

EFFECTS OF NANOPARTICLES ON THERMAL CHARACTERISTICS OF  
POLYAMIDE-6, POLYLACTIC ACID AND POLYSTYRENE  
INVOLVING VARIOUS FLAME RETARDANTS

A THESIS SUBMITTED TO  
THE GRADUATE SCHOOL OF NATURAL AND APPLIED SCIENCES  
OF  
MIDDLE EAST TECHNICAL UNIVERSITY

BY

HATİCE KAYA

IN PARTIAL FULFILLMENT OF THE REQUIREMENTS  
FOR  
THE DEGREE OF DOCTOR OF PHILOSOPHY  
IN  
POLYMER SCIENCE AND TECHNOLOGY

DECEMBER 2013



Approval of the thesis:

**EFFECTS OF NANOPARTICLES ON THERMAL CHARACTERISTICS  
OF POLYAMIDE-6, POLYLACTIC ACID AND POLYSTYRENE  
INVOLVING VARIOUS FLAME RETARDANTS**

submitted by **HATİCE KAYA** in partial fulfillment of the requirements for the degree of **Doctor of Philosophy in Polymer Science and Technology Department, Middle East Technical University** by,

Prof. Dr. Canan Özgen  
Dean, Graduate School of **Natural and Applied Sciences** \_\_\_\_\_

Prof. Dr. Teoman Tinçer  
Head of Department, **Polymer Science and Technology** \_\_\_\_\_

Prof. Dr. Jale Hacaloğlu  
Supervisor, **Chemistry Dept., METU** \_\_\_\_\_

Prof. Dr. Cevdet Kaynak  
Co-Supervisor, **Metallurgical and Mat. Eng. Dept., METU** \_\_\_\_\_

**Examining Committee Members:**

Prof. Dr. Teoman Tinçer  
Chemistry Dept., METU \_\_\_\_\_

Prof. Dr. Jale Hacaloğlu  
Chemistry Dept., METU \_\_\_\_\_

Prof. Dr. Erdal Bayramlı  
Chemistry Dept., METU \_\_\_\_\_

Prof. Dr. Nursel Dilsiz  
Chemical Engineering Dept., Gazi University \_\_\_\_\_

Prof. Dr. Göknur Bayram  
Chemical Engineering Dept., METU \_\_\_\_\_

**Date:** **25/12/2013**

**I hereby declare that all information in this document has been obtained and presented in accordance with academic rules and ethical conduct. I also declare that, as required by these rules and conduct, I have fully cited and referenced all material and results that are not original to this work.**

Name, Last name : Hatice KAYA

Signature :

## ABSTRACT

### EFFECTS OF NANOPARTICLES ON THERMAL CHARACTERISTICS OF POLYAMIDE-6, POLYLACTIC ACID AND POLYSTYRENE INVOLVING VARIOUS FLAME RETARDANTS

Kaya, Hatice

Ph.D., Department of Polymer Science and Technology

Supervisor : Prof. Dr. Jale Hacaloğlu

Co-Supervisor : Prof. Dr. Cevdet Kaynak

December 2013, 205 pages

In this work, the effects of addition of nanoparticles halloysite, (HNT), organically modified montmorillonites (MMT10A, MMT25A and MMT30B) and SiO<sub>2</sub> on thermal degradation characteristics of polyamide 6 (PA6), polylactide (PLA) and polystyrenes (PS and HIPS) involving flame retardants are investigated. The composites of PA6 and PLA involve phosphorus containing flame retardant, aluminium diethylphosphinate (AlPi). Composites HIPS involve mineral flame retardant, aluminium hydroxide and those of PS involve halogenated flame retardant, brominated epoxy (BE).

Addition of MMT25A does not affect thermal stability of PA6. On the other hand, thermal stability of PA6 decreases in the presence of HNT, and increases in the presence of MMT30B. Upon incorporation of AlPi thermal stability of PA6 decreases noticeably. Addition of nanoparticles to flame retarded PA6 affects both thermal stability and product patterns.

In the presence of AlPi, thermal stability of PLA is decreased due to the attack of phosphinate groups to carbonyl groups. Upon addition of MMT30B to PLA-AlPi, thermal stability of the composite is increased slightly. In addition, transesterification reactions between PLA and the organic modifier of the nanoclay are noted. Presence of SiO<sub>2</sub> affects mainly product patterns of AlPi, whereas, in the presence of HNT, the interactions between PLA and AlPi are hindered, and product patterns resemble to those of the pure forms.

Products involving head-to-head linkages, double and triple bonds are generated during the pyrolysis of HIPS in the presence of MMT10A. The addition of aluminium hydroxide enhances the effects of the clay.

Reactions between BE and PS, and upon addition of Sb<sub>2</sub>O<sub>3</sub>, reactions between BE and Sb<sub>2</sub>O<sub>3</sub> and between the products generated and PS are noticed. Addition of MMT10A hinders the interactions between BE and PS. On the other hand, the reactions of Sb<sub>2</sub>O<sub>3</sub> with bromines are increased in the presence of MMT10A.

Keywords: Polyamide 6, polylactic acid, polystyrene, flame retardant, nanoparticle, pyrolysis mass spectrometry, thermal degradation.

## ÖZ

### NANOPARTİKÜLLERİN ÇEŞİTLİ ALEV GECİKTİRİCİLER İÇEREN POLİAMİD-6, POLİLAKTİK ASİT VE POLİSTİRENİN ISIL ÖZELLİKLERİ ÜZERİNDEKİ ETKİLERİ

Kaya, Hatice

Doktora, Polimer Bilimi ve Teknolojisi Bölümü

Tez Yöneticisi : Prof. Dr. Jale Hacaloğlu

Ortak Tez Yöneticisi : Prof. Dr. Cevdet Kaynak

Aralık 2013, 205 sayfa

Bu çalışmada, halloysit, (HNT), organik olarak modifiye edilmiş killer (MMT10A, MMT25A ve MMT30B) ve SiO<sub>2</sub> gibi nanopartiküllerin eklenmesinin, alev geciktiriciler içeren poliamid 6 (PA6), polilaktik asit (PLA) ve polistiren (PS ve HIPS) kompozitlerinin ısıl bozunma karakterleri üzerindeki etkisi incelenmiştir. PA6 ve PLA kompozitleri fosfor içeren alev geciktirici olan alüminyum dietilfosfinat, (AlPi) içerir. HIPS kompozitleri mineral içeren alev geciktirici olan alüminyum hidroksit ve PS kompozitleri halojenli alev geciktirici olan bromlanmış epoksi, (BE) içerir.

MMT25A eklenmesi, PA6'nın ısıl kararlılığını etkilemez. Diğer taraftan, PA6'nın ısıl kararlılığı HNT varlığında azalırken MMT30B varlığında artar. AlPi eklenmesi üzerine PA6'nın ısıl kararlılığı önemli ölçüde azalır. Nanopartiküllerin eklenmesi alev geciktirici içeren PA6'nın hem ısıl kararlılığını hemde ürün dağılımını etkiler.

AlPi varlığında, PLA'in ısı kararlılığı fosfinat gruplarının karbonil gruplarına saldırması sonucu azalır. MMT30B eklenmesi PLA-AlPi kompozitinin ısı kararlılığını biraz artırır. Buna ek olarak, PLA ve nanokilin organik kısmı arasında transesterifikasyon reaksiyonları gözlenmiştir. SiO<sub>2</sub> varlığında çoğunlukla AlPi'nin ürün dağılımı etkilenirken, HNT varlığında PLA ve AlPi arasındaki etkileşimler engellendiğinden, ürün dağılımları saf formlarındakilere benzer.

MMT10A eklenmesiyle HIPS'nin pirolizi sırasında baş-baş katılması ve çift ve üçlü bağlar içeren ürünlerin oluşumu gözlenmiştir. Alüminyum hidroksit eklenmesi kilin etkisini artırır.

BE ve PS arasındaki reaksiyonlar ve Sb<sub>2</sub>O<sub>3</sub> eklenmesi üzerine, BE ve Sb<sub>2</sub>O<sub>3</sub> arasındaki reaksiyonlar ve oluşan ürünler ile PS arasındaki reaksiyonlar fark edilir. MMT10A eklenmesi BE ve PS arasındaki etkileşimi engeller. Diğer yandan, brom ile Sb<sub>2</sub>O<sub>3</sub> arasındaki reaksiyonlar MMT10A varlığında artar.

Anahtar Kelimeler: Poliamid 6, polilaktik asit, polistiren, alev geciktirici, nanopartikül, piroliz kütle spektrometresi, ısı bozunma



To My Mother,

## ACKNOWLEDGEMENTS

I would like to express my appreciation to my supervisor Prof. Dr. Jale Hacalođlu, for her guidance, support, understanding and endless helps throughout my whole study.

I would like to express my appreciation to my co-supervisor Prof. Dr. Cevdet Kaynak for his support and I am also grateful for him and his former Ph.D. student Dr. Nihat Ali Iřıtman for supplying the composite materials analyzed within this study.

I would like to thank to all my Ph.D. thesis committee members for their invaluable comments and contributions.

I would sincerely thank my manager Dr. Glendem Gnendi and my friends employed in MTA, for encouraging me to complete my thesis study.

I would like to thank to my labmates for their collaboration on my experimental studies in Mass Spectrometry Laboratory, Chemistry Department, METU.

The partial financial support of TBTAK through research fund 112T493 is also acknowledged.

Finally, I am indebted to my parents, my lovely brother, my husband and my little baby Melisa, for being always so supportive, giving love and having an understanding.

## TABLE OF CONTENTS

ABSTRACT .....	v
ÖZ .....	vii
ACKNOWLEDGEMENTS .....	x
TABLE OF CONTENTS .....	xi
LIST OF FIGURES .....	xv
LIST OF SCHEMES.....	xx
LIST OF TABLES .....	xxii
LIST OF ABBREVIATIONS .....	xxvi
CHAPTERS	
1. INTRODUCTION .....	1
1.1. Thermal Degradation .....	1
1.2. Thermal Degradation Techniques .....	2
1.2.1. Pyrolysis .....	3
1.2.1.1. Pyrolysis-Mass Spectrometry (Py-MS) .....	3
1.2.1.2. Pyrolysis-Gas Chromatography-Mass Spectrometry (Py-GC-MS) .....	4
1.3. Polymer Combustion .....	4
1.4. Flame Retardancy .....	6
1.4.1. Physical Action .....	7
1.4.2. Chemical Action.....	7
1.5. Flame Retardant Additives.....	8
1.5.1. Mineral Flame Retardants.....	8
1.5.1.1. Metal Hydroxides .....	9
1.5.1.2. Hydrocarbonates.....	10
1.5.1.3. Borates .....	10
1.5.2. Halogenated Flame Retardants .....	10
1.5.3. Phosphorated Flame Retardants.....	12

1.5.3.1. Metal Phosphinate Salts .....	14
1.5.4. Nitrogen Based Flame Retardants .....	14
1.5.5. Silicon Based Flame Retardants .....	15
1.5.5.1. Silicones .....	16
1.5.5.2. Silica.....	16
1.5.6. Nanometric Particles .....	16
1.5.6.1. Nanoclays .....	17
1.5.6.2. Carbon Nanotubes.....	18
1.6. Polyamide 6 (PA6) .....	18
1.6.1. Thermal Degradation of PA6. ....	19
1.6.2. Flame Retardancy of PA6. ....	21
1.7. Polylactide .....	23
1.7.1. Thermal Degradation of PLA. ....	23
1.7.2. Flame Retardancy of PLA.....	25
1.8. Polystyrene.....	26
1.8.1. Thermal Degradation of PS. ....	26
1.8.2. Flame Retardancy of PS.....	28
1.9. Aim of Work.....	30
2. EXPERIMENTAL.....	33
2.1. Materials .....	33
2.2. Direct Pyrolysis Mass Spectrometry .....	35
2.3. Data Analysis .....	36
3. RESULTS AND DISCUSSION.....	37
3.1. Thermal Degradation of Flame Retardant Additives .....	37
3.1.1. Organically Modified Montmorillonite.....	37
3.1.1.1. MMT10A.....	37
3.1.1.2. MMT25A.....	41
3.1.1.3. MMT30B .....	44
3.1.2. AlPi .....	48
3.1.3. Brominated Epoxy (BE).....	59
3.1.4. Sb <sub>2</sub> O <sub>3</sub> .....	65

3.2. Thermal Degradation of PA6 in the Presence of Nanoparticles and Flame Retardants .....	68
3.2.1. In the Presence of Nanoparticles.....	75
3.2.1.1. PA6-HNT .....	75
3.2.1.2. PA6-MMT25A .....	80
3.2.1.3. PA6-MMT30B.....	84
3.2.2. In the Presence of Flame Retardant, AlPi.....	89
3.2.3. In the Presence of Flame Retardant and Nanoparticles.....	94
3.2.3.1. PA6-AlPi-HNT .....	94
3.2.3.2. PA6-AlPi-MMT25A .....	99
3.2.3.3. PA6-AlPi-MMT30B .....	103
3.3. Thermal Degradation of PLA in the Presence of Nanoparticles and Flame Retardants .....	109
3.3.1. Flame Retarded PLA With or Without Nanoparticles .....	114
3.3.1.1. PLA-AlPi.....	114
3.3.1.2. PLA-AlPi-MMT30B .....	120
3.3.1.3. PLA-AlPi-SiO <sub>2</sub> .....	127
3.3.1.4. PLA-AlPi-HNT .....	132
3.4. Thermal Degradation of PS in the Presence of Nanoparticles and Flame Retardants. ....	138
3.4.1. Thermal Degradation of HIPS in the Presence of Nanoparticles and Flame Retardants .....	138
3.4.1.1. HIPS-ATH.....	141
3.4.1.2. HIPS-MMT10A.....	145
3.4.1.3. HIPS-ATH-MMT10A.....	151
3.4.2. Thermal Degradation of PS in the Presence of Nanoparticles and Flame Retardants .....	156
3.4.2.1. PS-BE.....	160
3.4.2.2. PS-BE-Sb <sub>2</sub> O <sub>3</sub> .....	165
3.4.2.3. PS-MMT10A.....	170
3.4.2.4. PS-BE-MMT10A.....	176
3.4.2.5. PS-BE-Sb <sub>2</sub> O <sub>3</sub> -MMT10A .....	182

4. CONCLUSION .....	189
REFERENCES .....	193
CURRICULUM VITAE .....	203

## LIST OF FIGURES

### FIGURES

Figure 1.1 The combustion cycle of polymers .....	5
Figure 1.2 Chemical structures of classical halogenated flame retardants .....	12
Figure 1.3 Structure of Organomodified MMT10A, MMT25A and MMT30B ....	17
Figure 3.1 a) The total ion current curve and mass spectra at b) 232 c) 299 d) and 384 °C recorded during the pyrolysis of MMT10A.....	38
Figure 3.2 Single ion pyrograms of some selected fragments detected during the pyrolysis of MMT10A. ....	40
Figure 3.3 a) The total ion current curve and mass spectra at b) 338 and c) 396°C recorded during the pyrolysis of MMT25A. ....	42
Figure 3.4 Single ion pyrograms of some selected fragments detected during the pyrolysis of pure MMT25A.....	43
Figure 3.5 a) The total ion current curve and mass spectra at b) 279 and c) 421°C recorded during the pyrolysis of MMT30B .....	45
Figure 3.6 Single ion pyrograms of some selected fragments detected during the pyrolysis of MMT30B.....	47
Figure 3.7 a) The total ion current curve and mass spectra at b) 390 and c) 440°C during the pyrolysis of AlPi. ....	48
Figure 3.8 Single ion pyrograms of some selected fragments detected during the pyrolysis of AlPi. ....	50
Figure 3.9 The daughter spectra of precursor fragment ions with m/z values 751, 659, 601, 543, 433 and 269 Da.....	52
Figure 3.10 The daughter spectra of precursor fragment ions with m/z values 505, 413 and 403 Da.....	55
Figure 3.11 The daughter spectra of precursor fragment ions with m/z values 169, 105 and 94 Da.....	57
Figure 3.12 a) The total ion current curve and b) mass spectrum of BE at 407 °C	59

Figure 3.13 Single ion pyrograms of some selected fragments detected during the pyrolysis of BE.....	61
Figure 3.14 a) The total ion current curve and b) mass spectrum of $Sb_2O_3$ at 495°C. ....	65
Figure 3.15 Single ion pyrograms of some selected fragments detected during the pyrolysis of $Sb_2O_3$ . ....	67
Figure 3.16 a) The total ion current curve and b) mass spectrum of PA6 at 449°C. ....	69
Figure 3.17 Single ion pyrograms of some selected fragments detected during the pyrolysis of PA6. ....	72
Figure 3.18 a) The total ion current curve and b) mass spectrum of PA6-HNT at 434°C. ....	76
Figure 3.19 Single ion pyrograms of some selected fragments detected during the pyrolysis of PA6-HNT.....	79
Figure 3.20 a) The total ion current curve and b) mass spectrum of PA6-MMT25A at 449°C.....	80
Figure 3.21 Single ion pyrograms of some selected fragments detected during the pyrolysis of PA6-MMT25A.....	83
Figure 3.22 a) The total ion current curve and b) mass spectrum of PA6-MMT30B at 455°C.....	84
Figure 3.23 Single ion pyrograms of some selected fragments detected during the pyrolysis of PA6-MMT30B.....	87
Figure 3.24 a) The total ion current curve and b) mass spectrum of PA6-AlPi at 433°C. ....	90
Figure 3.25 Single ion pyrograms of some selected fragments detected during the pyrolysis of PA6-AlPi.....	93
Figure 3.26 a) The total ion current curve and b) mass spectrum of PA6-AlPi-HNT at 438°C.....	95
Figure 3.27 Single ion pyrograms of some selected fragments detected during the pyrolysis of PA6-AlPi-HNT. ....	98
Figure 3.28 a) The total ion current curve and b) mass spectrum of PA6-AlPi-MMT25A at 452°C.....	99



Figure 3.29 Single ion pyrograms of some selected fragments detected during the pyrolysis of PA6-AIPi-MMT25A.....	102
Figure 3.30 a) The total ion current curve and the mass spectra at b) 393 and c) 451°C recorded during the pyrolysis of PA6-AIPi-MMT30B.....	104
Figure 3.31 Single ion pyrograms of some selected fragments detected during the pyrolysis of PA6-AIPi-MMT30B. ....	107
Figure 3.32 a) The total ion current curve and b) the mass spectra at 363°C recorded during the pyrolysis of PLA.....	110
Figure 3.33 Single ion pyrograms of some selected fragments detected during the pyrolysis PLA .....	113
Figure 3.34 a) The total ion current curve and the mass spectra at b) 328°C and c) 425°C recorded during the pyrolysis of PLA-AIPi.....	115
Figure 3.35 Single ion pyrograms of some selected fragments detected during the pyrolysis PLA-AIPi.....	118
Figure 3.36 a) The total ion current curve and the mass spectra at b) 340°C and c) 440°C recorded during the pyrolysis of PLA-AIPi-MMT30B .....	121
Figure 3.37 Single ion pyrograms of some selected fragments detected during the pyrolysis of I. PLA-AIPi, and II. PLA-AIPi-MMT30B. ....	124
Figure 3.38 The Single ion pyrograms of selected products recorded during the pyrolysis of I. MMT30B, II. PLA-AIPi, and III. PLA-AIPi-MMT30B.....	126
Figure 3.39 a) The total ion current curve and the mass spectra at b) 340°C and c) 415°C recorded during the pyrolysis of PLA-AIPi-SiO <sub>2</sub> .....	128
Figure 3.40 Single ion pyrograms of some selected fragments detected during the pyrolysis PLA-AIPi-SiO <sub>2</sub> . ....	131
Figure 3.41 a) The total ion current curve and the mass spectra at b) 310°C and c) 395°C recorded during the pyrolysis of PLA-AIPi-HNT.....	133
Figure 3.42 Single ion pyrograms of some selected fragments detected during the pyrolysis PLA-AIPi-HNT.....	136
Figure 3.43 a) The total ion current curve and b) mass spectrum of HIPS at 471 °C .....	139
Figure 3.44 Single ion pyrograms of some selected fragments detected during the pyrolysis of HIPS.....	140

Figure 3.45 a) The total ion current curve and b) mass spectrum of HIPS-ATH at 469°C .....	143
Figure 3.46 Single ion pyrograms of some selected fragments detected during the pyrolysis of HIPS-ATH .....	144
Figure 3.47 a) The total ion current curve and b) mass spectrum of HIPS-MMT10A at 449 °C.....	146
Figure 3.48 Single ion pyrograms of some selected fragments detected during the pyrolysis of HIPS-MMT10A .....	148
Figure 3.49 a) The total ion current curve and b) mass spectrum of HIPS-ATH-MMT10A at 441 °C.....	152
Figure 3.50 Single ion pyrograms of some selected fragments detected during the pyrolysis of HIPS-ATH-MMT10A .....	154
Figure 3.51 a) The total ion current curve and b) mass spectrum of PS at 441°C	157
Figure 3.52 Single ion pyrograms of some selected fragments detected during the pyrolysis of PS .....	159
Figure 3.53 a) The total ion current curve and b) mass spectrum of PS-BE at 448 °C .....	161
Figure 3.54 Single ion pyrograms of some selected fragments detected during the pyrolysis of PS-BE .....	163
Figure 3.55 a) The total ion current curve and the mass spectra at b) 393 c) 446 °C recorded during the pyrolysis of PS-BE-Sb <sub>2</sub> O <sub>3</sub> .....	166
Figure 3.56 Single ion pyrograms of some selected fragments detected during the pyrolysis of PS-BE-Sb <sub>2</sub> O <sub>3</sub> .....	168
Figure 3.57 a) The total ion current curve and b) mass spectrum of PS-MMT10A at 457°C.....	171
Figure 3.58 Single ion pyrograms of some selected fragments detected during the pyrolysis .....	174
Figure 3.59 Possible head-to-head compounds.....	175
Figure 3.60 a) The total ion current curve and the mass spectra at b) 372, c) 442 °C recorded during the pyrolysis of PS-BE-MMT10A .....	178
Figure 3.61 Single ion pyrograms of some selected fragments detected during the pyrolysis of PS-BE-MMT10A .....	181

Figure 3.62 a) The total ion current curve and the mass spectra at b) 384, c) 453 °C recorded during the pyrolysis of PS-BE-Sb <sub>2</sub> O <sub>3</sub> -MMT10A.....	184
Figure 3.63 Single ion pyrograms of some selected fragments detected during the pyrolysis of PS-BE-Sb <sub>2</sub> O <sub>3</sub> -MMT10A.....	187

## LIST OF SCHEMES

### SCHEMES

Scheme 1.1 Chain scission reactions .....	6
Scheme 1.2 Flame retardant mechanism of aluminium hydroxide .....	9
Scheme 1.3 Flame retardant mechanism of halogenated flame retardants, X may be Br or Cl .....	11
Scheme 1.4 Pyrophosphate structures formation from phosphoric acid condensation.....	13
Scheme 1.5 Generation of unsaturated structures after dehydration of terminal alcohols .....	13
Scheme 1.6 Thermal degradation of melamine.....	15
Scheme 1.7 Generation of caprolactam .....	20
Scheme 1.8 Generation of caprolactam, aldehyde, amide and cyanide end groups .....	20
Scheme 1.9 Possible thermal degradation reactions of PA6.....	21
Scheme 1.10 Possible thermal degradation reactions of PLA .....	24
Scheme 1.11 Synthesis of High-impact polystyrene .....	26
Scheme 1.12 Initiation reactions of PS .....	27
Scheme 1.13 Propagation reactions of .....	28
Scheme 1.14 Termination reactions of PS .....	28
Scheme 3.1 Possible structures and fragmentation pathways of aluminium phosphinates complex.....	54
Scheme 3.2 Thermal degradation pathways of brominated epoxy oligomer .....	63
Scheme 3.3 Formation of protonated oligomers .....	73
Scheme 3.4 Formation of C=N linkages and CN end groups.....	73
Scheme 3.5 Other possible reaction pathways for the evolution of H <sub>2</sub> O, CO <sub>2</sub> and NH <sub>3</sub> .....	74
Scheme 3.6 Nucleophilic attack of NH <sub>3</sub> to carbonyl groups .....	74

Scheme 3.7 Hydrolysis of PA6.....	75
Scheme 3.8 Trans-esterification reactions between the modifier of MMT and PA6 .....	86
Scheme 3.9 Trans-esterification and cis-elimination reactions of PLA.....	111
Scheme 3.10 Possible reactions between phosphinates and PLA .....	119
Scheme 3.11 Trans-esterification reactions between the modifier of MMT and PLA .....	127
Scheme 3.12 The degradation pathway of neat high impact polystyrene .....	141
Scheme 3.13 Possible generated radicals and their reactions.....	149
Scheme 3.14 Possible unsaturated and head to head compounds .....	150
Scheme 3.15 Disproportionation reaction of polystyrene .....	151

## LIST OF TABLES

### TABLES

Table 2.1 PA6 based samples.....	34
Table 2.2 PLA based samples .....	34
Table 2.3 HIPS based samples .....	34
Table 2.4 PS based samples .....	34
Table 3.1 The relative intensities, RI, of some selected intense and/or characteristic peaks recorded in pyrolysis spectrum of MMT10A at 232, 299 and 384 °C and the assignments made .....	39
Table 3.2 The relative intensities, RI, of some selected intense and/or characteristic peaks recorded in pyrolysis spectrum of AlPi at 400 and 440°C and the assignments made .....	58
Table 3.3 The relative intensities, RI, of some selected intense and/or characteristic peaks recorded in pyrolysis spectrum of BE at 407°C and the assignments made	60
Table 3.4 The relative intensities, RI, of some selected intense and/or characteristic peaks recorded in pyrolysis spectrum of Sb <sub>2</sub> O <sub>3</sub> at 495°C and the assignments made .....	66
Table 3.5 The relative intensities, RI, of some selected intense and/or characteristic peaks recorded in pyrolysis spectrum of PA6 at 449°C and the assignments made .....	70
Table 3.6 The relative intensities, RI, of some selected intense and/or characteristic peaks recorded in pyrolysis spectrum of PA6-HNT at 434°C and the assignments made.....	77
Table 3.7 The relative intensities, RI, of some selected intense and/or characteristic peaks recorded in pyrolysis spectrum of PA6-MMT25A at 345 and 449°C and the assignments made .....	81

Table 3.8 The relative intensities, RI, of some selected intense and/or characteristic peaks recorded in pyrolysis spectrum of PA6-MMT30B at 299 and 455°C and the assignments made .....	85
Table 3.9 The relative intensities, RI, of some selected intense and/or characteristic peaks recorded in pyrolysis spectrum of PA6-AlPi at 433°C and the assignments made .....	91
Table 3.10 The relative intensities, RI, of some selected intense and/or characteristic peaks recorded in pyrolysis spectrum of PA6-AlPi-HNT at 438°C and the assignments made .....	96
Table 3.11 The relative intensities, RI, of some selected intense and/or characteristic peaks recorded in pyrolysis spectrum of PA6-AlPi-MMT25A at 452°C and the assignments made.....	100
Table 3.12 The relative intensities, RI, of some selected intense and/or characteristic peaks recorded in pyrolysis spectrum of PA6-AlPi-MMT30B at 391 and 451°C and the assignments made .....	105
Table 3.13 The relative intensities, RI, of some selected intense and/or characteristic peaks recorded in pyrolysis spectrum of PLA at 363°C and the assignments made .....	112
Table 3.14 The relative intensities, RI, of some selected intense and/or characteristic peaks recorded in pyrolysis spectrum of PLA-AlPi at 325 and 425°C and the assignments made .....	116
Table 3.15 The relative intensities, RI, of some selected intense and/or characteristic peaks recorded in pyrolysis spectrum of PLA-AlPi-MMT30B at 340 and 440°C and the assignments made .....	122
Table 3.16 The relative intensities, RI, of some selected intense and/or characteristic peaks recorded in pyrolysis spectrum of PLA-AlPi-SiO <sub>2</sub> at 330 and 410°C and the assignments made.....	129
Table 3.17 The relative intensities, RI, of some selected intense and/or characteristic peaks recorded in pyrolysis spectrum of PLA-AlPi-HNT at 310 and 392°C and the assignments made.....	134

Table 3.18 The relative intensities, RI, of some selected intense and/or characteristic peaks recorded in pyrolysis spectrum of HIPS at 471 °C and the assignments made .....	139
Table 3.19 The relative intensities, RI, of some selected intense and/or characteristic peaks recorded in pyrolysis spectrum of HIPS-ATH at 469°C and the assignments made .....	143
Table 3.20 The relative intensities, RI, of some selected intense and/or characteristic peaks recorded in pyrolysis spectrum of HIPS-MMT10A at 449°C and the assignments made.....	147
Table 3.21 The relative intensities, RI, of some selected intense and/or characteristic peaks recorded in pyrolysis spectrum of HIPS-ATH-MMT10A at 441 °C and the assignments made .....	153
Table 3.22 The comparison of relative intensities, RI, of some selected intense and/or characteristic peaks recorded in pyrolysis spectrum of HIPS, HIPS-ATH, HIPS–MMT10A and HIPS-ATH-MMT10A and the assignments made.....	156
Table 3.23 The relative intensities, RI, of some selected intense and/or characteristic peaks recorded in pyrolysis spectrum of PS at 441°C and the assignments made .....	158
Table 3.24 The relative intensities, RI, of some selected intense and/or characteristic peaks recorded in pyrolysis spectrum of PS-BE at 448 °C and the assignments made .....	162
Table 3.25 The relative intensities, RI, of some selected intense and/or characteristic peaks recorded in pyrolysis spectrum of PS-BE-Sb <sub>2</sub> O <sub>3</sub> at 393 and 446°C and the assignments made .....	167
Table 3.26 The relative intensities, RI, of some selected intense and/or characteristic peaks recorded in pyrolysis spectrum of PS- MMT10A at 457°C and the assignments made .....	172
Table 3.27 The relative intensities, RI, of some selected intense and/or characteristic peaks recorded in pyrolysis spectrum of PS-BE-MMT10A at 372 and 442°C and the assignments made.....	179



Table 3.28 The relative intensities, RI, of some selected intense and/or characteristic peaks recorded in pyrolysis spectrum of PS-BE-Sb<sub>2</sub>O<sub>3</sub>-MMT10A at 384 and 453 °C and the assignments made ..... 185

## LIST OF ABBREVIATIONS

AlPi	aluminium diethylphosphinate
BE	tribromophenol end-capped brominated epoxy
BPO <sub>4</sub>	boron phosphate
BSi	borosilicate
CID	collision induced dissociation
DP-MS	direct pyrolysis mass spectrometry
DSC	differential scanning calorimeter
EI	electron impact
EVA	ethylene vinyl acetate
FTIR	Fourier transform infrared spectrometry
GC	gas chromatography
HDT	heat deflection temperature
HIPS	high-impact polystyrene
HNT	halloysite nanotubes
LDPE	low density polyethylene
LOI	limiting of oxygen index
MMT	modifier for montmorillonite
MMT10A	dimethyl, benzyl, hydrogenated tallow, quaternary ammonium modified montmorillonite
MMT25A	dimethyl, dehydrogenated tallow, 2-ethylhexyl quaternary ammonium modified montmorillonite
MMT30B	methyl, tallow, bis-2-hydroxyethyl, quaternary ammonium modified montmorillonite
MPP	melamine pyrophosphate
MS	mass spectrometry
NIST	National Institute of Standards and Technology
PA6	polyamide 6
PB	Polybutadiene

PE	Polyethylene
PHRR	peak heat release rate
PLA	polylactide or poly(lactic acid)
PMLR	peak mass loss rate
PMMA	poly(methyl methacrylate)
POSS	polyhedral oligosilsesquioxane
PP	Polypropylene
PS	Polystyrene
PST	polymer science and technologies
PVC	poly(vinyl chloride)
Py	Pyrolysis
RI	relative intensity
RP	red phosphorus
TGA	thermal gravimetric analysis
TIC	total ion current
UL	Underwriters laboratory
ZnB	zinc borate



## **CHAPTER 1**

### **INTRODUCTION**

#### **1.1 THERMAL DEGRADATION**

Polymer degradation covers destructions in the chemical and physical features of the polymers because of external physical or chemical stresses resulted from chemical reactions [1, 2]. Degradation may be thermal, oxidative, bio, mechanical, photo or catalytic.

The thermal degradation of polymers refers to the situation where polymers at elevated temperatures start to undergo chemical changes [2]. For improving a technology for polymer processing, for usage at high temperatures, and in understanding of thermal decomposition mechanisms for the synthesis of fire-safe products, thermal degradation of polymers is essential. It can be divided into three. The first one is complete degradation involving the decomposition of the main chain. The second one is the loose of side groups along with formation of volatile products and char residues. The last one is the formation of crosslinked polymers, thus, production of large amount of char releasing only small amount of volatiles. Studies on degradation mechanisms have aimed to increase the lifetime of polymers and also to rise the degradation rate of large-volume plastics, such as polyamides (PA), poly(vinyl chloride) (PVC), polystyrene (PS) and polyethylene (PE), to overcome the landfills filling with slowly degrading plastic wastes.

During processing, usually polymers are exposed to high temperatures and thermal degradation is important in modification of the properties of the starting materials [3]. Polymeric materials are subjected to serious damage during the thermal

degradation processes. For recycled polymers, this effect is especially significant since they undergo sequential cycles of low and high temperatures [4, 5].

For understanding the recycling, storage and usability of polymers, researches on thermal degradation is essential. Another serious subject is the flammability of polymers. Many fatalities and serious injuries have been caused by fires involving polymeric materials, mainly based from the smoke released during the burning of the polymers [6]. Especially in closed spaces, during thermal decomposition or burning the toxic gases evolved causes the destroying effects [1].

This work investigates the thermal degradation behavior and mechanism of some important polymers involving various flame retardant additives. To start with, a brief overview of thermal degradation techniques is presented, followed by the types of flame retardants. A brief overview on the thermal degradation and flame retardancy of the polymers analyzed is also presented.

## **1.2 THERMAL DEGRADATION TECHNIQUES**

Thermal analysis methods are useful not only in determination of suitable processing conditions but also in getting information on the relationships between polymer structure and thermal properties. Several various configurations of instrumentation have been improved to achieve degradation for quantitative and qualitative analysis. Thermogravimetry (TG), differential scanning calorimetry (DSC) and pyrolysis techniques have been used to analyze the thermal degradation of polymers. Fourier transform infrared spectrometry (FTIR) or mass spectrometry (MS) techniques have been used to investigate volatile products. The combined thermo analytical techniques, e.g., TG-MS or TG-FTIR, have been shown to be useful in searching structural properties of complex organic compounds [7]. The primary aim of thermal degradation is to rupture the polymer by increasing the quantity of decomposition products and to make them remove from the reaction zone to decrease secondary fragmentation. The combination of results obtained

from more than one thermal degradation technique supplies better information of the thermal decomposition mechanisms.

### **1.2.1 PYROLYSIS**

In general pyrolysis is thermal degradation in the absence of oxygen. The process includes many complex sets of reactions causing the formation of radicals. Thermal decomposition proceeds via a radical mechanism, initiated by homolysis of a bond, in the absence of specific reactions, such as elimination and retro Diels-Alder reaction [7, 8]. This creates a pair of free radicals as the first products, which can then undergo secondary reactions (rearrangement,  $\beta$ -scission, elimination, hydrogen abstraction, etc.) and abstraction of hydrogen from unreacted molecules to include them into the pyrolysis reaction cycle finally [9]. Pyrolysis, coupled to Fourier Transform Infrared, FTIR, spectrometry, mass spectrometry, MS, gas chromatography, GC, or GC/MS allows interpretation of thermal degradation products at least to a certain extent.

#### **1.2.1.1 PYROLYSIS – MASS SPECTROMETRY (DP-MS)**

Direct pyrolysis-mass spectrometry (DP-MS) is used to determine mainly the primary thermal degradation products to analyze the thermal degradation mechanisms. DP-MS enables the polymer degradation close to the ion source, so that the generating fragments are ionized and continually identified by repetitive mass scans nearly at the same time with their generation [10, 11]. Under high vacuum conditions, thermal decomposition products are quickly escaped from the hot zone in the mass spectrometer. Therefore, probability of secondary reactions and molecular collisions are decreased. As a result, primary pyrolysis products are mainly detected by the fast detection system [5]. Nevertheless, pyrolysis mass spectra of polymers are generally very complicated because of further decomposition of thermal degradation products throughout ionization. However, it is the only technique that permits identification of unstable products that may be quite important for understanding of thermal degradation mechanism.

### **1.2.1.2. PYROLYSIS-GAS CHROMATOGRAPHY-MASS SPECTROMETRY (Py-GC-MS)**

For separation and identification of the volatile pyrolysis products of polymers, pyrolysis-gas chromatography-mass spectrometry (Py-GC-MS) has been widely utilized. Also, this technique is suitable way to identify continuously the decomposition products quantitatively and qualitatively [12]. Using a GC coupled to a mass-selective detector proposes many benefits for studying the decomposition mechanism. The number of peaks present in the total ion chromatogram (TIC) is directly related to the number of compounds recorded by GC-MS. The relative concentration of each compound complies with the relative intensity of each peak. By analyzing known compounds or matching the spectrum with those in a GC-MS library, assigning of each degradation fragment can also be done.

### **1.3 POLYMER COMBUSTION**

Synthetic and natural polymers are used in many fields and under various environmental situations. However, using polymers can result loss of life and goods in case of a fire. Therefore, using flame retardants becomes a main part of the developments and applications of new materials to suppress ignition of the polymers, smoke and poisonous gas generation. Especially, the industries are interested in electronics, transportation and construction require flame retardants [13].

When subjected to enough heat, polymers degrade by producing flammable gases. These gases get mixed with the O<sub>2</sub> of the atmospheric air to generate a flammable mixture. Combustion starts in the existence of an exterior source or impulsively, if the activation energy of the ignition reaction is obtained. Heat is evolved by combustion, a part of which caused further pyrolysis of the substrate. If the released heat is sufficient to maintain the degradation ratio of the polymer over that needed to keep the concentration of the volatiles within the flammability



boundaries, then a self-sustaining ignition cycle is founded (Figure 1.1). Oxygen, heat and fuel are needed for the growing of a continuous fire. Carbon rich polymeric material, fuel, release combustible volatiles during thermal degradation processes [14–16]. The fire products depend on chemical composition of the polymer and the situations under which the burning process happens. For example, smoke is a mixture of complete combustion species such as H<sub>2</sub>O, CO<sub>2</sub> and acid gases and incomplete combustion species such as soot, CO and partially oxidized fuel gases. On the other hand, the solid residue is mainly ash and carbon which is oxidized metals. Smoke consisting CO, which is very poisonous, can be the main fire damage. In addition the escape from fire becomes difficult because of acid gases which are irritant for nasal passages and eyes and soot which absorbs light restricting visibility [17].

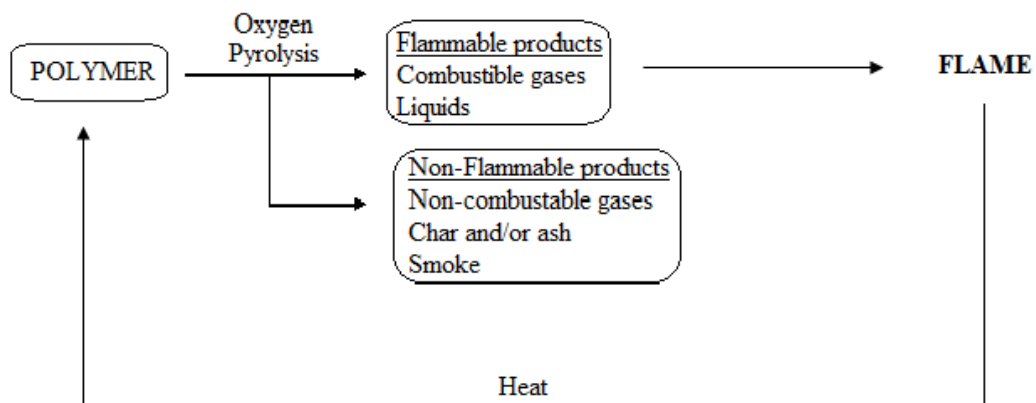


**Figure 1.1.** The ignition cycle of polymers.

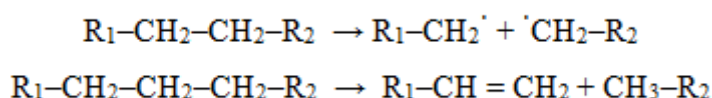
The thermal degradation of a polymer is endothermic, means needs energy. The energy supplied to the system must be greater than the covalent bond energy for most C-C bond about 200-400 kJ/mol. The decomposition mechanism of the polymer is managed by the presence or absence of oxygen in the gas and solid

phases and weakest bonds. Thermal degradation can be divided into two parts as oxidizing and non-oxidizing thermal degradation [18].

At high temperatures, chain scissions initiate the non-oxidizing thermal degradation. The first scission relies on various factors which are the presence of catalyst residues, the presence of oxygen atoms in the chain and the existence of weak bonds.

Chain scission can happen in two paths. First one is the homolysis reaction, cause the formation of free-radicals; in this case, these radicals initiate a chain reaction. Second one is the disproportionation, cause the generation of saturated and unsaturated compounds by the migration of hydrogen atoms (Scheme 1.1) [19].

**Scheme 1.1.** Chain scission reactions.



#### 1.4 FLAME RETARDANCY

The aim of flame retardancy is to hinder or terminate the polymer ignition. Flame retardancy may be achieved by chemical or physical processes. In polymer combustion, flame retardants can interfere in various steps such as ignition, pyrolysis, heating, propagation of thermal degradation. The principle ways of flame retardancy are described [20].

### **1.4.1 PHYSICAL ACTION**

By heat consumption, some of the flame retardant additives decrease the temperature. Thus, the reaction medium is cooled below the combustion temperature of the polymer. Aluminium or magnesium hydroxides are flame retardants affective by physical action. They start to liberate H<sub>2</sub>O vapor at about 200 and 300°C, respectively.

During the degradation of flame retardants, the flammable gaseous phase is diluted, with the generation of inert gases like NH<sub>3</sub>, CO<sub>2</sub> and H<sub>2</sub>O. Thus, the combustion probability is decreased by limiting the concentration of the flammable products.

In the thermal degradation process, combustion occurs in the gaseous phase and thermal decomposition takes place in the solid phase. The generation of a protective gaseous or solid coating among the gas and solid phase can be triggered by some flame retardant additives. The transfer of combustible volatile gases and oxygen is limited by this protective layer. Therefore, the amount of decomposition gases generated is reduced remarkably. In addition, the combustible gases can be physically isolated from the oxygen, thus, ignition process is hindered [19].

### **1.4.2 CHEMICAL ACTION**

By chemical modification, flame retardancy of the combustion process can occur in gaseous and condensed phases. The release of specific radicals such as Cl<sup>·</sup> and Br<sup>·</sup> in the gaseous phase by flame retardant additives can stop the combustion process. Very reactive radicals such as OH<sup>·</sup> and H<sup>·</sup> react with these formed radicals, thus, less reactive products are obtained. Change in the ignition pathway causes significant reduction in the heat of the reaction so temperature is decreased.

In the solid phase, flame retardants generate two kinds of chemical reactions. First of all, decomposition of the polymer chains can be initiated by the flame

retardants. By this way, the polymer removes from the flame by dripping. Secondly, the generation of a vitreous layer and/or carbonized at the surface of the polymer can be promoted by the flame retardant. This vitrified layer and/or char behaves as an isolating coating among the condensed and the gaseous phase.

Flame retardants can be subdivided into two groups as additive flame retardants and reactive flame retardants. Additive flame retardants are usually added during the transformation process and only react with the polymer at high temperature. On the other hand, reactive flame retardants are usually incorporated into the polymer chain during synthesis or by chemical grafting [19].

## **1.5 FLAME RETARDANT ADDITIVES**

### **1.5.1 MINERAL FLAME RETARDANTS**

All types of inorganic fillers can affect the thermal degradation of polymers in fire for various causes. First of all, it decreases the ingredient of flammable products. Also, it changes thermal properties and conductivity of the composite. Finally, it changes the viscosity of the composite. All these behaviors reduce the flammability of the polymer.

However, due to their acts at high temperatures, some mineral flame retardants are more preferred. The mostly preferred ones are hydroxycarbonates, zinc borates and metal hydroxides such as aluminium and magnesium hydroxides. Besides the common actions, these additives have a direct physical flame retardant action. When the temperature increases, mineral flame retardants degrade by absorbing heat. In addition, they can lead the vitreous layer and/or protective ceramic generation and release inert molecules such as H<sub>2</sub>O and CO<sub>2</sub> [19].

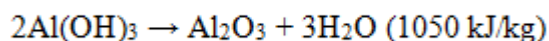
### 1.5.1.1 METAL HYDROXIDES

If a metal hydroxide releases water by endothermic decomposition at around decomposition temperature of the polymer, it may be used as a flame retardant. Metal hydroxides can also suppress the smoke. The definite mechanism has not been explained yet, but the most feasible comment is that carbon, generated from polymer degradation, and oxide, generated from metal hydroxide degradation, forms carbon dioxide without releasing any smoke [21, 22].

Aluminium hydroxide is the most preferred additive due to properties of non-toxic fume generation, ability to suppress smoke, safe handling and cost effectiveness [23, 24].

Aluminium hydroxide ( $\text{Al}(\text{OH})_3$ ) promotes the releasing of  $\text{H}_2\text{O}$  and forms alumina by decomposing at around 180 and 200°C (Scheme 1.2). This reaction happens in two stages. In the first stage an intermediate product boehmite  $\text{AlOOH}$  is formed by endothermic decomposition [25].

**Scheme 1.2.** Flame retardant mechanism of aluminium hydroxide.



The reaction of aluminium hydroxide has various influences on the polymer ignition. First of all it cools down the polymer by absorbing 1050 kJ/kg energy. In addition, isolating layer is formed by  $\text{Al}_2\text{O}_3$ . Furthermore, the formation of  $\text{Al}_2\text{O}_3$  behaves as a protecting coating among the flame and the polymer. And finally, combustible gases are diluted by the released water vapors and protective gas layer is formed [19].

### **1.5.1.2 HYDROCARBONATES**

Only calcium and magnesium carbonates release carbon dioxide below 1000°C, all other carbonates release it at higher temperatures. Magnesium carbonate has the lowest evolution temperature at 550°C. Hydroxycarbonates are an alternative to metal hydroxides although they are less popular. Besides loss of H<sub>2</sub>O, magnesite and hydromagnesite, are also effective as they decompose by endothermic process and by releasing CO<sub>2</sub> at high temperatures [19].

### **1.5.1.3 BORATES**

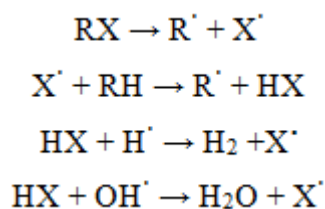
Mostly used borates are zinc borates such as 2ZnO·3B<sub>2</sub>O<sub>3</sub>·3.5H<sub>2</sub>O. They decompose by absorbing 503 kJ/kg energy in the temperature range 290 to 450°C. Also, they release water, boric acid (B(OH)<sub>3</sub>) and boron oxide (B<sub>2</sub>O<sub>3</sub>). In addition, a protective vitreous layer is formed by B<sub>2</sub>O<sub>3</sub> which softens at 350°C and flows above 500°C. Furthermore, if polymers contain oxygen atoms, boric acid promotes dehydration and the generation of a carbonized coating. As a consequence, polymer is kept away from oxygen and heat and thus, evolution of flammable gases is decreased [19].

### **1.5.2 HALOGENATED FLAME RETARDANTS**

The kind of halogen is important for the action of halogenated flame retardants. Iodine and fluorine containing composites are not useful as flame retardants because they do not step in the ignition process. For instance, most of the polymers are less thermally stable than fluorine containing composites, thus, fluorine containing composites do not evolve fluorine radicals at around or below the degradation temperature of the polymers [26]. However, most commercial polymers are more thermally stable than iodine containing composites, thus, evolve halogen radicals during polymer processing. Besides, chlorine and bromine can readily be evolved and take part in the ignition process as C-Cl and C-Br bond energies are low.

OH<sup>•</sup> and H<sup>•</sup>, highly reactive free-radicals, are released during the decomposition of the polymer. Thus, in the gaseous phase, combustion is continued via progressive-chain mechanism. These additives also release halogen radicals that react with these reactive radicals to stop the chain degradation and thus, the polymer ignition. Halogen radicals are much less reactive than OH<sup>•</sup> and H<sup>•</sup> (Scheme 1.3).

**Scheme 1.3.** Flame retardant mechanism of halogenated flame retardants, X may be Br or Cl.



HX, which is the very expressive flame retardant compound, is reproduced by the reaction between X<sup>•</sup> radical and RH. Furthermore, HX has a physical action on the ignition process by forming protective gaseous coating and diluting fuel gases due to nonflammable properties. Also, HX promotes the generation of a solid protective layer by catalyzing the oxidation of the solid phase. In Figure 1.2, the most widespread halogenated flame retardants are demonstrated.

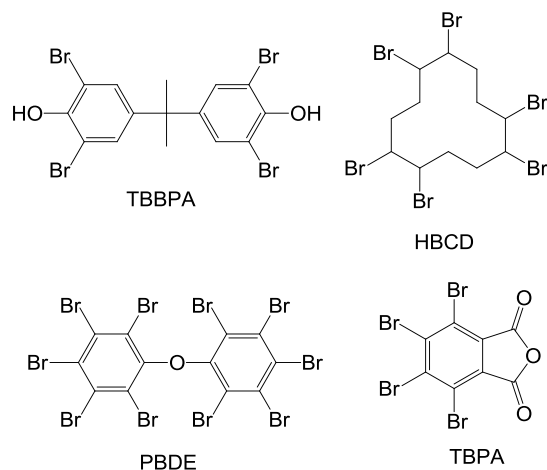


**Figure 1.2.** Chemical structures of classical halogenated flame retardants.

The most commonly preferred halogenated flame retardant is tetrabromobisphenol A (TBBPA). Particularly in epoxy resins, it is usually incorporated as a reactive flame retardant. The other most preferred halogenated flame retardant is polybromodiphenylether (PBDE). Ten bromine atoms can be added to a diphenylether [19].

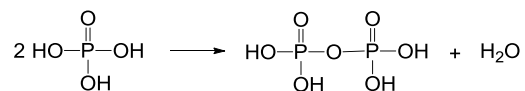
### 1.5.3 PHOSPHORATED FLAME RETARDANTS

The types of phosphorus based flame retardants are very broad, covering red phosphorus, phosphine oxides, phosphinates, phosphonates and phosphates. These phosphorated flame retardants can be added to the polymer chain during synthesis or used as additives. They are effective in the gas and/or solid phase.

The phosphorus containing additives promote the phosphoric acid formation. Pyrophosphate structures are generated by the condensation of phosphoric acid (Scheme 1.4).

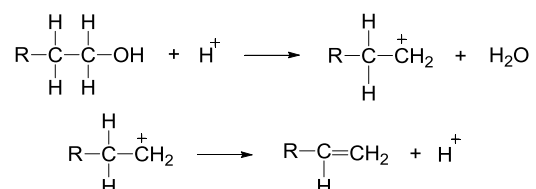


**Scheme 1.4.** Pyrophosphate structures formation from phosphoric acid condensation.



The gas phase is diluted by the released water. In addition, dehydration reaction of the –OH end groups is catalyzed by phosphoric acid and pyro-phosphoric acid and this reaction promotes the production of carbocations and unsaturated structures (Scheme 1.5). At elevated temperatures, this situation results in production of carbonized or crosslinked compounds.

**Scheme 1.5.** Generation of unsaturated structures after dehydration of terminal alcohols.



At elevated temperatures, ortho- and pyro-phosphoric acids are converted to meta-phosphoric acid,  $\text{PO}_3\text{H}$ , and their related polymers,  $(\text{PO}_3\text{H})_n$ . The carbon and the phosphate anion lead to the generation of char. The polymer is insulated and guarded by char from the flame. Furthermore, it restricts oxygen diffusion, which decreases combustion, and restricts the volatilization of products thus, hinders the generation of new free-radicals.

As in the case of halogenated additives, also phosphorus containing additives may generate active radicals, like  $\text{HPO}\cdot$ ,  $\text{PO}_2\cdot$  and  $\text{PO}\cdot$ . These less reactive radicals react with highly reactive  $\text{OH}\cdot$  and  $\text{H}\cdot$  radicals. Volatile phosphorus containing flame retardants are the most efficient ignition inhibitors because phosphorus radicals are ten times more powerful than chlorine and five times more powerful than bromine radicals [27].

Phosphorated additives are remarkably more efficient in polymers containing nitrogen and/or oxygen. If the polymer does not have a suitable reactive group in the polymer chain, it cannot participate to charring. In this situation, besides the phosphorated flame retardant, a charring additive, like pentaerythritol, has to be added [28].

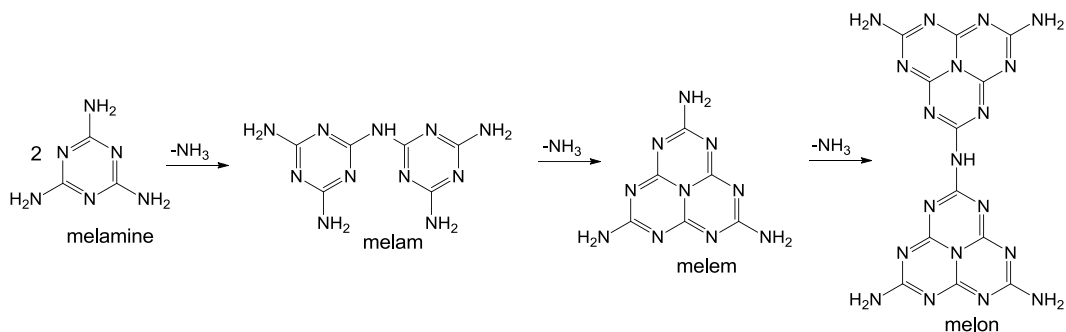
#### **1.5.3.1 METAL PHOSPHINATE SALTS**

Phosphorated additives can react in the condensed phase and the vapor phase. In the condensed phase starts the generation of char and in the vapor phase, phosphorus inhibits the flame by releasing active radicals [29, 30]. The activity of phosphorus depends on various factors: chemical structure and oxidation state of the flame retardants, presence or absence of heteroatoms in the polymer matrix and presence or absence of other additives such as metal salts, borates and melamine [30-33].

#### **1.5.4 NITROGEN BASED FLAME RETARDANTS**

Melamine is a crystalline compound containing 67 wt% nitrogen atoms and has a melting point at 345°C [26]. Melamine sublimates at around 350°C. With sublimation, the temperature is reduced by absorbing energy from the surroundings. Melamine decomposes by elimination of ammonia at high temperatures. This promotes the production of thermally stable condensates, such as melam, melem and melon and dilutes oxygen and flammable gases (Scheme 1.6) [34].

**Scheme 1.6.** Thermal degradation of melamine.



Melamine volatilization and decomposition occur at similar rates. However, if melamine evaporation is hindered, for instance, by the generation of an insulating barrier, production of melam, melem and melon becomes marked. The production of these compounds creates protective coating in the condensed phase and causes an endothermic process. Moreover, with strong acids melamine may generate thermally stable salts such as melamine pyrophosphate, melamine phosphate, and melamine cyanurate. Melamine salts have different flame retardancy behavior. Melamine salts decompose when heated. Then re-generated melamine evaporates and meets more cascade condensation [34]. Therefore, the condensed phase action of salts is much greater.

### 1.5.5 SILICON BASED FLAME RETARDANTS

Flammability can be improved with the contribution of a low amount of silicon-containing products, such as silicates, silsesquioxanes, organosilanes, silicas and silicones. They can be incorporated into the polymer chain during synthesis or as additives after synthesis.

### **1.5.5.1 SILICONES**

Silicones have perfect high heat resistance, thermal stability and restricted evolution of poisonous gas during thermal degradation. They can be incorporated into the polymer chain during synthesis or mixed directly with the polymer matrix.

### **1.5.5.2 SILICA**

Gilman et al. searched the flame retardancy of polypropylene in the presence of various silica gel structures [35]. They investigated the effect of silica gels with various surface silanol concentration, particle size and pore volume. The drastic impact of silica gel pore volume on the HRR of polypropylene including 10% wt. silica was detected by cone calorimeter tests. Heat release rate decreased drastically with the addition of high pore volume silica. Flammability properties were not affected by the particle size, but they were significantly affected by the surface silanol concentration. The flammability was decreased at higher silica gel pore volume because larger pores supplied to locate polypropylene and by increasing molten viscosity.

### **1.5.6 NANOMETRIC PARTICLES**

Nanometric particles when spreaded in polymer matrix, increase fire resistance, and improve thermal and mechanical properties. The low loading of nanoparticle to polymers improves their flame retardancy. The flame retardancy performance of nanoparticles strongly relies on the chemical structure of the nanoparticle.

There are three types of nanoparticles. First type involves the layered compounds, defined by 1 nanometric dimension (usually smaller than 100 nm) and called as 2D nanoparticles such as nanoclays, montmorillonite (MMT). Second type consists of fibrous compounds defined by elongated compounds with 2 nanometric dimensions and called as 1D nanoparticles like carbon nanotubes and sepiolite. Third type involves particulate compounds defined by 3 nanometric dimensions

and called as 0D nanoparticles such as spherical silica nanoparticles and polyhedral oligosilsesquioxane (POSS) [19].

### 1.5.6.1 NANOCCLAYS

By modifying of nanoclays with organic cations such as alkyl imidazol(idin)ium cations, alkyl ammonium or alkyl phosphonium, the clay layers distribution among the matrix of polymer becomes easier. As a conclusion organomodified nanoclays are obtained. Some common examples of modified nanoclays are, dimethyl, benzyl, hydrogenated tallow, quaternary ammonium modified montmorillonite, MMT10A, dimethyl, dehydrogenated tallow, 2-ethylhexyl quaternary ammonium modified montmorillonite, MMT25A, and methyl, tallow, bis-2-hydroxyethyl, quaternary ammonium modified montmorillonite, MMT30B. In Figure 1.3, the structures of the modifiers are demonstrated.

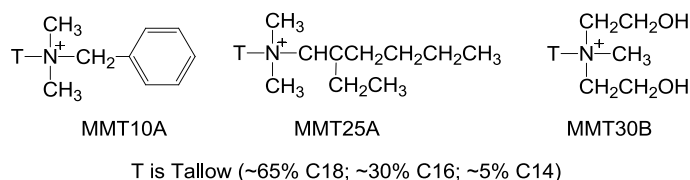


**Figure 1.3** Structure of organomodified MMT10A, MMT25A and MMT30B

During combustion, in the matrix of polymer an insulating barrier is obtained by the addition of a comparatively small amount of organomodified nanoclay [36, 37]. By heating, the replacement of the clay nanolayers to the surface becomes easier with the reduction in the viscosity of nanocomposite. Furthermore, the organomodifier decomposed by heat transfer creates extremely protonic sites on the surface. This layer catalyzes the char production [38, 39]. Thus, a protective

barrier is formed by gathering of the clay on the surface. This barrier restricts heat transfer, O<sub>2</sub> diffusion into the polymer and evaporation of flammable fragments. In addition, production of gas bubbles, which is started by the degradation of both the polymer chain and the quaternary ammonium organomodifiers, increases the nanoclay migration.

### **1.5.6.2 CARBON NANOTUBES**

Carbon nanotubes show extraordinary properties that can be utilized in different areas such as macroscopic material composites and nanodevices. Because of their high aspect ratio, carbon nanotubes generate a network with even little loading. They promote important increase of various features such as mechanical [40], rheological [41-43] and flame retardant [44-46] features.

Low loading rate (<3 wt%) of carbon nanotubes is sufficient to increase the flame retardancy of many polymers such as copolymer of ethylene vinyl acetate, EVA [40], polystyrene, PS [43], poly(methyl methacrylate), PMMA [44], polyamide-6, PA6 [45], low density polyethylene, LDPE [46] and polypropylene, PP [47].

Halloysite nanotubes (HNT) are inexpensive, environmentally safe and naturally occurring nanotubes. On the other hand, due to their toxicity for human health and environment, there are concerns about the usage of carbon nanotubes. Halloysite nanotubes are useful in various areas such as, personal care products, drug delivery vehicles, electronic components, and additives in polymers and plastic. Recently, nanocomposites incorporated with HNT are investigated. It shows significantly enhanced properties, for instance, greater thermal stability, flame retardancy and mechanical strength and so on [48].

## **1.6 POLYAMIDE 6**

In the areas of construction and engineering, polyamides are an important class of polymers, due to their high fatigue resistance and melting point, and excellent

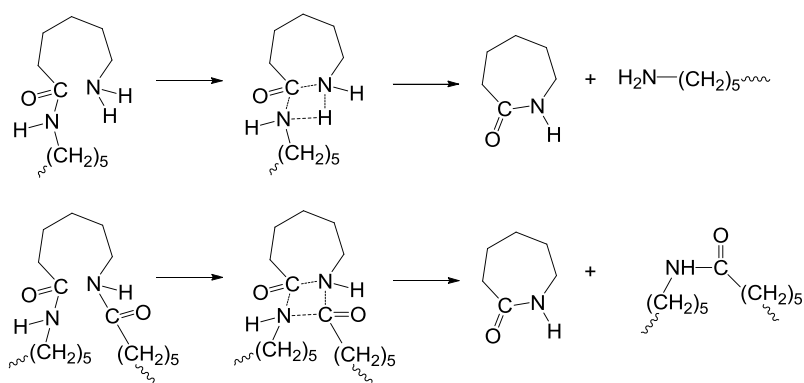
tensile properties, chemical and abrasion resistance, [49, 50]. In addition, it has many advantages such as high resistances to attrition, organic solvents and oil and good mechanical properties. Polyamide 6 (PA6) is an important class of polyamides. Because it has high heat distortion temperature, PA6 may be used in high temperature conditions. All these properties make PA6 attracted for several applications.

On the other hand, discoloration and reduction in its mechanical properties are detected when polyamide 6 is subjected to heat for an extended time. Furthermore, PA6 has low limiting oxygen index (LOI), thus, it ignites readily. Even though polyamides have self-extinguishing properties because of their wide dripping and shrinkage, most polyamides are classified as V2 by the Underwriters Laboratory UL-94 test. Thus, in order to increase its usage, thermal decomposition behaviors of PA6 have been investigated widely [51-56].

#### **1.6.1. THERMAL DEGRADATION OF POLYAMIDE 6**

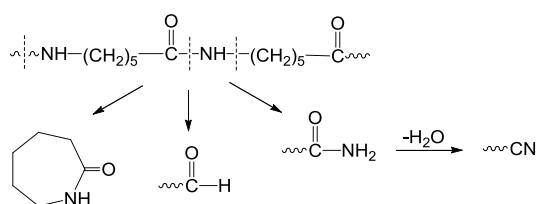
Polyamides decompose in a very complex way and can produce many different products. The principal degradation product of PA6 is the cyclic monomer (Scheme 1.7), caprolactam. Production of oligomeric fragments with vinyl chain ends and nitrile and also generation of HCN, H<sub>2</sub>O, CO, NH<sub>3</sub> and CO<sub>2</sub> have been noted [52, 54, 56].

**Scheme 1.7.** Generation of caprolactam.



Dussel et al. [57] performed the pyrolysis of PA6 in the temperature range of 530 - 800°C. They found amines, amides and nitriles as thermal decomposition products and suggested homolytic scission of C-N bonds (Scheme 1.8).

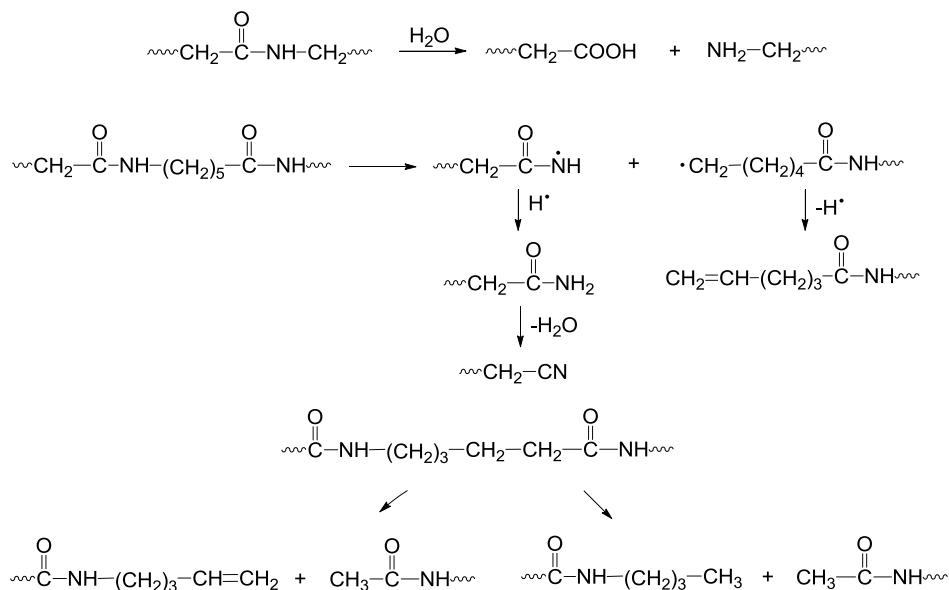
**Scheme 1.8.** Generation of caprolactam, aldehyde, amide and cyanide end groups.



Hornsby et al. [58] proposed that in the presence of water, peptide bond hydrolysis is predominant. However, at high temperatures, scission of N-alkylamide bonds or CH<sub>2</sub>-CH<sub>2</sub> linkages which are in a β-position relative to the carbonyl group is also probable (Scheme 1.9).



**Scheme 1.9.** Possible thermal degradation reactions of PA6.



### 1.6.2 FLAME RETARDANCY OF POLYAMIDE 6

As mentioned before, PA6 is flammable because of low LOI. Various studies were performed to improve its flammability [59-63]. Song et al. [59] studied the organoclay added polyamide 6 nanocomposites in which flame retardants were magnesium hydroxide and red phosphorus. PA6 flammability and mechanical properties were searched in the presence of organoclay. Better mechanical and flame retarded properties were demonstrated by addition of nanocomposites compared to the flame retarded PA6 and interactions between organoclay, magnesium hydroxide and red phosphorus were detected.

Wilkie et al. [60] determined decline in the peak heat release rate, PHRR, in polyamide 6/clay nanocomposites. The primary decomposition of PA6 is mainly intramolecular aminolysis reaction by generating  $\beta$ -caprolactam. By the higher addition of clay, the relative yield of  $\beta$ -caprolactam among all degradation products was decreased and the viscosity of condensates was enhanced. Therefore,

it was found that in the presence of clay inter-chain reactions were increased with the degrading polymer chains were trapped in the clay during thermal degradation.

Braun and coworkers [61] studied the fire retardancy mechanism of melamine polyphosphate (MPP) and aluminium phosphinate (AlPi) in glass fiber reinforced polyamide 6,6 by analyzing the thermal degradation behavior and flammability. AlPi vaporizes and reacts efficiently as a flame stopper. Moreover, MPP dilutes fuel in the gaseous phase and shows an expressive protective coating in the solid phase. By using AlPi and MPP together lead to charring. It was concluded that zinc borate (ZnB) presence increased the improvement in the solid phase more by the generation of boron aluminium phosphates.

Recently, Isitman et al. [62] investigated organoclay effect on glass fiber reinforced/flame retarded polyamide 6. In glass fiber reinforced PA6, melamine, zinc borate and phosphorus based flame retardants were used at various levels. TGA, LOI, UL94 and cone calorimetry were used to determine the thermal stability and combustion behaviors. Reduction in the PHRR, improvement in LOI and retarding in ignition were observed for the nanocomposites containing flame retardant and nanoclays. In addition, the generation of a glassy boron/aluminium phosphate layer was observed at the nanoscale.

Lately, Isbasar et al. [63] investigated the thermal decomposition of PA6 involving melamine and a boron and silicon involving oligomer (BSi), borophosphate ( $BPO_4$ ) or zinc borate (ZnB) by DP-MS. Boron compounds increased the interactions among melamine and PA6 and affected their degradation products remarkably. It was observed that ZnB produced a glassy surface limiting the liberation of the degradation products of melamine. Moreover, a reduction in the decomposition fragments of melamine was observed in the presence of BSi.

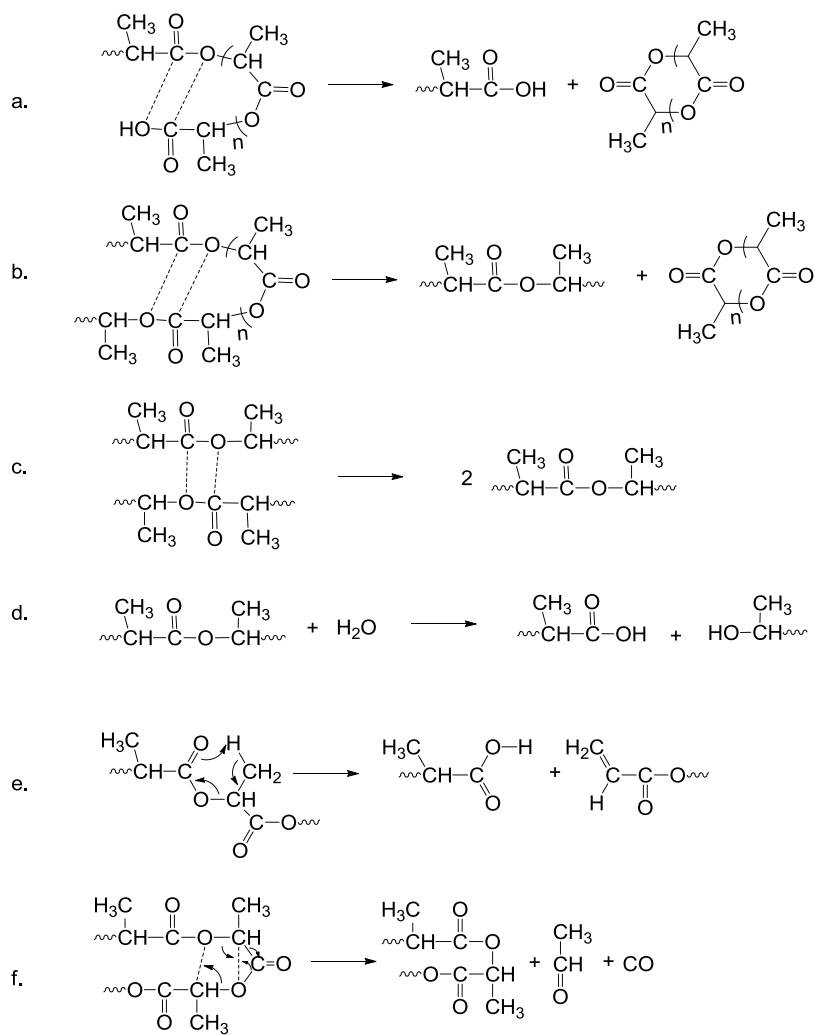
## **1.7 POLYLACTIDE**

Poly lactide or poly(lactic acid) (PLA), is important in the modern industrial field. Poly(lactic acid) has various advantages such as biodegradability, good thermal and mechanical properties, gas permeability, reproducibility from renewable resources. Furthermore, it has very low toxicity to the human body and the environment. Thus, it has been investigated in terms of scientific interest and was used in a wide range of areas such as tissue engineering, drug delivery, textiles and packaging [64]. PLA composite materials were used in household products such as casing for personal computers and mobile phones and used as a bio-based thermoplastic resin in composites, automobile parts and electronics.

### **1.7.1 THERMAL DEGRADATION OF POLYLACTIDE**

By heating of PLA over 250°C, volatile components, such as lactide, methylketene, acetaldehyde, CO, CO<sub>2</sub> and cyclic oligomers are generated [65]. Possible non-radical thermal degradation reactions of PLA are demonstrated in Scheme 1.10 [65]. Intramolecular trans-esterification reactions generate the lactide and cyclic oligomers. The intermolecular trans-esterification, hydrolytic degradation and cis-elimination reactions reduce the molecular weight. The production of double bonds at the chain terminals is obtained by the cis-elimination reaction. In addition, non-radical, backbiting ester interchange mechanism can generate lactide, oligomers, or CO and acetaldehyde.

**Scheme 1.10.** Possible thermal degradation reactions of PLA.



### 1.7.2 FLAME RETARDANCY OF POLYLACTIDE

Unfortunately, PLA has some disadvantages among with its advantages. For instance, it has poor heat stability, low moisture stability, low heat deflection temperature (HDT) and high flammability. Thus, for extended applications of PLA in electrical industry flame retardancy is crucial.

Thermal characteristics of polylactide/clay nanocomposites were investigated by Pluta et al. [66] in inert and oxidative conditions. In helium atmosphere, decomposition temperature of nanocomposites was enhanced almost 10°C, on the other hand in air, degradation temperature was increased by 25°C. However, the microcomposites showed almost the same thermal resistance in each case. Thus, the development in thermal stability of nanocomposites was referred to the distinction in the morphologic properties of both compounds.

Thermogravimetry analysis was applied on the poly(l-lactide)/organoclay by Paul et al. [67]. In the presence of about 3 wt% nanoclay, TG analysis indicated an increase in the thermal stability of the polymer nanocomposite. This effect was depended on the type and property of the filler, such as functionality and chemistry of the ammonium cation and alkyl chain size. It was found that nanocomposite including Na<sup>+</sup>-MMT had higher thermal stability and degradation temperature was increased by about 40°C.

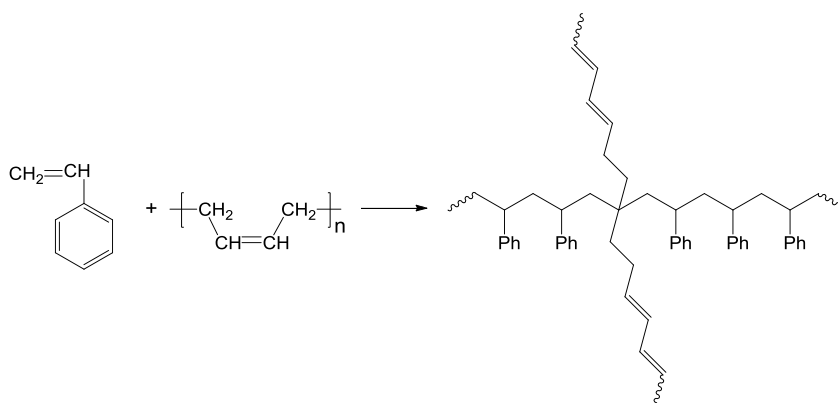
Recently, Isitman et al. [68] studied the effects of nanoparticle geometry on flammability of PLA composites including AlPi using three types of nanofillers, namely plate-like montmorillonite, rod-like halloysite and spherical nanosilica. Flame retardancy was found to enhance in the order of halloysite, nanosilica and montmorillonite indicating that the surface area is important in flame retardancy. In the presence of montmorillonite a thicker montmorillonite/aluminium phosphate char was generated by preventing the formation of intumescent char due to wide surface area of montmorillonite enables fast transferring and collection of montmorillonites on subjected polymer surface.

## 1.8 POLYSTYRENE

Polystyrene (PS) is a large-volume, clear, hard and brittle commodity polymer. It can be foamed or rigid. It has a broad range of uses, in packaging, CD and DVD cases and containers [69].

High-impact polystyrene (HIPS) is mainly utilized for building materials, electronic instruments and electrical appliances. It contains polystyrene and polybutadiene phase. The preparation of HIPS is given in Scheme 1.11. Although HIPS has high impact resistance, it is very flammable.

**Scheme 1.11.** Synthesis of high-impact polystyrene.

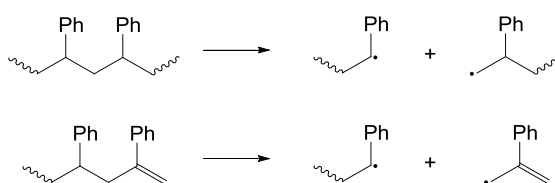


### 1.8.1 THERMAL DEGRADATION OF POLYSTYRENE

The thermal decomposition of PS with different tacticities (aPS, sPS and iPS) and modified PS have been studied in detail in the literature and random chain scission is accepted as the primary mechanism [70-75]. This includes initiation, propagation and termination reactions.

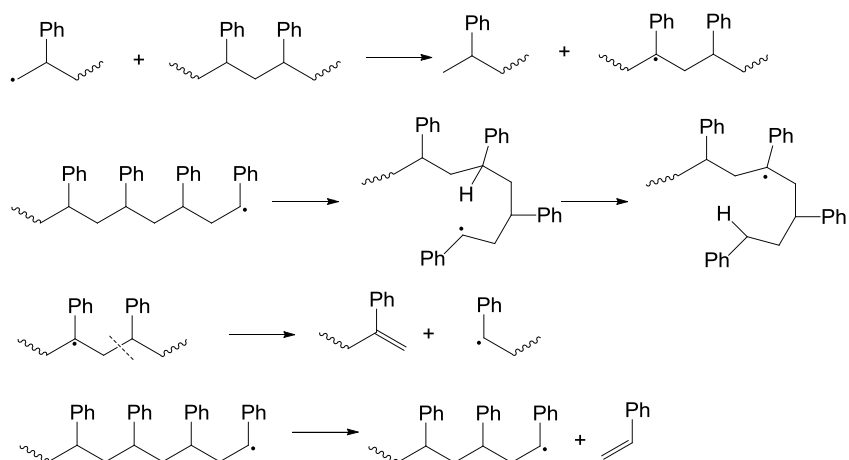
Initiation reactions involve cleavage of a C-C bond of the polymer chain to generate radicals. There are two types of initiation reactions (Scheme 1.12). The first one is random chain scission, in which a primary radical and a secondary benzyl radical are formed. Secondary benzyl radical has a strong resonance. The second one is chain-end scission. In which a secondary benzyl radical and a resonance stabilized allyl benzene radical is formed.

**Scheme 1.12.** Initiation reactions of PS.



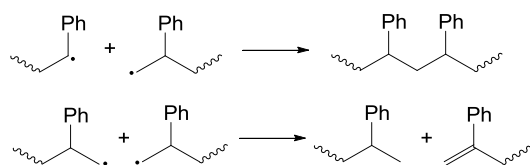
In the propagation step a series of H-abstraction and  $\beta$ -decomposition reactions are observed (Scheme 1.13). H-abstraction reactions divided into two. The first one is the intermolecular abstractions, in which the radicals abstract the hydrogen from a different molecule. The intermolecular abstraction on the tertiary carbon atoms with the formation of tertiary radical is more probable because of the formation of higher stability resonance stabilized benzyl radical. The second one is the intramolecular H-abstractions or back biting reactions, in which, five-, six- or seven-membered ring intermediates can be formed by the radicals of secondary benzyl radical and primary radical. In addition, the tertiary benzyl radical can form a secondary benzyl radical and an unsaturated end by the break of the C-C bond in  $\beta$  position. The last one is  $\beta$ -decomposition reactions, in which a monomer and another secondary benzyl radical are generated.

**Scheme 1.13.** Propagation reactions of PS.



There are two types of second-order termination reactions (Scheme 1.14). The first one is recombination reactions. The second one is disproportionation reactions of radicals as shown in Scheme 1.14 [76].

**Scheme 1.14.** Termination reactions of PS.



## 1.8.2 FLAME RETARDANCY OF POLYSTYRENE

Like other organic compounds, polystyrene is also flammable. As a consequence, modification of PS by addition of flame retardants is crucial. Many researches on



flame retardancy of PS were appeared in the literature. Luijk and co-workers examined the thermal degradation and the thermal stability of HIPS– antimony oxide –decabromodiphenylether composite with thermogravimetry (TG), pyrolysis-mass spectrometry (Py-MS) and pyrolysis-gas chromatography-mass spectrometry (Py-GC-MS). They determined generation of antimonybromides, antimonyoxybromides and brominated higher styrene oligomers [77].

Jakab et al. [78] analyzed the thermal degradation of HIPS containing decabromodibenzyl (Br10-DB), decabromodiphenyl ether (Br10-DPE) and antimony trioxide ( $\text{Sb}_2\text{O}_3$ ) by pyrolysis-mass spectrometry (Py-MS), pyrolysis-gas chromatography/mass spectrometry (Py-GC/MS) and thermogravimetry/mass spectrometry (TG/MS) techniques. They found that  $\text{Sb}_2\text{O}_3$  reduced the thermal stability of the flame retardants and polystyrene. The brominated additives were decomposed by various pathways. Bromotoluene formation was the significant reaction of Br10-DB flame retardants. On the other hand, in the Br10-DPE decomposition, brominated dibenzofurans (DBF) was generated by intermolecular ring closure.

Wilkie et al. [79] determined that by the addition of clay to polystyrene, inter-chain reactions became significant and by increasing clay ingredients not only the extent of inter-chain reactions but also those of radical recombination reactions, hydrogen abstraction reactions, and formations of head-to-head compounds and conjugated double bonds were increased.

Grause et al. analyzed the thermal degradation of brominated flame retarded HIPS in the presence of antimony trioxide ( $\text{Sb}_2\text{O}_3$ ) by TGA. They found that these additives reduced the activation energy [80].

Recently, Isitman et al. [81] studied the effect of micro- and nanocomposite formation of nanoclays and aluminium hydroxide on the flammability of HIPS, in terms of cone calorimetric fire properties, LOI and horizontal burning rates. Higher LOI and mechanical properties, lower burning rates and mass loss rates,

char enhancement and reductions in PHRR were obtained for nanocomposites relative to microcomposites. Again, Isitman et al. [82] investigated the fire behaviors of polystyrene-brominated-epoxy-blend-based nanocomposites. They found a noticeable decrease in PHRR and enhancement in LOI of organoclay nanocomposites. And also, the overall effectiveness of the fire-retardant was increased with the combination of the vapor-phase (by radical scavenger), and the solid-phase (by char formation) activities.

## 1.9 AIM OF WORK

The aim of this study is to investigate the effects of various nanoparticles on thermal degradation characteristics of polyamide 6, (PA6), polylactide, (PLA), polystyrene, (PS) and high impact polystyrene, (HIPS) composites involving flame retardants. PA6 and PLA composites analyzed involved aluminium diethylphosphinate, (AlPi), a common phosphorous containing flame retardant for esters. The nanofiller used in PA6 composites was either halloysite nanotube, (HNT) or organically modified montmorillonite, MMT25A (dimethyl, dehydrogenated tallow, 2-ethylhexyl quaternary ammonium modified montmorillonite), or MMT30B (methyl, tallow, bis-2-hydroxyethyl, quaternary ammonium modified montmorillonite). In case of PLA, HNT or MMT30B or silicon dioxide, (SiO<sub>2</sub>) was used as the nanofiller.

Both of the HIPS and PS composites contained organically modified montmorillonite, MMT10A (dimethyl, benzyl, hydrogenated tallow, quaternary ammonium modified montmorillonite) as the nanofiller. However, aluminium hydroxide, (Al(OH)<sub>3</sub>), was used as the flame retardant for HIPS whereas, tribromophenol end-capped brominated epoxy, (BE), and antimony trioxide, (Sb<sub>2</sub>O<sub>3</sub>) were used as the flame retardants in PS composites.

For analyzing the effects of nanoparticles on thermal characteristics of the polymers, DP-MS analyses of each component of the composite and various combinations of the components were performed systematically. MS/MS/MS

analyses were also applied to elucidate the structures of the thermal degradation products. The collision induced dissociation experiments were acquired at different energies to provide fragmentation pathways to generate informative, structurally significant daughter ions.



## CHAPTER 2

### EXPERIMENTAL

#### 2.1 MATERIALS

Materials analyzed in this study, polyamide 6, (PA6), polylactide, (PLA), polystyrene, (PS) and high impact polystyrene, (HIPS) composites involving nanoclay, have been prepared by Dr. Nihat Ali Isitman during his Ph.D. studies in the Department of Metallurgical and Materials Engineering at METU [68, 81, 82]. The compositions of the composites analyzed are given in Table 2.1 to Table 2.4 PA6 was obtained from DSM Akulon. Polylactide, ( $M_w \sim 190,000 \text{ g}\cdot\text{mol}^{-1}$ ) was supplied from Cargill Dow and PS ( $M_w \sim 192,000 \text{ g}\cdot\text{mol}^{-1}$ ) was provided by Aldrich (St. Louis, MO, USA). High-impact polystyrene (HIPS) was an extrusion grade high-impact resin (Dow Styron A-Tech 1175).

The phosphinate salt (aluminium diethylphosphinate, AlPi, Exolit OP 1240) was marketed by Clariant (Germany). Montmorillonite nanoclays (MMT10A, MMT25A and MMT30B) were obtained from Southern Clay Products, Gonzales, TX, USA. Nanosilica was a dimethyldichlorosilane treated fumed silica (Aerosil R 974) provided by Evonik Degussa (Germany). Halloysite, a clay mineral predominantly in the form of nanotubes, was supplied from Aldrich. The brominated flame retardant was a tribromophenol end-capped (BE) oligomer (molecular weight  $15,000 \text{ g}\cdot\text{mol}^{-1}$ ,  $\sim 53\text{wt}\%$  Br) purchased from ICL Industrial Products (Beersheba, Israel). Antimony trioxide,  $\text{Sb}_2\text{O}_3$  (99.9%) was an industrial-grade product provided by a Chinese source. Aluminium hydroxide (ATH) was provided from Nabaltec Apyral-16. The preparations of each composite were explained in detail in the previous literature [68, 81, 82].

**Table 2.1** PA6 based samples.

weight percent	PA6	ALPI	HNT	MMT25A	MMT30B
PA6-ALPI	80	20			
PA6-ALPI-HNT	80	17	3		
PA6-ALPI-MMT25A	80	17		3	
PA6-ALPI-MMT30B	80	17			3
PA6-HNT	97		3		
PA6-MMT25A	97			3	
PA6-MMT30B	97				3

**Table 2.2** PLA based samples.

weight percent	PLA	ALPI	HNT	MMT30B	SiO <sub>2</sub>
PLA-ALPI	80	20			
PLA-ALPI-HNT	80	17	3		
PLA-ALPI-MMT30B	80	17		3	
PLA-ALPI-SiO <sub>2</sub>	80	17			3

**Table 2.3** HIPS based samples.

weight percent	HIPS	ATH	MMT10A
HIPS-MMT10A	97		3
HIPS-ATH	75	25	
HIPS-MMT10A-ATH	72	25	3

**Table 2.4** PS based samples.

weight percent	PS	BE	MMT10A	Sb <sub>2</sub> O <sub>3</sub>
PS-MMT10A	95		5	
PS-BE	80	20		
PS-BE-MMT10A	75	20	5	
PS-BE- Sb <sub>2</sub> O <sub>3</sub>	77	20		3
PS-BE- Sb <sub>2</sub> O <sub>3</sub> -MMT10A	72	20	5	3

## 2.2 DIRECT PYROLYSIS MASS SPECTROMETRY

Direct pyrolysis mass spectrometry analyses of PA6, PS and HIPS composites were done by Waters Micromass Quattro Micro GC Mass Spectrometer coupled to a direct insertion probe. It has a mass range of 10-1500 Da. The temperature was increased to 50 °C at a rate of 5 °C·min<sup>-1</sup>, then was increased to 650 °C at a rate of 10 °C·min<sup>-1</sup> and held at 650 °C for 5 additional minutes during pyrolysis. The time of pyrolysis is about 70 minutes. About 0.010 mg samples were pyrolyzed in quartz sample vials. 70 eV EI mass spectra at a mass scan rate of 1 scan·s<sup>-1</sup> was simultaneously recorded during pyrolysis.

The direct insertion probe pyrolysis mass spectrometry (DIP-MS) system used for the thermal analyses of PLA composites consists of a 5973 HP quadrupole mass spectrometer coupled to a JHP SIS direct insertion probe pyrolysis system (T<sub>max</sub>=445°C). It has a mass range of 10-700 Da. About 0.010 mg samples were pyrolyzed in flared glass sample vials. The temperature was risen at a rate of 10 °C·min<sup>-1</sup>. 70 eV EI mass spectra at a mass scan rate of 2 scan·s<sup>-1</sup> was recorded during pyrolysis.

The pyrolysis mass spectrometry analyses were repeated several times to ensure reproducibility. Every time almost exactly the identical trends were obtained.

Collision induced dissociation experiments were done by Waters Micromass Quattro Micro GC triple quadrupole Mass Spectrometer coupled to a direct insertion probe, using argon as the collision gas (P=0.5 bar) and 65, 40, 30 and 20 eV EI ionization. The daughter spectra of the precursor ions were recorded while pyrolyzing (0.010 mg) samples in quartz sample vials at the temperatures at which the yield of the selected precursor ion was maximized. Relationships between the various ions were established by product-ion spectra on fragment ions formed in-source and by precursor-ion spectra.

## 2.3 DATA ANALYSIS

Direct pyrolysis mass spectrometry (DP-MS) technique has many advances, amongst the different techniques applied to search pyrolysis fragments. In DP-MS technique, the high vacuum system immediately removes the decomposition products from the heating zone, thus, condensation and secondary reactions are almost totally hindered and unstable thermal decomposition fragments can be also identified. As a result, more precise degradation mechanism can be obtained by the application of this technique. Scanning total ion current (TIC) as a function of temperature enables the identification of components as a function of volatilities and thermal stability. However, during the DP-MS analysis, thermal decomposition fragments further decompose during ionization. Therefore, the pyrolysis mass spectra of polymers are generally very complicated. Moreover, all the products with the same mass to charge ratio have additions to the intensity of the same peak in the mass spectrum. Thus, in DP-MS analysis, the changes in the peak intensities as a function of temperature, single ion pyrograms, have great importance [83, 84].

The pyrolysis mass spectra of polymers and composites involving more than one component are even more complex. Thus, systematic analyses have to be performed. For this purpose, DP-MS analyses of each component of the composites and various mixtures of the components have to be performed separately.



## CHAPTER 3

### RESULTS AND DISCUSSION

In this work, the effects of various nanoclays which were MMT10A, MMT25A, MMT30B, halloysite and nanosilica on thermal degradation characteristics of polyamide 6, polylactide and polystyrene involving phosphorous containing flame retardant aluminium diethylphosphinate, (AlPi), halogen containing flame retardant tribromophenol end-capped oligomer, (BE) or metal containing flame retardant aluminium hydroxide, (Al(OH)<sub>3</sub>), or antimony oxide, (Sb<sub>2</sub>O<sub>3</sub>) were studied systematically by direct pyrolysis mass spectrometry (DP-MS) technique. In order to determine the influences of these additives on thermal degradation of the polymers, pyrolysis mass spectrometry analyses of each component and different combinations of the components were performed.

#### 3.1 THERMAL DEGRADATION OF FLAME RETARDANT ADDITIVES

##### 3.1.1 Organically Modified Montmorillonite

###### 3.1.1.1 MMT10A

The variation of total ion yield as a function of temperature (TIC) curve recorded during the pyrolysis of dimethyl, benzyl, hydrogenated tallow, quaternary ammonium modified montmorillonite (MMT10A) is given in Figure 3.1. Three overlapping broad peaks are present in the TIC curve with maxima at around 232, 299 and 384°C (Figure 3.1). However, all the mass spectra recorded at the peak maxima are almost identical, showing intense peaks at  $m/z = 58, 91, 134$  Da due to  $\text{CH}_2\text{N}(\text{CH}_3)_2$ ,  $\text{CH}_2\text{C}_6\text{H}_5$  and  $\text{CH}_2\text{N}(\text{CH}_3)\text{CH}_2\text{C}_6\text{H}_5$ , respectively.

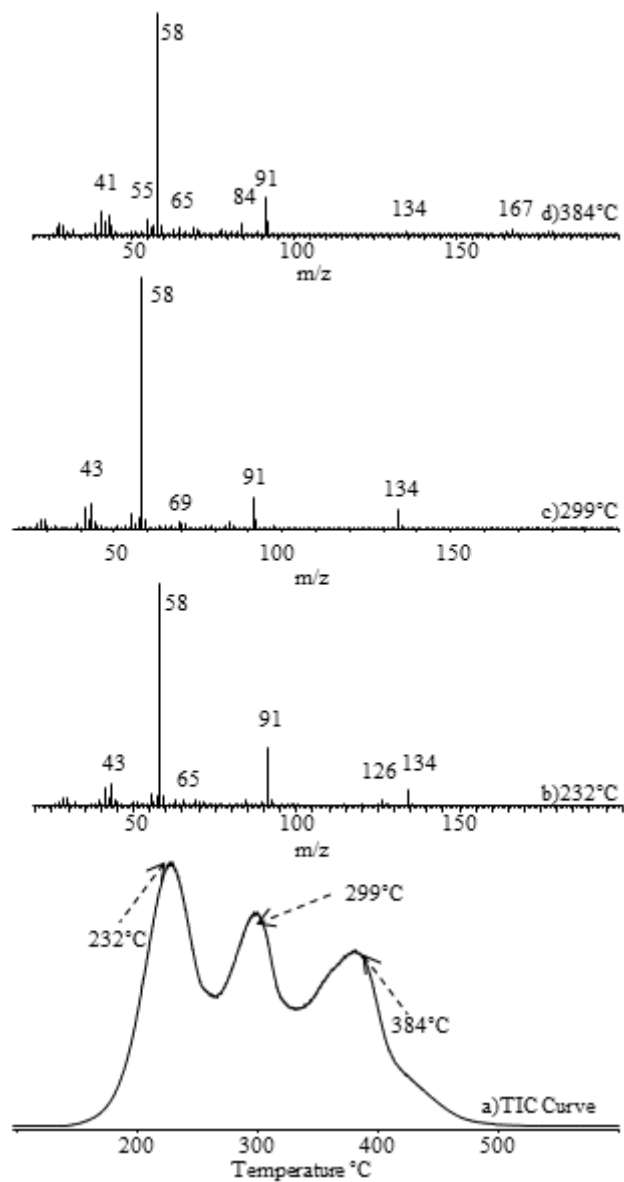


**Figure 3.1.** a) The total ion current curve and mass spectra at b) 232 c) 299 d) and 384°C recorded during the pyrolysis of MMT10A.

In Table 3.1, the relative intensities of intense and/or characteristic peaks recorded in the spectrum and the assignments made are summarized.

**Table 3.1.** The relative intensities, RI, of some selected intense and/or characteristic peaks recorded in pyrolysis spectrum of MMT10A at 232, 299 and 384°C and the assignments made.

m/z	RI			Assignment
	232°C	299°C	384°C	
43	86	96	93	CH <sub>2</sub> NCH <sub>3</sub> , C <sub>3</sub> H <sub>7</sub>
58	1000	1000	1000	CH <sub>2</sub> N(CH <sub>3</sub> ) <sub>2</sub> , C <sub>4</sub> H <sub>11</sub>
59	38	24	40	CH <sub>2</sub> NH(CH <sub>3</sub> ) <sub>2</sub>
65	29	13	33	C <sub>5</sub> H <sub>5</sub>
78			21	C <sub>6</sub> H <sub>6</sub>
84	24	25	52	C <sub>6</sub> H <sub>12</sub>
89	18	4.7	14	C <sub>7</sub> H <sub>5</sub>
90	5.5	2.1	3.4	C <sub>7</sub> H <sub>6</sub>
91	260	126	178	CH <sub>2</sub> C <sub>6</sub> H <sub>5</sub>
92	21	30	62	CH <sub>3</sub> C <sub>6</sub> H <sub>5</sub>
126	26	1.2	3.0	C <sub>9</sub> H <sub>18</sub>
134	66	71		CH <sub>2</sub> N(CH <sub>3</sub> )CH <sub>2</sub> C <sub>6</sub> H <sub>5</sub>
135	8.2	9.4		N(CH <sub>3</sub> ) <sub>2</sub> CH <sub>2</sub> C <sub>6</sub> H <sub>5</sub>
167			21	NC <sub>12</sub> H <sub>9</sub> , C <sub>13</sub> H <sub>11</sub>
179			14	(CHC <sub>6</sub> H <sub>5</sub> )C(C <sub>6</sub> H <sub>5</sub> )
269			4.1	(CHC <sub>6</sub> H <sub>5</sub> ) <sub>2</sub> C(C <sub>6</sub> H <sub>5</sub> )
359			2.2	(CHC <sub>6</sub> H <sub>5</sub> ) <sub>3</sub> C(C <sub>6</sub> H <sub>5</sub> )
449			0.8	(CHC <sub>6</sub> H <sub>5</sub> ) <sub>4</sub> C(C <sub>6</sub> H <sub>5</sub> )

Single ion pyrograms of some characteristic products are shown in Figure 3.2, involved significant differences. (CH<sub>3</sub>)<sub>2</sub>NCH<sub>2</sub>C<sub>6</sub>H<sub>5</sub> (135 Da) yielded a single ion pyrogram with two maxima at around 249 and 297°C. At low temperature it decomposed to low mass fragments such as CH<sub>3</sub>NCH<sub>2</sub> (43 Da) and C<sub>7</sub>H<sub>8</sub> (92 Da) by McLafferty rearrangement. In addition, peaks, due to series of products with formula (CHC<sub>6</sub>H<sub>5</sub>)<sub>x</sub>C(C<sub>6</sub>H<sub>5</sub>), generated by the polymerization of phenyl group (m/z = 179, 269, 359, 449, 539, 629, 719 and 809 Da for x = 1 to 8) were detected.

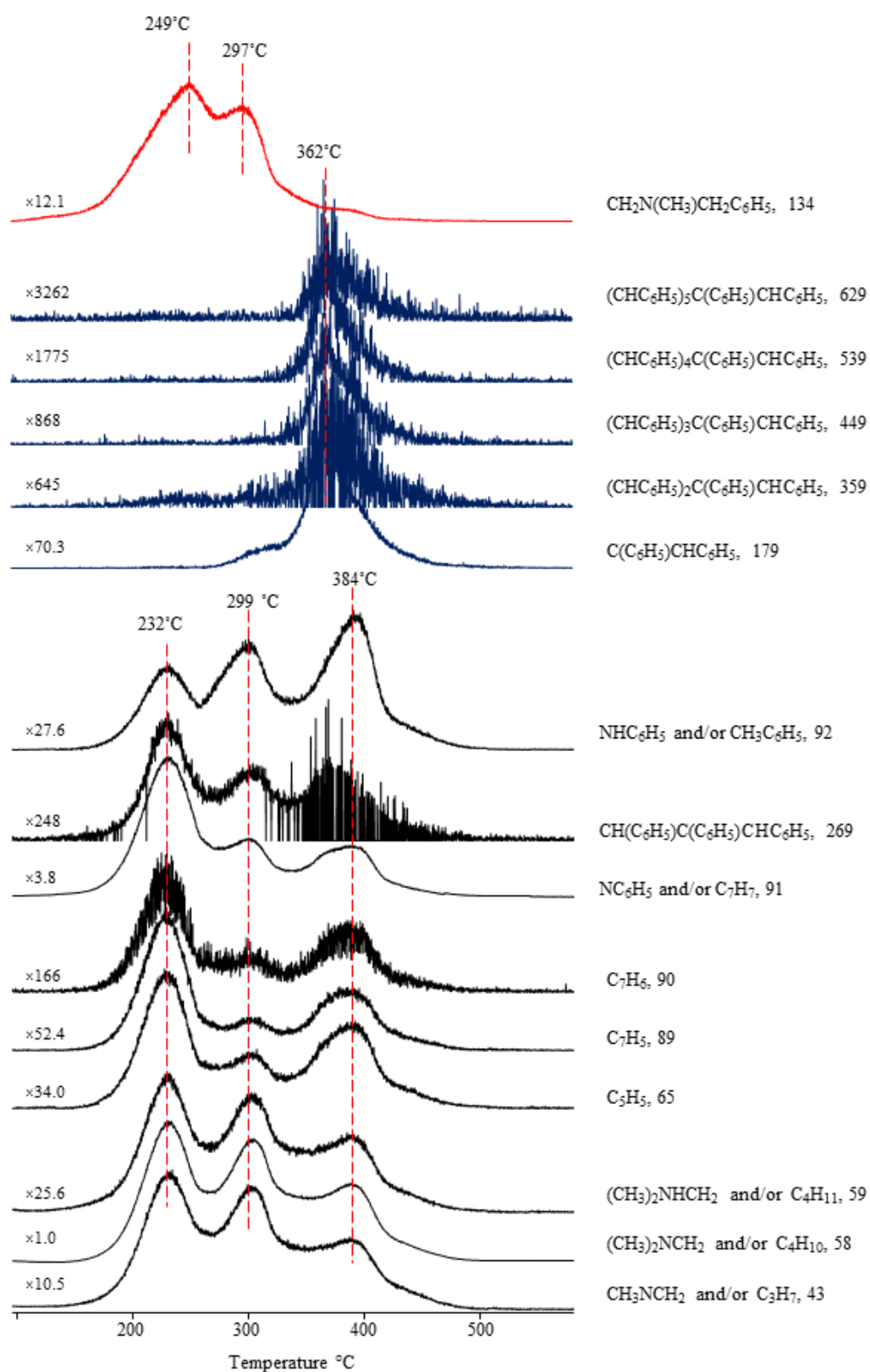


**Figure 3.2.** Single ion pyrograms of some selected fragments detected during the pyrolysis of MMT10A.

### 3.1.1.2. MMT25A

Pyrolysis of pure dimethyl, dehydrogenated tallow, 2-ethylhexyl quaternary ammonium organically modified montmorillonite (MMT25A) yielded a TIC curve involving overlapping two peaks with maxima at around 338 and 396°C (Figure 3.3). Organic part of MMT25A decomposes mainly by losing alkyl groups from hydrocarbon chain at elevated temperatures. On the other hand, amines evaporate at low temperatures. Intense peaks at  $m/z = 58, 269, 297$  Da due to  $\text{CH}_2\text{N}(\text{CH}_3)_2$  and/or  $\text{C}_4\text{H}_{10}$ ,  $\text{NC}_{19}\text{H}_{27}$  and  $\text{NC}_{21}\text{H}_{31}$  respectively, were detected in the pyrolysis mass spectra.

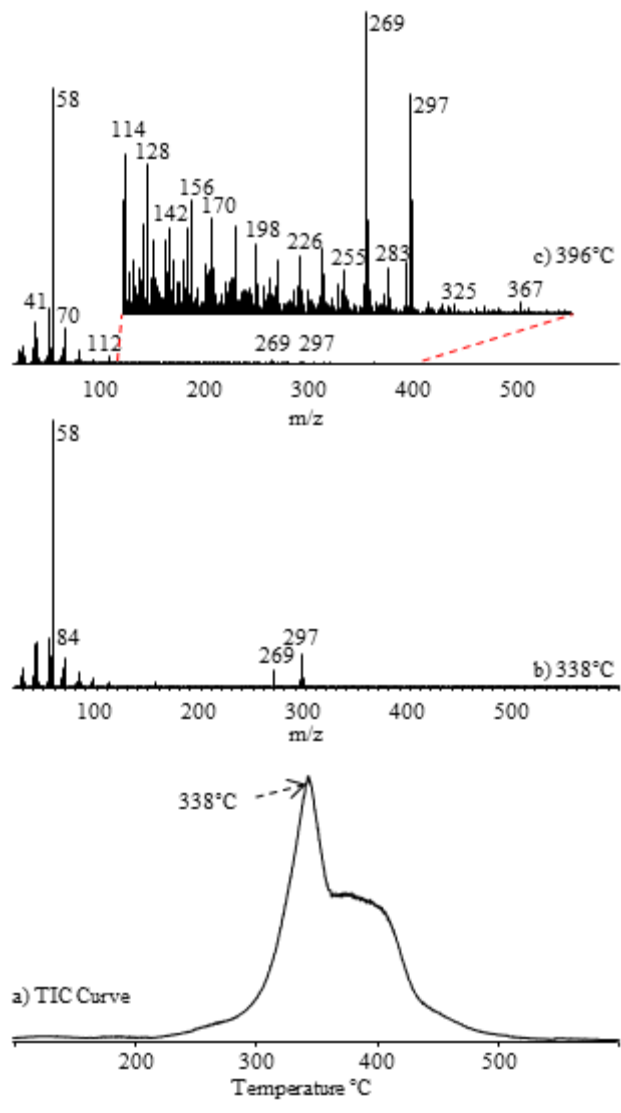


**Figure 3.3.** a) The total ion current curve and mass spectra at b) 338 and c) 396°C recorded during the pyrolysis of MMT25A.

The single ion pyrograms of fragment ions noticed some differences as shown in Figure 3.4. Evaporation of amines was observed at around 338°C. On the other hand, high mass tallow chains decomposed at high temperatures at around 396°C. Peaks, due to hydrocarbon chains with formula  $(CH_2)_x$  and/or products with formula  $N(CH_2)_{x-1}$  ( $m/z = 56, 70, 84, 98, \dots$  and 210 Da for  $x = 4$  to 15) were detected at around 338 and 396°C. In addition, weak peaks, due to hydrocarbon chains with formula  $(C_xH_{2x+2})$  ( $m/z = 72, 86, 100, \dots$  and 240 Da for  $x = 5$  to 17) were detected at around 338 and 396°C. The intensity of low-mass peaks was more pronounced than high-mass peaks. Because, long hydrocarbon chains formed during pyrolysis are ionized again to form low-mass fragments. Moreover, low mass fragments may directly be evolved at the early stages of pyrolysis and may be produced by the ionization of high mass fragments at elevated temperatures.

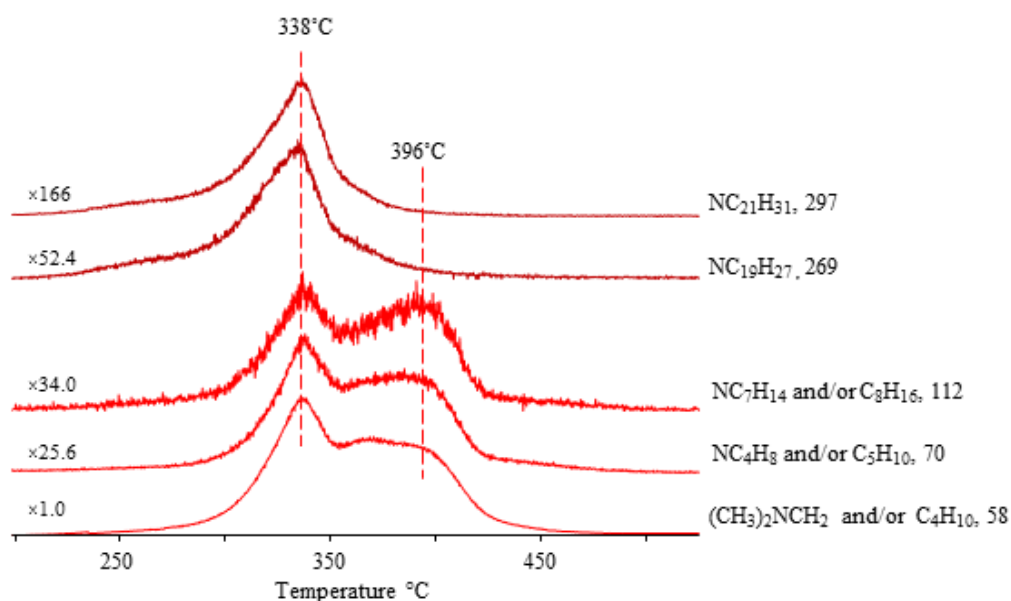


**Figure 3.4.** Single ion pyrograms of some selected fragments detected during the pyrolysis of pure MMT25A.

### 3.1.1.3. MMT30B

Pyrolysis of pure methyl, tallow, bis-2-hydroxyethyl, quaternary ammonium modified montmorillonite nanoclay (MMT30B) yielded a TIC curve with two maxima at around 279 and 421°C (Figure 3.5). Intense peaks at  $m/z = 58, 88, 269, 297$  Da due to  $\text{CH}_2\text{N}(\text{CH}_3)_2$  and/or  $\text{C}_4\text{H}_{10}$ ,  $\text{CH}_2\text{N}(\text{C}_2\text{H}_4\text{OH})\text{CH}_3$ ,  $\text{N}(\text{C}_2\text{H}_4\text{OH})_2\text{C}_{12}\text{H}_{21}$  and  $\text{N}(\text{C}_2\text{H}_4\text{OH})_2\text{C}_{14}\text{H}_{25}$  respectively, were observed in the pyrolysis mass spectra.



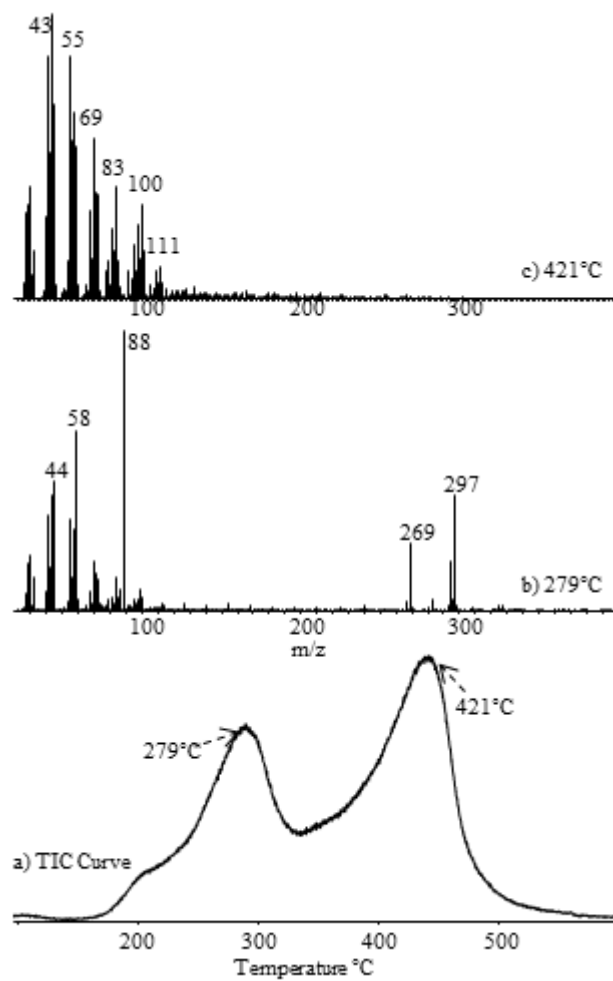


**Figure 3.5.** a) The total ion current curve and mass spectra at b) 279 and c) 421°C during the pyrolysis of MMT30B.

The single ion pyrograms of some selected fragment ions showed some differences as shown in Figure 3.6. As in the case of MMT25A, evaporation of products of the amines was observed at low temperatures. On the other hand, decomposition of high mass tallow chains was occurred at elevated temperatures. In this region, the most intense peak was  $C_3H_7$  (43 Da). The peaks due to  $C_4H_7$  (55 Da),  $C_5H_9$  (69 Da),  $C_6H_{11}$  (83 Da) and  $C_7H_{16}$  (100 Da) were also present in the mass spectra. In addition, weak peaks that can be attributed to  $C_{10}H_{13}$  (133 Da),  $C_{12}H_{22}$  (165 Da),  $C_{14}H_{29}$  (197 Da),  $C_{16}H_{32}$  (224 Da) and  $C_{18}H_{36}$  (252 Da) were observed.

Moreover, peaks, due to hydrocarbon chains with formula  $(CH_2)_x$  and/or products with formula  $N(CH_2)_{x-1}$  ( $m/z = 56, 70, 84, 98, \dots$  and 210 Da for  $x = 4$  to 15) were detected at around 279 and 421 °C. Low mass fragments may directly be evolved at the early stages of pyrolysis and at elevated temperatures, by the dissociative ionization of high mass fragments.

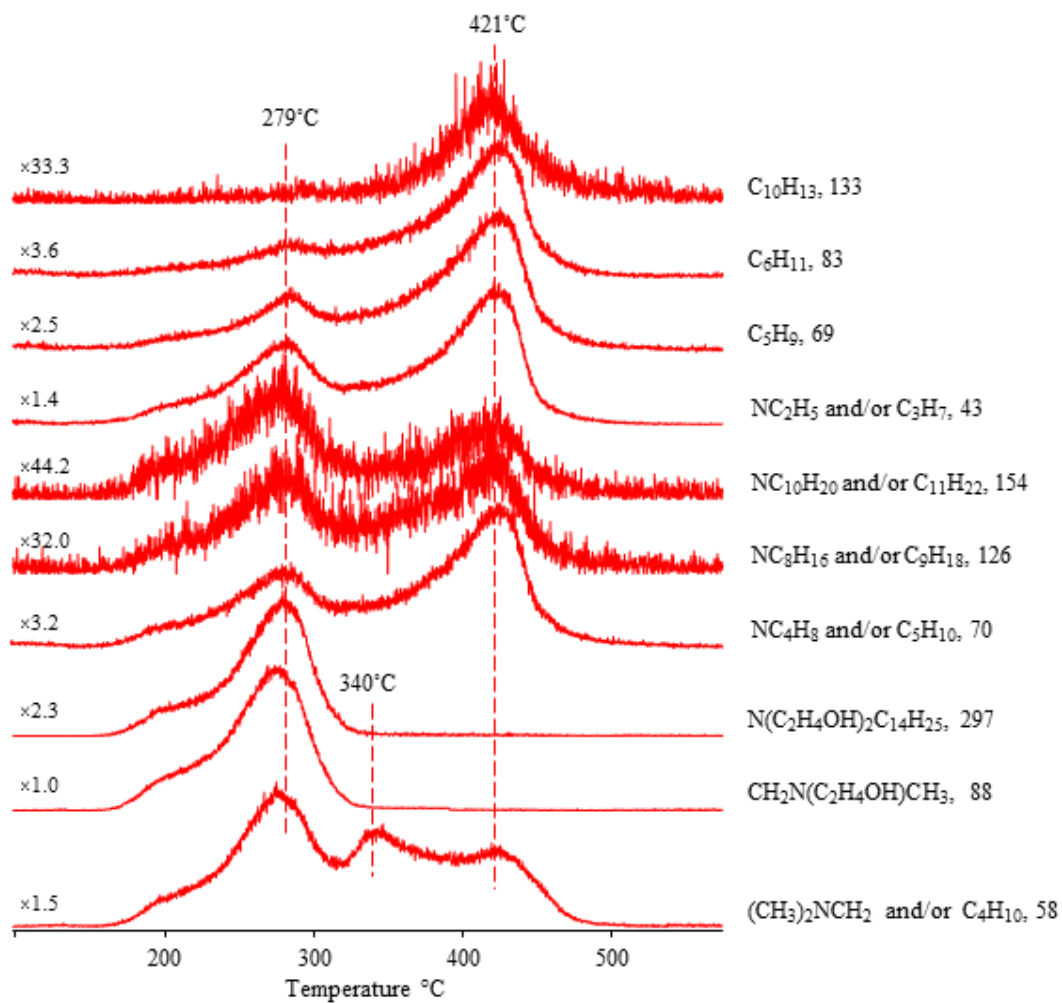


**Figure 3.6.** Single ion pyrograms of some selected fragments detected during the pyrolysis of MMT30B.

### 3.1.2. AlPi

Thermal decomposition of pure aluminium diethylphosphinate (AlPi) mostly detected in two regions. The TIC curve showed two overlapping peaks with maxima at around 390 and 440°C (Figure 3.7). Typical fragmentation pattern of AlPi, intense peaks at  $m/z = 269$ , 601 and 659 Da and less abundant ones, at 751, 543, 505, 433, 375, 315 and 169 Da due to complex structures involving Al-O-P linkages, was detected in the pyrolysis mass spectra recorded at both 390 and 440°C.

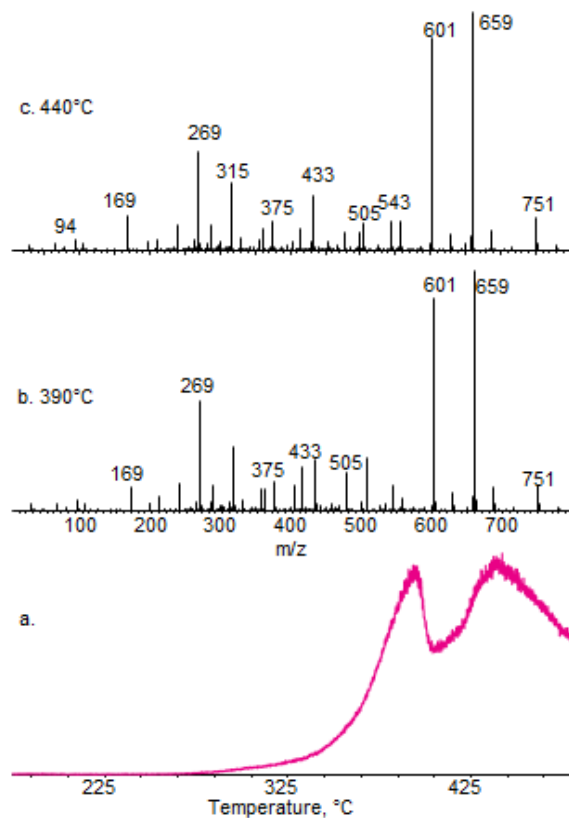


**Figure 3.7.** a) The total ion current curve and mass spectra at b) 390 and c) 440°C during the pyrolysis of AlPi.

The single ion pyrograms of most of the abundant and/or characteristic products are analysed and grouped according to their trends (Figure 3.8). The first group showing identical evolution profiles contains the fragments with m/z values 751, 659, 601, 543, 433, 375, 315 and 269 Da. Two broad overlapping peaks at 390 and 440 °C with similar intensity are present in the single ion pyrograms. In a recent study, generation of four coordinate dimeric compounds containing Al-O-P linkages were suggested during the pyrolysis of AlPi [85]. The trends in the evolution profiles show that these species may directly be eliminated at around 390°C or may be generated by decomposition of a network structure involving these fragments as repeating units at around 440°C.

The second group contains only few fragments of relatively low abundance and with m/z values 505, 413, 403, 311 and 211 Da. They also show two peaks in their evolution profiles but, the relative intensity of the high temperature peak is noticeably low, indicating that the probability of their generation especially at high temperatures is not of significant importance.

Third group contains even less abundant fragments with low m/z values 65, 94, 105, 122, and 169 Da, that may directly be associated with P(OH)<sub>2</sub>, C<sub>2</sub>H<sub>5</sub>P(OH)<sub>2</sub>, (C<sub>2</sub>H<sub>5</sub>)<sub>2</sub>PO, (C<sub>2</sub>H<sub>5</sub>)<sub>2</sub>PO<sub>2</sub>H and (C<sub>2</sub>H<sub>5</sub>PO)<sub>2</sub>OH. They show single ion profiles with a shoulder at around 390°C and a maximum at around 445°C. Thus, it may be thought that they are mainly formed by degradation of the first and second group products at around 390°C and by degradation of poly(alkylphosphinate)s which are generated only to a limited extent.

Single ion pyrograms of P(OH)<sub>2</sub> (65 Da), C<sub>2</sub>H<sub>5</sub>P(OH)<sub>2</sub> (94 Da), (C<sub>2</sub>H<sub>5</sub>)<sub>2</sub>PO (105 Da), (C<sub>2</sub>H<sub>5</sub>PO)<sub>2</sub>OH (169 Da), Al[O<sub>2</sub>P(C<sub>2</sub>H<sub>5</sub>)<sub>2</sub>]<sub>2</sub>(H<sub>2</sub>P<sub>2</sub>O<sub>5</sub>) (413 Da), Al[O<sub>2</sub>P(C<sub>2</sub>H<sub>5</sub>)<sub>2</sub>]<sub>2</sub>(H<sub>2</sub>P<sub>2</sub>O<sub>5</sub>)(O<sub>2</sub>PC<sub>2</sub>H<sub>5</sub>) (505 Da), Al[O<sub>2</sub>P(C<sub>2</sub>H<sub>5</sub>)<sub>2</sub>]<sub>2</sub> (269 Da), Al<sub>2</sub>(O<sub>2</sub>P(C<sub>2</sub>H<sub>5</sub>)<sub>2</sub>)<sub>4</sub>OPO (601 Da) and Al<sub>2</sub>[O<sub>2</sub>P(C<sub>2</sub>H<sub>5</sub>)<sub>2</sub>]<sub>5</sub> (659 Da) are presented in Figure 3.8 as representative examples of each group.

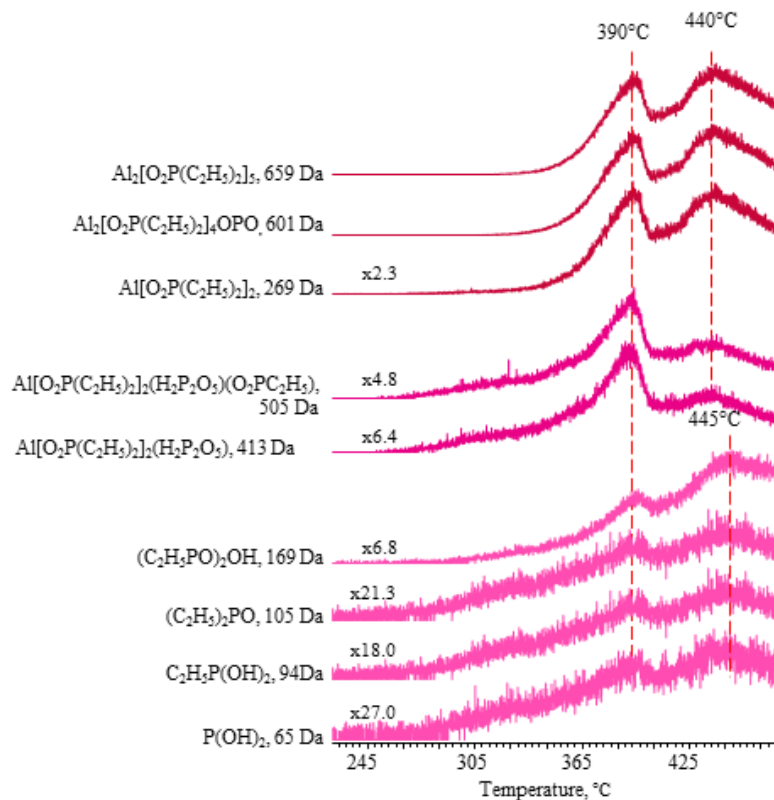


**Figure 3.8.** Single ion pyrograms of some selected fragments detected during the pyrolysis of AlPi.

In order to confirm the proposed structures, collision induced dissociation experiments were carried out at different collision energies (40, 30 and 20 eV) to provide fragmentation pathways to generate informative, structurally significant product ions. In Figure 3.9 the daughter spectra of precursor fragment ions with  $m/z$  values 751, 659, 601, 543, 433 and 269 Da, the main members of the first group, are given.

Few peaks are present in the CID spectra of fragments with  $m/z$  values 751, 659 and 601 Da obtained even at high energies. The precursor ion peak is absent in the CID spectra of 751 Da fragment ion. On the other hand, those of 659 and 601 Da fragment ions are quite intense. Moreover, they all decompose to yield intense 433 Da daughter ion. Only a single peak at 659 Da is present in the low energy CID spectrum of the

fragment ion with  $m/z=751$  Da indicating a neutral loss of 92 Da, that may be associated with  $C_2H_5PO_2$  (Figure 3.9a). When the energy is increased, an intense peak at 433 Da and weak peaks at 601 and 269 Da are appeared. The 20 eV CID spectrum of the fragment ion with  $m/z=659$  Da shows precursor ion peak as the base peak together with a moderate peak at 433 Da (Figure 3.9b). The 433 Da peak becomes the base peak in the high energy CID spectrum and weak peaks at 587 and 375 Da appear in the spectrum. Similarly, in the low energy CID spectrum of 601 Da fragment ion, only, the precursor ion peak, as the base peak, and intense 433 Da peak are present (Figure 3.9c). 601 Da peak totally disappear in the high energy CID spectra, the 433 Da peak becomes again the base peak and weak peaks at 375, 329, 313 and 269 Da are appeared.

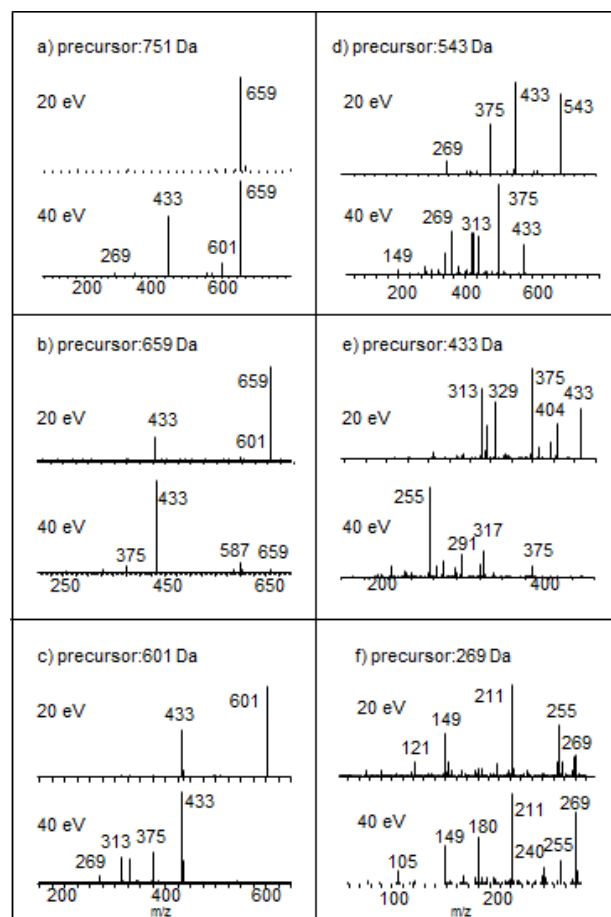


**Figure 3.9.** The daughter spectra of precursor fragment ions with m/z values 751, 659, 601, 543, 433 and 269 Da.



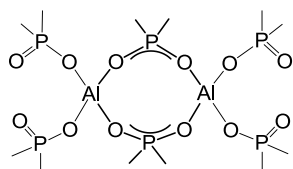
Contrary to the limited fragmentation of the precursors ions with  $m/z$  values 751, 659, 601 Da, extensive fragmentations are detected in the CID spectra of the ions with  $m/z=543$ , 433 and 269 Da pointing out lower stability in accordance with their low intensities in the pyrolysis mass spectra. The CID spectra of the fragments with  $m/z$  values 543 and 433 Da involve peaks at 433, 375 and 269 Da indicating presence of similar units (Figure 3.9d and e).

The prominent peaks in the CID spectrum of the ion with  $m/z=269$  Da are at 269, 255, 240, 211, 180, 149 and 105 Da (Figure 3.9f). Taking into account the neutral losses and the fragmentation pattern recorded, the daughter ions can be attributed to  $(C_2H_5)_2PO$  (105 Da),  $HAIO_2P(C_2H_5)_2$  (149 Da),  $O_2AlO_2P(C_2H_5)_2$  (180 Da),  $C_2H_5PO_2AlO_2PC_2H_5$  (211 Da),  $C_2H_5PO_2AlO_2P(C_2H_5)_2$  (240 Da) and the precursor ion to  $(C_2H_5)_2PO_2AlO_2P(C_2H_5)_2$  (269 Da) in accordance with our previous assignments [85].

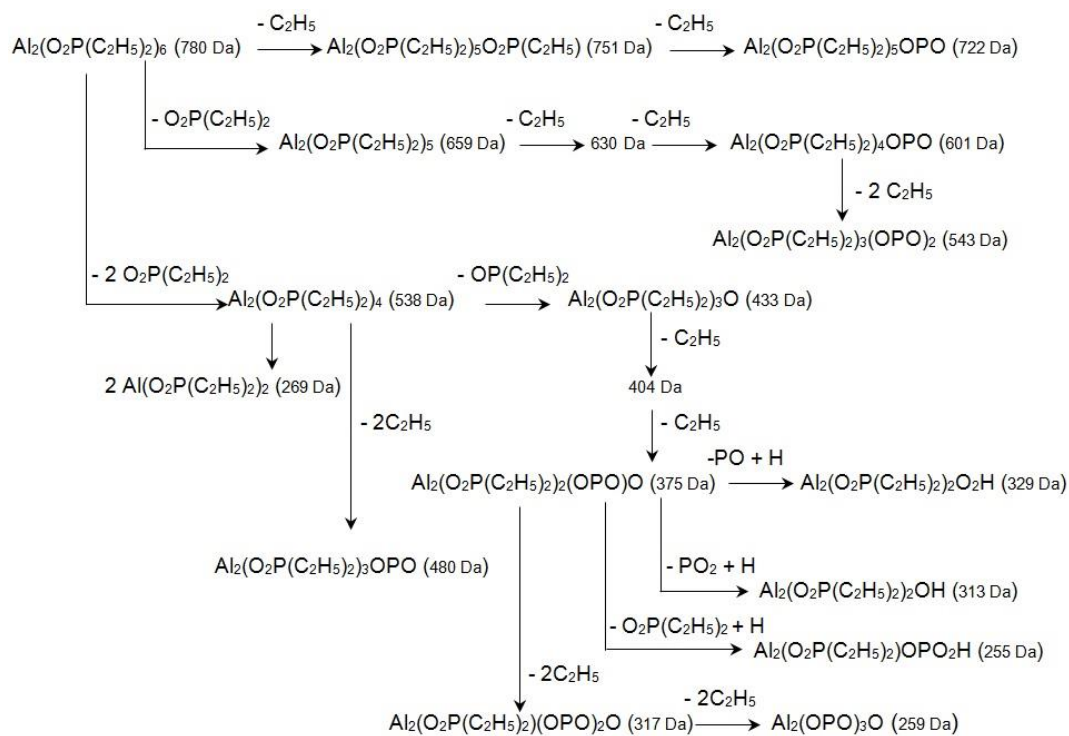
The CID results reveal that 751, 659, 601 and 543 Da fragment ions involve a stem unit with  $m/z$  value 433 Da that may be attributed to  $OAl_2(O_2P(C_2H_5)_2)_3$  fragment. The most prominent fragment ions and the neutral losses corresponding to presumably assigned structures for these fragments are revised and the possible structure for the four coordinate dimeric compound involving Al-O-P linkages generated during pyrolysis yielding the intense fragment ions during pyrolysis and/or dissociative ionization processes are proposed as shown in Scheme 3.1a and 3.1b [86, 87].

**Scheme 3.1.** Possible structure and fragmentation pathways of the aluminium phosphinates complex

**a)** Possible structure of four coordinate aluminium phosphinates complex



**b)** Possible fragmentation pathways of the complex during pyrolysis and/or ionization



In Figure 3.10 the daughter spectra of the precursor fragment ions with  $m/z$  values 505, 413 and 403 Da are presented. Intense peaks at 413 and 269 Da are present in the CID spectra of both fragment ions with  $m/z$  values 505 and 413 Da indicating elimination of  $C_2H_5PO_2$  (92 Da) and  $H_2P_2O_5$ . In contrast, extensive fragmentation is observed the CID spectra when 403 Da fragment is chosen as the precursor ion. The most prominent peak at 311 Da may be related with the fragment formed by loss of  $C_2H_5PO_2$  (92 Da) from the precursor ion 403 Da. Successive loses of  $C_2H_5$  groups and  $C_2H_5PO$  yields 269 Da fragment, the common ion in the daughter spectra of the precursor ions with  $m/z$  values 505 and 413 Da.

Among the few other thermal degradation products having similar evolution profiles with 505, 413 and 403 Da fragments, the fragment with  $m/z=211$  Da yields a CID spectrum with a base peak at 153 Da indicating successive loses of two ethyl groups and weak peaks at 92 and 77 Da that can readily be associated with  $C_2H_5PO_2$  (92 Da) and  $C_2H_5PHO$  (77 Da) fragments. As a consequence, the fragment with  $m/z=211$  Da is associated with a dimeric structure,  $((C_2H_5)_2PO)_2H$ .

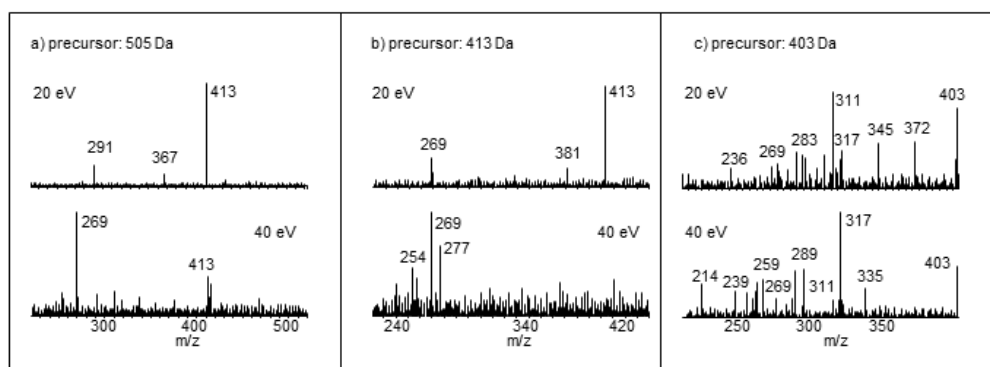


**Figure 3.10.** The daughter spectra of precursor fragment ions with  $m/z$  values 505, 413 and 403 Da.

Thus, it may be concluded that 505, 413 and 403 Da fragments all contain  $\text{Al}(\text{O}_2\text{P}(\text{C}_2\text{H}_5)_2)_2$  (269 Da) fragment involving also  $\text{H}_2\text{P}_2\text{O}_5$  as a substituent. 505 and 413 Da are presumably assigned to  $\text{Al}(\text{O}_2\text{P}(\text{C}_2\text{H}_5)_2)_2(\text{O}_2\text{PC}_2\text{H}_5)(\text{H}_2\text{P}_2\text{O}_5)$  (505 Da) and  $\text{Al}(\text{O}_2\text{P}(\text{C}_2\text{H}_5)_2)_2(\text{H}_2\text{P}_2\text{O}_5)$  (413 Da) possessing phosphinate oligomers. On the other hand, 403 Da fragment may be presumably assigned to  $\text{Al}(\text{OP})_4(\text{C}_2\text{H}_5)_3(\text{OH})_5\text{O}$  and/or  $\text{Al}(\text{OP})_3(\text{C}_2\text{H}_5)_4(\text{OH})_7$  that may also generate  $\text{Al}(\text{OP})_3(\text{OH})_5\text{O}$  (269 Da) having a less stable structure. Considering the trends in the evolution profiles, it can further be suggested that the elimination of oligomers of alkyl phosphinates takes place at slightly higher temperatures than fragments involving monomeric and dimeric four coordinate compounds involving Al-O-P linkages.

The CID spectrum of the fragment ion with  $m/z=169$  Da presents peaks at 105, and 77 Da indicating losses of  $\text{PO}_2\text{H}$  (64 Da), and  $\text{C}_2\text{H}_5\text{PO}_2$  (92 Da) (Figure 3.11). While those of the fragment ion with  $m/z=105$  Da show peaks at 77 and 49 Da that can be attributed to  $\text{C}_2\text{H}_5\text{PHO}$  and  $\text{H}_2\text{PO}$ . And, finally, the daughter spectra of 94 Da shows base peak at 65 Da and a weak mother ion peak confirming the structure  $\text{C}_2\text{H}_5\text{P}(\text{OH})_2$ . Thus, 169 Da fragment may be attributed to  $(\text{C}_2\text{H}_5\text{PO})_2\text{OH}$ . As the single ion profiles of these fragments are identical it can be stated that the last group of thermal decomposition products involve oligomers of alkyl phosphinates.

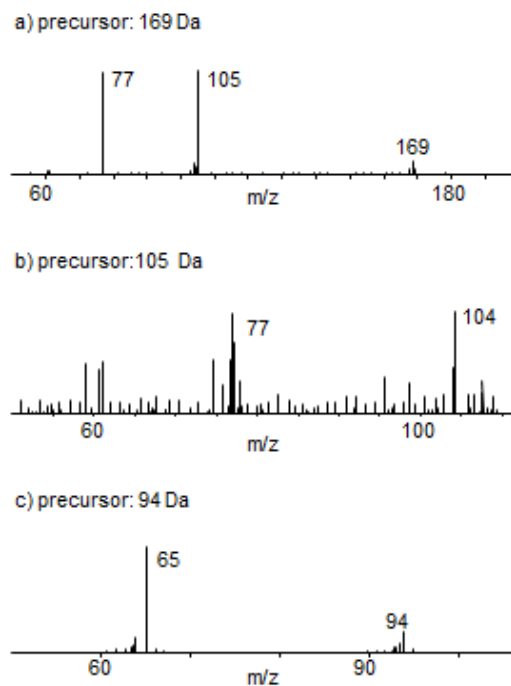


**Figure 3.11.** The daughter spectra of precursor fragment ions with  $m/z$  values 169, 105 and 94 Da.

In Table 3.2, the relative intensities of intense and/or characteristic peaks recorded in the spectrum of pure AlPi and the assignments made are summarized.

**Table 3.2.** The relative intensities, RI, of some selected intense and/or characteristic peaks recorded in pyrolysis spectrum of AlPi at 400 and 440°C and the assignments made.

m/z	RI		Assignment
	400°C	440°C	
49	5.0		H <sub>2</sub> PO
65	21	33	P(OH) <sub>2</sub>
77	18	17	C <sub>2</sub> H <sub>5</sub> PHO
94	46	50	C <sub>2</sub> H <sub>5</sub> P(OH) <sub>2</sub>
105	35	43	(C <sub>2</sub> H <sub>5</sub> ) <sub>2</sub> PO
122	11	14	(C <sub>2</sub> H <sub>5</sub> ) <sub>2</sub> PO <sub>2</sub> H
149	6.7	4.7	HAlO <sub>2</sub> P(C <sub>2</sub> H <sub>5</sub> ) <sub>2</sub>
153	4.3		(C <sub>2</sub> H <sub>5</sub> PO) <sub>2</sub> H
169	103	142	(C <sub>2</sub> H <sub>5</sub> PO) <sub>2</sub> OH
180		3.5	O <sub>2</sub> AlO <sub>2</sub> P(C <sub>2</sub> H <sub>5</sub> ) <sub>2</sub>
211	52	51	((C <sub>2</sub> H <sub>5</sub> ) <sub>2</sub> PO) <sub>2</sub> H and/or C <sub>2</sub> H <sub>5</sub> PO <sub>2</sub> AlO <sub>2</sub> PC <sub>2</sub> H <sub>5</sub>
240	125	97	C <sub>2</sub> H <sub>5</sub> PO <sub>2</sub> AlO <sub>2</sub> P(C <sub>2</sub> H <sub>5</sub> ) <sub>2</sub>
255	12	16	Al <sub>2</sub> (O <sub>2</sub> P(C <sub>2</sub> H <sub>5</sub> ) <sub>2</sub> )OPO <sub>2</sub> H
259	8.6	5.9	Al <sub>2</sub> (OPO) <sub>3</sub> O
269	486	428	(C <sub>2</sub> H <sub>5</sub> ) <sub>2</sub> PO <sub>2</sub> AlO <sub>2</sub> P(C <sub>2</sub> H <sub>5</sub> ) <sub>2</sub>
311	38	11	Al(OP) <sub>3</sub> (C <sub>2</sub> H <sub>5</sub> ) <sub>2</sub> (OH) <sub>5</sub>
313	17	17	Al <sub>2</sub> (O <sub>2</sub> P(C <sub>2</sub> H <sub>5</sub> ) <sub>2</sub> ) <sub>2</sub> OH
317	15	25	Al <sub>2</sub> (O <sub>2</sub> P(C <sub>2</sub> H <sub>5</sub> ) <sub>2</sub> )(OPO) <sub>2</sub> O
329	46	46	Al <sub>2</sub> (O <sub>2</sub> P(C <sub>2</sub> H <sub>5</sub> ) <sub>2</sub> ) <sub>2</sub> O <sub>2</sub> H
355	93	50	HI(C <sub>2</sub> H <sub>5</sub> AlO <sub>2</sub> P(C <sub>2</sub> H <sub>5</sub> ) <sub>2</sub> ) <sub>2</sub>
375	115	102	Al <sub>2</sub> (O <sub>2</sub> P(C <sub>2</sub> H <sub>5</sub> ) <sub>2</sub> ) <sub>2</sub> (OPO)O
403	78	32	Al(OP) <sub>4</sub> (C <sub>2</sub> H <sub>5</sub> ) <sub>3</sub> (OH) <sub>5</sub> O and/or Al(OP) <sub>3</sub> (C <sub>2</sub> H <sub>5</sub> ) <sub>4</sub> (OH) <sub>7</sub>
404	15	18	OAl <sub>2</sub> (O <sub>2</sub> PC <sub>2</sub> H <sub>5</sub> )(O <sub>2</sub> P(C <sub>2</sub> H <sub>5</sub> ) <sub>2</sub> ) <sub>2</sub>
413	168	83	Al(O <sub>2</sub> P(C <sub>2</sub> H <sub>5</sub> ) <sub>2</sub> ) <sub>2</sub> (H <sub>2</sub> P <sub>2</sub> O <sub>5</sub> )
433	223	210	OAl <sub>2</sub> (O <sub>2</sub> P(C <sub>2</sub> H <sub>5</sub> ) <sub>2</sub> ) <sub>3</sub>
505	207	107	Al(O <sub>2</sub> P(C <sub>2</sub> H <sub>5</sub> ) <sub>2</sub> ) <sub>2</sub> (H <sub>2</sub> P <sub>2</sub> O <sub>5</sub> )(O <sub>2</sub> PC <sub>2</sub> H <sub>5</sub> )
543	108	112	Al <sub>2</sub> (O <sub>2</sub> P(C <sub>2</sub> H <sub>5</sub> ) <sub>2</sub> ) <sub>3</sub> (OPO) <sub>2</sub>
601	902	856	Al <sub>2</sub> (O <sub>2</sub> P(C <sub>2</sub> H <sub>5</sub> ) <sub>2</sub> ) <sub>4</sub> OPO
630	26	16	Al <sub>2</sub> (O <sub>2</sub> PC <sub>2</sub> H <sub>5</sub> )(O <sub>2</sub> P(C <sub>2</sub> H <sub>5</sub> ) <sub>2</sub> ) <sub>4</sub>
659	1000	1000	Al <sub>2</sub> (O <sub>2</sub> P(C <sub>2</sub> H <sub>5</sub> ) <sub>2</sub> ) <sub>5</sub>
751	102	128	Al <sub>2</sub> (O <sub>2</sub> P(C <sub>2</sub> H <sub>5</sub> ) <sub>2</sub> ) <sub>5</sub> O <sub>2</sub> P(C <sub>2</sub> H <sub>5</sub> )
780	5.6	4.6	Al <sub>2</sub> (O <sub>2</sub> P(C <sub>2</sub> H <sub>5</sub> ) <sub>2</sub> ) <sub>6</sub>

### 3.1.3. Brominated Epoxy (BE)

In this study, oligomeric brominated flame retardant was preferred because of decreased toxicity, mechanical properties, melt flow characteristics and thermal stability among the conventional non-oligomeric types. The TIC curve of pure brominated epoxy oligomer showed a single peak with a maximum at around 407°C (Figure 3.12). The most intense peak in the pyrolysis mass spectrum recorded at 407°C is at 43 Da due to CH<sub>3</sub>CO fragment. Tetrabromo bisphenol A (525-533 Da) and HBr (80-82 Da) were detected to be the major decomposition products. Tribromophenol (328-334 Da), bromoacetone (136-138 Da) and acetone (58 Da) were observed.

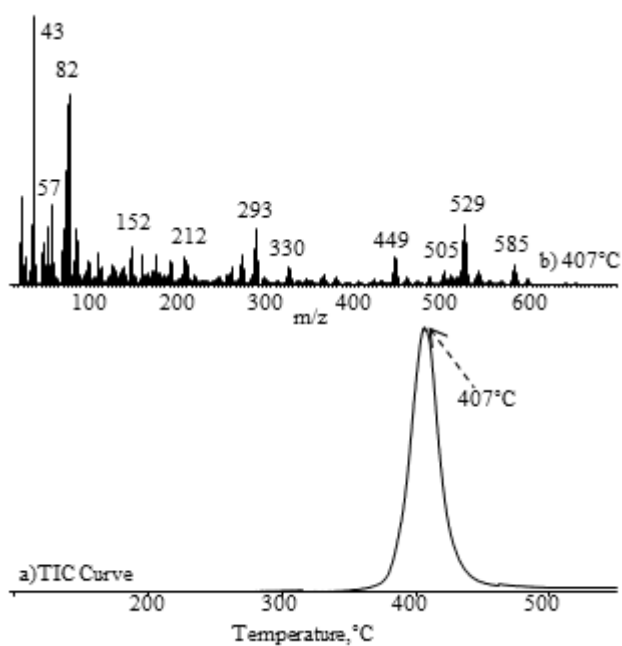


**Figure 3.12.** a) The total ion current curve and b) mass spectrum of BE at 407 °C.

In Table 3.3, the relative intensities of intense and/or characteristic peaks recorded in the spectrum and the assignments made are summarized.

**Table 3.3.** The relative intensities, RI, of some selected intense and/or characteristic peaks recorded in pyrolysis spectrum of BE at 407°C and the assignments made.

m/z	RI	Assignment
43	1000	CH <sub>3</sub> CO, CH <sub>2</sub> COH
57	217	CH <sub>3</sub> COCH <sub>2</sub>
58	25	CH <sub>3</sub> COCH <sub>3</sub>
79, 81	427, 357	Br
80, 82	677, 713	HBr
91	163	C <sub>6</sub> H <sub>5</sub> CH <sub>2</sub>
94, 96	34, 16	CH <sub>3</sub> Br
136, 138	12, 23	CH <sub>3</sub> COCH <sub>2</sub> Br
291-295	135,208,89	C <sub>6</sub> H <sub>2</sub> Br <sub>2</sub> C <sub>2</sub> H <sub>3</sub> O <sub>2</sub>
328-334	26,64,57,24	Br <sub>3</sub> C <sub>6</sub> H <sub>2</sub> OH
462-468	16, 26, 22, 8	HO(Br <sub>2</sub> )C <sub>6</sub> H <sub>2</sub> C(CH <sub>3</sub> ) <sub>2</sub> C <sub>6</sub> H <sub>3</sub> BrOH
525-533	52,162,225,153,39	HO(Br <sub>2</sub> )C <sub>6</sub> H <sub>2</sub> CCH <sub>3</sub> C <sub>6</sub> H <sub>2</sub> (Br <sub>2</sub> )OH
540-548	14,35,52,32,10	HO(Br <sub>2</sub> )C <sub>6</sub> H <sub>2</sub> C(CH <sub>3</sub> ) <sub>2</sub> C <sub>6</sub> H <sub>2</sub> (Br <sub>2</sub> )OH
581-589	15,48,70,43,12	C <sub>3</sub> H <sub>5</sub> O <sub>2</sub> (Br <sub>2</sub> )C <sub>6</sub> H <sub>2</sub> CCH <sub>3</sub> C <sub>6</sub> H <sub>2</sub> (Br <sub>2</sub> )OH
637-645	0.1, 3, 7, 4, 1.5	C <sub>3</sub> H <sub>5</sub> O <sub>2</sub> (Br <sub>2</sub> )C <sub>6</sub> H <sub>2</sub> CCH <sub>3</sub> C <sub>6</sub> H <sub>2</sub> (Br <sub>2</sub> )C <sub>3</sub> H <sub>5</sub> O <sub>2</sub>

Single ion pyrograms of degradation products showed slight differences thus, it can be thought that the degradation occurred through different reaction pathways (Figure 3.13).



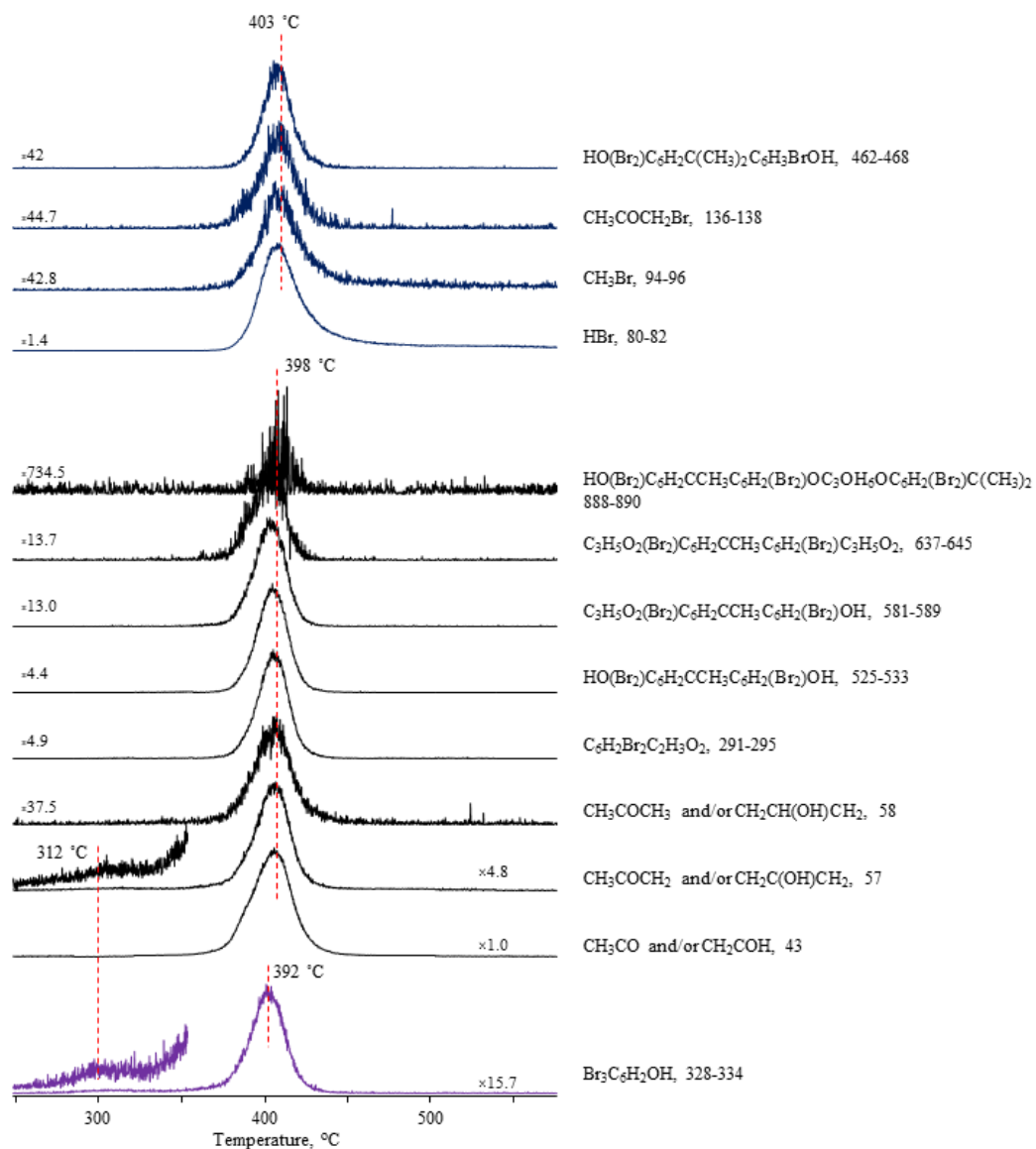
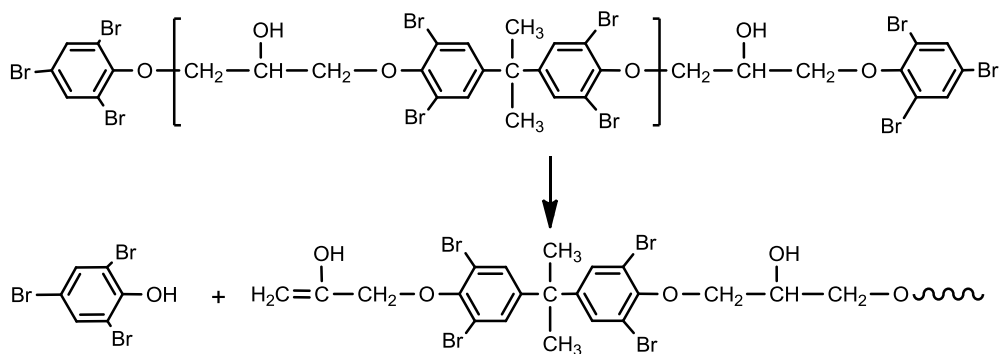


**Figure 3.13.** Single ion pyrograms of some selected fragments detected during the pyrolysis of BE.

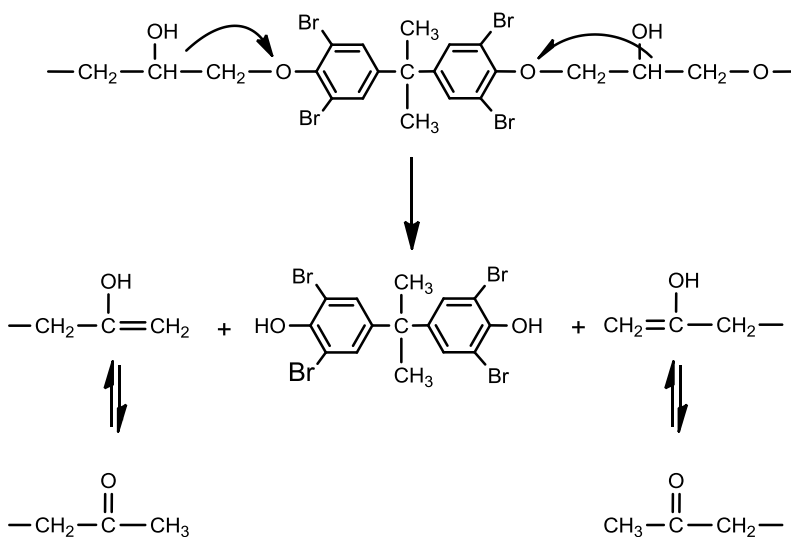
The single ion evolution profile of tribromophenol (328-334 Da) showed two peaks with maxima at around 312 and 392°C. Products due to the decomposition of epoxy linkages such as CH<sub>3</sub>CO or CH<sub>2</sub>COH (43 Da), CH<sub>3</sub>COCH<sub>2</sub> or CH<sub>2</sub>COHCH<sub>2</sub> (57 Da), CH<sub>3</sub>COCH<sub>3</sub> or CH<sub>2</sub>COHCH<sub>3</sub> (58 Da) and tetrabromobisphenol A (540-548 Da) and all the fragments involving bisphenol A units reached maximum yield at around 398°C. However, the evolution of HBr (80-82 Da), CH<sub>3</sub>Br (94-96 Da) and CH<sub>3</sub>COCH<sub>2</sub>Br (136-138 Da) were maximized at slightly elevated temperatures, at around 403°C. In addition to tribromophenol, evolution of CH<sub>3</sub>COCH<sub>2</sub> or CH<sub>2</sub>C(OH)CH<sub>2</sub> (57 Da) was also noticed at around 312°C. Therefore, it can be concluded that thermal decomposition of the epoxy oligomer started by loss of end groups (Scheme 3.2a). The evolution of tetrabromobisphenol A and other fragments involving bisphenol A units and also the fragments involving the epoxy linkages observed at slightly higher temperatures. Tetrabromobisphenol A was the major product among the products involving bisphenol A. Its formation may be explained by the mechanism proposed by Blazso et al. as shown in Scheme 3.2b. [88]. However, although, Blazso et al. noted the evolution of hydrogen bromide and tetrabromobisphenol A in the same temperature region under the high vacuum conditions, in this study, elimination of HBr was occurred at slightly higher temperatures, together with minor amounts of bromomethane, bromoacetone and tribromobisphenol A. These may be caused by the attack of HBr to epoxy units even under high vacuum conditions (Scheme 3.2c). In fact, in the EI mass spectrum of tetrabromobisphenol A and tribromophenol, HBr peak is not present. However, it should necessarily be generated during the thermal degradation of the epoxy oligomers. Moreover, detection of high mass fragments such as C<sub>3</sub>H<sub>5</sub>O<sub>2</sub>(Br<sub>2</sub>)C<sub>6</sub>H<sub>2</sub>CCH<sub>3</sub>C<sub>6</sub>H<sub>2</sub>(Br<sub>2</sub>)C<sub>3</sub>H<sub>5</sub>O<sub>2</sub> (637–645 Da) and HO(Br<sub>2</sub>)C<sub>6</sub>H<sub>2</sub>CCH<sub>3</sub>C<sub>6</sub>H<sub>2</sub>(Br<sub>2</sub>)OC<sub>3</sub>OH<sub>6</sub>OC<sub>6</sub>H<sub>2</sub>(Br<sub>2</sub>)C(CH<sub>3</sub>)<sub>2</sub> (888-890 Da) showed that random cleavages along the main chain also took place as an opposing thermal degradation pathway.

**Scheme 3.2.** Thermal degradation pathways of brominated epoxy oligomer.

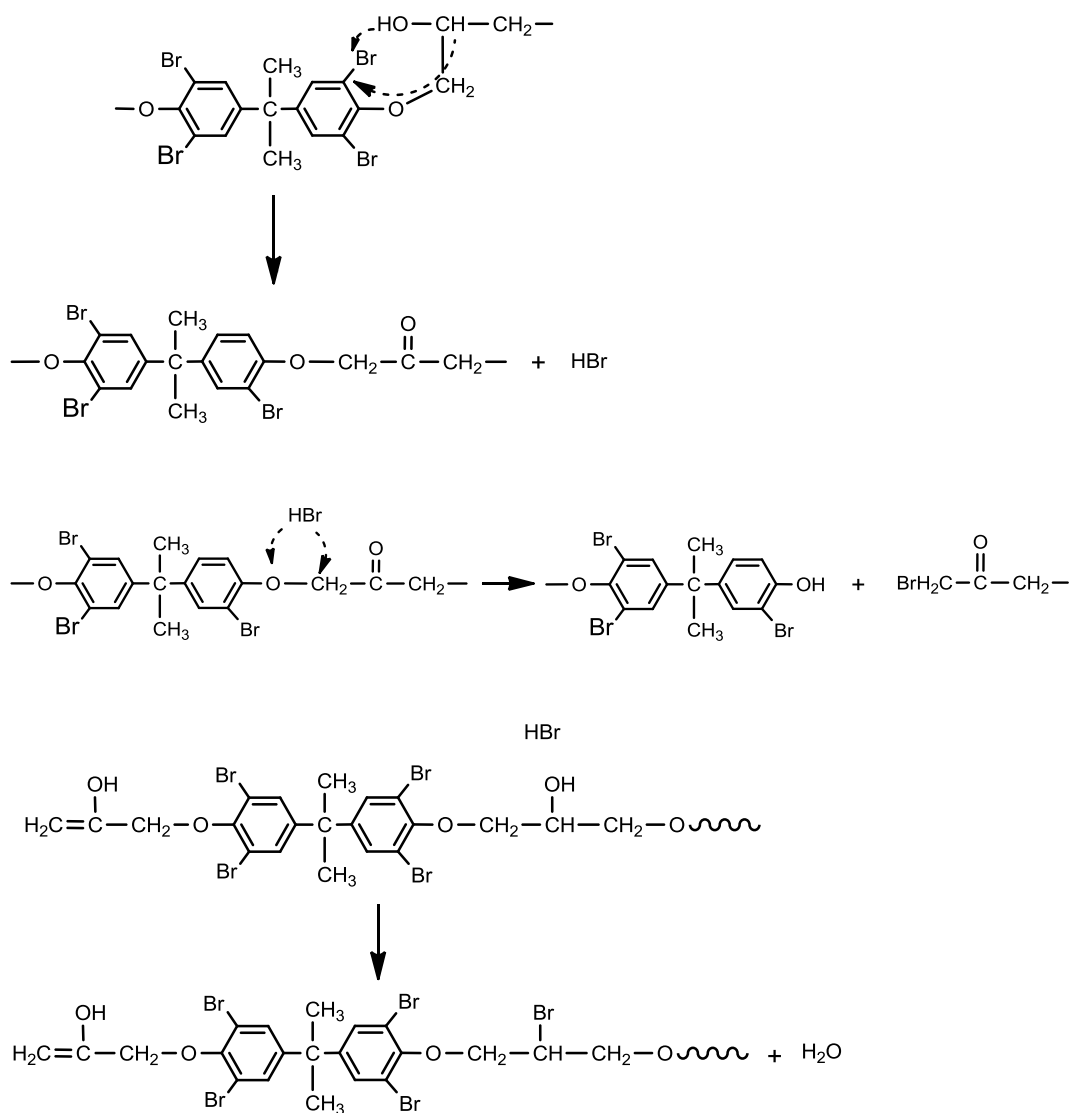
**a) Loss of end groups**



**b) Generation of tetrabromobisphenol A**



c) Generation of HBr, CH<sub>3</sub>Br and BrCH<sub>2</sub>COCH<sub>3</sub>



### 3.1.4. $\text{Sb}_2\text{O}_3$

The TIC curve of pure  $\text{Sb}_2\text{O}_3$  and the mass spectrum recorded at  $495^\circ\text{C}$ , at the peak maximum, is given in Figure 3.14. Several oxides were detected contrary to our expectations. Besides the starting compound,  $\text{Sb}_2\text{O}_3$ ,  $\text{Sb}_2\text{O}_2$ ,  $\text{Sb}_3\text{O}_x$ , where  $x=1$  to  $5$ ,  $\text{Sb}_4\text{O}_x$  where  $x=3$  or  $7$  and  $\text{Sb}_5\text{O}_x$  where  $x=2$  or  $7$  and Sb oligomers,  $\text{Sb}_x$  for  $x=1$  to  $4$ , were also identified.

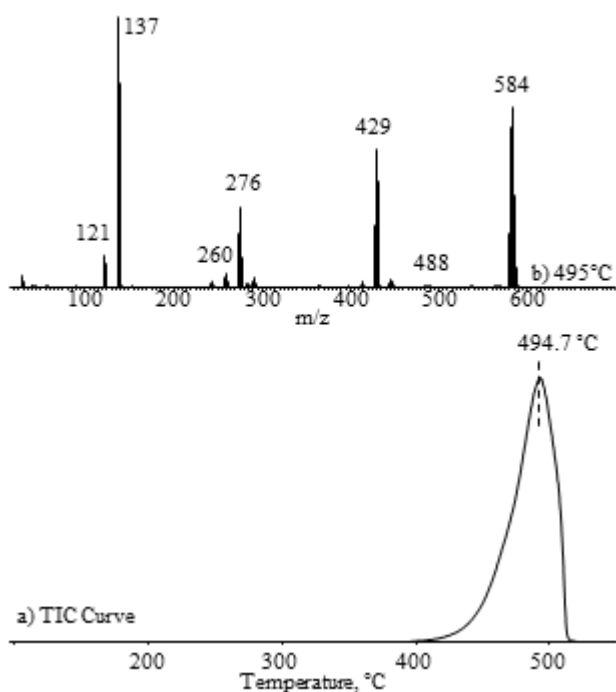


**Figure 3.14.** a) The total ion current curve and b) mass spectrum of  $\text{Sb}_2\text{O}_3$  at  $495^\circ\text{C}$ .

The relative yield of  $\text{Sb}_2\text{O}_3$  (290-294 Da) was quite weak. The base peak was due to SbO (137-139 Da).  $\text{Sb}_4\text{O}_6$  (580-588 Da),  $\text{Sb}_3\text{O}_4$  (427-433 Da) and  $\text{Sb}_2\text{O}_2$  (274-278 Da) were the other abundant products. All products followed identical evolution profiles and maximized at around  $495^\circ\text{C}$ . Evaporation of  $\text{Sb}_4\text{O}_6$  was

confirmed as previous literature findings [78, 89]. Yet, to our knowledge antimony oxides involving more than four Sb atoms was not detected before. Therefore, it may be concluded that a glassy network structure was produced under the high vacuum conditions. In Table 3.4, the relative intensities of intense and/or characteristic peaks recorded in the spectrum and the assignments made are summarized.

**Table 3.4.** The relative intensities, RI, of some selected intense and/or characteristic peaks recorded in pyrolysis spectrum of  $\text{Sb}_2\text{O}_3$  at  $495^\circ\text{C}$  and the assignments made.

m/z	RI	Assignment
121, 123	119, 88	Sb
242-246	15, 21, 8	$\text{Sb}_2$
363-369	1.8, 4, 3, 0.7	$\text{Sb}_3$
484-492	3, 8, 9, 5, 0.8	$\text{Sb}_4$
137, 139	1000, 755	SbO
274-278	199, 296, 111	$\text{Sb}_2\text{O}_2$
290-294	22, 37, 12	$\text{Sb}_2\text{O}_3$
379-385	0.3,1.0,0.7,0.2	$\text{Sb}_3\text{O}$
395-401	0.5,1.3,0.9,0.2	$\text{Sb}_3\text{O}_2$
411-417	8,17,13,3	$\text{Sb}_3\text{O}_3$
427-433	230, 515, 392, 101	$\text{Sb}_3\text{O}_4$
443-449	10,25,18,5	$\text{Sb}_3\text{O}_5$
536	1.6	$\text{Sb}_4\text{O}_3$
568	5.2	$\text{Sb}_4\text{O}_5$
580-588	199, 590, 665, 338, 69	$\text{Sb}_4\text{O}_6$
600	0.2	$\text{Sb}_4\text{O}_7$

Single ion pyrograms of some intense and/or characteristic fragments recorded during the pyrolysis of  $\text{Sb}_2\text{O}_3$  are given in Figure 3.15. All products showed almost the same trends in their evolution profiles. Thus, it can be concluded that they were generated energetically through the same decomposition pathway, through one step thermal degradation mechanism.

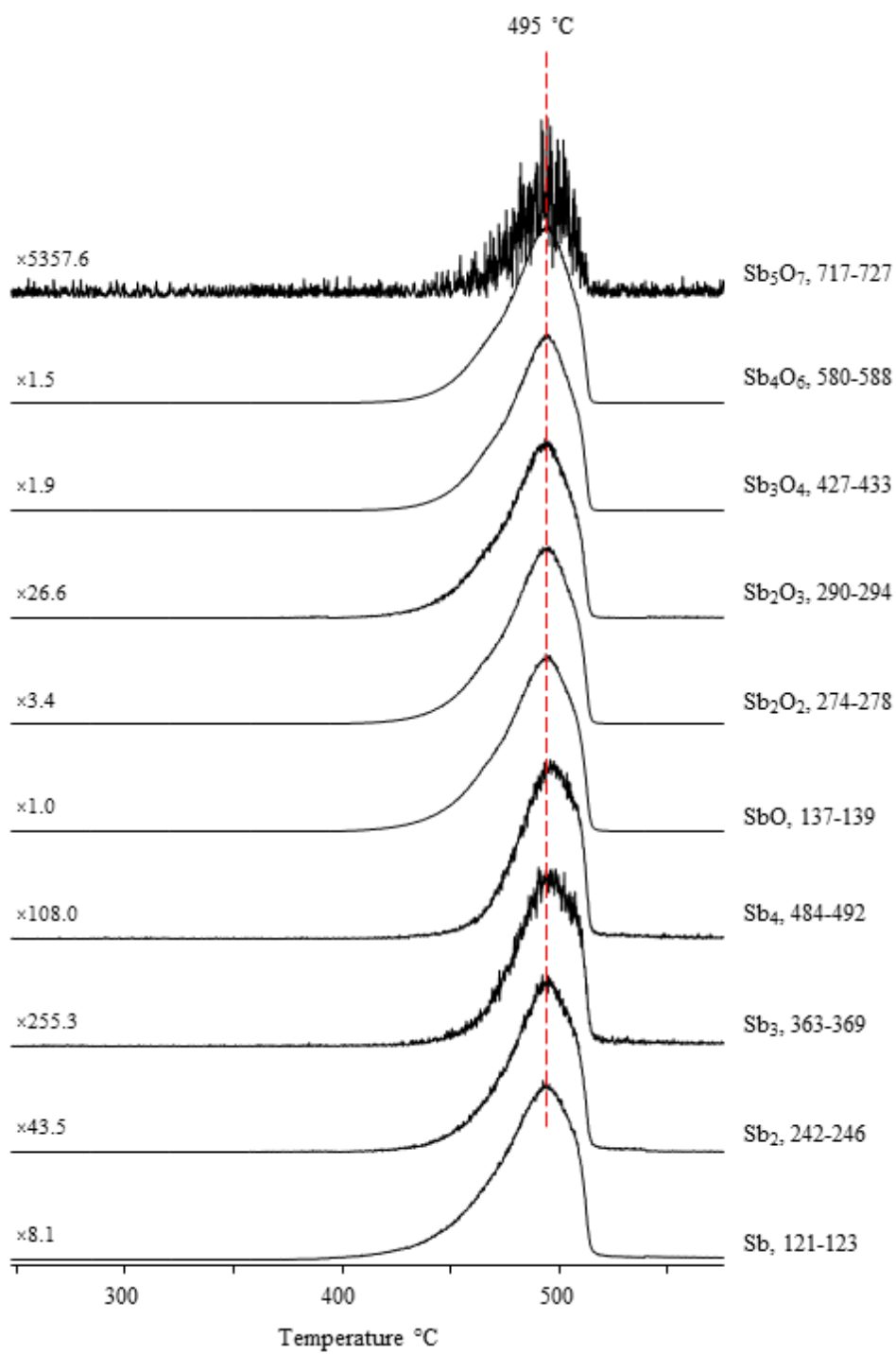


**Figure 3.15.** Single ion pyrograms of some selected fragments detected during the pyrolysis of  $\text{Sb}_2\text{O}_3$ .

### 3.2 THERMAL DEGRADATION OF POLYAMIDE 6 IN THE PRESENCE OF NANOPARTICLES AND FLAME RETARDANTS

For understanding the effects of nanoclays on thermal degradation properties of polyamide 6 composites, PA6 involving 3% MMT25A, 3 or 5% MMT30B, 3% HNT or 20% ALPI, PA6 involving 17% ALPI and 3% MMT25A, 3% MMT30B or 3% HNT were studied by DP-MS technique separately (Table 2.1).

The variation of total ion current as a function of temperature (TIC) curve recorded during the pyrolysis of PA6 showed a single peak having a maximum at 449°C (Figure 3.16). The pyrolysis mass spectra showed intense peaks at  $m/z = 114, 96, 84, 69, 55, 41, 30$  and  $18$  Da associated with protonated monomer, MH,  $C_5H_{10}CN$ ,  $C_2H_8CO$ ,  $C_5H_9$ ,  $C_4H_7$ ,  $C_3H_5$ ,  $CH_2NH_2$  and  $H_2O$ , respectively, mostly due to dissociative ionization of the monomer and its oligomers. Peaks due to series of fragments with formula  $M_xH$ , protonated oligomers ( $m/z = 227, 340, 453$  and  $566$  Da for  $x = 2$  to  $5$ ),  $M_xOH$  ( $m/z = 130, 243, 356, 469$  and  $582$  Da for  $x = 1$  to  $5$ ),  $M_xCONH_2$  ( $m/z = 157, 270, 383$  and  $496$  Da for  $x = 1$  to  $4$ ),  $M_xC=NCH_2CH_2$  ( $m/z = 167, 280, 393, 506,$  and  $619$  Da for  $x = 1$  to  $5$ ),  $M_xHC=NCH_2CH_2$  ( $m/z = 168, 281, 394, 507$  and  $620$  Da for  $x = 1$  to  $5$ ) and  $M_xCN$  ( $m/z = 139, 252, 365, 478$  and  $591$  Da for  $x = 1$  to  $5$ ) were detected.



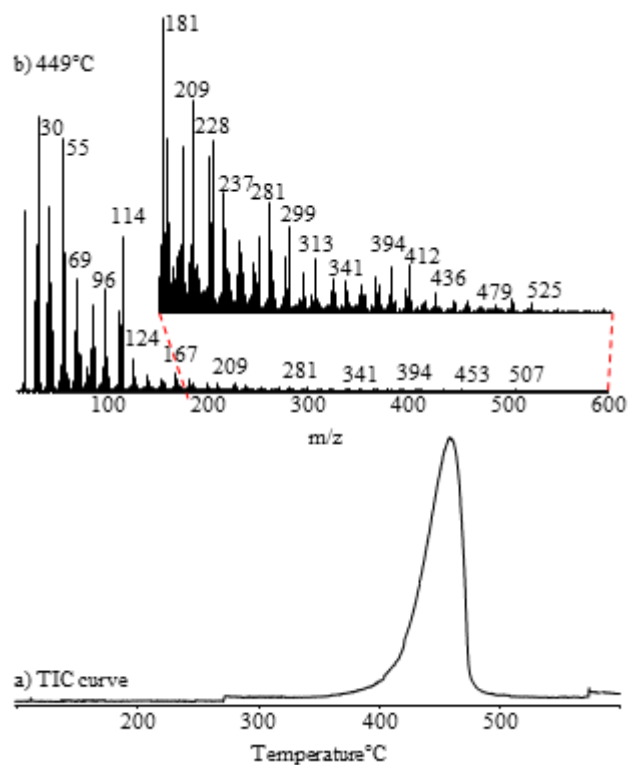


**Figure 3.16.** a) The total ion current curve and b) mass spectrum of PA6 at 449°C.

In Table 3.5, the relative intensities of intense and/or characteristic peaks recorded in the spectrum and the assignments made are summarized.

**Table 3.5.** The relative intensities, RI, of some selected intense and/or characteristic peaks recorded in pyrolysis spectrum of PA6 at 449°C and the assignments made.

m/z	RI	Assignment
18	616	H <sub>2</sub> O
30	1000	CH <sub>2</sub> NH <sub>2</sub>
41	655	C <sub>3</sub> H <sub>5</sub>
42	382	COCH <sub>2</sub> and/or C <sub>3</sub> H <sub>6</sub>
44	225	CONH <sub>2</sub> and/or CO <sub>2</sub>
45	49	CO <sub>2</sub> H
55	896	C <sub>4</sub> H <sub>7</sub>
69	401	C <sub>5</sub> H <sub>9</sub>
84	311	COC <sub>4</sub> H <sub>8</sub>
96	366	C <sub>5</sub> H <sub>10</sub> CN
111	286	C <sub>5</sub> H <sub>10</sub> NHCN
299	10	NCNH(CH <sub>2</sub> ) <sub>5</sub> MC(OH)(NH <sub>2</sub> )NHCH <sub>3</sub>
113	233	M
114	561	MH
227	14	M <sub>2</sub> H
340	3.6	M <sub>3</sub> H
453	1.5	M <sub>4</sub> H
566	0.5	M <sub>5</sub> H
130	8.3	MOH
243	6.3	M <sub>2</sub> OH
356	1.1	M <sub>3</sub> OH
469	0.4	M <sub>4</sub> OH
582	0.1	M <sub>5</sub> OH
139	50	MCN
252	5.6	M <sub>2</sub> CN
365	2.4	M <sub>3</sub> CN
478	0.8	M <sub>4</sub> CN
591	0.3	M <sub>5</sub> CN
157	29	MCONH <sub>2</sub>
270	3.0	M <sub>2</sub> CONH <sub>2</sub>
383	1.9	M <sub>3</sub> CONH <sub>2</sub>
496	0.4	M <sub>4</sub> CONH <sub>2</sub>
167	62	MC=NCH <sub>2</sub> CH <sub>2</sub>
280	3.7	M <sub>2</sub> C=NCH <sub>2</sub> CH <sub>2</sub>
393	1.9	M <sub>3</sub> C=NCH <sub>2</sub> CH <sub>2</sub>
506	0.4	M <sub>4</sub> C=NCH <sub>2</sub> CH <sub>2</sub>
619	0.2	M <sub>5</sub> C=NCH <sub>2</sub> CH <sub>2</sub>

**Table 3.5.** continued

m/z	RI	Assignment
168	41	MHC=NCH <sub>2</sub> CH <sub>2</sub>
281	14	M <sub>2</sub> HC=NCH <sub>2</sub> CH <sub>2</sub>
394	7.2	M <sub>3</sub> HC=NCH <sub>2</sub> CH <sub>2</sub>
507	1.2	M <sub>4</sub> HC=NCH <sub>2</sub> CH <sub>2</sub>
620	0.3	M <sub>5</sub> HC=NCH <sub>2</sub> CH <sub>2</sub>

The single ion pyrograms of all fragment ions showed same trends indicating that thermal decomposition of the polymer took place energetically almost through the same decomposition pathways (Figure 3.17).

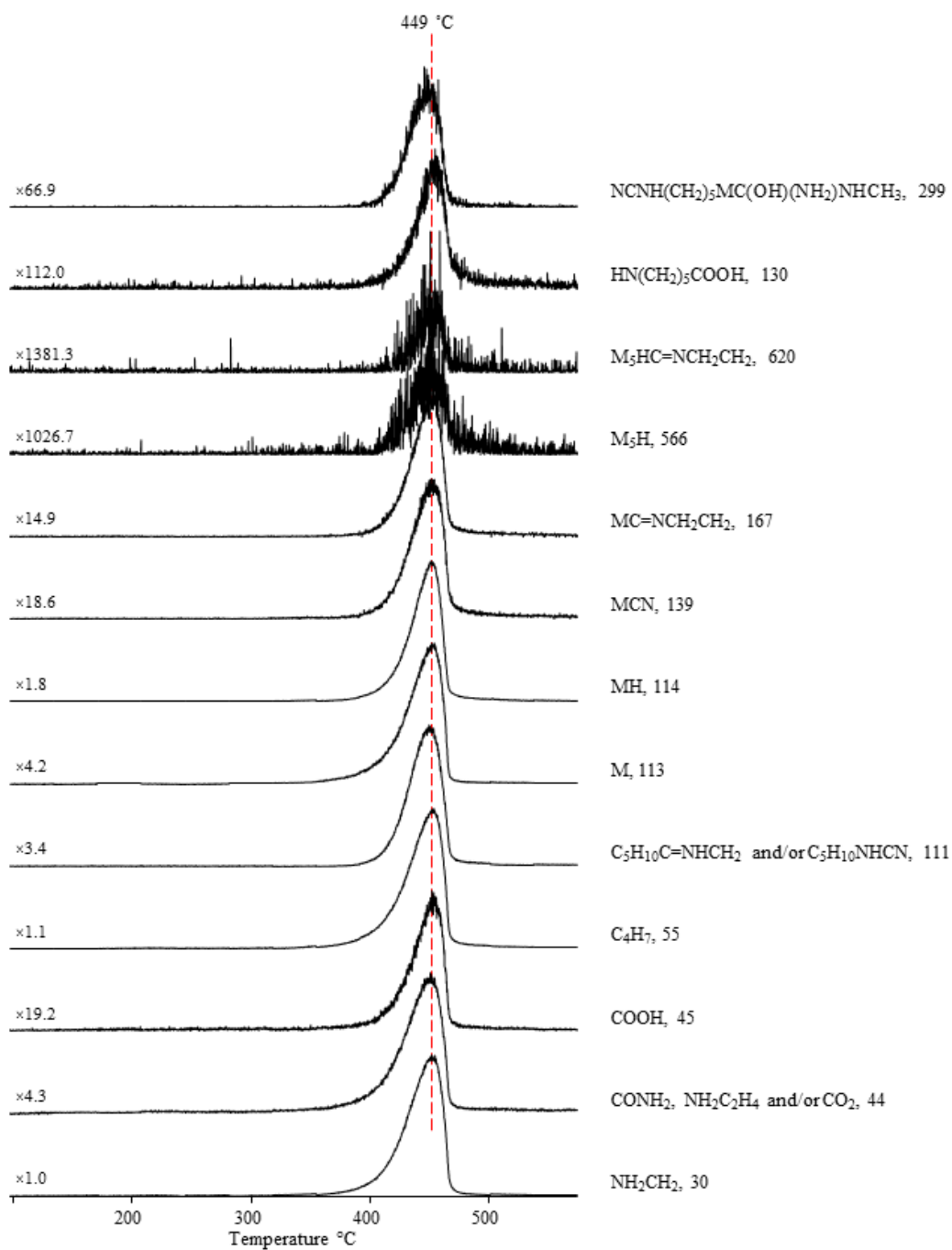
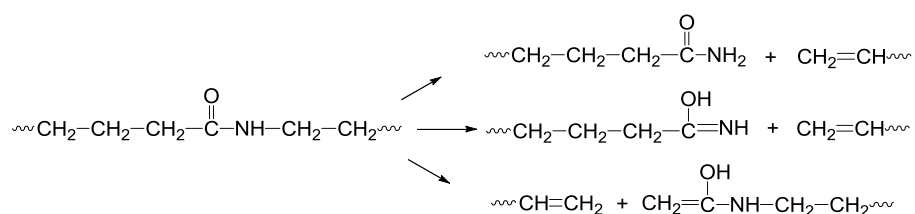


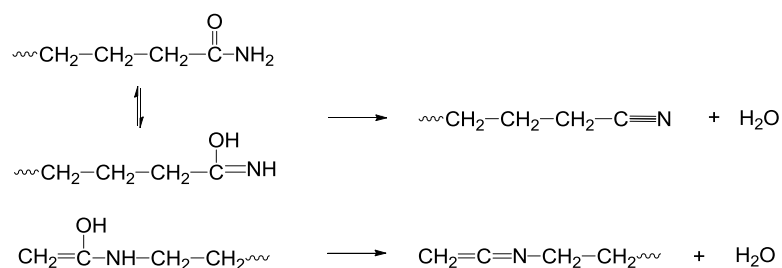
**Figure 3.17.** Single ion pyrograms of some selected fragments detected during the pyrolysis of PA6.

It has been established that caprolactam and cyclic oligomers were mainly generated via different reaction pathways [51-56]. Generations of H<sub>2</sub>O, CO<sub>2</sub> and NH<sub>3</sub> were also noted. During the pyrolysis and/or dissociative ionization processes the protonated monomer and oligomers can be produced by McLafferty type rearrangement reactions or by H-transfer to NH group, as demonstrated in Scheme 3.3. Then by the loss of H<sub>2</sub>O, fragments involving C=N linkages or CN end groups might be produced, as shown in Scheme 3.4 [90].

**Scheme 3.3.** Formation of protonated oligomers.

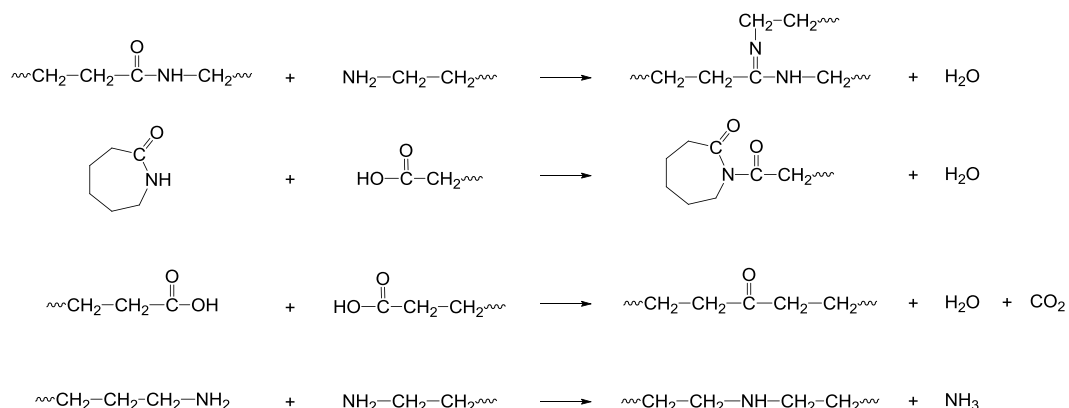


**Scheme 3.4.** Formation of C=N linkages and CN end groups.



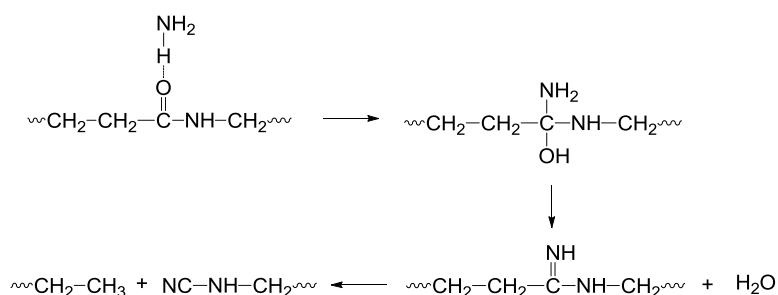
Several reaction pathways of generation of H<sub>2</sub>O, such as intermolecular aminolysis, reaction of caprolactam with the acid end groups, condensation of carboxylic chain ends to yield also CO<sub>2</sub> and condensation of the amine chain ends to yield NH<sub>3</sub> were suggested in the literature (Scheme 3.5) [54].

**Scheme 3.5.** Other possible reaction pathways for the evolution of H<sub>2</sub>O, CO<sub>2</sub> and NH<sub>3</sub>.



Another prospect is the reactions between ammonia and carbonyl groups to give derivatives of imine by evolution of H<sub>2</sub>O and CN end groups by H-transfer reactions (Scheme 3.6) Presence of C<sub>5</sub>H<sub>10</sub>NHCN (m/z = 111) and NCNH(CH<sub>2</sub>)<sub>5</sub>MC(OH)(NH<sub>2</sub>)NHCH<sub>3</sub> (m/z = 299) confirmed the suggested mechanism [90].

**Scheme 3.6.** Nucleophilic attack of NH<sub>3</sub> to carbonyl groups.



Products containing COOH end groups such as  $\text{HN}(\text{CH}_2)_5\text{COOH}$  (130 Da) can be produced by the hydrolysis of PA6 chains (Scheme 3.7) [63].

**Scheme 3.7.** Hydrolysis of PA6.



### 3.2.1. IN THE PRESENCE OF NANOPARTICLES

#### 3.2.1.1. PA6-HNT

As expected, no product was observed during the direct pyrolysis of pure HNT, up to 650°C. In the presence of 3 wt% HNT, pyrolysis of Polyamide 6 yielded a TIC curve with a maximum at around 434°C, indicating that the thermal stability of PA6 chains was decreased in the presence of HNT (Figure 3.18). The pyrolysis mass spectra showed intense peaks at  $m/z = 114, 111, 96, 69, 55, 41, 30$  and 18 Da related with MH,  $\text{C}_5\text{H}_{10}\text{NHCN}$ ,  $\text{C}_5\text{H}_{10}\text{CN}$ ,  $\text{C}_5\text{H}_9$ ,  $\text{C}_4\text{H}_7$ ,  $\text{C}_3\text{H}_5$ ,  $\text{CH}_2\text{NH}_2$  and  $\text{H}_2\text{O}$ , respectively, mostly by dissociative ionization of the monomer and oligomers.

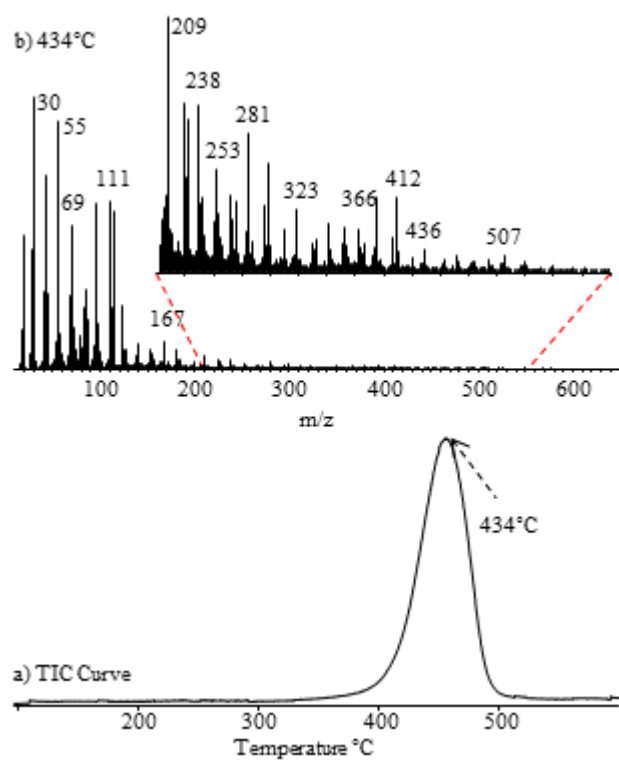


**Figure 3.18.** a) The total ion current curve and b) mass spectrum of PA6-HNT at 434°C.

In Table 3.6, the relative intensities of intense and/or characteristic peaks recorded in the spectrum and the assignments made are summarized.



**Table 3.6.** The relative intensities, RI, of some selected intense and/or characteristic peaks recorded in pyrolysis spectrum of PA6-HNT at 434°C and the assignments made.

m/z	RI	Assignment
18	495	H <sub>2</sub> O
30	1000	CH <sub>2</sub> NH <sub>2</sub>
41	712	C <sub>3</sub> H <sub>5</sub>
42	391	COCH <sub>2</sub> and/or C <sub>3</sub> H <sub>6</sub>
44	274	CONH <sub>2</sub> and/or CO <sub>2</sub>
45	35	CO <sub>2</sub> H
55	913	C <sub>4</sub> H <sub>7</sub>
69	529	C <sub>5</sub> H <sub>9</sub>
84	290	COC <sub>4</sub> H <sub>8</sub>
96	608	C <sub>5</sub> H <sub>10</sub> CN
111	620	C <sub>5</sub> H <sub>10</sub> NHCN
299	21	NCNH(CH <sub>2</sub> ) <sub>5</sub> MC(OH)(NH <sub>2</sub> )NHCH <sub>3</sub>
113	226	M
114	580	MH
139	96	MCN
167	101	MC=NCH <sub>2</sub> CH <sub>2</sub>
566	0.4	M <sub>5</sub> H
620	0.5	M <sub>5</sub> HC=NCH <sub>2</sub> CH <sub>2</sub>
130	7.5	MOH
243	6.1	M <sub>2</sub> OH
356	1.4	M <sub>3</sub> OH
469	0.5	M <sub>4</sub> OH
582	0.2	M <sub>5</sub> OH

Most of the diagnostic fragments noted during the degradation of neat Polyamide 6 followed almost same evolution profiles when produced during the degradation of PA6-HNT (Figure 3.19). However, in the presence of HNT, thermal decomposition of PA6 was shifted to lower temperatures. Also, some distinctions were noticed in the evolution profiles of hydrolysis and aminolysis fragments. In the presence of HNT, the relative yields of the products generated by aminolysis reactions such as C<sub>5</sub>H<sub>10</sub>NHCN (m/z = 111 Da) and NCNH(CH<sub>2</sub>)<sub>5</sub>MC(OH)(NH<sub>2</sub>)NHCH<sub>3</sub> (m/z = 299 Da), were enhanced about 2.1 and 1.6 folds respectively. In addition, the evolution profiles of these fragments shifted slightly to lower temperatures. This indicates that HNT enhance the

possibility of the interactions among carbonyl groups and ammonia (Scheme 3.6) [90]. Actually, as a result of the enhancement in the aminolysis reactions, the relative yield of H<sub>2</sub>O should also be enhanced. On the contrary, reduction in the evolution of H<sub>2</sub>O was noticed. The enhancement in the relative yields of fragments including COOH end groups such as NH(CH<sub>2</sub>)<sub>5</sub>COOH (130 Da), M<sub>x</sub>NH(CH<sub>2</sub>)<sub>5</sub>COOH (m/z = 243, 356, 469 and 582 Da for x = 1 to 4) that may also be formed by hydrolysis of PA6 chains, may be a possible reason. Moreover, the evolution of these fragments was maximized at slightly elevated temperatures, at around 446°C.

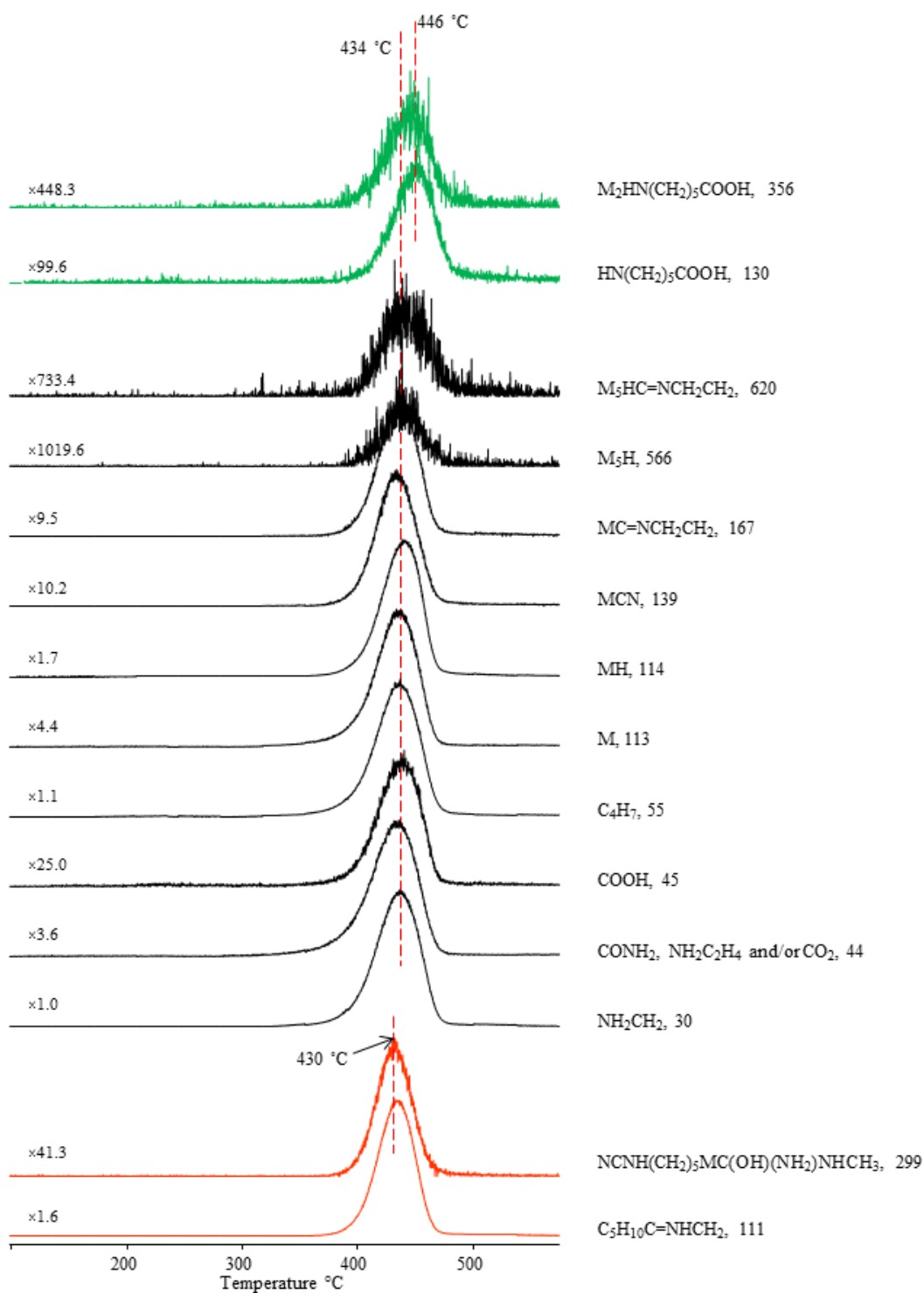


**Figure 3.19.** Single ion pyrograms of some selected fragments detected during the pyrolysis of PA6-HNT.

### 3.2.1.2. PA6-MMT25A

In the presence of MMT25A (3 wt%), pyrolysis of PA6 yielded a TIC curve with a maximum at around 449°C (Figure 3.20). The pyrolysis mass spectra again showed intense peaks at  $m/z = 114, 96, 84, 69, 55, 41, 30$  and 18 Da related with  $\text{MH}, \text{C}_5\text{H}_{10}\text{CN}, \text{C}_4\text{H}_8\text{CO}, \text{C}_5\text{H}_9, \text{C}_4\text{H}_7, \text{C}_3\text{H}_5, \text{CH}_2\text{NH}_2$  and  $\text{H}_2\text{O}$ , respectively. In Table 3.7, the relative intensities intense and/or characteristic peaks recorded in the spectrum and the assignments made are summarized.

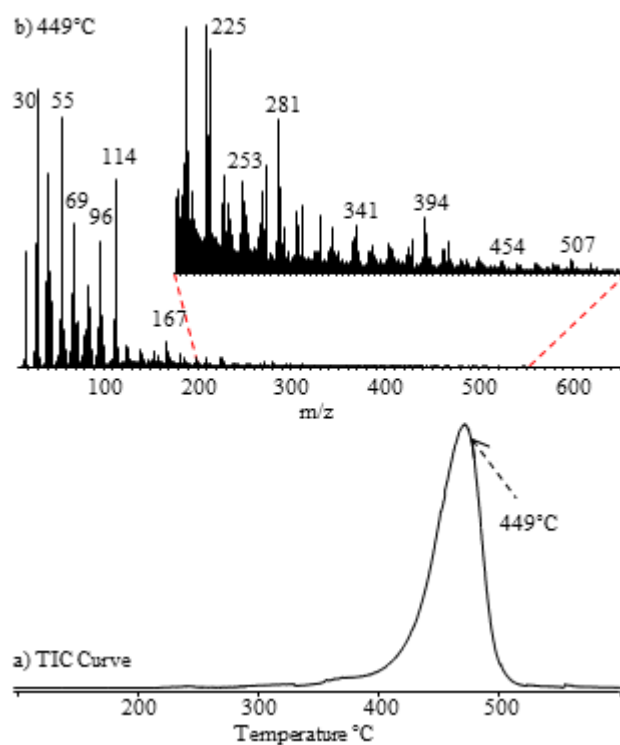


**Figure 3.20.** a) The total ion current curve and b) mass spectrum of PA6-MMT25A at 449°C.

**Table 3.7.** The relative intensities, RI, of some selected intense and/or characteristic peaks recorded in pyrolysis spectrum of PA6-MMT25A at 345 and 449°C and the assignments made.

m/z	RI		Assignment
	345 °C	449°C	
18		414	H <sub>2</sub> O
30		1000	CH <sub>2</sub> NH <sub>2</sub>
41		697	C <sub>3</sub> H <sub>5</sub>
42		342	COCH <sub>2</sub> and/or C <sub>3</sub> H <sub>6</sub>
44		235	CONH <sub>2</sub> and/or CO <sub>2</sub>
45		57	CO <sub>2</sub> H
55		901	C <sub>4</sub> H <sub>7</sub>
69		515	C <sub>5</sub> H <sub>9</sub>
84		290	COC <sub>4</sub> H <sub>8</sub>
96		455	C <sub>5</sub> H <sub>10</sub> CN
111		168	C <sub>5</sub> H <sub>10</sub> NHCN
113		221	M
114		675	MH
130		16	MOH
139		61	MCN
167		92	MC=NCH <sub>2</sub> CH <sub>2</sub>
299		10	NCNH(CH <sub>2</sub> ) <sub>5</sub> MC(OH)(NH <sub>2</sub> )NHCH <sub>3</sub>
566		0.7	M <sub>5</sub> H
620		0.2	M <sub>5</sub> HC=NCH <sub>2</sub> CH <sub>2</sub>
58	158	84	(CH <sub>3</sub> ) <sub>2</sub> NCH <sub>2</sub> and/or C <sub>4</sub> H <sub>10</sub>
269	12	4.9	NC <sub>19</sub> H <sub>27</sub>
297	20	3.7	NC <sub>21</sub> H <sub>31</sub>

Single ion pyrograms of some of the characteristic products are shown in Figure 3.21. The trends noticed in the evolution profiles of thermal decomposition fragments of Polyamide 6 were almost same to those analyzed for PA6-HNT. The fragments with m/z values 111 and 299 Da that were related with products produced by interactions of NH<sub>3</sub> and carbonyl groups, and hydrolysis products demonstrated same trends with those noted for PA6-HNT. Yet their relative yields were changed noticeably. Contrary to what was observed for PA6-HNT, reduction in the yields of fragments produced by aminolysis reactions of PA6, thus, decrease in the yield of H<sub>2</sub>O was recorded. Significant reduction in the yield of fragments,

produced by aminolysis reactions,  $(\text{CH}_2)_5\text{NHCN}$  (111 Da) and  $\text{NCNH}(\text{CH}_2)_5\text{MC}(\text{OH})(\text{NH}_2)\text{NHCH}_3$  (299 Da) was observed, about 1.6 and 1.4 folds respectively compare to pure PA6. On the other hand, the enhancement in the relative yields of products including COOH end groups such as,  $\text{CO}_2$  (44 Da),  $\text{COOH}$  (45 Da) and  $\text{HN}(\text{CH}_2)_5\text{COOH}$  (130 Da), that may also be formed by hydrolysis of PA6 chains, was observed. Drastic increase was noted in the relative yields of  $\text{HN}(\text{CH}_2)_5\text{COOH}$  (130 Da), about 2.1 folds compare to neat PA6. That may be another possible cause of the decrease in the yield of  $\text{H}_2\text{O}$ .

Typical thermal decomposition fragments of MMT25A were started to show up in the pyrolysis mass spectra at around  $220^\circ\text{C}$  and were maximized at around  $345^\circ\text{C}$ . Therefore, it can be concluded that the decomposition of MMT25A was shifted to elevated temperatures in the presence of PA6 (Section 3.1.1.2). Therefore, it can be concluded that the thermal stability of MMT25A was enhanced slightly due to the interactions with PA6. On the other hand thermal stability of PA6 did not influenced by the presence of MMT25A.

The pyrolysis mass spectra recorded at around  $345^\circ\text{C}$  was dominated by typical peaks of MMT25A such as 58, 269 and 297 Da associated with  $(\text{CH}_3)_2\text{NCH}_2$ ,  $\text{NC}_{19}\text{H}_{27}$  and  $\text{NC}_{21}\text{H}_{31}$ , respectively. However, due to the similarity between the structures, contribution of thermal decomposition fragments of PA6 especially around  $449^\circ\text{C}$  have to be considered (Figure 3.21).

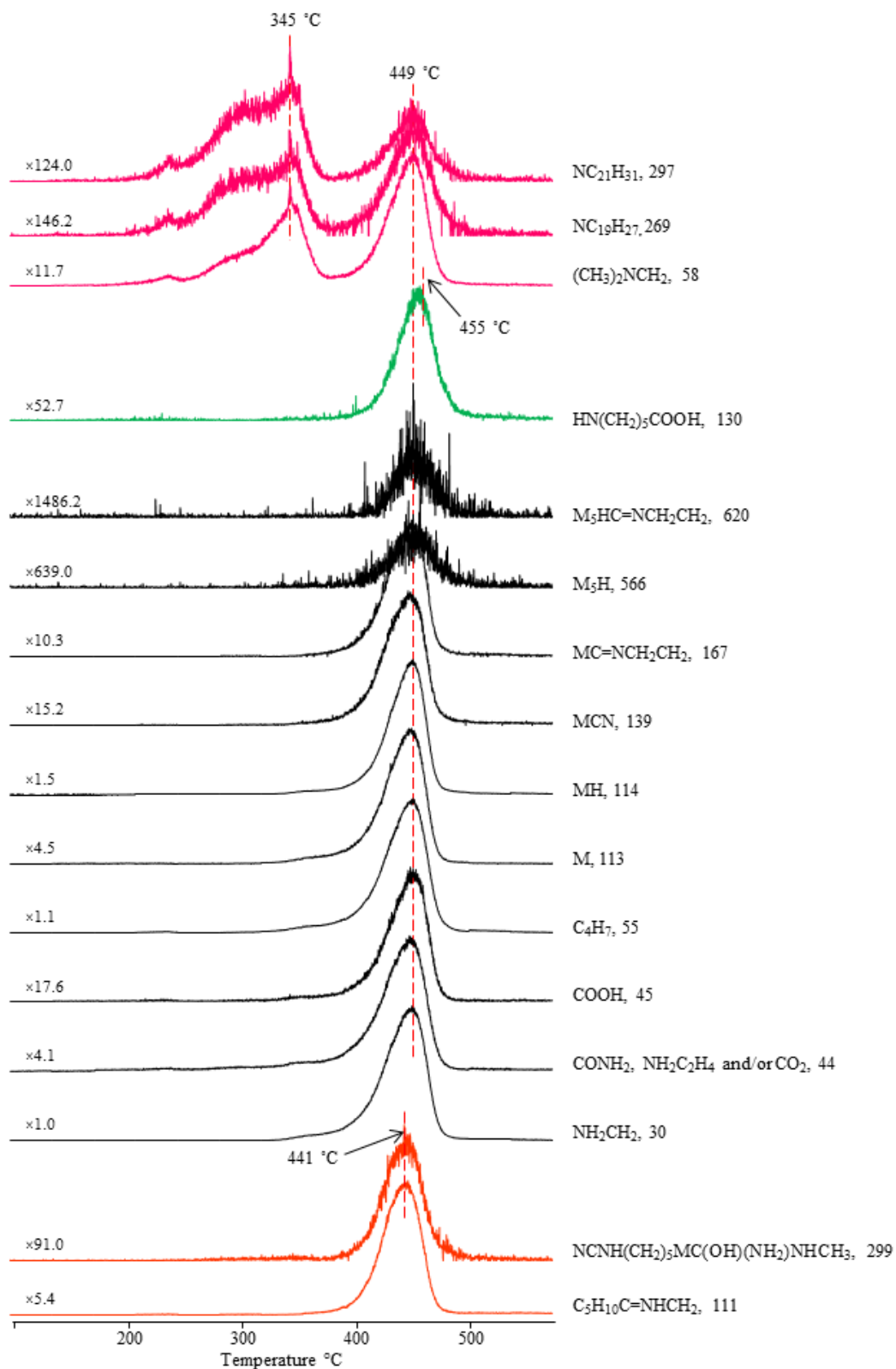


**Figure 3.21.** Single ion pyrograms of some selected fragments detected during the pyrolysis of PA6-MMT25A.

### 3.2.1.3. PA6-MMT30B

In the presence of MMT30B (3 wt%), pyrolysis of PA6 yielded a TIC curve with a maximum at around 455°C (Figure 3.22). The pyrolysis mass spectra showed intense peaks at  $m/z = 114, 96, 84, 69, 55, 41, 30$  and  $18$  Da related with  $MH, C_5H_{10}CN, C_4H_8CO, C_5H_9, C_4H_7, C_3H_5, CH_2NH_2$  and  $H_2O$ , respectively. In Table 3.8, the relative intensities of some of the intense and/or characteristic peaks recorded in the spectrum and the assignments made are summarized.

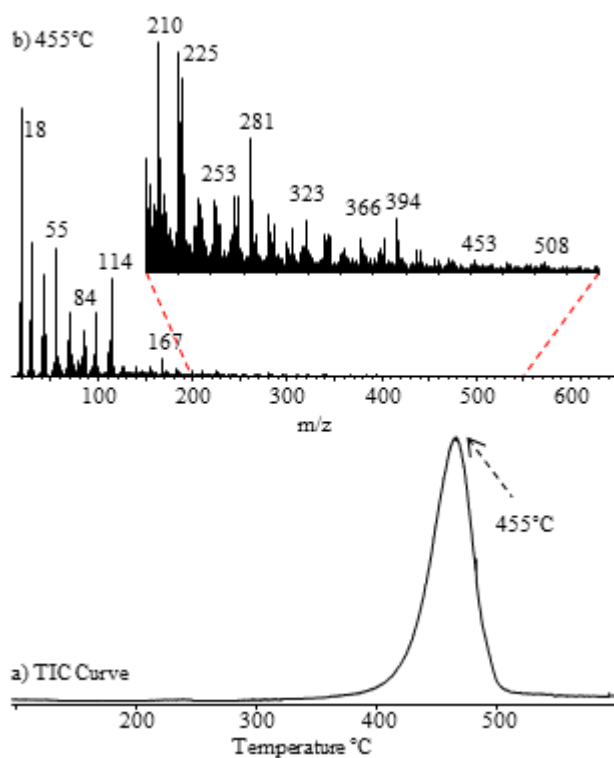


**Figure 3.22.** a) The total ion current curve and b) mass spectrum of PA6-MMT30B at 455°C.



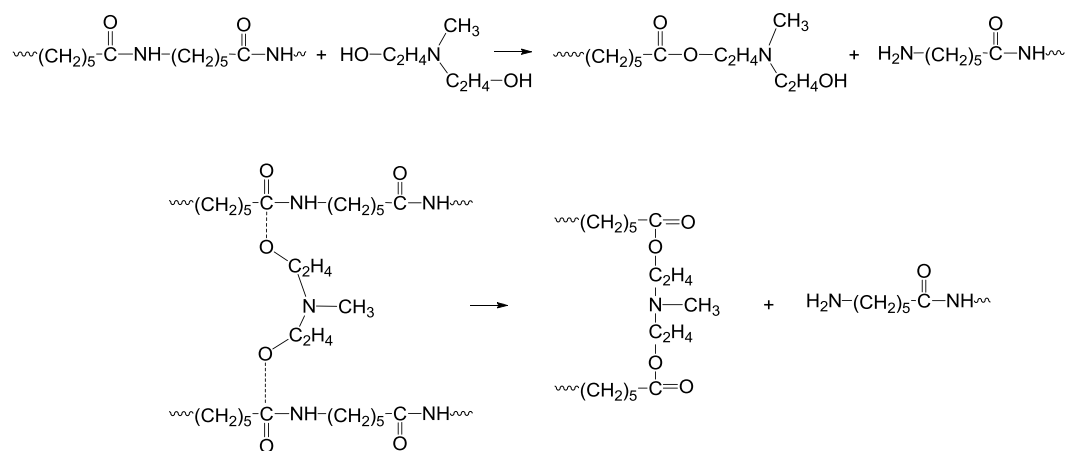
**Table 3.8.** The relative intensities, RI, of some selected intense and/or characteristic peaks recorded in pyrolysis spectrum of PA6-MMT30B at 292 and 455 °C and the assignments made

m/z	RI		Assignment
	292 °C	455 °C	
18		1000	H <sub>2</sub> O
30		497	CH <sub>2</sub> NH <sub>2</sub>
41		376	C <sub>3</sub> H <sub>5</sub>
42		199	COCH <sub>2</sub> and/or C <sub>3</sub> H <sub>6</sub>
44		155	CONH <sub>2</sub> and/or CO <sub>2</sub>
45		27	CO <sub>2</sub> H
55		480	C <sub>4</sub> H <sub>7</sub>
69		240	C <sub>5</sub> H <sub>9</sub>
84		170	COC <sub>4</sub> H <sub>8</sub>
96		236	C <sub>5</sub> H <sub>10</sub> CN
111		86	C <sub>5</sub> H <sub>10</sub> NHCN
113		130	M
114		365	MH
130		9.0	MOH
139		37	MCN
167		72	MC=NCH <sub>2</sub> CH <sub>2</sub>
299		4.2	NCNH(CH <sub>2</sub> ) <sub>5</sub> MC(OH)(NH <sub>2</sub> )NHCH <sub>3</sub>
566		0.4	M <sub>5</sub> H
620		0.2	M <sub>5</sub> HC=NCH <sub>2</sub> CH <sub>2</sub>
58	10.9	43	(CH <sub>3</sub> ) <sub>2</sub> NCH <sub>2</sub> and/or C <sub>4</sub> H <sub>10</sub>
88	9.2	7.1	CH <sub>2</sub> N(C <sub>2</sub> H <sub>4</sub> OH)CH <sub>3</sub>
268		6.7	N(C <sub>2</sub> H <sub>4</sub> OH) <sub>2</sub> C <sub>12</sub> H <sub>20</sub> and/or COOC <sub>2</sub> H <sub>4</sub> N(CH <sub>3</sub> )C <sub>2</sub> H <sub>4</sub> OH
296		3.5	N(C <sub>2</sub> H <sub>4</sub> OH) <sub>2</sub> C <sub>14</sub> H <sub>24</sub> and/or C <sub>2</sub> H <sub>4</sub> COOC <sub>2</sub> H <sub>4</sub> N(CH <sub>3</sub> )C <sub>2</sub> H <sub>4</sub> OH

The pyrolysis mass spectra detected at around 236 and 292 °C was dominated by typical peaks of MMT30B; yet, significant differences in the relative intensities of diagnostic peaks were noticed, indicating presence of some interactions among MMT30B and PA6 (Figure 3.23). Generation of units involving CO-OC<sub>2</sub>H<sub>4</sub>N may be proposed by trans-esterification reactions between the PA6 and hydroxy ethylene groups of ammonium salt, as shown in Scheme 3.8. Slight enhancement in the intensity of the peak at 297 Da due to C<sub>2</sub>H<sub>4</sub>COOC<sub>2</sub>H<sub>4</sub>N(CH<sub>3</sub>)C<sub>2</sub>H<sub>4</sub>OH may be thought as a direct evidence for this proposed mechanism. In addition,

diagnostic peaks of PA6 were recorded at around 455°C, slightly elevated temperature than the related value for the pure polymer. Incorporation of MMT 30B increased thermal stability of PA6 chains slightly.

**Scheme 3.8.** Trans-esterification reactions between the modifier of MMT and PA6.



Single ion pyrograms of characteristic fragments such as  $\text{CH}_2\text{NH}_2$  (30 Da),  $\text{CO}_2$  (44 Da),  $\text{COOH}$  (45 Da),  $\text{HN(CH}_2)_5\text{COOH}$  (130 Da),  $\text{MC=NCH}_2\text{CH}_2$  (167 Da),  $\text{C}_5\text{H}_{10}\text{NHCN}$  (111 Da) and  $\text{NCNH(CH}_2)_5\text{MC(OH)(NH}_2\text{)NHCH}_3$  (299 Da) are given in Figure 3.23.

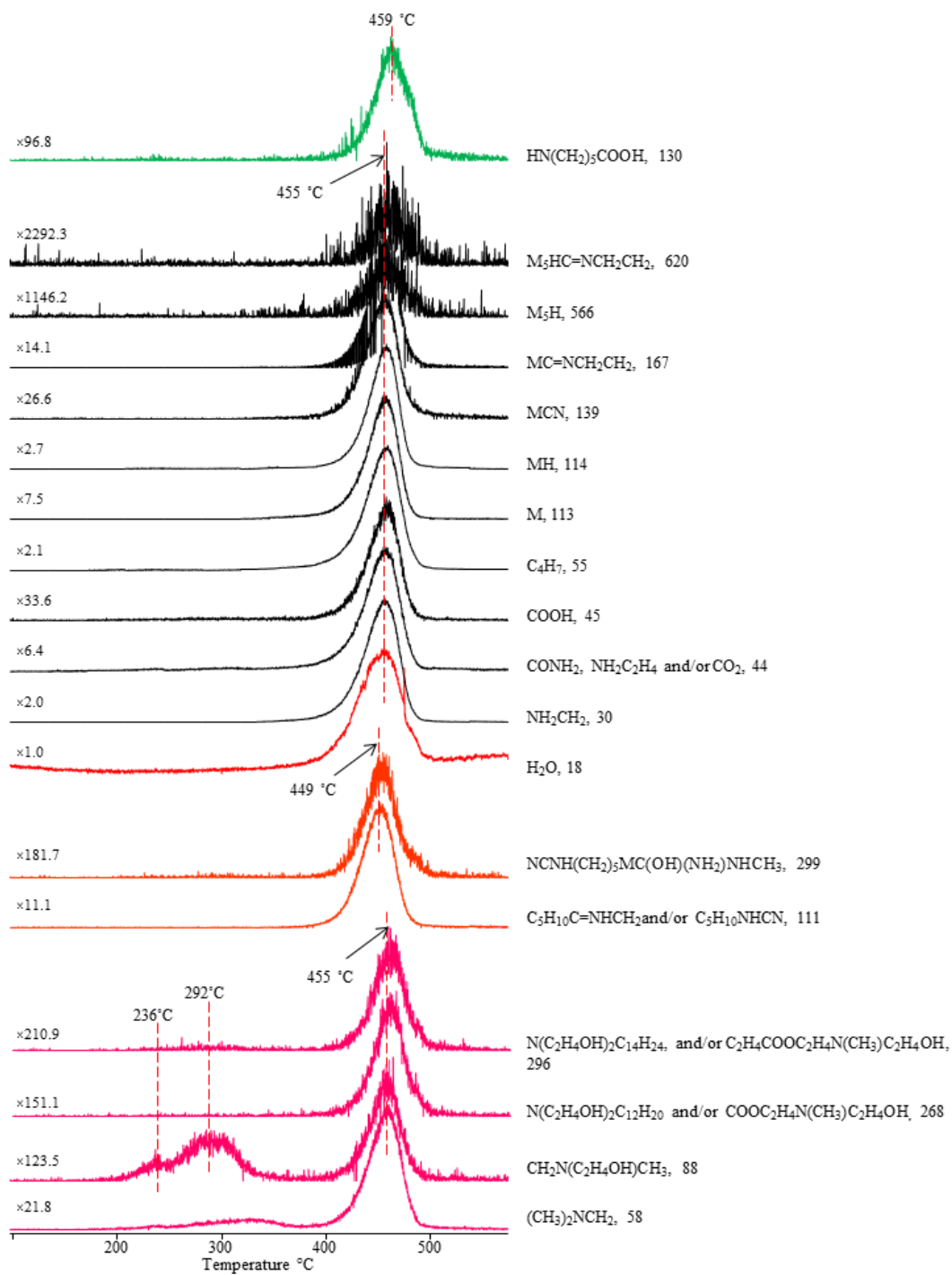


**Figure 3.23.** Single ion pyrograms of some selected fragments detected during the pyrolysis of PA6-MMT30B.

The trends recognized in the evolution profiles of thermal decomposition fragments of PA6 were same to those recorded for PA6-MMT25A. The fragments with  $m/z$  values 111 and 299 Da that were related with products produced by interactions of  $\text{NH}_3$  and carbonyl groups, and hydrolysis products showed same trends with those recorded for PA6-MMT25A. However, in the presence of MMT30B the pyrolysis mass spectra showed base peak due to  $\text{H}_2\text{O}$  evolution. In addition, contrary to what were observed in the presence of HNT and MMT25A, the relative yields of almost all products was enhanced except those of the fragments generated by aminolysis reactions such as the fragments with  $m/z$  values of 111 and 299 Da. As in the case of PA-MMT25A, a noticeable reduction in the yield of these fragments was observed, about 1.4 and 1.6 folds respectively.

Although there was a reduction in the yields of aminolysis products, evolution of  $\text{H}_2\text{O}$  was noticeably pronounced. In addition, the yield of fragments generated by hydrolysis of PA6 such as,  $\text{HN}(\text{CH}_2)_5\text{COOH}$  (130 Da),  $\text{CO}_2$  (44 Da) and  $\text{COOH}$  (45 Da) were increased. The enhancement was about 2.3 folds for 130 Da.

Typical thermal decomposition fragments of MMT30B were started to show up in the pyrolysis mass spectra at around  $200^\circ\text{C}$  and were maximized at around  $292^\circ\text{C}$ . Therefore, it can be concluded that the decomposition of MMT30B ( $279^\circ\text{C}$ ) shifted to elevated temperatures in the presence of PA6 (Section 3.1.1.3). The high temperature slight may be explained by trans-esterification reactions between the PA6 and MMT30B (Scheme 3.8). Therefore, it can be concluded that the thermal stability of MMT30B was increased because of the interactions with PA6.

When the weight % of MMT30B was increased to 5 wt%, the maximum in the TIC curve was recorded at around  $457^\circ\text{C}$ , almost identical to what was observed for the sample involving 3 wt% MMT30B. The pyrolysis mass spectra showed again intense peaks at  $m/z = 114, 96, 84, 69, 55, 41, 30$  and 18 Da related with  $\text{MH}$ ,  $\text{C}_5\text{H}_{10}\text{CN}$ ,  $\text{C}_4\text{H}_8\text{CO}$ ,  $\text{C}_5\text{H}_9$ ,  $\text{C}_4\text{H}_7$ ,  $\text{C}_3\text{H}_5$ ,  $\text{CH}_2\text{NH}_2$  and  $\text{H}_2\text{O}$ , respectively as in the case of 3 wt% MMT30B addition of PA6.

The addition of 3 wt% and 5 wt% MMT30B to PA6 did not show any noticeable influence on the thermal degradation of PA-MMT30B nanocomposite. Almost all single ion evolution profiles showed similar trend. However, generation of H<sub>2</sub>O was noticed in the same temperature region with fragments produced by aminolysis reactions in the presence of 5 wt% MMT30B. These products showed identical evolution profiles and maximized at lower temperatures pointing out increase in intermolecular interactions among the PA6 chains in the presence of higher wt% nanoclay.

### **3.2.2 IN THE PRESENCE OF FLAME RETARDANT, AlPi**

In the presence of 20 wt% AlPi, pyrolysis of PA6 yielded a TIC curve with a maximum at around 433°C (Figure 3.24). The pyrolysis mass spectra showed intense peaks at  $m/z = 114, 111, 96, 84, 55, 41, 30$  and 18 Da related with MH, C<sub>5</sub>H<sub>10</sub>NHCN, C<sub>5</sub>H<sub>10</sub>CN, C<sub>4</sub>H<sub>8</sub>CO, C<sub>4</sub>H<sub>7</sub>, C<sub>3</sub>H<sub>5</sub>, CH<sub>2</sub>NH<sub>2</sub> and H<sub>2</sub>O, respectively. The single ion evolution profiles of PA6 based products were almost identical to those noted during the degradation of PA6 (Figure 3.17). Nevertheless, a significant increase in the relative yield of monomer compared to diagnostic degradation fragments was noted. The ratios of peak intensities due to M/CH<sub>2</sub>NH<sub>2</sub> were 4.2 for PA6 and 1.7 for PA6-AlPi respectively. Also base peak was changed to 55 Da due to C<sub>4</sub>H<sub>7</sub>. In addition typical fragmentation pattern of AlPi, intense peaks at  $m/z = 65, 94, 269,$  and 660 Da due to P(OH)<sub>2</sub>, C<sub>2</sub>H<sub>5</sub>P(OH)<sub>2</sub>, (C<sub>2</sub>H<sub>5</sub>)<sub>2</sub>PO<sub>2</sub>AlO<sub>2</sub>P(C<sub>2</sub>H<sub>5</sub>)<sub>2</sub> and HAl<sub>2</sub>(O<sub>2</sub>P(C<sub>2</sub>H<sub>5</sub>)<sub>2</sub>)<sub>5</sub> respectively, were observed in the pyrolysis mass spectra recorded at around 429°C.

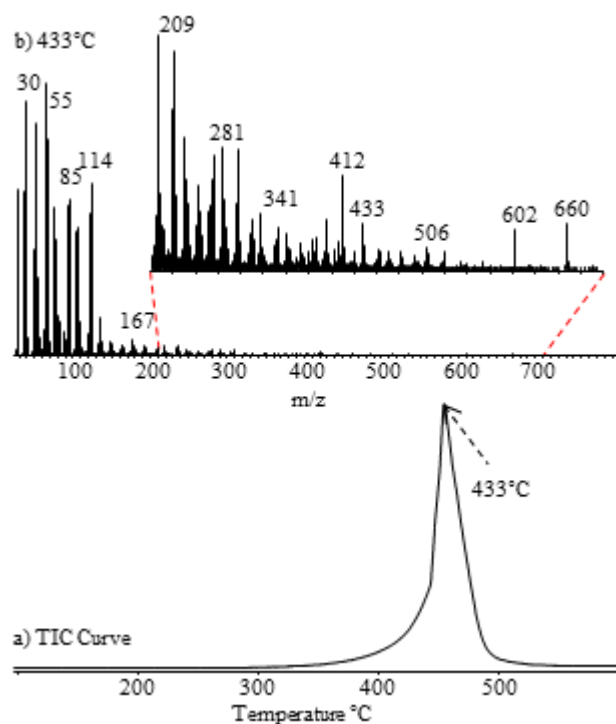


**Figure 3.24.** a) The total ion current curve and b) mass spectrum of PA6-AlPi at 433°C.

In Table 3.9, the relative intensities of intense and/or characteristic peaks recorded in the spectrum and the assignments made are summarized.

**Table 3.9.** The relative intensities, RI, of some selected intense and/or characteristic peaks recorded in pyrolysis spectrum of PA6-ALPi at 433°C and the assignments made.

m/z	RI	Assignment
17	143	OH and/or NH <sub>3</sub>
18	614	H <sub>2</sub> O
30	938	CH <sub>2</sub> NH <sub>2</sub>
41	858	C <sub>3</sub> H <sub>5</sub>
42	643	COCH <sub>2</sub> and/or C <sub>3</sub> H <sub>6</sub>
44	286	CONH <sub>2</sub> and/or CO <sub>2</sub>
45	39	CO <sub>2</sub> H
55	1000	C <sub>4</sub> H <sub>7</sub>
69	425	C <sub>5</sub> H <sub>9</sub>
84	549	COC <sub>4</sub> H <sub>8</sub>
96	470	C <sub>5</sub> H <sub>10</sub> CN
111	387	C <sub>5</sub> H <sub>10</sub> NHCN
113	525	M
114	637	MH
130	5.0	MOH
139	54	MCN
167	54	MC=NCH <sub>2</sub> CH <sub>2</sub>
299	20	NCNH(CH <sub>2</sub> ) <sub>5</sub> MC(OH)(NH <sub>2</sub> )NHCH <sub>3</sub>
566	1.2	M <sub>5</sub> H
620	0.5	M <sub>5</sub> HC=NCH <sub>2</sub> CH <sub>2</sub>
65	545	P(OH) <sub>2</sub>
94	459	C <sub>2</sub> H <sub>5</sub> P(OH) <sub>2</sub>
98	125	H <sub>3</sub> PO <sub>4</sub>
169	10	(C <sub>2</sub> H <sub>5</sub> PO) <sub>2</sub> OH
269	15	(C <sub>2</sub> H <sub>5</sub> ) <sub>2</sub> PO <sub>2</sub> AlO <sub>2</sub> P(C <sub>2</sub> H <sub>5</sub> ) <sub>2</sub>
404	3.3	OAl <sub>2</sub> (O <sub>2</sub> PC <sub>2</sub> H <sub>5</sub> )(O <sub>2</sub> P(C <sub>2</sub> H <sub>5</sub> ) <sub>2</sub> ) <sub>2</sub>
660	7.5	HAAl <sub>2</sub> (O <sub>2</sub> P(C <sub>2</sub> H <sub>5</sub> ) <sub>2</sub> ) <sub>5</sub>

Single ion pyrograms of some of the characteristic products are shown in Figure 3.25. In the presence of AlPi, the pyrolysis mass spectra showed most intense peak 55 Da due to  $C_4H_7$ . The relative yields of almost all products were enhanced in the presence of AlPi. Although, degradation of PA6 chains was started almost at same temperatures as the neat PA6, the yields were maximized significantly at lower temperatures and the decomposition was completed over a small temperature interval. Therefore, it can be concluded that the thermal stability of PA6 chains were reduced and the rate of depolymerization was increased in the presence of AlPi.

An enhancement in the relative yields of the fragments generated by aminolysis reactions, by intermolecular interactions of  $NH_3$  and carbonyl groups, such as  $NCNH(CH_2)_5MC(OH)(NH_2)NHCH_3$  (299 Da) and  $C_5H_{10}NHCN$  (111 Da) was also observed (Scheme 3.6). The relative yield of  $C_5H_{10}NHCN$  was increased about 1.5 folds in the presence of AlPi. Moreover, these fragments showed identical evolution profiles with those of almost all other thermal degradation of PA6 based products as in the case of neat PA6.

However, the relative yields of fragments including COOH end groups such as  $NH(CH_2)_5COOH$  (130 Da) and COOH (45 Da) were decreased about 1.7 and 1.3 folds, respectively. Moreover, the relative yields of fragments including C=N linkages and CN end groups such as  $MC=NCH_2CH_2$  (167 Da) and  $M_3HC=NCH_2CH_2$  (620 Da) were also decreased slightly. This situation may be thought as a direct evidence for the change in thermal decomposition pathways of PA6 in the presence of AlPi.

The pyrolysis mass spectra recorded at around 425 and 429°C was dominated by typical peaks of AlPi; yet, significant differences in the relative intensities of diagnostic peaks were noticed, indicating presence of some interactions among AlPi and PA6 (Figure 3.25). In the presence of PA6, decomposition of AlPi retarded but decomposition was completed over a small temperature interval, pointing out the increase in decomposition rate (Section 3.1.2).



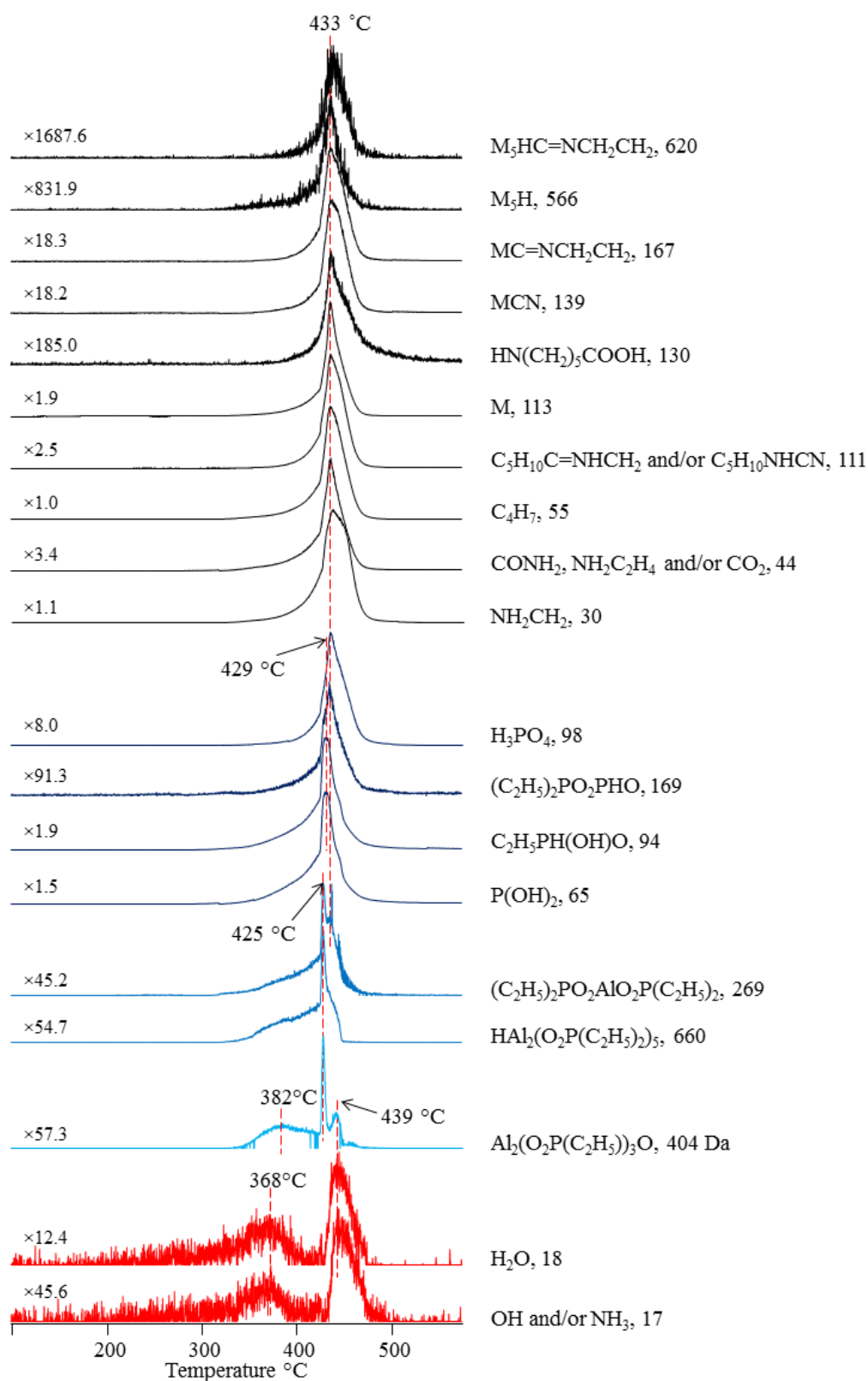


**Figure 3.25.** Single ion pyrograms of some selected fragments detected during the pyrolysis of PA6-AlPi

### 3.2.3 IN THE PRESENCE OF FLAME RETARDANCE AND NANOPARTICLES

#### 3.2.3.1. PA6-AlPi-HNT

In the presence of HNT (3 wt%) and AlPi (17 wt%), pyrolysis of PA6 yielded a TIC curve with a maximum at around 438°C (Figure 3.26). Typical fragmentation pattern of PA6, intense peaks at  $m/z = 114, 113, 111, 96, 84, 55, 41, 30$  and 18 Da due to MH, M,  $C_5H_{10}NHCN$ ,  $C_5H_{10}CN$ ,  $C_5H_{10}NHCN$ ,  $C_5H_{10}CN$ ,  $C_4H_7$ ,  $C_3H_5$ ,  $CH_2NH_2$  and  $H_2O$ , respectively, was observed in the pyrolysis mass spectra recorded at 438°C. In addition typical fragmentation pattern of AlPi, intense peaks at  $m/z = 65, 94, 269,$  and 660 Da due to  $P(OH)_2$ ,  $C_2H_5P(OH)_2$ ,  $(C_2H_5)_2PO_2AlO_2P(C_2H_5)_2$  and  $HAl_2(O_2P(C_2H_5)_2)_5$  respectively, were observed in the pyrolysis mass spectra recorded at around 434 °C.

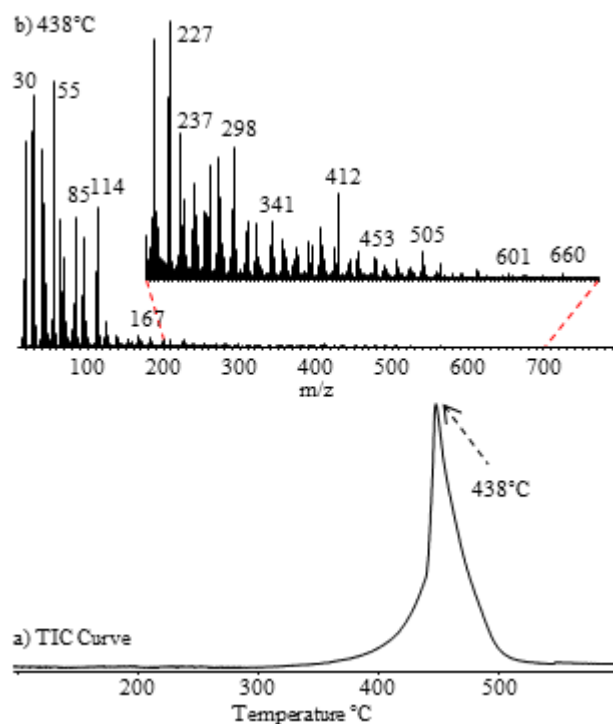


**Figure 3.26.** a) The total ion current curve and b) mass spectrum of PA6-AlPi-HNT at 438°C.

In Table 3.10, the relative intensities of intense and/or characteristic peaks recorded in the spectrum and the assignments made are summarized.

**Table 3.10.** The relative intensities, RI, of some selected intense and/or characteristic peaks recorded in pyrolysis spectrum of PA6-AlPi-HNT at 438°C and the assignments made.

m/z	RI	Assignment
17	256	OH and/or NH <sub>3</sub>
18	779	H <sub>2</sub> O
30	950	CH <sub>2</sub> NH <sub>2</sub>
41	745	C <sub>3</sub> H <sub>5</sub>
42	542	COCH <sub>2</sub> and/or C <sub>3</sub> H <sub>6</sub>
44	239	CONH <sub>2</sub> and/or CO <sub>2</sub>
45	32	CO <sub>2</sub> H
55	1000	C <sub>4</sub> H <sub>7</sub>
69	334	C <sub>5</sub> H <sub>9</sub>
84	454	COC <sub>4</sub> H <sub>8</sub>
96	343	C <sub>5</sub> H <sub>10</sub> CN
113	451	M
114	523	MH
111	282	C <sub>5</sub> H <sub>10</sub> NHCN
298	14	NCNH(CH <sub>2</sub> ) <sub>5</sub> MC(OH)(NH <sub>2</sub> )NHCH <sub>2</sub>
566	1.0	M <sub>5</sub> H
130	3.5	MOH
243	3.1	M <sub>2</sub> OH
356	2.3	M <sub>3</sub> OH
469	0.3	M <sub>4</sub> OH
582	0.3	M <sub>5</sub> OH
139	40	MCN
252	9.5	M <sub>2</sub> CN
365	2.1	M <sub>3</sub> CN
167	40	MC=NCH <sub>2</sub> CH <sub>2</sub>
280	13	M <sub>2</sub> C=NCH <sub>2</sub> CH <sub>2</sub>
393	2.5	M <sub>3</sub> C=NCH <sub>2</sub> CH <sub>2</sub>
168	30	MHC=NCH <sub>2</sub> CH <sub>2</sub>
281	8.8	M <sub>2</sub> HC=NCH <sub>2</sub> CH <sub>2</sub>
394	5.5	M <sub>3</sub> HC=NCH <sub>2</sub> CH <sub>2</sub>
507	1.4	M <sub>4</sub> HC=NCH <sub>2</sub> CH <sub>2</sub>
620	0.3	M <sub>5</sub> HC=NCH <sub>2</sub> CH <sub>2</sub>
65	481	P(OH) <sub>2</sub>
94	413	C <sub>2</sub> H <sub>5</sub> P(OH) <sub>2</sub>
98	94	H <sub>3</sub> PO <sub>4</sub>
169	7.8	(C <sub>2</sub> H <sub>5</sub> PO) <sub>2</sub> OH
269	6.6	(C <sub>2</sub> H <sub>5</sub> ) <sub>2</sub> PO <sub>2</sub> AlO <sub>2</sub> P(C <sub>2</sub> H <sub>5</sub> ) <sub>2</sub>
404	0.6	OAl <sub>2</sub> (O <sub>2</sub> PC <sub>2</sub> H <sub>5</sub> )(O <sub>2</sub> P(C <sub>2</sub> H <sub>5</sub> ) <sub>2</sub> ) <sub>2</sub>
602	0.1	HAl <sub>2</sub> (O <sub>2</sub> P(C <sub>2</sub> H <sub>5</sub> ) <sub>2</sub> ) <sub>4</sub> OPO
660	0.6	HAl <sub>2</sub> (O <sub>2</sub> P(C <sub>2</sub> H <sub>5</sub> ) <sub>2</sub> ) <sub>5</sub>

Single ion pyrograms of some characteristic products are shown in Figure 3.27. In the presence of HNT the pyrolysis mass spectra showed the base peak at 55 Da due to  $C_4H_7$  as in the case of PA6-AlPi. However, the relative yield of all products, except those of  $NH_3$  and  $H_2O$  evolution, was decreased compared to PA6-AlPi.

Although, the evolution of  $NH_3$  and  $H_2O$  was enhanced, a reduction in the yields of the products, originated by the aminolysis reactions such as  $C_5H_{10}NHCN$  (111 Da) and  $NCNH(CH_2)_5MC(OH)(NH_2)NHCH_2$  (298 Da) and the products generated by hydrolysis reactions such as,  $HN(CH_2)_5COOH$  (130 Da),  $MNH(CH_2)_5COOH$  (243 Da),  $CO_2$  (44 Da) and  $COOH$  (45 Da), was noted.

Moreover, the products involving acid end groups such as  $MxOH$  ( $m/z = 130, 243, 356, 469, 582$  Da for  $x = 1$  to 5) and C=N linkages or CN end groups such as  $MxCN$  ( $m/z = 139, 252$  and  $365$  Da for  $x = 1$  to 3),  $MxC=NCH_2CH_2$  ( $m/z = 167, 280$  and  $393$  Da for  $x = 1$  to 3) and  $MxHC=NCH_2CH_2$  ( $m/z = 168, 281, 394, 507$  and  $620$  Da for  $x = 1$  to 5) showed broader peaks in their evolution profiles indicating a reduction in the rate of evolution of these products, in the presence of HNT.

In addition, the relative yields of AlPi based products decreased significantly compared to PA6-AlPi. For instance, the relative yields of products with  $m/z$  values 602 and 660 Da were decreased about 2.6 and 2.4 folds respectively. On the other hand, the relative yields of low mass fragments of AlPi based products were almost constant. Thus, it can be concluded that in the presence of HNT, interactions between PA6 and phosphinate were hindered.

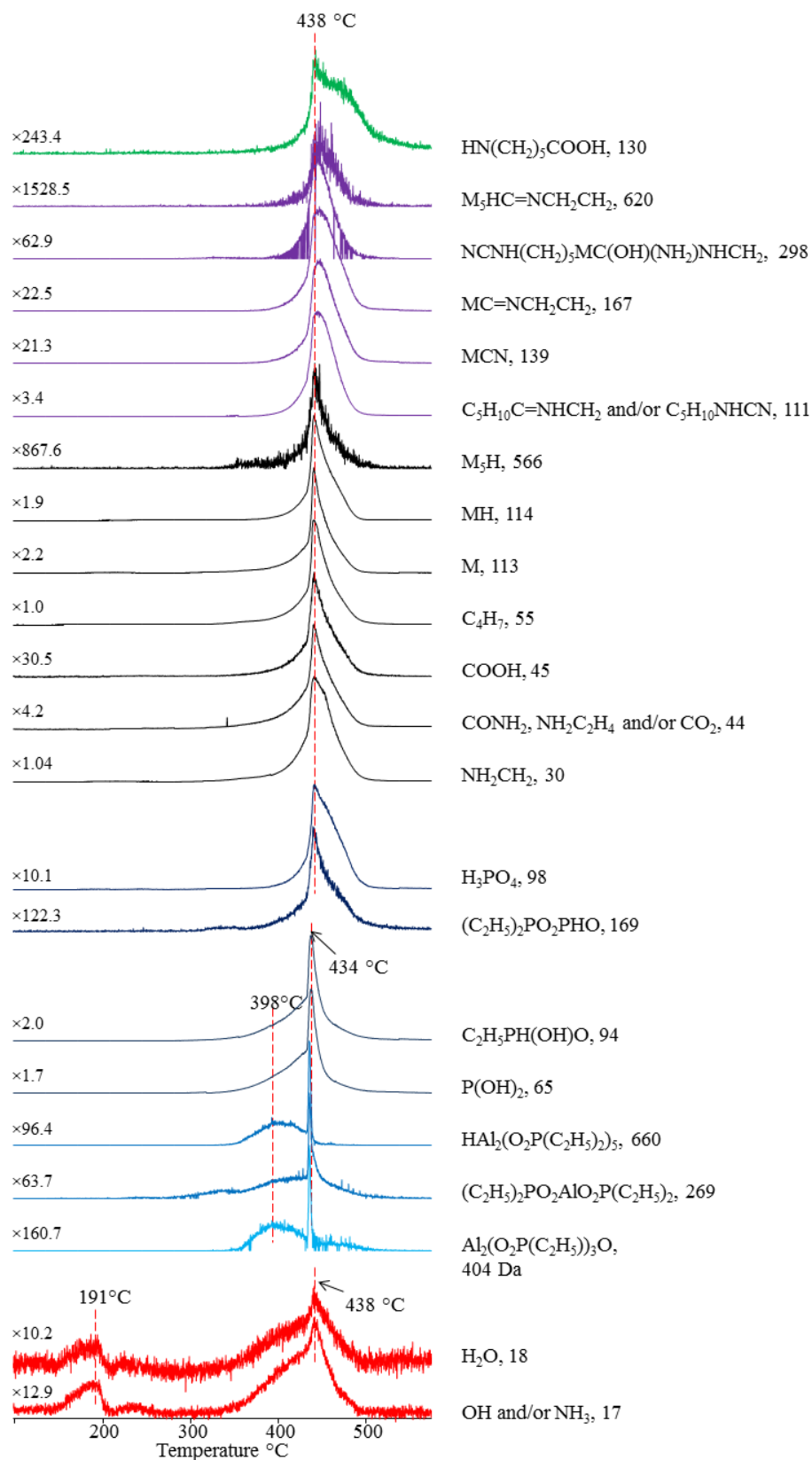


**Figure 3.27.** Single ion pyrograms of some selected fragments detected during the pyrolysis of PA6-AlPi-HNT.

### 3.2.3.2. PA6-ALPI-MMT25A

In the presence of MMT25A (3 wt%) and AlPi (17 wt%), pyrolysis of PA6 yielded a TIC curve with a maximum at around 452°C (Figure 3.28). Typical fragmentation pattern of PA6, intense peaks at  $m/z = 114, 113, 111, 96, 84, 69, 55, 41, 30$  and 18 Da due to MH, M,  $C_5H_{10}NHCN$ ,  $C_5H_{10}CN$ ,  $C_4H_8CO$ ,  $C_5H_9$ ,  $C_4H_7$ ,  $C_3H_5$ ,  $CH_2NH_2$  and  $H_2O$ , respectively, were noted in the pyrolysis mass spectra recorded at 452°C. Moreover, diagnostic peaks of AlPi, at 65, 94 and 169 Da due to  $P(OH)_2$ ,  $C_2H_5P(OH)_2$  and  $(C_2H_5PO)_2OH$  respectively, were observed in the pyrolysis mass spectra recorded at around 433°C. In Table 3.11, the relative intensities of intense and/or characteristic peaks recorded in the spectrum and the assignments made are summarized.

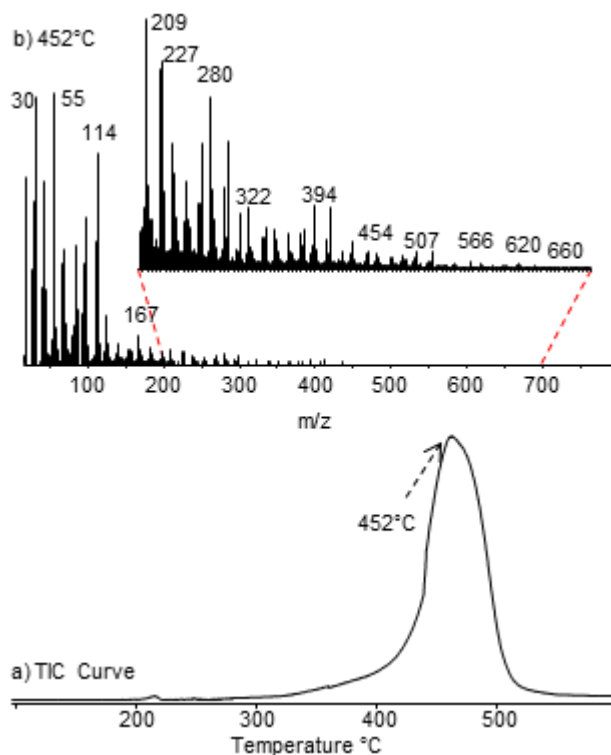


**Figure 3.28.** a) The total ion current curve and b) mass spectrum of PA6-AlPi-MMT25A at 452°C.

**Table 3.11.** The relative intensities, RI, of some selected intense and/or characteristic peaks recorded in pyrolysis spectrum of PA6-AlPi-MMT25A at 452°C and the assignments made.

m/z	RI		Assignment
	433 °C	452°C	
17	261		OH and/or NH <sub>3</sub>
18	1000		H <sub>2</sub> O
44		272	CONH <sub>2</sub> and/or CO <sub>2</sub>
30		982	CH <sub>2</sub> NH <sub>2</sub>
55		1000	C <sub>4</sub> H <sub>7</sub>
111		453	C <sub>5</sub> H <sub>10</sub> NHCN
113		459	M
114		777	MH
139		76	MCN
167		102	MC=NCH <sub>2</sub> CH <sub>2</sub>
298		29	NCNH(CH <sub>2</sub> ) <sub>5</sub> MC(OH)(NH <sub>2</sub> )NHCH <sub>2</sub>
130		8.3	MOH
243		6.2	M <sub>2</sub> OH
356		4.1	M <sub>3</sub> OH
469		0.8	M <sub>4</sub> OH
582		0.5	M <sub>5</sub> OH
566		1.7	M <sub>5</sub> H
620		1.1	M <sub>5</sub> HC=NCH <sub>2</sub> CH <sub>2</sub>
65	795		P(OH) <sub>2</sub>
94	734		C <sub>2</sub> H <sub>5</sub> P(OH) <sub>2</sub>
98	118		H <sub>3</sub> PO <sub>4</sub>
169	20		(C <sub>2</sub> H <sub>5</sub> PO) <sub>2</sub> OH
404	6.8		OAl <sub>2</sub> (O <sub>2</sub> PC <sub>2</sub> H <sub>5</sub> )(O <sub>2</sub> P(C <sub>2</sub> H <sub>5</sub> ) <sub>2</sub> ) <sub>2</sub>
660	19		HAl <sub>2</sub> (O <sub>2</sub> P(C <sub>2</sub> H <sub>5</sub> ) <sub>2</sub> ) <sub>5</sub>
58	50	66	(CH <sub>3</sub> ) <sub>2</sub> NCH <sub>2</sub> and/or C <sub>4</sub> H <sub>10</sub>
269	27	8.3	NC <sub>19</sub> H <sub>27</sub> and/or (C <sub>2</sub> H <sub>5</sub> ) <sub>2</sub> PO <sub>2</sub> AlO <sub>2</sub> P(C <sub>2</sub> H <sub>5</sub> ) <sub>2</sub>
297	8.4	10	NC <sub>21</sub> H <sub>31</sub>



Single ion pyrograms of some characteristic products are shown in Figure 3.29. In the presence of MMT25A, the base peak in the pyrolysis mass spectra was at 55 Da due to  $C_4H_7$ , as in the cases of PA6-ALPi and PA6-ALPi-HNT. Yet, drastic enhancement in the yield of high mass products of PA6 was noted compared to PA6-ALPi and PA6-ALPi-HNT. These findings confirmed the change in thermal degradation pathways of PA6 in the presence of MMT25A and also indicated that the thermal stability of PA6 chains was enhanced in the presence of MMT25A. On the other hand, the relative yields of high mass ALPi products were decreased compared to PA6-ALPi.

The enhancement observed in the evolution of  $H_2O$  was about 1.7 folds, as a consequence an enhancement in the yields of the products related with the hydrolysis reactions such as  $NH(CH_2)_5COOH$  (130 Da),  $M_xNH(CH_2)_5COOH$  ( $m/z = 243, 356, 469$  and  $582$  Da for  $x = 1$  to  $4$ ) were noted. The yields of these fragments were maximized at higher temperatures, at around  $477^\circ C$ . Furthermore, increase in the yields of fragments including  $C=N$  linkages or  $CN$  end groups such as  $MCN$  (139 Da),  $MC=NCH_2CH_2$  (167 Da) and  $M_5HC=NCH_2CH_2$  (620 Da) were regarded as an indication of enhanced possibility of these interactions in the presence of MMT25A. Enhancement in the possibility of intermolecular reactions between PA6 chains could be resulted from the barrier effect of clay layers retarding the release of decomposition products from the nanoclay.

However, the single ion evolution profiles of MMT25A based fragments such as  $(CH_3)_2NCH_2$  (58 Da),  $NC_{19}H_{27}$  (269 Da) and  $NC_{21}H_{31}$  (297 Da) were appeared just above  $200^\circ C$  and continued over a broad temperature range pointing out significant disparities (Figure 3.29). Again, contribution of thermal degradation fragments of PA6 was quite significant at the high temperature evolution of MMT25A based products.

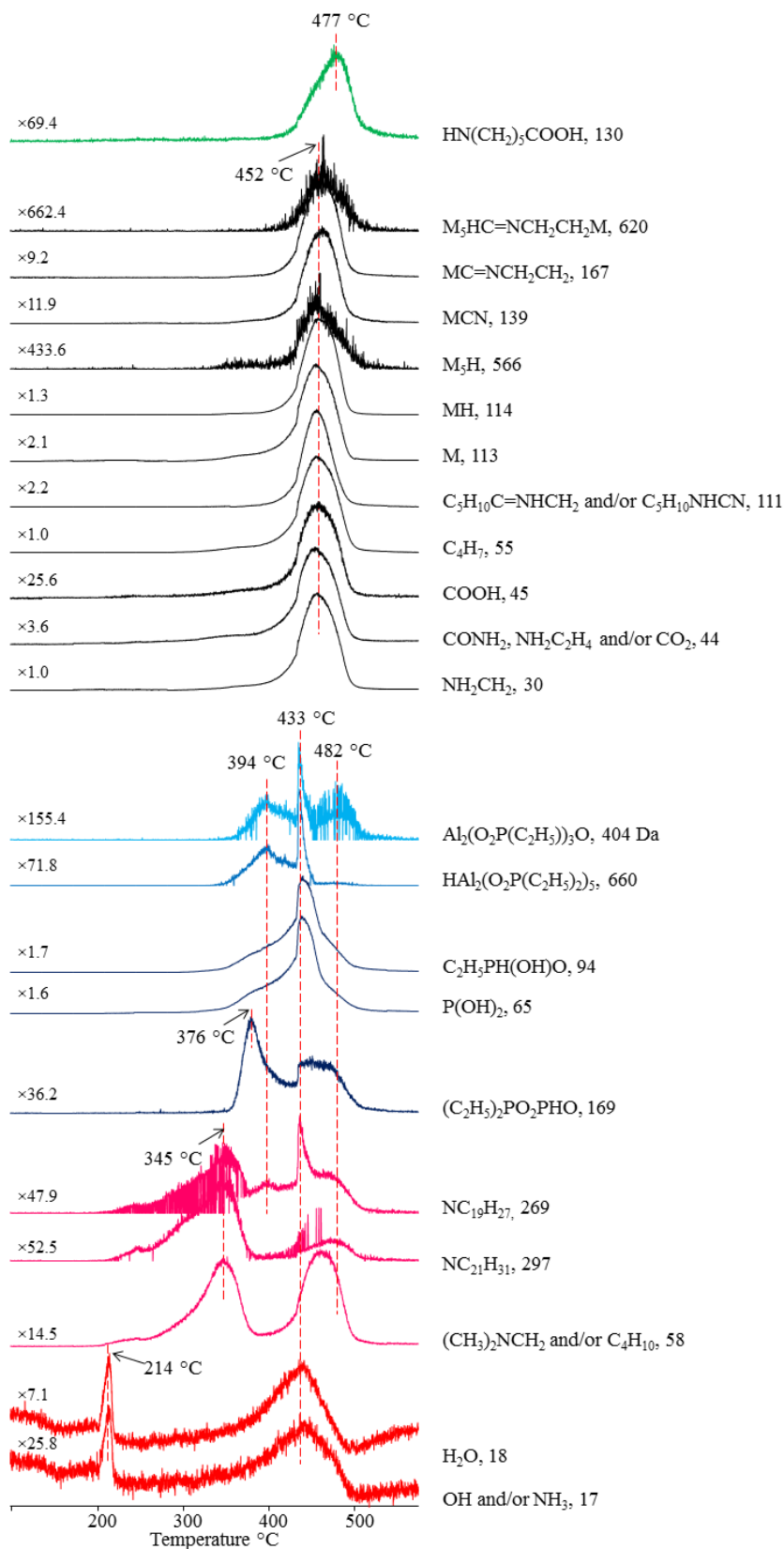


**Figure 3.29.** Single ion pyrograms of some selected fragments detected during the pyrolysis of PA6-AIPi-MMT25A

### 3.2.3.3. PA6-ALPi-MMT30B

In the presence of MMT30B (3 wt%) and ALPi (17 wt%), pyrolysis of PA6 yielded a TIC curve with a maximum at around 451°C and a shoulder at around 393°C (Figure 3.30). Typical fragmentation pattern of PA6, intense peaks at  $m/z = 114, 113, 111, 96, 84, 55, 41, 30$  and 18 Da due to MH, M,  $C_5H_{10}NHCN$ ,  $C_5H_{10}CN$ ,  $C_4H_8CO$ ,  $C_4H_7$ ,  $C_3H_5CH_2NH_2$  and  $H_2O$ , respectively, was noted in the pyrolysis mass spectrum recorded at 451°C. In addition characteristic intense peaks of ALPi, at 65, 94, 269, and 169 Da due to  $P(OH)_2$ ,  $C_2H_5P(OH)_2$ ,  $(C_2H_5)_2PO_2AlO_2P(C_2H_5)_2$  and  $(C_2H_5PO)_2OH$  respectively, were observed in the pyrolysis mass spectra recorded at around 392 and 466°C. In Table 3.12, the relative intensities of intense and/or characteristic peaks recorded in the spectrum and the assignments made are summarized.

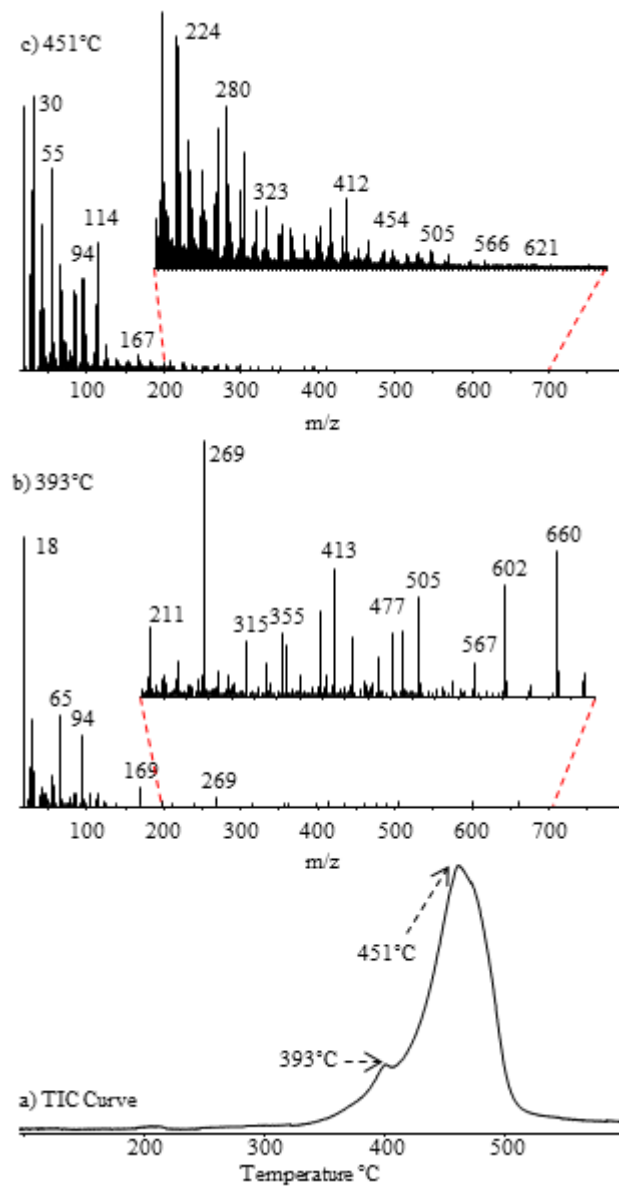


**Figure 3.30.** a) The total ion current curve and the mass spectra at b) 393 and c) 451°C recorded during the pyrolysis of PA6-AlPi-MMT30B.

**Table 3.12.** The relative intensities, RI, of some selected intense and/or characteristic peaks recorded in pyrolysis spectrum of PA6-AlPi-MMT30B at 391 and 451 °C and the assignments made.

m/z	RI		Assignment
	391 °C	451 °C	
17	315	323	OH and/or NH <sub>3</sub>
18	1000	966	H <sub>2</sub> O
44		218	CONH <sub>2</sub> and/or CO <sub>2</sub>
30		1000	CH <sub>2</sub> NH <sub>2</sub>
45		31	CO <sub>2</sub> H
55		733	C <sub>4</sub> H <sub>7</sub>
111		235	C <sub>5</sub> H <sub>10</sub> NHCN
113		276	M
114		462	MH
130		5.2	MOH
243		3.2	M <sub>2</sub> OH
356		1.6	M <sub>3</sub> OH
139		39	MCN
167		50	MC=NCH <sub>2</sub> CH <sub>2</sub>
298		12	NCNH(CH <sub>2</sub> ) <sub>5</sub> MC(OH)(NH <sub>2</sub> )NHCH <sub>2</sub>
566	1.0	0.8	M <sub>5</sub> H
620		0.4	M <sub>5</sub> HC=NCH <sub>2</sub> CH <sub>2</sub>
65	332	380	P(OH) <sub>2</sub>
94	260	334	C <sub>2</sub> H <sub>5</sub> P(OH) <sub>2</sub>
98		129	H <sub>3</sub> PO <sub>4</sub>
169	68	10	(C <sub>2</sub> H <sub>5</sub> PO) <sub>2</sub> OH
269	35	5.6	(C <sub>2</sub> H <sub>5</sub> ) <sub>2</sub> PO <sub>2</sub> AlO <sub>2</sub> P(C <sub>2</sub> H <sub>5</sub> ) <sub>2</sub>
404	2.7		OAl <sub>2</sub> (O <sub>2</sub> PC <sub>2</sub> H <sub>5</sub> )(O <sub>2</sub> P(C <sub>2</sub> H <sub>5</sub> ) <sub>2</sub> ) <sub>2</sub>
660	21		HAl <sub>2</sub> (O <sub>2</sub> P(C <sub>2</sub> H <sub>5</sub> ) <sub>2</sub> ) <sub>5</sub>
58		45	(CH <sub>3</sub> ) <sub>2</sub> NCH <sub>2</sub> and/or C <sub>4</sub> H <sub>10</sub>
88		6.7	CH <sub>2</sub> N(C <sub>2</sub> H <sub>4</sub> OH)CH <sub>3</sub>
268	2.2	5.1	N(C <sub>2</sub> H <sub>4</sub> OH) <sub>2</sub> C <sub>12</sub> H <sub>20</sub> and/or COOC <sub>2</sub> H <sub>4</sub> N(CH <sub>3</sub> )C <sub>2</sub> H <sub>4</sub> OH
297	3.0	5.2	N(C <sub>2</sub> H <sub>4</sub> OH) <sub>2</sub> C <sub>14</sub> H <sub>25</sub> and/or C <sub>2</sub> H <sub>5</sub> COOC <sub>2</sub> H <sub>4</sub> N(CH <sub>3</sub> )C <sub>2</sub> H <sub>4</sub> OH

Single ion pyrograms of some characteristic products are shown in Figure 3.31. In the presence of MMT30B, the pyrolysis mass spectra showed the base peak at 30 Da due to  $\text{CH}_2\text{NH}_2$ , unlike what was observed for PA6-ALPi. Moreover, the pyrolysis mass spectrum of PA6-ALPi-MMT30B recorded at 451°C demonstrated noticeable changes compared to that of PA6-ALPi composite; the relative intensities of both PA6 and ALPi based fragment peaks were changed noticeably. In the presence of MMT30B, relative abundance of monomer was decreased about 1.4 folds.

The trends observed in the single ion evolution profiles of PA6 based products were changed significantly. The yield of fragments generated by hydrolysis reactions such as the series of  $\text{M}_x\text{NH}(\text{CH}_2)_5\text{COOH}$  ( $m/z = 130, 243$  and  $356$  Da for  $x = 0$  to  $2$ ), were maximized at elevated temperatures, at around 479°C. In addition, the products involving C=N linkages such as  $\text{MC}=\text{NCH}_2\text{CH}_2$  (167 Da) and  $\text{M}_5\text{HC}=\text{NCH}_2\text{CH}_2$  (620 Da) were maximized at slightly higher temperatures, at around 460°C. The high mass fragments of  $\text{M}_x\text{H}$  ( $m/z = 453, 566$  and  $679$  Da for  $x = 4$  to  $6$ ) had a higher yield at low temperatures. It may be thought that interactions between high mass oligomers with phosphinates cause the degradation of these fragments at early stages in the presence of MMT30B.

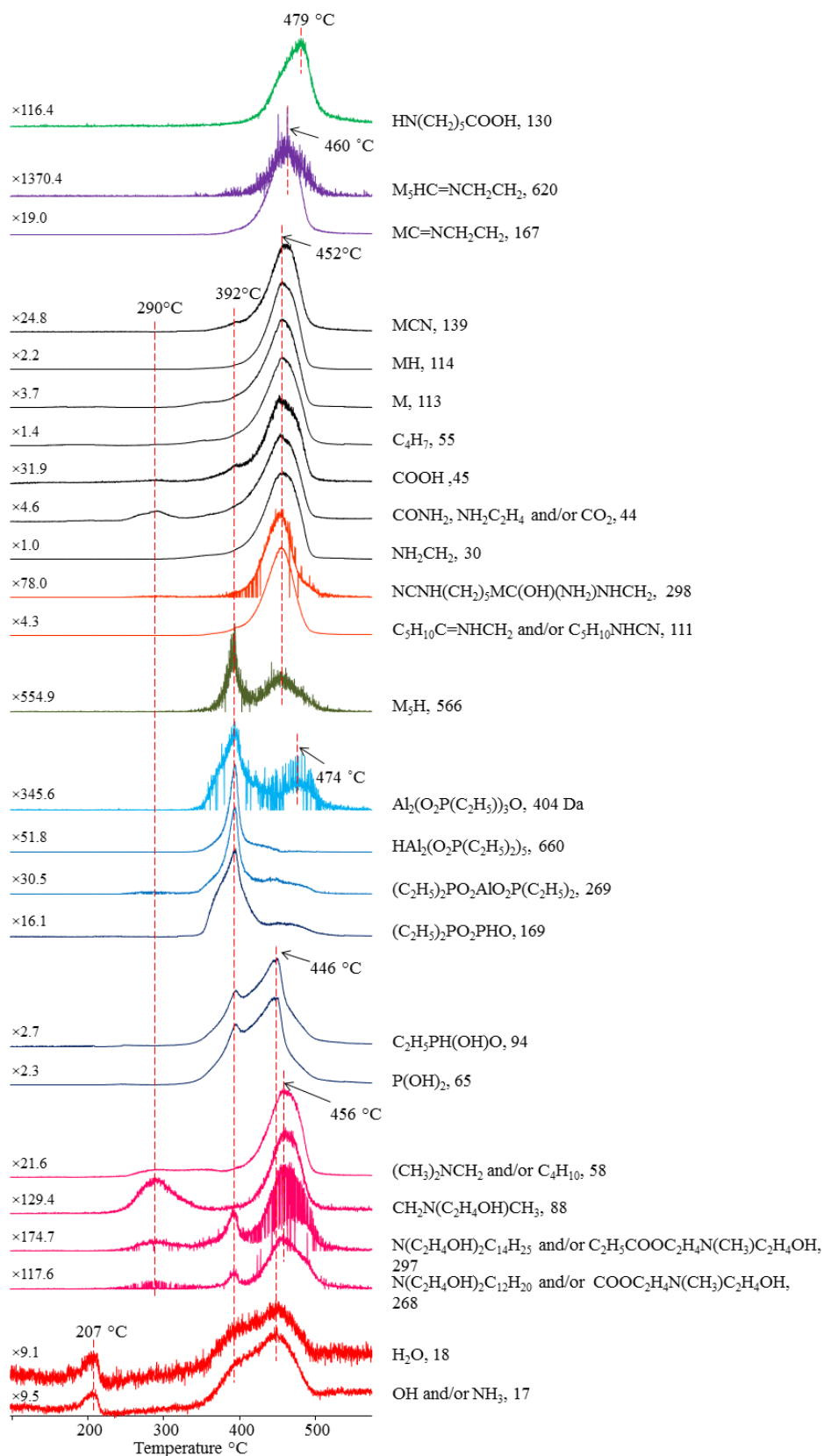


**Figure 3.31.** Single ion pyrograms of some selected fragments detected during the pyrolysis of PA6-AlPi-MMT30B.

Although about 6.7 folds enhancement in the yield of  $\text{NH}_3$  was recorded, a slight reduction in the yields of the fragments originated by aminolysis reactions such as  $\text{NCNH}(\text{CH}_2)_5\text{MC}(\text{OH})(\text{NH}_2)\text{NHCH}_2$  (298 Da) and  $\text{C}_5\text{H}_{10}\text{NHCN}$  (111 Da) was noted. However, contrary to expectations, the significant increase, about 1.9 folds, in the yield of  $\text{H}_2\text{O}$  was accompanied by the increase in the yields of fragments generated by hydrolysis reactions such as,  $\text{HN}(\text{CH}_2)_5\text{COOH}$  (130 Da),  $\text{MNH}(\text{CH}_2)_5\text{COOH}$  (243 Da),  $\text{CO}_2$  (44 Da) and  $\text{COOH}$  (45 Da).

The pyrolysis mass spectra recorded at around  $290^\circ\text{C}$  and  $392^\circ\text{C}$  were dominated by typical peaks of MMT30B and AlPi; yet, significant varieties in the relative intensities and evolution profiles of diagnostic peaks were noticed. (Figure 3.31). Furthermore, the evolution profile of the product with  $m/z$  value 44 Da due to  $\text{CO}_2$ ,  $\text{CONH}_2$  and/or  $\text{NH}_2\text{C}_2\text{H}_4$  showed weak peak at around  $290^\circ\text{C}$  that might be associated with decomposition of the modifier of MMT30B.

Significant changes with respect to PA6-AlPi were noticed in the single ion evolution profiles of AlPi based products for PA6-AlPi-MMT30B. Evolution of fragments produced by depolymerization continued over a broader temperature region indicating a reduction in rate of depolymerization. The relative yields of diethylphosphinic acid based products were increased significantly. The relative yield of  $(\text{C}_2\text{H}_5)_2\text{P}_2\text{O}_3\text{H}$  (169 Da) was increased more than 8-folds compared to PA6-AlPi. In the presence of MMT30B, the single ion evolution profiles of thermal decomposition fragments of PA6 showed a shoulder at  $392^\circ\text{C}$ . Release of alkyl amines and/or fragments generated by trans-esterification reactions between the modifier of MMT and PA6 (such as 268 and 297 Da) and most of AlPi based products were recorded at around this temperature. From these results it may be thought that in the presence of MMT30B, interactions among amine and carbonyl groups and phosphinates took place during the pyrolysis of PA6-AlPi-MMT30B composite. And, low temperature peaks present in the evolution profiles of thermal decomposition fragments of PA6 may be due to the release of fragments from the modifier of MMT having the same  $m/z$  values. Also, the low temperature peak in the single ion evolution profiles of  $\text{P}(\text{OH})_2$  (65 Da) and  $\text{C}_2\text{H}_5\text{P}(\text{OH})_2$  (94 Da) may



be thought to be produced by reactions of phosphinate groups and amines. The effect of MMT30B may be resulted from the dispersion of clay layers within the polymer chains, causing an increase in the interactions between PA6 and AlPi.

### **3.3 THERMAL DEGRADATION OF POLY(LACTIC ACID) IN THE PRESENCE OF FLAME RETARDANTS AND NANOPARTICLES**

For understanding the effects of nanoclays on thermal degradation characteristics of poly(lactic acid) composites, PLA involving 20% AlPi, PLA involving 17% AlPi and 3% MMT30B, 3% HNT or 3% SiO<sub>2</sub> were studied by DP-MS technique separately (Table 2.2).

Pyrolysis of pure PLA yielded a TIC curve with a broad peak at around 363°C (Figure 3.32). The base peak is at  $m/z = 56$  Da due to CH<sub>3</sub>CHCO, the common product of lactide and its oligomers produced mainly during pyrolysis by random chain scissions or by ionization of higher mass pyrolysis products. This recommendations are also valid for abundant low mass products such as C<sub>2</sub>H<sub>4</sub> and/or CO (28 Da), C<sub>2</sub>H<sub>3</sub>O (43 Da), C<sub>2</sub>H<sub>4</sub>O and/or CO<sub>2</sub> (44 Da), C<sub>2</sub>H<sub>4</sub>OH and/or CO<sub>2</sub>H (45 Da). The mass spectrum recorded at 363°C is dominated by the series of peaks at  $m/z = 72n-88$  for  $n=2$  to 12; with formula (C<sub>2</sub>H<sub>4</sub>CO<sub>2</sub>)<sub>x</sub>C<sub>2</sub>H<sub>4</sub>CO for  $x=0$  to 10 due to fragments generated by elimination of the neutral molecules CO<sub>2</sub> and acetaldehyde from cyclic oligomers produced by trans-esterification reactions (Figure 3.32).

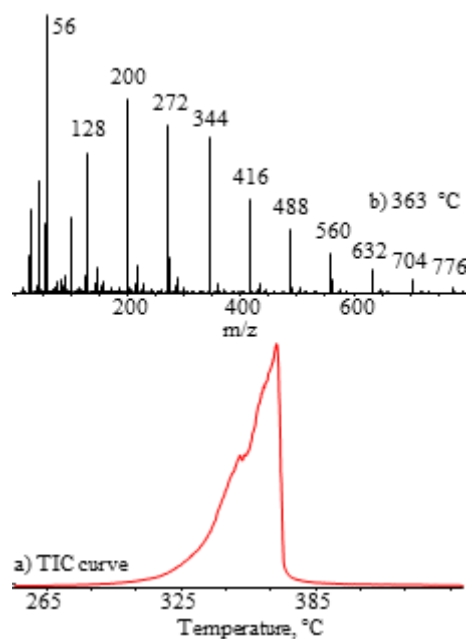
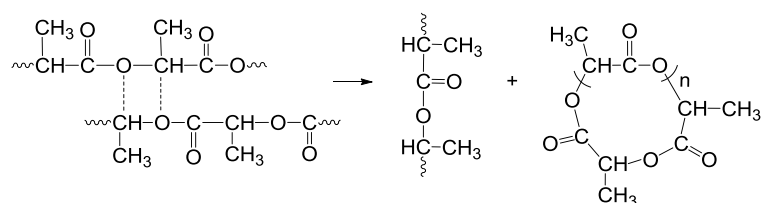


**Figure 3.32.** a) The total ion current curve and b) the mass spectra at 363 °C recorded during the pyrolysis of PLA.

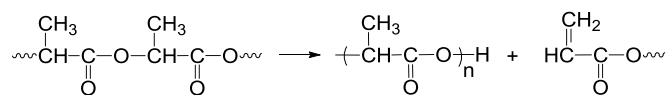
The molecular ions of cyclic oligomers, produced are not stable even with the soft ionization techniques. The reaction mechanism, for generation of cyclic oligomers by inter and/or intra trans-esterification reactions, is given in Scheme 3.9a. The second, less intense series of peaks with  $m/z = 72n+73$  for  $n=2$  to 12 with formula  $(C_2H_4CO_2)_xH$  ( $m/z= 73, 145, 217$  and  $289$  Da for  $x=1$  to 4) are associated with fragments produced by cis-elimination reactions (Scheme 3.9b). Besides the peaks at  $m/z = 72n-44$  for  $n=2$  to 5; are related to  $(C_2H_4CO_2)_xC_2H_4$  fragments ( $m/z=100, 172, 244,$  and  $316$  Da for  $x=1$  to 4) most probably generated by homolysis reactions.

**Scheme 3.9** Trans-esterification and cis-elimination reactions of PLA.

a. Trans-esterification



b. cis-elimination



In Table 3.13, the relative intensities of intense and/or characteristic peaks recorded in the spectrum and the assignments made are summarized.

**Table 3.13.** The relative intensities, RI, of some selected intense and/or characteristic peaks recorded in pyrolysis spectrum of PLA at 363°C and the assignments made.

m/z	RI	Assignment
28	304	C <sub>2</sub> H <sub>4</sub> and/or CO
43	387	C <sub>2</sub> H <sub>3</sub> O
44	106	C <sub>2</sub> H <sub>4</sub> O and/or CO <sub>2</sub>
45	380	C <sub>2</sub> H <sub>4</sub> OH and/or CO <sub>2</sub> H
56	1000	C <sub>2</sub> H <sub>4</sub> CO
72	17	C <sub>2</sub> H <sub>4</sub> CO <sub>2</sub>
73	17	C <sub>2</sub> H <sub>4</sub> CO <sub>2</sub> H
100	329	C <sub>2</sub> H <sub>4</sub> COOC <sub>2</sub> H <sub>4</sub>
172	10	(C <sub>2</sub> H <sub>4</sub> COO) <sub>2</sub> C <sub>2</sub> H <sub>4</sub>
244	15	(C <sub>2</sub> H <sub>4</sub> COO) <sub>3</sub> C <sub>2</sub> H <sub>4</sub>
316	11	(C <sub>2</sub> H <sub>4</sub> COO) <sub>4</sub> C <sub>2</sub> H <sub>4</sub>
128	574	(C <sub>2</sub> H <sub>4</sub> CO <sub>2</sub> )C <sub>2</sub> H <sub>4</sub> CO
200	847	(C <sub>2</sub> H <sub>4</sub> CO <sub>2</sub> ) <sub>2</sub> C <sub>2</sub> H <sub>4</sub> CO
272	611	(C <sub>2</sub> H <sub>4</sub> CO <sub>2</sub> ) <sub>3</sub> C <sub>2</sub> H <sub>4</sub> CO
344	552	(C <sub>2</sub> H <sub>4</sub> CO <sub>2</sub> ) <sub>4</sub> C <sub>2</sub> H <sub>4</sub> CO
416	406	(C <sub>2</sub> H <sub>4</sub> CO <sub>2</sub> ) <sub>5</sub> C <sub>2</sub> H <sub>4</sub> CO
488	260	(C <sub>2</sub> H <sub>4</sub> CO <sub>2</sub> ) <sub>6</sub> C <sub>2</sub> H <sub>4</sub> CO
560	141	(C <sub>2</sub> H <sub>4</sub> CO <sub>2</sub> ) <sub>7</sub> C <sub>2</sub> H <sub>4</sub> CO
632	90	(C <sub>2</sub> H <sub>4</sub> CO <sub>2</sub> ) <sub>8</sub> C <sub>2</sub> H <sub>4</sub> CO
704	47	(C <sub>2</sub> H <sub>4</sub> CO <sub>2</sub> ) <sub>9</sub> C <sub>2</sub> H <sub>4</sub> CO
776	23	(C <sub>2</sub> H <sub>4</sub> CO <sub>2</sub> ) <sub>10</sub> C <sub>2</sub> H <sub>4</sub> CO
145	97	(C <sub>2</sub> H <sub>4</sub> CO <sub>2</sub> ) <sub>2</sub> H
217	94	(C <sub>2</sub> H <sub>4</sub> CO <sub>2</sub> ) <sub>3</sub> H
289	62	(C <sub>2</sub> H <sub>4</sub> CO <sub>2</sub> ) <sub>4</sub> H

Single ion pyrograms of low mass fragments C<sub>2</sub>H<sub>4</sub> and/or CO (28 Da), C<sub>2</sub>H<sub>3</sub>O (43 Da), C<sub>2</sub>H<sub>4</sub>O and/or CO<sub>2</sub> (44 Da), C<sub>2</sub>H<sub>4</sub>OH and/or CO<sub>2</sub>H (45 Da) and C<sub>2</sub>H<sub>4</sub>CO (56 Da), products generated by cis-elimination reactions (C<sub>2</sub>H<sub>4</sub>CO<sub>2</sub>)<sub>x</sub>H (m/z=145 and 217 Da for x=2 and 3), products generated by elimination of the neutral molecules CO<sub>2</sub> and acetaldehyde from cyclic oligomers produced by trans-esterification reactions, (C<sub>2</sub>H<sub>4</sub>CO<sub>2</sub>)<sub>x</sub>C<sub>2</sub>H<sub>4</sub>CO (m/z=128, 200 and 488 Da for x= 1, 2 and 6) and C<sub>2</sub>H<sub>4</sub>COOC<sub>2</sub>H<sub>4</sub> (100 Da) are shown in Figure 3.33.

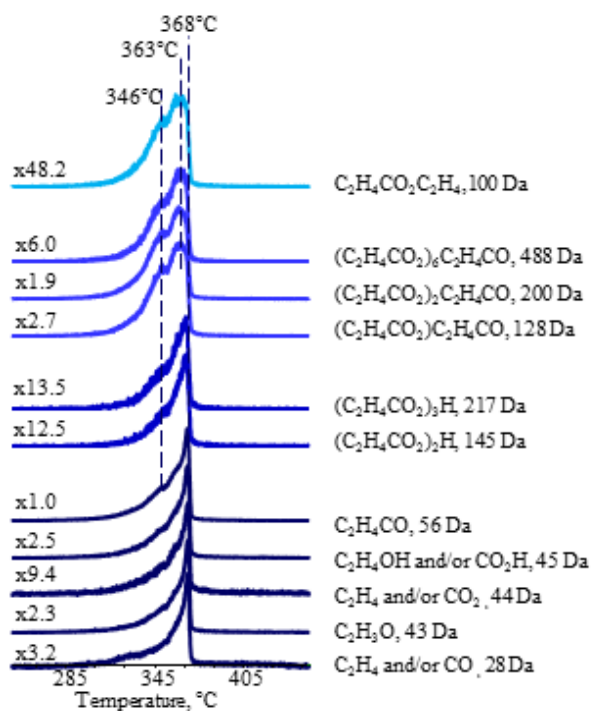


**Figure 3.33.** Single ion pyrograms of some selected fragments detected during the pyrolysis PLA.

Contrary to the results of Kopinke et al., some differences are noticed in the single ion profiles of thermal degradation products of PLA [12, 91]. The single ion pyrograms of the fragments produced by trans-esterification reactions such as  $(C_2H_4CO_2)C_2H_4CO$  (128 Da),  $(C_2H_4CO_2)_2C_2H_4CO$  (200 Da) and  $(C_2H_4CO_2)_6C_2H_4CO$  (488 Da) showed two overlapping peaks with maxima at 346 and 363°C, indicating that thermal degradation of PLA starts by trans-esterification reactions. The fragments due to cis-eliminations such as  $(C_2H_4CO_2)_2H$  (145 Da),  $(C_2H_4CO_2)_3H$  (217 Da) and  $(C_2H_4CO_2)_4H$  (289 Da) showed identical trends with low mass fragments such as  $C_2H_4CO$  (56 Da),  $CO_2H$  and/or  $C_2H_5O$  (45 Da), and  $C_2H_4O$  and/or  $CO_2$  (44 Da). All the other ion traces, which are clear in the averaged mass spectra of the two decomposition peaks have identical shapes, indicating only two dominating decomposition pathways which are chain homolysis and trans-esterification reactions.

### 3.3.1. FLAME RETARDED POLY(LACTIC ACID) WITH OR WITHOUT NANOPARTICLES

#### 3.3.1.1. PLA-ALPi

Recently, Isitman et al. determined that the fire retardancy of PLA was enhanced by incorporation of ALPi and fire risks were decreased as a consequence of higher limiting oxygen index, LOI, lower peak heat release rate, PHRR, and lower peak mass loss rates, PMLR [68]. It was determined that flammability characteristics of PLA with the addition of ALPi, according to UL-94 vertical burn test, can be defined as V2. LOI value was increased from 23 to 27.5 upon addition of 20% of ALPi. Furthermore, decrease in the PHRR from  $578 \text{ kWm}^{-2}$  to  $443 \text{ kWm}^{-2}$  was detected indicating the improvement of fire retardancy. However, TGA results indicated a reduction in thermal stability of PLA in the presence of ALPi [68]. TGA results are confirmed with direct pyrolysis mass spectrometry results.

The TIC curve of PLA involving 20 wt% ALPi, and the mass spectra recorded at the maxima are presented in Figure 3.34. It is clear from the pyrolysis mass spectra that release of degradation products of PLA and ALPi occurs at around 328 and 425°C respectively, indicating an important reduction in thermal stability of PLA. Maximum ion yield of PLA was decreased from 368°C to 327°C. The characteristic intense peaks of ALPi, likely assigned to  $(\text{C}_2\text{H}_5)_2\text{PO}_2\text{AlO}_2\text{P}(\text{C}_2\text{H}_5)_2$  (269 Da),  $\text{Al}(\text{O}_2\text{P}(\text{C}_2\text{H}_5)_2)_2(\text{H}_2\text{P}_2\text{O}_5)$  (413 Da),  $\text{Al}_2(\text{O}_2\text{P}(\text{C}_2\text{H}_5)_2)_3\text{O}$  (433 Da),  $\text{Al}(\text{O}_2\text{P}(\text{C}_2\text{H}_5)_2)_2(\text{H}_2\text{P}_2\text{O}_5)(\text{O}_2\text{PC}_2\text{H}_5)$  (505 Da),  $\text{Al}_2(\text{O}_2\text{P}(\text{C}_2\text{H}_5)_2)_4\text{OPO}$  (601 Da) and  $\text{Al}_2(\text{O}_2\text{P}(\text{C}_2\text{H}_5)_2)_5$  (659 Da) according to CID experiments (Section 3.1.2), are present in the pyrolysis mass spectra of PLA-ALPi recorded at around 425°C. Weak peaks due to diethylphosphinic acid  $(\text{C}_2\text{H}_5)_2\text{PO}_2\text{H}$  (122 Da), fragment that may be associated with low mass oligomers of alkyl phosphinates such as  $((\text{C}_2\text{H}_5)_2\text{PO})_2\text{H}$  (211 Da),  $(\text{C}_2\text{H}_5)_2\text{PO}_2\text{PC}_2\text{H}_5\text{O}$  (197 Da), and  $(\text{C}_2\text{H}_5\text{PO})_2\text{OH}$  (169 Da) and related fragment ions  $(\text{C}_2\text{H}_5)_2\text{PO}$  (105 Da),  $\text{C}_2\text{H}_5\text{P}(\text{OH})_2$  (94 Da) and  $\text{P}(\text{OH})_2$  (65 Da) are also detected.

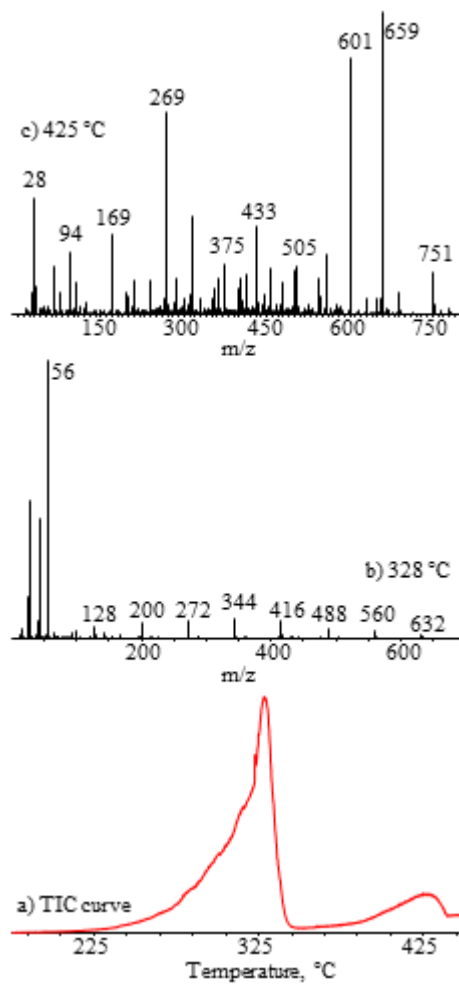


**Figure 3.34.** a) The total ion current curve and the mass spectra at b) 328 and c) 425°C recorded during the pyrolysis of PLA-AIPi.

Although, the mass spectra contain the diagnostic peaks for PLA and AlPi, the fragmentation patterns recorded involve noticeable changes with respect to corresponding pure forms. In Table 3.14, the relative intensities of intense and/or characteristic peaks recorded in the spectrum and the assignments made are summarized.

**Table 3.14.** The relative intensities, RI, of some selected intense and/or characteristic peaks recorded in pyrolysis spectrum of PLA-AlPi at 325 and 425°C and the assignments made.

m/z	RI		Assignment
	325°C	425°C	
28	449		C <sub>2</sub> H <sub>4</sub> and/or CO
43	388		C <sub>2</sub> H <sub>3</sub> O
44	98		C <sub>2</sub> H <sub>4</sub> O and/or CO <sub>2</sub>
45	336		C <sub>2</sub> H <sub>4</sub> OH and/or CO <sub>2</sub> H
56	1000		C <sub>2</sub> H <sub>4</sub> CO
72	3.2		C <sub>2</sub> H <sub>4</sub> CO <sub>2</sub>
100	29		C <sub>2</sub> H <sub>4</sub> COOC <sub>2</sub> H <sub>4</sub>
128	47		(C <sub>2</sub> H <sub>4</sub> CO <sub>2</sub> ) <sub>2</sub> C <sub>2</sub> H <sub>4</sub> CO
145	8.3		(C <sub>2</sub> H <sub>4</sub> CO <sub>2</sub> ) <sub>2</sub> H
200	62		(C <sub>2</sub> H <sub>4</sub> CO <sub>2</sub> ) <sub>2</sub> C <sub>2</sub> H <sub>4</sub> CO
217	5.5	10	(C <sub>2</sub> H <sub>4</sub> CO <sub>2</sub> ) <sub>3</sub> H
488	29		(C <sub>2</sub> H <sub>4</sub> CO <sub>2</sub> ) <sub>6</sub> C <sub>2</sub> H <sub>4</sub> CO
65	18	183	P(OH) <sub>2</sub>
94	18	192	C <sub>2</sub> H <sub>5</sub> P(OH) <sub>2</sub>
105	3.1	89	(C <sub>2</sub> H <sub>5</sub> ) <sub>2</sub> PO
122	3.5	36	(C <sub>2</sub> H <sub>5</sub> ) <sub>2</sub> PO <sub>2</sub> H
149	0.8	17	CO <sub>2</sub> P(C <sub>2</sub> H <sub>5</sub> ) <sub>2</sub> O
169	13	264	(C <sub>2</sub> H <sub>5</sub> PO) <sub>2</sub> OH
177		5.7	C <sub>2</sub> H <sub>4</sub> CO <sub>2</sub> P(C <sub>2</sub> H <sub>5</sub> ) <sub>2</sub> O
197	4.5	62	(C <sub>2</sub> H <sub>5</sub> ) <sub>2</sub> PO <sub>2</sub> PC <sub>2</sub> H <sub>5</sub> O
211		93	((C <sub>2</sub> H <sub>5</sub> ) <sub>2</sub> PO) <sub>2</sub> H and/or C <sub>2</sub> H <sub>5</sub> PO <sub>2</sub> AlO <sub>2</sub> PC <sub>2</sub> H <sub>5</sub>
269		616	(C <sub>2</sub> H <sub>5</sub> ) <sub>2</sub> PO <sub>2</sub> AlO <sub>2</sub> P(C <sub>2</sub> H <sub>5</sub> ) <sub>2</sub>
353		58	(C <sub>2</sub> H <sub>5</sub> PO <sub>2</sub> ) <sub>3</sub> (C <sub>2</sub> H <sub>5</sub> POH)
413	1.9	110	Al(O <sub>2</sub> P(C <sub>2</sub> H <sub>5</sub> ) <sub>2</sub> ) <sub>2</sub> (H <sub>2</sub> P <sub>2</sub> O <sub>5</sub> )
433	4.1	257	OAl <sub>2</sub> (O <sub>2</sub> P(C <sub>2</sub> H <sub>5</sub> ) <sub>2</sub> ) <sub>3</sub>
455		142	((C <sub>2</sub> H <sub>5</sub> ) <sub>2</sub> PO <sub>2</sub> ) <sub>3</sub> (C <sub>2</sub> H <sub>5</sub> PO <sub>2</sub> )
505	4.4	139	Al(O <sub>2</sub> P(C <sub>2</sub> H <sub>5</sub> ) <sub>2</sub> ) <sub>2</sub> (H <sub>2</sub> P <sub>2</sub> O <sub>5</sub> )(O <sub>2</sub> PC <sub>2</sub> H <sub>5</sub> )
601		816	Al <sub>2</sub> (O <sub>2</sub> P(C <sub>2</sub> H <sub>5</sub> ) <sub>2</sub> ) <sub>4</sub> OPO
659		1000	Al <sub>2</sub> (O <sub>2</sub> P(C <sub>2</sub> H <sub>5</sub> ) <sub>2</sub> ) <sub>5</sub>



In the presence of AlPi, reduction in thermal stability of PLA and more than 8-folds decrease in the trans-esterification and cis-elimination reactions were noticed. According to shapes and relative intensities, evolution profiles of AlPi based fragments showed noticeable changes. The multiplication factors for pure AlPi based fragments are also given in parenthesis for comparison of the distribution of these products. Fragments of AlPi related with four coordinate compounds involving Al-O-P linkages showed a single peak at around 425°C.

Single ion pyrograms of some of the selected fragments of PLA, such as C<sub>2</sub>H<sub>4</sub> and/or CO (28 Da), C<sub>2</sub>H<sub>4</sub>O and/or CO<sub>2</sub> (44 Da), C<sub>2</sub>H<sub>4</sub>CO (56 Da), (C<sub>2</sub>H<sub>4</sub>CO<sub>2</sub>)<sub>x</sub>H (145 and 217 Da for x=2 and 3), (C<sub>2</sub>H<sub>4</sub>CO<sub>2</sub>)<sub>x</sub>C<sub>2</sub>H<sub>4</sub>CO (128, 200, and 488 Da for x=1, 2 and 6 respectively) and C<sub>2</sub>H<sub>4</sub>CO<sub>2</sub>C<sub>2</sub>H<sub>4</sub> (100 Da) and those of AlPi, namely P(OH)<sub>2</sub> (65 Da), C<sub>2</sub>H<sub>5</sub>P(OH)<sub>2</sub> (94 Da), (C<sub>2</sub>H<sub>5</sub>)<sub>2</sub>PO (105 Da), (C<sub>2</sub>H<sub>5</sub>PO)<sub>2</sub>OH (169 Da), Al(O<sub>2</sub>P(C<sub>2</sub>H<sub>5</sub>)<sub>2</sub>)<sub>2</sub>(H<sub>2</sub>P<sub>2</sub>O<sub>5</sub>) (413 Da), Al(O<sub>2</sub>P(C<sub>2</sub>H<sub>5</sub>)<sub>2</sub>)<sub>2</sub>(O<sub>2</sub>PC<sub>2</sub>H<sub>5</sub>)(H<sub>2</sub>P<sub>2</sub>O<sub>5</sub>) (505 Da), (C<sub>2</sub>H<sub>5</sub>)<sub>2</sub>PO<sub>2</sub>AlO<sub>2</sub>P(C<sub>2</sub>H<sub>5</sub>)<sub>2</sub> (269 Da), Al<sub>2</sub>(O<sub>2</sub>P(C<sub>2</sub>H<sub>5</sub>)<sub>2</sub>)<sub>4</sub>(OPO) (601 Da), Al<sub>2</sub>(O<sub>2</sub>P(C<sub>2</sub>H<sub>5</sub>)<sub>2</sub>)<sub>5</sub> (659 Da), CO<sub>2</sub>P(C<sub>2</sub>H<sub>5</sub>)<sub>2</sub>O (149 Da), C<sub>2</sub>H<sub>4</sub>CO<sub>2</sub>P(C<sub>2</sub>H<sub>5</sub>)<sub>2</sub>O (177 Da), (C<sub>2</sub>H<sub>5</sub>PO<sub>2</sub>)<sub>3</sub>(C<sub>2</sub>H<sub>5</sub>POH) (353 Da) and ((C<sub>2</sub>H<sub>5</sub>)<sub>2</sub>PO<sub>2</sub>)<sub>3</sub>(C<sub>2</sub>H<sub>5</sub>PO<sub>2</sub>) (455 Da) recorded during the pyrolysis of PLA-AlPi are shown in Figure 3.35.

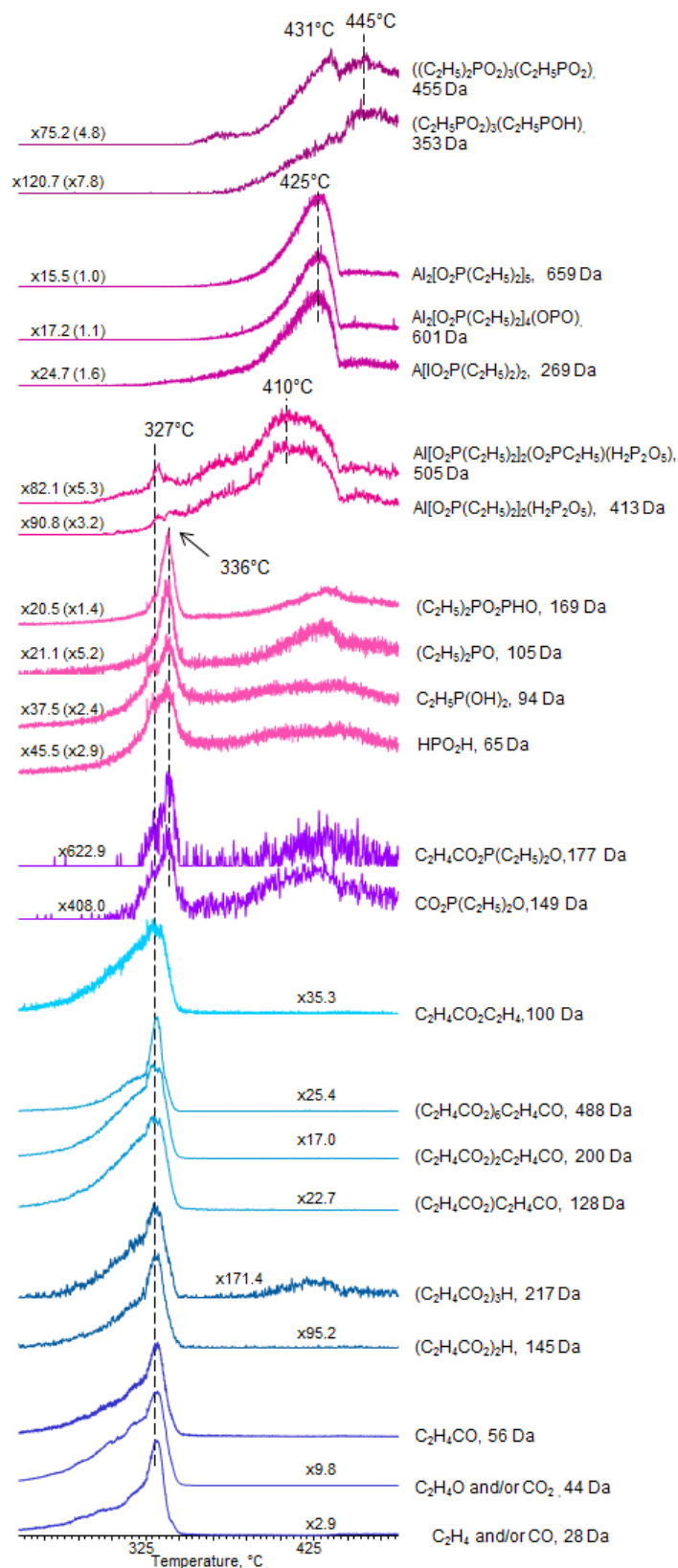
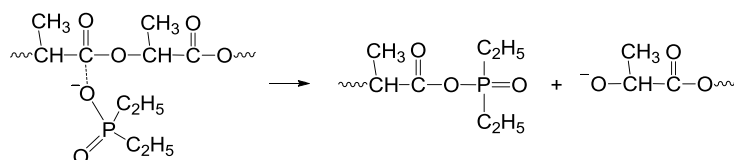


**Figure 3.35.** Single ion pyrograms of some selected fragments detected during the pyrolysis PLA-AlPi.

Another difference is the evolution of low mass alkyl phosphinates, phosphate oligomers and related fragments in the temperature region where PLA degradation took place. The relative yields of these products were enhanced 4 to 9-folds compared to those observed for pure AlPi. Therefore, it can be concluded that the interactions between PLA and AlPi prevent principally trans-esterification reactions and produce low mass phosphinate oligomers and diethylphosphinic acid resulting the decomposition of PLA chains at lower temperatures. Extensive fragmentation of PLA chains can be explained by the mechanism given in Scheme 3.10.

**Scheme 3.10.** Possible reactions between phosphinates and PLA



Increase in the relative yield of  $(\text{C}_2\text{H}_5\text{PO})_2\text{OH}$  (169) was also recorded. New peaks appeared at 122, 353 and 455 Da due to diethyl phosphinic acid,  $(\text{C}_2\text{H}_5)_2\text{PO}_2\text{H}$ ,  $(\text{C}_2\text{H}_5\text{PO}_2)_3(\text{C}_2\text{H}_5\text{POH})$  and  $((\text{C}_2\text{H}_5)_2\text{PO}_2)_3(\text{C}_2\text{H}_5\text{PO}_2)$  respectively. These products reached maximum yield at slightly higher temperatures than the AlPi based fragments. Also, new peaks at 149 and 177 Da, though significantly weak may be associated with  $\text{CO}_2\text{P}(\text{C}_2\text{H}_5)_2\text{O}$  and  $\text{C}_2\text{H}_4\text{CO}_2\text{P}(\text{C}_2\text{H}_5)_2\text{O}$  respectively, were detected. Presence of these peaks supports the proposed mechanism in Scheme 3.10. The relative yields of these fragments were maximized at around  $335^\circ\text{C}$  as low mass phosphinate oligomers. Unfortunately the yields of the new products detected were not sufficient to perform CID experiments for further support for explanation of the structures.

### 3.3.1.2. PLA-AIPi-MMT30B

Isitman et al. showed that methyl tallow bis-2-hydroxyethyl, quaternary ammonium modified montmorillonite, MMT30B was spreaded in composite homogeneously. By addition of MMT30B no enhancement was observed in flammability properties. On the contrary, when MMT30B was introduced the positive effect of AIPi on flammability was eliminated. Also, increase in LOI from 23 to 27.5 upon addition of the AIPi, was unaffected by addition of MMT30B. However, PHRR of PLA was decreased drastically from  $578 \text{ kWm}^{-2}$  to  $283 \text{ kWm}^{-2}$  by addition MMT30B indicating char thickening through combustion. These results show that presence of MMT30B does not cause positive development in properties of combustion, instead makes it more difficult to deflagrate [68].

In the presence of MMT30B, pyrolysis of PLA-AIPi composite yielded a TIC curve with an intense peak at around  $340^\circ\text{C}$  and a weak one at around  $440^\circ\text{C}$  (Figure 3.36). The enhancement in the thermal stability of PLA is detected immediately with the addition of MMT30B. Again, the pyrolysis mass spectra recorded at around  $340^\circ\text{C}$  showed base peak at  $m/z = 56$  Da due to  $\text{CH}_3\text{CHCO}$ . The characteristic intense peaks of AIPi based products,  $(\text{C}_2\text{H}_5)_2\text{PO}$  (105 Da),  $(\text{C}_2\text{H}_5\text{PO})_2\text{OH}$  (169 Da),  $(\text{C}_2\text{H}_5)_2\text{PO}_2\text{AlO}_2\text{P}(\text{C}_2\text{H}_5)_2$  (269 Da),  $\text{Al}(\text{O}_2\text{P}(\text{C}_2\text{H}_5)_2)_2(\text{H}_2\text{P}_2\text{O}_5)$  (413 Da),  $\text{Al}_2(\text{O}_2\text{P}(\text{C}_2\text{H}_5)_2)_3\text{O}$  (433 Da),  $\text{Al}(\text{O}_2\text{P}(\text{C}_2\text{H}_5)_2)_2(\text{H}_2\text{P}_2\text{O}_5)(\text{O}_2\text{PC}_2\text{H}_5)$  (505 Da),  $\text{Al}_2(\text{O}_2\text{P}(\text{C}_2\text{H}_5)_2)_4\text{OPO}$  (601 Da) and  $\text{Al}_2(\text{O}_2\text{P}(\text{C}_2\text{H}_5)_2)_5$  (659 Da) are present in the pyrolysis mass spectra of PLA-AIPi-MMT30B recorded at around  $440^\circ\text{C}$ .

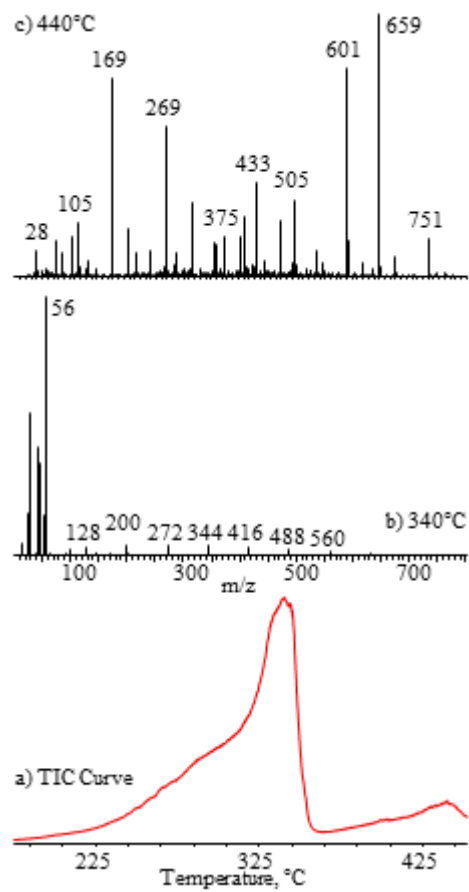


**Figure 3.36.** a) The total ion current curve and the mass spectra at b) 340°C and c) 440°C recorded during the pyrolysis of PLA-AIPi-MMT30B.

However, no significant change was noted in the relative yields of characteristic thermal degradation products of PLA compared to PLA-AlPi, thermal stability and product distribution of AlPi were affected by the presence of MMT30B. In Table 3.15, the relative intensities of intense and/or characteristic peaks recorded in the spectrum and the assignments made are summarized.

**Table 3.15.** The relative intensities, RI, of some selected intense and/or characteristic peaks recorded in pyrolysis spectrum of PLA-AlPi-MMT30B at 340 and 440°C and the assignments made.

m/z	RI		Assignment
	340°C	440°C	
28	544		C <sub>2</sub> H <sub>4</sub> and/or CO
43	408		C <sub>2</sub> H <sub>3</sub> O
44	101		C <sub>2</sub> H <sub>4</sub> O and/or CO <sub>2</sub>
45	358		C <sub>2</sub> H <sub>4</sub> OH and/or CO <sub>2</sub> H
56	1000		C <sub>2</sub> H <sub>4</sub> CO
72	5.5		C <sub>2</sub> H <sub>4</sub> CO <sub>2</sub>
100	25		C <sub>2</sub> H <sub>4</sub> COOC <sub>2</sub> H <sub>4</sub>
128	34		(C <sub>2</sub> H <sub>4</sub> CO <sub>2</sub> ) <sub>2</sub> C <sub>2</sub> H <sub>4</sub> CO
145	13		(C <sub>2</sub> H <sub>4</sub> CO <sub>2</sub> ) <sub>2</sub> H
200	42		(C <sub>2</sub> H <sub>4</sub> CO <sub>2</sub> ) <sub>2</sub> C <sub>2</sub> H <sub>4</sub> CO
217	6.3		(C <sub>2</sub> H <sub>4</sub> CO <sub>2</sub> ) <sub>3</sub> H
488	23		(C <sub>2</sub> H <sub>4</sub> CO <sub>2</sub> ) <sub>6</sub> C <sub>2</sub> H <sub>4</sub> CO
65	12	153	P(OH) <sub>2</sub>
94	12	175	C <sub>2</sub> H <sub>5</sub> P(OH) <sub>2</sub>
105	5.7	239	(C <sub>2</sub> H <sub>5</sub> ) <sub>2</sub> PO
122	2.7	29	(C <sub>2</sub> H <sub>5</sub> ) <sub>2</sub> PO <sub>2</sub> H
149	1.0	11	CO <sub>2</sub> P(C <sub>2</sub> H <sub>5</sub> ) <sub>2</sub> O
169	13	881	(C <sub>2</sub> H <sub>5</sub> PO) <sub>2</sub> OH
177	0.7	5.5	C <sub>2</sub> H <sub>4</sub> CO <sub>2</sub> P(C <sub>2</sub> H <sub>5</sub> ) <sub>2</sub> O
269		650	(C <sub>2</sub> H <sub>5</sub> ) <sub>2</sub> PO <sub>2</sub> AlO <sub>2</sub> P(C <sub>2</sub> H <sub>5</sub> ) <sub>2</sub>
353	0.2	22	(C <sub>2</sub> H <sub>5</sub> PO <sub>2</sub> ) <sub>3</sub> (C <sub>2</sub> H <sub>5</sub> POH)
413	1.4	289	Al(O <sub>2</sub> P(C <sub>2</sub> H <sub>5</sub> ) <sub>2</sub> ) <sub>2</sub> (H <sub>2</sub> P <sub>2</sub> O <sub>5</sub> )
433	2.4	403	OAl <sub>2</sub> (O <sub>2</sub> P(C <sub>2</sub> H <sub>5</sub> ) <sub>2</sub> ) <sub>3</sub>
505	3.5	341	Al(O <sub>2</sub> P(C <sub>2</sub> H <sub>5</sub> ) <sub>2</sub> ) <sub>2</sub> (H <sub>2</sub> P <sub>2</sub> O <sub>5</sub> )(O <sub>2</sub> PC <sub>2</sub> H <sub>5</sub> )
601		852	Al <sub>2</sub> (O <sub>2</sub> P(C <sub>2</sub> H <sub>5</sub> ) <sub>2</sub> ) <sub>4</sub> OPO
659		1000	Al <sub>2</sub> (O <sub>2</sub> P(C <sub>2</sub> H <sub>5</sub> ) <sub>2</sub> ) <sub>5</sub>
17	0.5		OH
31	4.1		CH <sub>2</sub> OH
296	1.1		N(C <sub>2</sub> H <sub>4</sub> OH) <sub>2</sub> C <sub>14</sub> H <sub>24</sub>

It is clear from the pyrolysis mass spectra that evolution of degradation fragments of PLA and AlPi occurred at around 340 and 440 °C respectively, indicating a slight increase in thermal stability of PLA and AlPi compared to PLA-AlPi. Single ion pyrograms of some of the representative thermal decomposition fragments of PLA, C<sub>2</sub>H<sub>4</sub> and/or CO (28 Da), C<sub>2</sub>H<sub>4</sub>CO (56 Da), protonated oligomers generated by cis-elimination reactions such as (C<sub>2</sub>H<sub>4</sub>CO<sub>2</sub>)<sub>2</sub>H (145 Da) and (C<sub>2</sub>H<sub>4</sub>CO<sub>2</sub>)<sub>2</sub>H (217 Da), and diagnostic products of cyclic oligomers (C<sub>2</sub>H<sub>4</sub>CO<sub>2</sub>)C<sub>2</sub>H<sub>4</sub>CO (128 Da), (C<sub>2</sub>H<sub>4</sub>CO<sub>2</sub>)C<sub>2</sub>H<sub>4</sub>CO (200 Da) are shown in Figure 3.37. The corresponding ones recorded during the degradation of PLA-AlPi composite are also included for comparison. Two overlapping peaks with maxima at 330 and 353°C are present in the evolution profiles of fragments produced by cis-elimination and transesterification reactions. The relative yields of group of fragment ions associated with (C<sub>2</sub>H<sub>4</sub>CO<sub>2</sub>)<sub>x</sub>H where x=1 to 4, were increased more than 1.5-folds when 20 wt% AlPi was replaced by 17 wt% AlPi and nanofiller involving 3 wt% MMT30B, although those of cyclic oligomers were not affected.

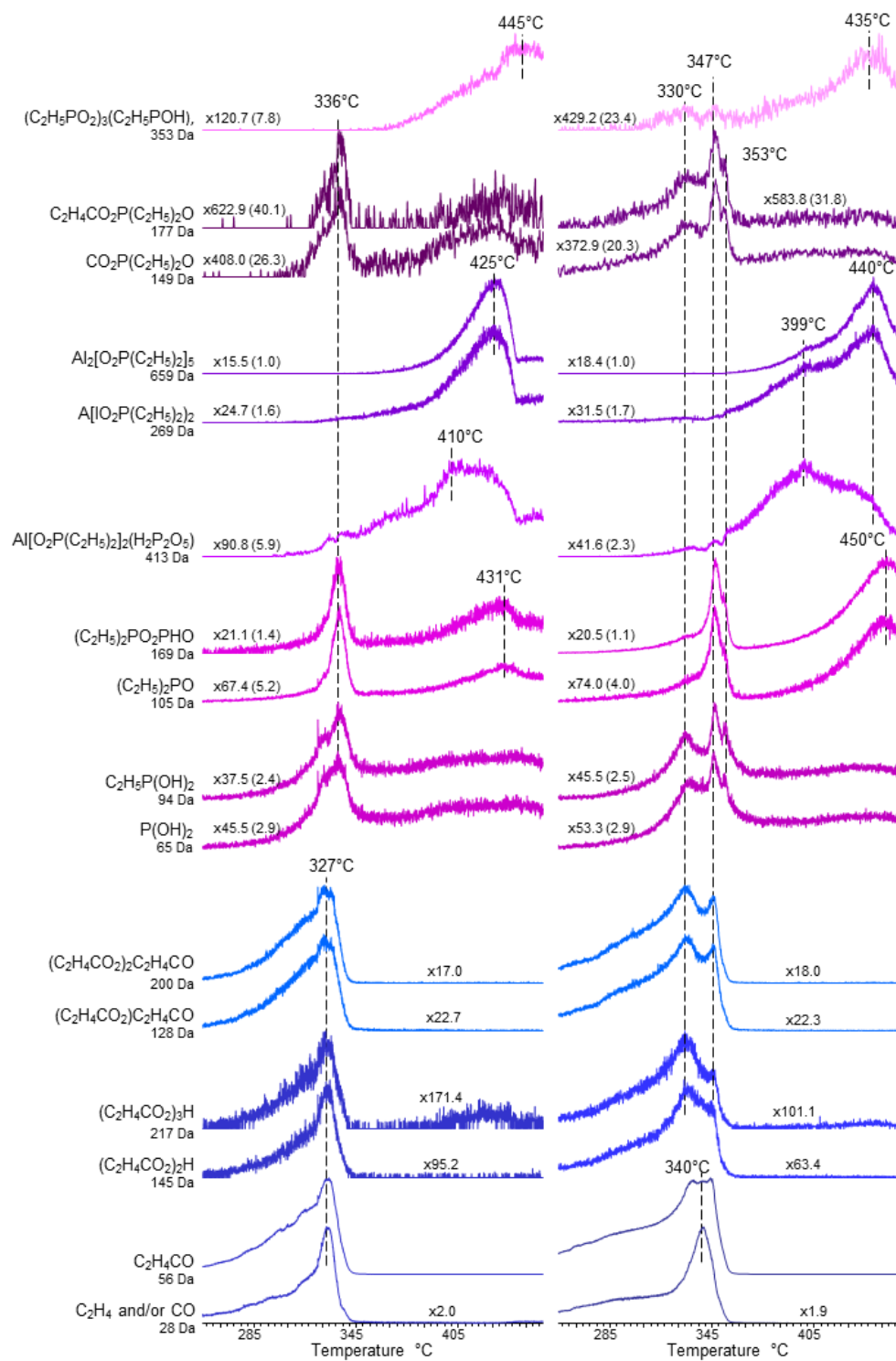


**Figure 3.37.** Single ion pyrograms of some selected fragments detected during the pyrolysis of I. PLA-AIPi, and II. PLA-AIPi-MMT30B.



The relative yields of thermal decomposition fragments of AlPi related with oligomers of phosphinates (i.e.  $(C_2H_5PO)_2OH$  (169 Da) and  $(C_2H_5)_2PO$  (105 Da)) and fragments involving oligomers of phosphinates as substituents (i.e.  $Al(O_2P(C_2H_5)_2)_2(H_2P_2O_5)$  (413 Da)) were slightly increased, when compared with PLA-AlPi. The increase was even more significant for  $(C_2H_5PO)_2OH$  (169 Da) and  $(C_2H_5)_2PO$  (105 Da) at high temperatures. Although, the relative yields of diethylphosphinic acid and  $P(OH)_2$  were not affected, a low temperature peak with a maximum at around 330°C was observed in their evolution profiles indicating formation of these products through different processes.

As a consequence of Lewis acid base interaction between phosphinates and carbonyl groups of PLA (Scheme 3.10) generation of fragments involving CO-P linkages such as  $CO_2P(C_2H_5)_2O$  (149 Da) and  $C_2H_4CO_2P(C_2H_5)_2O$  (177 Da), oligomers of phosphinates (i.e.  $(C_2H_5PO_2)_3(C_2H_5POH)$  (353 Da)) and diethylphosphinic acid  $(C_2H_5)_2PO_2H$  was observed. In the presence of MMT30B, the relative yields of fragments involving CO-P linkages increased in the temperature region where decomposition of PLA based products took place. On the other hand, the reduction in the yields of high mass oligomers of phosphinates in the high temperature region was noted.

By incorporation of MMT30B to the PLA-AlPi composite, evolution of alkyl amines was recorded at around 320 °C. This value was significantly higher than that detected during the pyrolysis of the pure MMT30B (279°C). The high temperature shift may be explained by the interaction between the PLA and MMT30B. Although, only few of the several peaks present in the MMT30B spectra were present in the spectra of PLA-AlPi-MMT30B, weak peaks at 17 and 31 Da that can directly be related with OH and  $CH_2OH$  groups were noticed. Single ion pyrograms of these fragments are given in Figure 3.38. The corresponding ones recorded during the pyrolysis of MMT30B and PLA-AlPi composite are also included for comparison. Possibility of trans-esterification reactions between the PLA and hydroxy ethylene groups of ammonium salt, generation of units involving  $CO-OC_2H_4N$  may be proposed as shown in Scheme

3.11. The increase in the relative yields of products with general formula  $(\text{COC}_2\text{H}_4\text{O})_x\text{H}$  where  $x=1$  to 3 supports the suggested trans-esterification reactions. In addition, the high temperature release of thermal decomposition fragments of PLA, at around  $347^\circ\text{C}$ , only few degrees above the temperature where the yields of OH and  $\text{CH}_2\text{OH}$  were maximized, may be considered as a further support for presence of chains cross-linked by trans-esterification reactions between hydroxide and carbonyl groups of PLA increasing the thermal stability slightly.

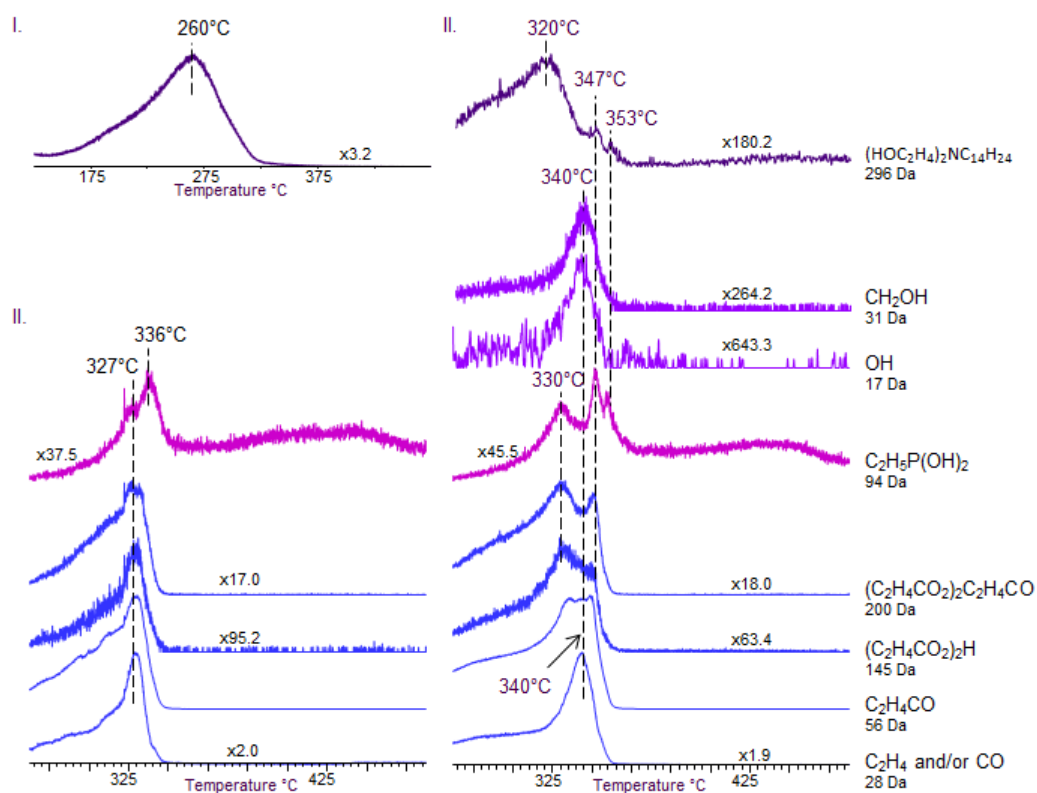
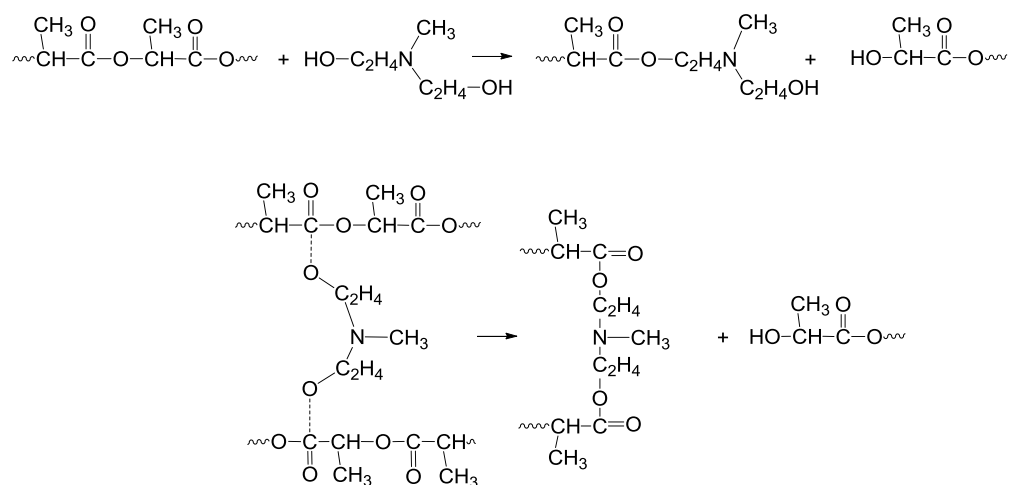


**Figure 3.38.** The single ion pyrograms of selected products recorded during the pyrolysis of I. MMT30B, II. PLA-AIPi, and III. PLA-AIPi-MMT30B.

**Scheme 3.11.** Trans-esterification reactions between the modifier of MMT and PLA



It may be concluded that in the presence of MMT30B, decomposition of ammonium salt initiated by trans-esterification reactions, generating PLA chains with slightly higher thermal stability. In addition, the nano-confinement of degrading molecules surrounded by the clay layers promoted reactions between phosphinates so, increasing the yield of fragments involving related oligomers.

### 3.3.1.3. PLA-AIPi- SiO<sub>2</sub>

In this study, nanosilica was a dimethyldichlorosilane treated fumed silica. Flame retardancy of nanosilica on PLA was studied by Isitman et al. [68]. Results showed that although SiO<sub>2</sub> spreaded homogeneously, a little aggregation was observed. According to the UL-94 vertical burn test, flammability of PLA-AIPi-SiO<sub>2</sub> was defined as V2 again. However, LOI value was decreased from 27.5 to 26.5 upon replacement of 15% of AIPi by SiO<sub>2</sub>. In addition, decrease in the PHRR from 443 kWm<sup>-2</sup> to 416 kWm<sup>-2</sup> was detected by addition of SiO<sub>2</sub> [68].

In the presence of SiO<sub>2</sub>, pyrolysis of PLA-AIPi composite yielded a TIC curve with a maximum at around 340 and 415°C (Figure 3.39). The pyrolysis mass

spectra of PLA showed the base peak at  $m/z = 56$  Da due to  $C_2H_4CO$  at around  $328^\circ C$ . The characteristic intense peaks of AlPi based products,  $P(OH)_2$  (65 Da),  $C_2H_5P(OH)_2$  (94 Da),  $(C_2H_5PO)_2OH$  (169 Da),  $(C_2H_5)_2PO_2AlO_2P(C_2H_5)_2$  (269 Da),  $Al(O_2P(C_2H_5)_2)_2(H_2P_2O_5)$  (413 Da),  $Al(O_2P(C_2H_5)_2)_2(H_2P_2O_5)(O_2PC_2H_5)$  (505 Da),  $Al_2(O_2P(C_2H_5)_2)_4OPO$  (601 Da) and  $Al_2(O_2P(C_2H_5)_2)_5$  (659 Da) are present in the pyrolysis mass spectra of PLA-AlPi recorded at around  $415^\circ C$ .

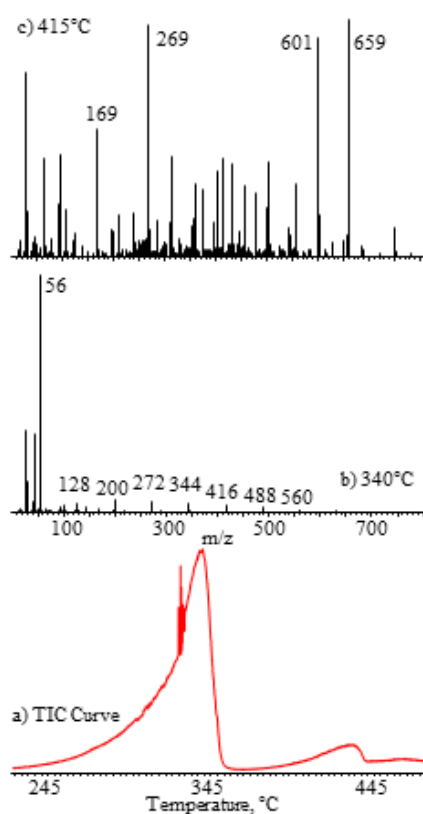


**Figure 3.39.** a) The total ion current curve and the mass spectra at b)  $340^\circ C$  and c)  $415^\circ C$  recorded during the pyrolysis of PLA-AlPi-SiO<sub>2</sub>.

Thermal stability of PLA was not changed in the presence of SiO<sub>2</sub>. Only the relative yields of fragments generated by the trans-esterification and cis-

elimination reactions decreased slightly, when compared with PLA-AlPi composite. Nevertheless, product distribution and thermal stability of AlPi were changed. In Table 3.16, the relative intensities of intense and/or characteristic peaks recorded in the spectrum and the assignments made are summarized.

**Table 3.16.** The relative intensities, RI, of some selected intense and/or characteristic peaks recorded in pyrolysis spectrum of PLA-AlPi-SiO<sub>2</sub> at 330 and 410°C and the assignments made.

m/z	RI		Assignment
	330°C	410°C	
28	342		C <sub>2</sub> H <sub>4</sub> and/or CO
43	332		C <sub>2</sub> H <sub>3</sub> O
44	82		C <sub>2</sub> H <sub>4</sub> O and/or CO <sub>2</sub>
45	305		C <sub>2</sub> H <sub>4</sub> OH and/or CO <sub>2</sub> H
56	1000		C <sub>2</sub> H <sub>4</sub> CO
72	3.2		C <sub>2</sub> H <sub>4</sub> CO <sub>2</sub>
100	28		C <sub>2</sub> H <sub>4</sub> COOC <sub>2</sub> H <sub>4</sub>
128	36		(C <sub>2</sub> H <sub>4</sub> CO <sub>2</sub> ) <sub>2</sub> C <sub>2</sub> H <sub>4</sub> CO
145	6.1		(C <sub>2</sub> H <sub>4</sub> CO <sub>2</sub> ) <sub>2</sub> H
200	49		(C <sub>2</sub> H <sub>4</sub> CO <sub>2</sub> ) <sub>2</sub> C <sub>2</sub> H <sub>4</sub> CO
217	3.9		(C <sub>2</sub> H <sub>4</sub> CO <sub>2</sub> ) <sub>3</sub> H
488	19		(C <sub>2</sub> H <sub>4</sub> CO <sub>2</sub> ) <sub>6</sub> C <sub>2</sub> H <sub>4</sub> CO
65	16	386	P(OH) <sub>2</sub>
94	18	473	C <sub>2</sub> H <sub>5</sub> P(OH) <sub>2</sub>
105	4.4	189	(C <sub>2</sub> H <sub>5</sub> ) <sub>2</sub> PO
122	3.8	64	(C <sub>2</sub> H <sub>5</sub> ) <sub>2</sub> PO <sub>2</sub> H
169	15	525	(C <sub>2</sub> H <sub>5</sub> PO) <sub>2</sub> OH
269	0.6	1000	(C <sub>2</sub> H <sub>5</sub> ) <sub>2</sub> PO <sub>2</sub> AlO <sub>2</sub> P(C <sub>2</sub> H <sub>5</sub> ) <sub>2</sub>
311	0.3	141	Al(OP) <sub>3</sub> (C <sub>2</sub> H <sub>5</sub> ) <sub>2</sub> (OH) <sub>5</sub>
353		85	(C <sub>2</sub> H <sub>5</sub> PO <sub>2</sub> ) <sub>3</sub> (C <sub>2</sub> H <sub>5</sub> POH)
403	0.6	375	Al(OP) <sub>4</sub> (C <sub>2</sub> H <sub>5</sub> ) <sub>3</sub> (OH) <sub>5</sub> O and/or Al(OP) <sub>3</sub> (C <sub>2</sub> H <sub>5</sub> ) <sub>4</sub> (OH) <sub>7</sub>
413	0.7	498	Al(O <sub>2</sub> P(C <sub>2</sub> H <sub>5</sub> ) <sub>2</sub> ) <sub>2</sub> (H <sub>2</sub> P <sub>2</sub> O <sub>5</sub> )
505	1.4	453	Al(O <sub>2</sub> P(C <sub>2</sub> H <sub>5</sub> ) <sub>2</sub> ) <sub>2</sub> (H <sub>2</sub> P <sub>2</sub> O <sub>5</sub> )(O <sub>2</sub> PC <sub>2</sub> H <sub>5</sub> )
601		885	Al <sub>2</sub> (O <sub>2</sub> P(C <sub>2</sub> H <sub>5</sub> ) <sub>2</sub> ) <sub>4</sub> OPO
659		975	Al <sub>2</sub> (O <sub>2</sub> P(C <sub>2</sub> H <sub>5</sub> ) <sub>2</sub> ) <sub>5</sub>

Single ion pyrograms of some of the selected fragments of PLA such as  $C_2H_4$  and/or CO (28 Da),  $C_2H_4CO$  (56 Da), protonated oligomers generated by cis-elimination reactions such as  $(C_2H_4CO_2)_2H$  (145 Da) and  $(C_2H_4CO_2)_2H$  (217 Da), and diagnostic products of cyclic oligomers  $(C_2H_4CO_2)C_2H_4CO$  (128 Da) and  $(C_2H_4CO_2)C_2H_4CO$  (200 Da) and AlPi involving four coordinates compounds with Al-O-P linkages, namely  $Al_2[O_2P(C_2H_5)_2]_5$  (659 Da) and  $(C_2H_5)_2PO_2AlO_2P(C_2H_5)_2$  (269 Da), fragments involving oligomers of phosphinates as substituents such as  $Al(O_2P(C_2H_5)_2)_2(H_2P_2O_5)$  (413 Da),  $Al(OP)_4(C_2H_5)_3(OH)_5O$  and/or  $Al(OP)_3(C_2H_5)_4(OH)_7$  (403 Da),  $Al(OP)_3(C_2H_5)_2(OH)_5$  (311 Da) and phosphinates such as  $(C_2H_5PO)_2OH$  (169 Da),  $(C_2H_5)_2PO$  (105 Da),  $C_2H_5P(OH)_2$  (94 Da) and  $P(OH)_2$  (65 Da) recorded during the pyrolysis of PLA-AlPi-SiO<sub>2</sub> are shown in Figure 3.40.

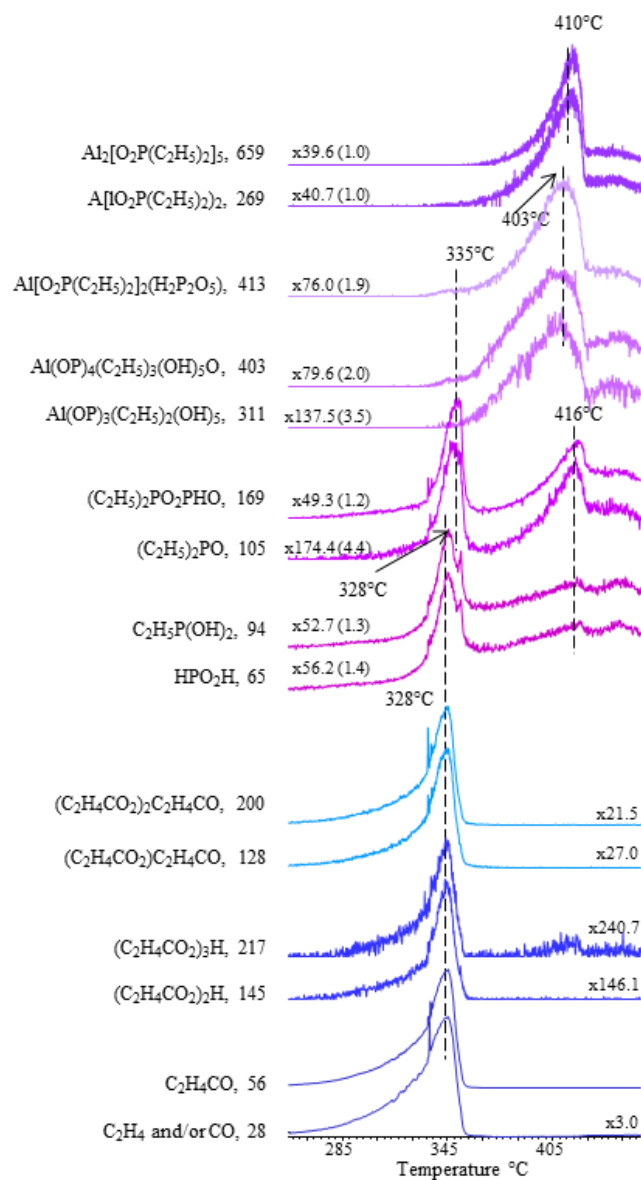


**Figure 3.40.** Single ion pyrograms of some selected fragments detected during the pyrolysis PLA-AlPi-SiO<sub>2</sub>.

In case of PLA-AIPi-SiO<sub>2</sub>, the PLA based fragments were maximized at around 328°C. On the other hand, noticeable decrease in degradation products of AIPi, the dimeric four coordinate compounds involving Al-O-P linkages, was recorded with a maximum yield at around 410°C. The reduction in the relative yield of these fragments was more than 2-folds, more than the expected value due to the replacement of 15 wt% AIPi by SiO<sub>2</sub>. The yields of fragments involving only phosphorous compounds such as (C<sub>2</sub>H<sub>5</sub>PO)<sub>2</sub>OH (169 Da), (C<sub>2</sub>H<sub>5</sub>)<sub>2</sub>PO (105 Da), C<sub>2</sub>H<sub>5</sub>P(OH)<sub>2</sub> (94 Da) and P(OH)<sub>2</sub> (65 Da) decreased but to a lower extent. These fragments reached maximum yield at around 335 and 416°C. Moreover, the products generated by Lewis acid base reactions of phosphinates and PLA such as CO<sub>2</sub>P(C<sub>2</sub>H<sub>5</sub>)<sub>2</sub>O (149 Da) and C<sub>2</sub>H<sub>4</sub>CO<sub>2</sub>P(C<sub>2</sub>H<sub>5</sub>)<sub>2</sub>O (177 Da) were almost totally disappeared. However, slight increase in the relative yields of Al(O<sub>2</sub>P(C<sub>2</sub>H<sub>5</sub>)<sub>2</sub>)<sub>2</sub>(O<sub>2</sub>P(C<sub>2</sub>H<sub>5</sub>))(H<sub>2</sub>P<sub>2</sub>O<sub>5</sub>) (505 Da), Al(O<sub>2</sub>P(C<sub>2</sub>H<sub>5</sub>)<sub>2</sub>)<sub>2</sub>(H<sub>2</sub>P<sub>2</sub>O<sub>5</sub>) (413 Da), Al(OP)<sub>4</sub>(C<sub>2</sub>H<sub>5</sub>)<sub>3</sub>(OH)<sub>5</sub>O and/or Al(OP)<sub>3</sub>(C<sub>2</sub>H<sub>5</sub>)<sub>4</sub>(OH)<sub>7</sub> (403 Da) and Al(OP)<sub>3</sub>(C<sub>2</sub>H<sub>5</sub>)<sub>2</sub>(OH)<sub>5</sub> (311 Da) fragments associated with monomeric aluminium phosphinate compounds was noted. In fact, among the AIPi based products, the relative yields of fragments involving only phosphorous compounds and monomeric aluminium phosphinate compounds increased. Therefore, it may be concluded that generation of dimeric four coordinate compounds involving Al-O-P linkages was hindered, and the yields of monomeric aluminium phosphinate compounds that may further decompose during pyrolysis and/or ionization to low mass phosphorous compounds were enhanced, in the presence of SiO<sub>2</sub>.

#### 3.3.1.4. PLA-AIPi-HNT

Earlier studies showed that HNT spreaded inhomogeneously [68]. By addition of HNT no improvement was observed in flammability properties of PLA-AIPi composite. On the contrary, when HNT was added the positive effect of AIPi on ignition was lost. In addition, LOI value decreased slightly from 27.5 to 27.0 by the addition of HNT. Moreover, PHRR was increased from 443 Wm<sup>-2</sup> to 511 kWm<sup>-2</sup> by addition of HNT [68].



In the presence of HNT, pyrolysis of PLA-AlPi composite yielded a TIC curve with a maximum at around 310 and 395°C (Figure 3.41). Again, the pyrolysis mass spectra showed the base peak at  $m/z = 56$  Da due to  $C_2H_4CO$  at around 310°C. The characteristic intense peaks of AlPi based products,  $P(OH)_2$  (65 Da),  $C_2H_5P(OH)_2$  (94 Da),  $(C_2H_5PO)_2OH$  (169 Da),  $(C_2H_5)_2PO_2AlO_2P(C_2H_5)_2$  (269 Da),  $Al(OP)_3(C_2H_5)_4(OH)_7$  (403 Da),  $Al(O_2P(C_2H_5)_2)_2(H_2P_2O_5)(O_2PC_2H_5)$  (505 Da),  $Al_2(O_2P(C_2H_5)_2)_4OPO$  (601 Da) and  $Al_2(O_2P(C_2H_5)_2)_5$  (659 Da) are also present in the pyrolysis mass spectra of PLA-AlPi-HNT recorded at around 390°C.

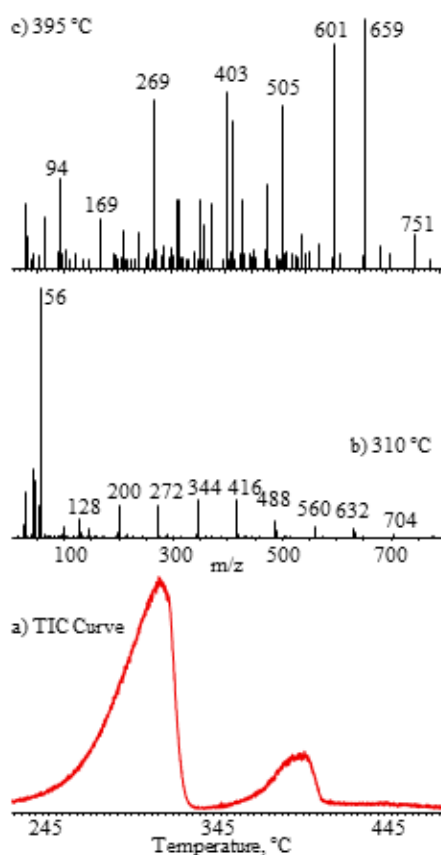


**Figure 3.41.** a) The total ion current curve and the mass spectra at b) 310°C and c) 395°C recorded during the pyrolysis of PLA-AlPi-HNT.

In the presence of HNT, thermal stability of PLA was reduced significantly and relative intensities of peaks related with generation of cyclic and protonated oligomers were increased. In Table 3.17, the relative intensities of intense and/or characteristic peaks recorded in the spectrum and the assignments made are summarized.

**Table 3.17.** The relative intensities, RI, of some selected intense and/or characteristic peaks recorded in pyrolysis spectrum of PLA-AlPi-HNT at 310 and 392°C and the assignments made.

m/z	RI		Assignment
	310°C	392°C	
28	198		C <sub>2</sub> H <sub>4</sub> and/or CO
43	309		C <sub>2</sub> H <sub>3</sub> O
44	63		C <sub>2</sub> H <sub>4</sub> O and/or CO <sub>2</sub>
45	249		C <sub>2</sub> H <sub>4</sub> OH and/or CO <sub>2</sub> H
56	1000		C <sub>2</sub> H <sub>4</sub> CO
72	2.8		C <sub>2</sub> H <sub>4</sub> CO <sub>2</sub>
100	44		C <sub>2</sub> H <sub>4</sub> COOC <sub>2</sub> H <sub>4</sub>
128	67		(C <sub>2</sub> H <sub>4</sub> CO <sub>2</sub> )C <sub>2</sub> H <sub>4</sub> CO
145	11		(C <sub>2</sub> H <sub>4</sub> CO <sub>2</sub> ) <sub>2</sub> H
200	131		(C <sub>2</sub> H <sub>4</sub> CO <sub>2</sub> ) <sub>2</sub> C <sub>2</sub> H <sub>4</sub> CO
217	14		(C <sub>2</sub> H <sub>4</sub> CO <sub>2</sub> ) <sub>3</sub> H
488	73		(C <sub>2</sub> H <sub>4</sub> CO <sub>2</sub> ) <sub>6</sub> C <sub>2</sub> H <sub>4</sub> CO
65	10	243	P(OH) <sub>2</sub>
94	18	395	C <sub>2</sub> H <sub>5</sub> P(OH) <sub>2</sub>
105		60	(C <sub>2</sub> H <sub>5</sub> ) <sub>2</sub> PO
122	3.5	51	(C <sub>2</sub> H <sub>5</sub> ) <sub>2</sub> PO <sub>2</sub> H
169	6.1	133	(C <sub>2</sub> H <sub>5</sub> PO) <sub>2</sub> OH
269		689	(C <sub>2</sub> H <sub>5</sub> ) <sub>2</sub> PO <sub>2</sub> AlO <sub>2</sub> P(C <sub>2</sub> H <sub>5</sub> ) <sub>2</sub>
311		173	Al(OP) <sub>3</sub> (C <sub>2</sub> H <sub>5</sub> ) <sub>2</sub> (OH) <sub>5</sub>
403		687	Al(OP) <sub>4</sub> (C <sub>2</sub> H <sub>5</sub> ) <sub>3</sub> (OH) <sub>5</sub> O and/or Al(OP) <sub>3</sub> (C <sub>2</sub> H <sub>5</sub> ) <sub>4</sub> (OH) <sub>7</sub>
413		566	Al(O <sub>2</sub> P(C <sub>2</sub> H <sub>5</sub> ) <sub>2</sub> ) <sub>2</sub> (H <sub>2</sub> P <sub>2</sub> O <sub>5</sub> )
505	7.5	684	Al(O <sub>2</sub> P(C <sub>2</sub> H <sub>5</sub> ) <sub>2</sub> ) <sub>2</sub> (H <sub>2</sub> P <sub>2</sub> O <sub>5</sub> )(O <sub>2</sub> PC <sub>2</sub> H <sub>5</sub> )
601		804	Al <sub>2</sub> (O <sub>2</sub> P(C <sub>2</sub> H <sub>5</sub> ) <sub>2</sub> ) <sub>4</sub> OPO
659		1000	Al <sub>2</sub> (O <sub>2</sub> P(C <sub>2</sub> H <sub>5</sub> ) <sub>2</sub> ) <sub>5</sub>

Single ion pyrograms of some of the representative fragments of PLA such as  $C_2H_4$  and/or  $CO$  (28 Da),  $C_2H_4CO$  (56 Da), protonated oligomers such as  $(C_2H_4CO_2)_2H$  (145 Da) and  $(C_2H_4CO_2)_2H$  (217 Da), and diagnostic products of cyclic oligomers  $(C_2H_4CO_2)C_2H_4CO$  (128 Da) and  $(C_2H_4CO_2)C_2H_4CO$  (200 Da)  $(C_2H_4CO_2)_xH$  and AlPi involving four coordinates compounds with Al-O-P linkages, namely  $Al_2[O_2P(C_2H_5)_2]_5$  (659 Da) and  $(C_2H_5)_2PO_2AlO_2P(C_2H_5)_2$  (269 Da), fragments involving oligomers of phosphinates as substituents such as  $Al(O_2P(C_2H_5)_2)_2(H_2P_2O_5)$  (413 Da),  $Al(OP)_4(C_2H_5)_3(OH)_5O$  and/or  $Al(OP)_3(C_2H_5)_4(OH)_7$  (403 Da),  $Al(OP)_3(C_2H_5)_2(OH)_5$  (311 Da) and phosphinates such as  $(C_2H_5PO)_2OH$  (169 Da),  $(C_2H_5)_2PO$  (105 Da),  $C_2H_5P(OH)_2$  (94 Da) and  $P(OH)_2$  (65 Da) recorded during the pyrolysis of PLA-AlPi-SiO<sub>2</sub> are shown in Figure 3.42.

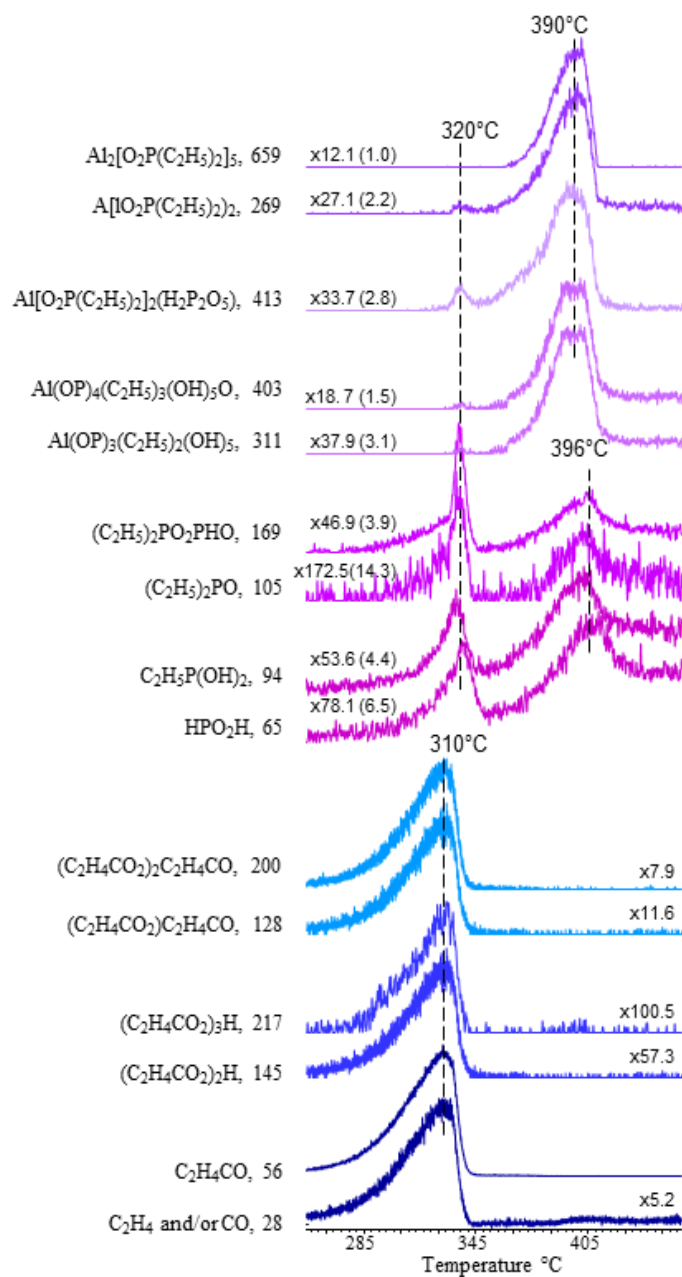


**Figure 3.42.** Single ion pyrograms of some selected fragments detected during the pyrolysis PLA-AlPi-HNT.

The thermal stability of PLA-AIPi-HNT composite was decreased significantly compared to PLA-AIPi. Thermal degradation of PLA based products decreased about 17°C. The decrease in the yields of the thermal decomposition of AIPi based products was not so significant. The temperature, at which the yields of dimeric four coordinate compounds involving Al-O-P linkages were maximized, shifted to 390°C from 425°C upon replacement of 15 % AIPi by HNT.

With the addition of HNT, the relative yields of fragments due to trans-esterification and cis-elimination reactions were increased more than 2-folds. On the other hand, the relative yields of these fragments were still lower than those recorded for the pure PLA. In addition, significant changes in the relative yields of characteristic products of AIPi were detected. The relative yields of four coordinate compounds including Al-O-P linkages slightly enhanced compared to PLA-AIPi. The enhancement in the relative yields of fragments with m/z values 505, 403, 413 and 311 Da was much more pronounced, almost about 4-folds.

The release of  $(C_2H_5PO)_2OH$  (169 Da),  $(C_2H_5)_2PO$  (105 Da),  $C_2H_5P(OH)_2$  (94 Da) and  $P(OH)_2$  (65 Da) was decreased significantly at around 320°C. However, their relative intensities were increased at around 396°C. The products generated by reactions of phosphinates and PLA such as  $CO_2P(C_2H_5)_2O$  (149 Da) and  $C_2H_4CO_2P(C_2H_5)_2O$  (177 Da) again were not detected as in case of PLA-AIPi-SiO<sub>2</sub>. Therefore, it may be thought that the interactions between PLA and AIPi based products were hindered in the presence of HNT. The increases in the relative yields of fragments associated with trans-esterification and cis-elimination reactions compared to PLA-AIPi and those of dimeric four coordinate compounds involving Al-O-P linkages supported this proposal. It may be concluded that, the interactions between PLA and AIPi were decreased in the presence of HNT and each of them decomposed as in the pure forms at least to a certain extent.

### 3.4 THERMAL DEGRADATION OF POLYSTYRENE IN THE PRESENCE OF NANOPARTICLES AND FLAME RETARDANTS

#### 3.4.1. THERMAL DEGRADATION OF HIGH IMPACT POLYSTYRENE IN THE PRESENCE OF NANOPARTICLE AND FLAME RETARDANT

For understanding the effects of nanoclays on thermal degradation characteristics of high impact polystyrene composites, HIPS involving 25% ATH or 3% MMT10A and HIPS involving 25% ATH and 3% MMT10A were studied by DP-MS technique separately (Table 2.3).

The variation of total ion yield as a function of temperature (TIC) curve and the mass spectrum of HIPS recorded at the peak maximum, at 471°C, are shown in Figure 3.43. Major component generated from the thermal decomposition of HIPS under vacuum was the styrene monomer. Other common products were dimer and trimer,  $\alpha$ -methylstyrene, toluene, benzene and ethylbenzene. The TIC curve recorded during the pyrolysis of HIPS showed a broad peak with a maximum at 471°C (Figure 3.43). Typical fragmentation pattern for styrene was recorded in the pyrolysis mass spectra of HIPS, involving intense peaks at  $m/z = 51, 78, 91$  and  $104$  Da due to  $C_4H_3$ ,  $C_6H_6$ ,  $C_6H_5CH_2$  and  $CH_2CHC_6H_5$ , M respectively. Furthermore, weak peaks at  $105, 115, 118, 129, 194$  and  $208$  Da due to MH,  $C_3H_2C_6H_5$ ,  $C_3H_5C_6H_5$ ,  $C_4H_4C_6H_5$ ,  $C_6H_5CH_2CHCHC_6H_5$  and  $C_6H_5CHCHCH(C_6H_5)CH_3$ , D respectively, were observed, indicating that the thermal degradation of HIPS took place via depolymerization generating mostly the monomer and low mass oligomers and by breaking and rearrangement of phenyl group from the monomer and dimer. In Table 3.18, the relative intensities of intense and/or characteristic peaks recorded in the spectrum and the assignments made are summarized.

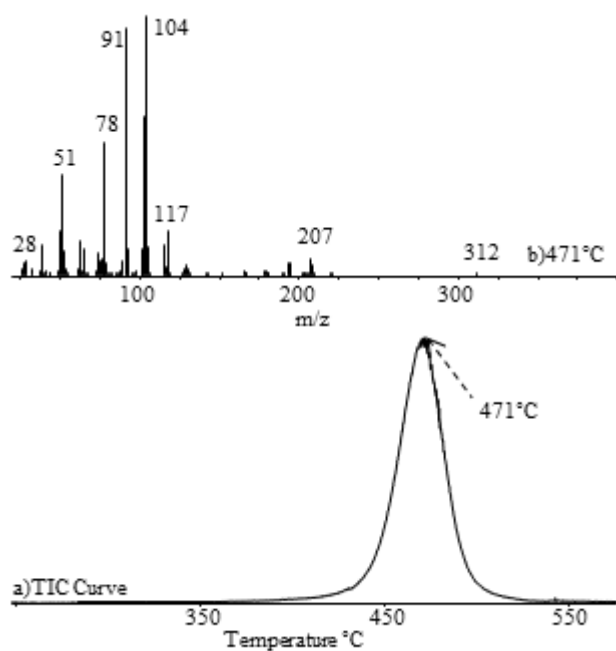


**Figure 3.43.** a) The total ion current curve and b) mass spectrum of HIPS at 471 °C.

**Table 3.18.** The relative intensities, RI, of some selected intense and/or characteristic peaks recorded in pyrolysis spectrum of HIPS at 471 °C and the assignments made.

m/z	RI	Assignment
51	385	C <sub>4</sub> H <sub>3</sub>
78	513	C <sub>6</sub> H <sub>6</sub>
91	947	C <sub>6</sub> H <sub>5</sub> CH <sub>2</sub>
92	100	C <sub>6</sub> H <sub>5</sub> CH <sub>3</sub>
104	1000	CH <sub>2</sub> CHC <sub>6</sub> H <sub>5</sub> , M and/or C <sub>2</sub> H <sub>4</sub> C <sub>6</sub> H <sub>4</sub>
105	106	CH <sub>2</sub> CH <sub>2</sub> C <sub>6</sub> H <sub>5</sub> and/or C <sub>2</sub> H <sub>5</sub> C <sub>6</sub> H <sub>4</sub>
115	113	C <sub>3</sub> H <sub>2</sub> C <sub>6</sub> H <sub>5</sub>
118	23	C <sub>3</sub> H <sub>5</sub> C <sub>6</sub> H <sub>5</sub>
129	35	C <sub>4</sub> H <sub>4</sub> C <sub>6</sub> H <sub>5</sub>
194	46	C <sub>6</sub> H <sub>5</sub> CH <sub>2</sub> CHCHC <sub>6</sub> H <sub>5</sub>
207	62	M <sub>2</sub> -H and/or C <sub>14</sub> H <sub>7</sub> O <sub>2</sub>
208	40	St <sub>2</sub>
312	3.0	St <sub>3</sub>

The evolution profiles of all fragment ions showed identical trends as expected. In Figure 3.44, single ion pyrograms of  $C_6H_6$  (78 Da),  $C_6H_5CH_2$  (91 Da),  $C_6H_5CH_3$  (92 Da), M (104 Da), MH (105 Da),  $C_3H_2C_6H_5$  (115 Da),  $C_4H_4C_6H_5$  (129 Da) and  $M_2-H$  (207 Da) are presented. Thus, it can be concluded that they were generated energetically through the same decomposition pathway, through one step thermal degradation mechanism.

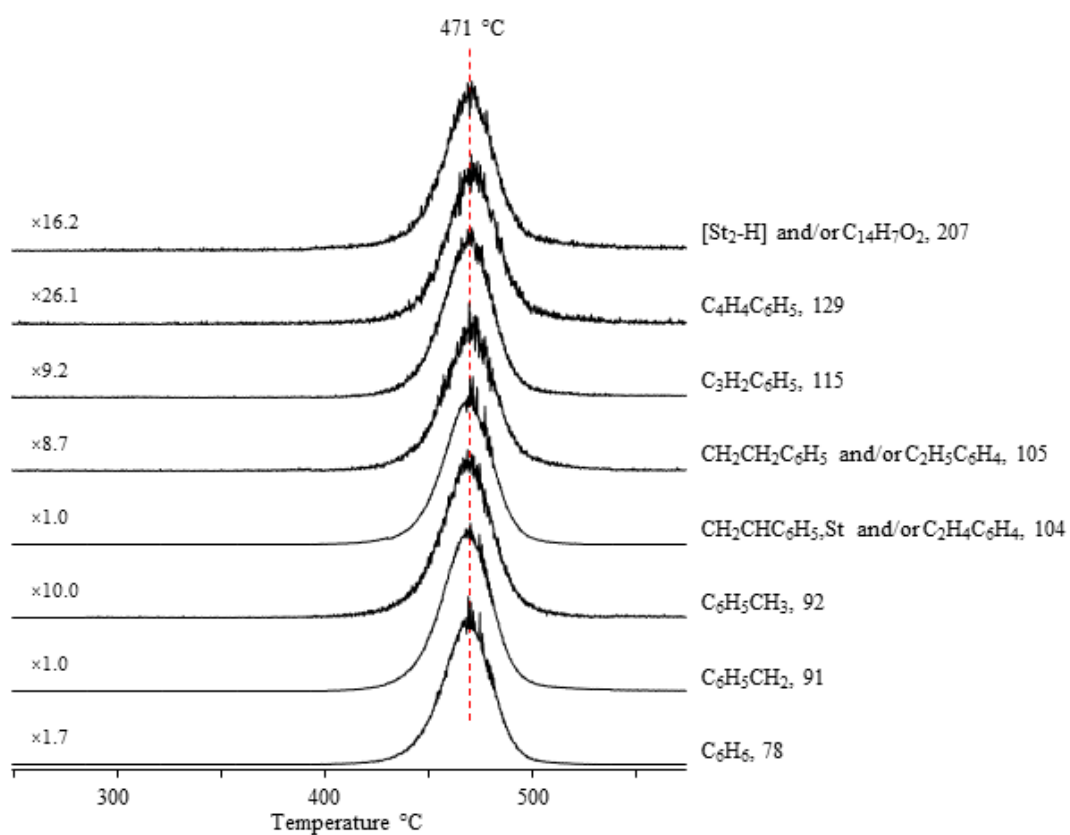
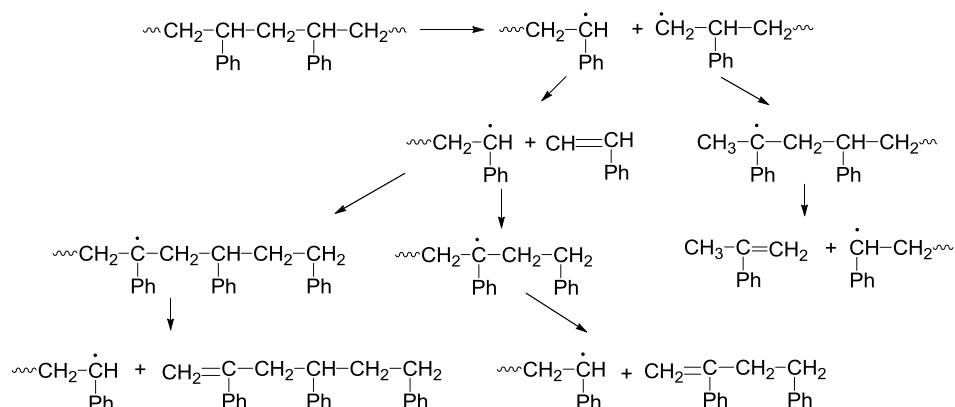


**Figure 3.44.** Single ion pyrograms of some selected fragments detected during the pyrolysis of HIPS.



The degradation pathway of neat high impact polystyrene occurs by chain scission continued by depolymerization and the production of the styrene monomer, dimer, and trimer, is demonstrated in Scheme 3.12 [92-99]. Generated primary radicals are converted to the tertiary radicals due to their enhanced stability. By  $\beta$ -scission, tertiary radical leads to the generation of  $\alpha$ -methyl styrene (118 Da) and another secondary radical. Therefore, during the degradation, the most abundant radical is the secondary radical and the most generated fragment is styrene, because, styrene is generated continuously by  $\beta$ -scission. However, secondary radicals are not stable, so, some of them are transformed to tertiary radical by hydrogen transfer as shown in Scheme 3.12, and styrene, dimer and trimer can be generated by this way. During the degradation of neat high impact polystyrene, the main generated compounds have carbon-carbon double bonds [79].

**Scheme 3.12.** The degradation pathway of neat high impact polystyrene.



### 3.4.1.1. HIPS-ATH

In a recent study [81], it has been shown that the addition of 25 wt% ATH was enough to decrease the peak heat release rate, PHRR, detected for HIPS by ~50%.

In addition, the peak mass loss rate, PMLR was decreased from ~31% to ~20% when 25 wt% ATH was added to HIPS. Furthermore, the limiting oxygen index, LOI, was increased about 1.5% with respect to the neat HIPS. No charring was observed during the decomposition of HIPS [81]. On the other hand, upon heating to 600°C, 15.6 wt% char residue was observed for HIPS-ATH composite, indicating that upon dehydration, a residue of about 60 wt% of the initial ATH mass remained in the solid phase [81].

In the presence of ATH, pyrolysis of HIPS yielded a broad peak with maximum at 469°C (Figure 3.45). HIPS-ATH composite decomposes mainly to C<sub>7</sub>H<sub>7</sub> (91 Da). Other intense peaks in the mass spectrum of HIPS-ATH composite at 469°C, were at 78, 104, 105 and 115 Da associated with C<sub>6</sub>H<sub>6</sub>, CH<sub>2</sub>CHC<sub>6</sub>H<sub>5</sub> (M), MH, C<sub>3</sub>H<sub>2</sub>C<sub>6</sub>H<sub>5</sub> and moderate peaks at 118, 129 and 208 Da due to C<sub>3</sub>H<sub>5</sub>C<sub>6</sub>H<sub>5</sub>, C<sub>4</sub>H<sub>4</sub>C<sub>6</sub>H<sub>5</sub> and M<sub>2</sub> respectively, indicating that the depolymerization reactions were decreased to a certain extent. In addition, the decomposition of HIPS took place almost at the same temperature region. In Table 3.19, the relative intensities of intense and/or characteristic peaks recorded in the spectrum and the assignments made are summarized.

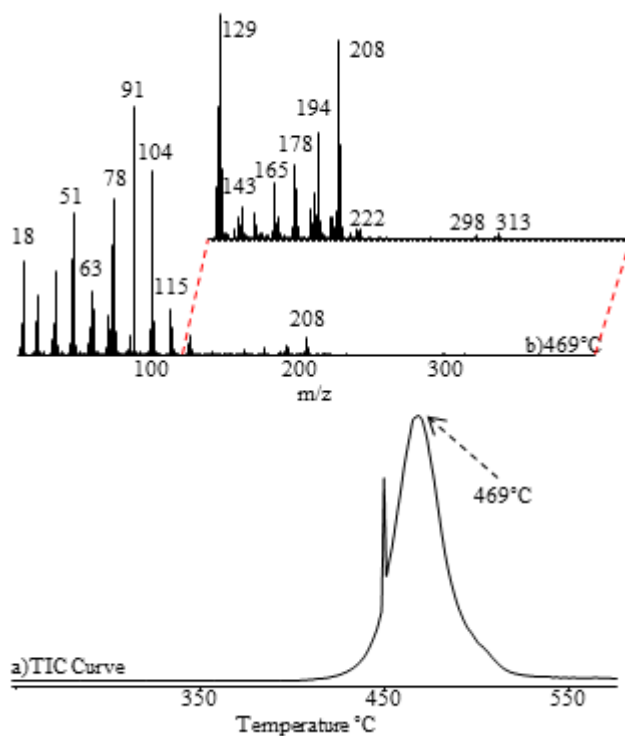


**Figure 3.45.** a) The total ion current curve and b) mass spectrum of HIPS-ATH at 469°C.

**Table 3.19.** The relative intensities, RI, of some selected intense and/or characteristic peaks recorded in pyrolysis spectrum of HIPS-ATH at 469°C and the assignments made.

m/z	RI	Assignment
18	395	H <sub>2</sub> O
78	651	C <sub>6</sub> H <sub>6</sub>
91	1000	C <sub>6</sub> H <sub>5</sub> CH <sub>2</sub>
92	114	C <sub>6</sub> H <sub>5</sub> CH <sub>3</sub>
104	746	CH <sub>2</sub> CHC <sub>6</sub> H <sub>5</sub> , St and/or C <sub>2</sub> H <sub>4</sub> C <sub>6</sub> H <sub>4</sub>
105	136	CH <sub>2</sub> CH <sub>2</sub> C <sub>6</sub> H <sub>5</sub> and/or C <sub>2</sub> H <sub>5</sub> C <sub>6</sub> H <sub>4</sub>
115	174	C <sub>3</sub> H <sub>2</sub> C <sub>6</sub> H <sub>5</sub>
118	25	C <sub>3</sub> H <sub>5</sub> C <sub>6</sub> H <sub>5</sub>
129	79	C <sub>4</sub> H <sub>4</sub> C <sub>6</sub> H <sub>5</sub>
194	38	C <sub>6</sub> H <sub>5</sub> CH <sub>2</sub> CHCHC <sub>6</sub> H <sub>5</sub>
207	8.1	M <sub>2</sub> -H and/or C <sub>14</sub> H <sub>7</sub> O <sub>2</sub>
208	73	St <sub>2</sub>
312	0.6	St <sub>3</sub>

The evolution profiles of almost all fragment ions showed identical trends as expected. Thus, it can be concluded that they were generated energetically through the same decomposition pathway or through the same thermal degradation mechanism. Although the relative yields of almost all products were increased, the relative yields of monomer, dimer and trimer were decreased. Thus, it can be thought that in the presence of ATH depolymerization reactions were suppressed. In Figure 3.46, single ion pyrograms of H<sub>2</sub>O (18 Da), C<sub>6</sub>H<sub>6</sub> (78 Da), C<sub>6</sub>H<sub>5</sub>CH<sub>2</sub> (91 Da), C<sub>6</sub>H<sub>5</sub>CH<sub>3</sub> (92 Da), M (104 Da), MH (105 Da), C<sub>3</sub>H<sub>2</sub>C<sub>6</sub>H<sub>5</sub> (115 Da), C<sub>4</sub>H<sub>4</sub>C<sub>6</sub>H<sub>5</sub> (129 Da) and M<sub>2</sub>-H (207 Da) are presented.

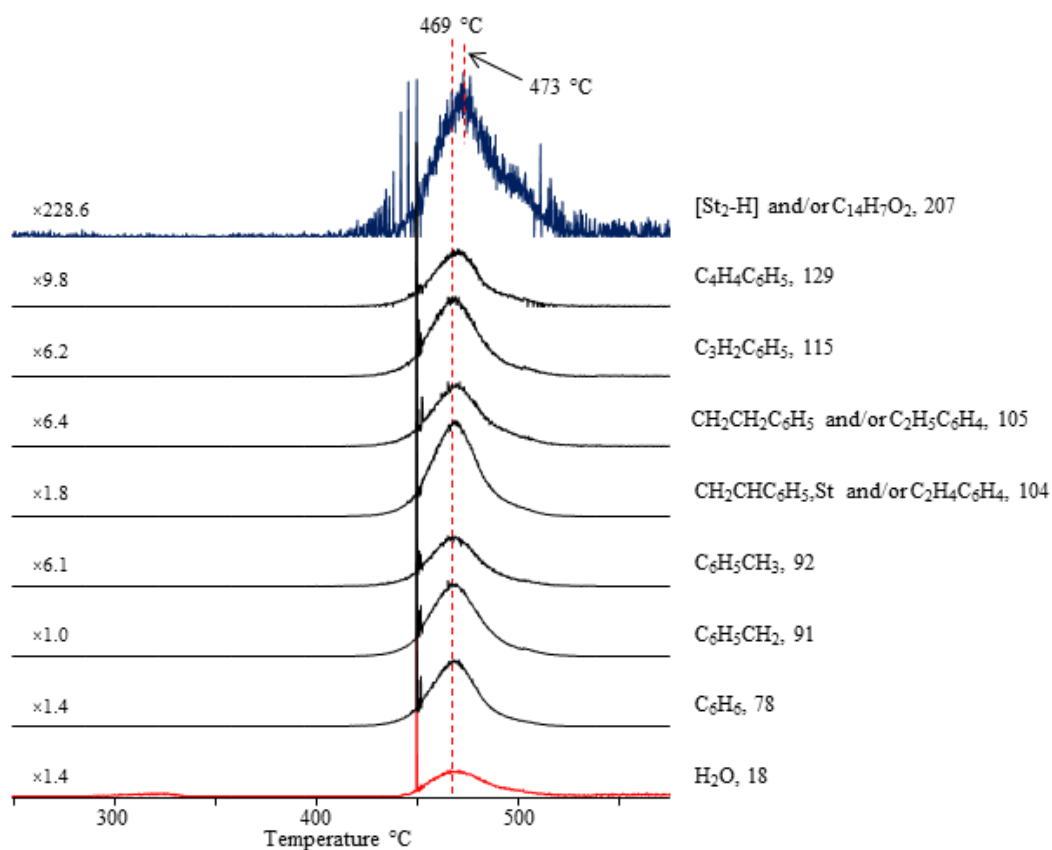


**Figure 3.46.** Single ion pyrograms of some selected fragments detected during the pyrolysis of HIPS-ATH.

### 3.4.1.2. HIPS-MMT10A

In a recent study [81], it has been defined that the addition of 3 wt% MMT10A was enough to decrease the PHRR by ~30% compared to neat HIPS. In addition, the PMLR was decreased from ~31% to ~23%. Furthermore, the percentage of char residues was 3.1% for HIPS-MMT10A composite, while no charring was occurred during the pyrolysis of neat HIPS. It can be concluded that the solid phase flame retardancy of organoclay comes from carbonaceous char formation [81].

In the presence of MMT10A, the TIC curve showed a peak with maximum at 449°C (Figure 3.47).  $C_6H_5CH_2$  (91 Da) was the most abundant fragment in the pyrolysis mass spectra of HIPS-MMT10A composite. Other intense peaks at 78, 104, 105 and 115 Da due to  $C_6H_6$ ,  $CH_2CHC_6H_5$  (M), MH and  $C_3H_2C_6H_5$ , and also less intense peaks at 118, 129, 178, 193, 208 and 220 Da due to  $C_3H_5C_6H_5$ ,  $C_4H_4C_6H_5$ ,  $C_6H_5CCC_6H_5$ ,  $C_6H_5CHCHCHC_6H_5$ ,  $M_2$  and  $CH_2(C_6H_5)CC(C_6H_5)CHCH_3$  respectively, were observed in the pyrolysis mass spectrum recorded at 449°C. Thus, it can be concluded that depolymerization reactions yielding mainly the monomer were inhibited at least to a certain extent. In addition, the decomposition of HIPS was shifted to lower temperatures, about 22°C, indicating that the thermal stability of HIPS chains reduced in the presence of nanoclay.

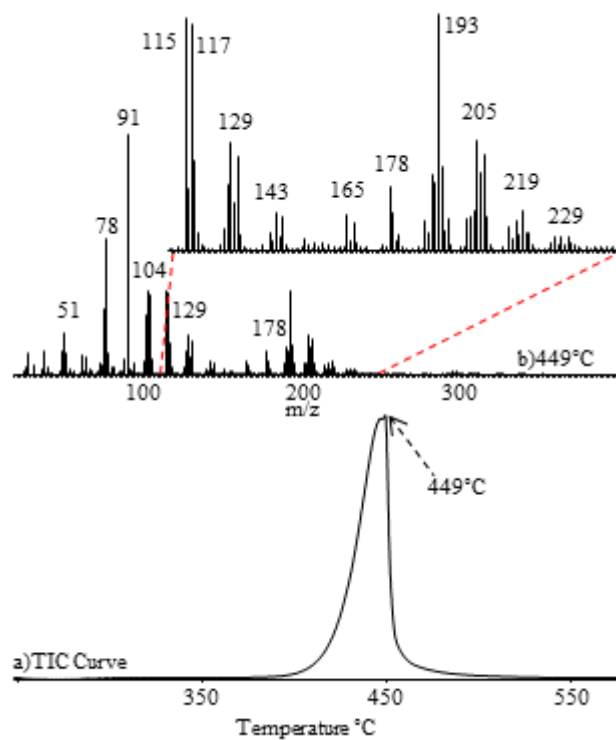


**Figure 3.47.** a) The total ion current curve and b) mass spectrum of HIPS-MMT10A at 449 °C.

In Table 3.20, the relative intensities of intense and/or characteristic peaks recorded in the spectrum and the assignments made are summarized.

**Table 3.20.** The relative intensities, RI, of some selected intense and/or characteristic peaks recorded in pyrolysis spectrum of HIPS-MMT10A at 449°C and the assignments made.

m/z	RI	Assignment
78	559	C <sub>6</sub> H <sub>6</sub>
91	1000	C <sub>6</sub> H <sub>5</sub> CH <sub>2</sub>
92	127	C <sub>6</sub> H <sub>5</sub> CH <sub>3</sub>
104	349	CH <sub>2</sub> CHC <sub>6</sub> H <sub>5</sub> , M and/or C <sub>2</sub> H <sub>4</sub> C <sub>6</sub> H <sub>4</sub>
105	328	CH <sub>2</sub> CH <sub>2</sub> C <sub>6</sub> H <sub>5</sub> and/or C <sub>2</sub> H <sub>5</sub> C <sub>6</sub> H <sub>4</sub>
115	336	C <sub>3</sub> H <sub>2</sub> C <sub>6</sub> H <sub>5</sub>
118	138	C <sub>3</sub> H <sub>5</sub> C <sub>6</sub> H <sub>5</sub>
129	164	C <sub>4</sub> H <sub>4</sub> C <sub>6</sub> H <sub>5</sub>
178	91	C <sub>6</sub> H <sub>5</sub> CCC <sub>6</sub> H <sub>5</sub>
180	15	C <sub>6</sub> H <sub>5</sub> CHCHC <sub>6</sub> H <sub>5</sub>
182	6.7	C <sub>6</sub> H <sub>5</sub> CH <sub>2</sub> CH <sub>2</sub> C <sub>6</sub> H <sub>5</sub>
193	353	C <sub>6</sub> H <sub>5</sub> CHCHCHC <sub>6</sub> H <sub>5</sub>
196	51	C <sub>6</sub> H <sub>5</sub> CH <sub>2</sub> CH <sub>2</sub> CH <sub>2</sub> C <sub>6</sub> H <sub>5</sub>
204	61	CH <sub>2</sub> C(C <sub>6</sub> H <sub>5</sub> )CCC <sub>6</sub> H <sub>5</sub>
206	115	CH <sub>2</sub> C(C <sub>6</sub> H <sub>5</sub> )C(C <sub>6</sub> H <sub>5</sub> )CH <sub>2</sub>
207	142	M <sub>2</sub> -H and/or C <sub>14</sub> H <sub>7</sub> O <sub>2</sub>
208	52	St <sub>2</sub> , CH <sub>3</sub> C(C <sub>6</sub> H <sub>5</sub> )C(CH <sub>3</sub> )C <sub>6</sub> H <sub>5</sub> , CH <sub>2</sub> C(C <sub>6</sub> H <sub>5</sub> )CH(CH <sub>3</sub> )C <sub>6</sub> H <sub>5</sub>
218	25	CH <sub>2</sub> C(C <sub>6</sub> H <sub>5</sub> )CH(C <sub>6</sub> H <sub>5</sub> )CCH
220	28	CH <sub>2</sub> (C <sub>6</sub> H <sub>5</sub> )CC(C <sub>6</sub> H <sub>5</sub> )CHCH <sub>3</sub>
222	8.2	CH <sub>2</sub> C(C <sub>6</sub> H <sub>5</sub> )C(C <sub>6</sub> H <sub>5</sub> )(CH <sub>3</sub> ) <sub>2</sub>
300	10	M(C <sub>6</sub> H <sub>5</sub> )CH <sub>2</sub> CH <sub>2</sub> CH <sub>2</sub> C <sub>6</sub> H <sub>5</sub>
306	2.3	CH(C <sub>6</sub> H <sub>5</sub> )CHC(C <sub>6</sub> H <sub>5</sub> )C(C <sub>6</sub> H <sub>5</sub> )CCH
312	3.8	St <sub>3</sub> , CH <sub>3</sub> CH(C <sub>6</sub> H <sub>5</sub> )CH <sub>2</sub> CH(C <sub>6</sub> H <sub>5</sub> )C(C <sub>6</sub> H <sub>5</sub> )CH <sub>2</sub>
194	125	MCHC <sub>6</sub> H <sub>5</sub>
298	10	M <sub>2</sub> CHC <sub>6</sub> H <sub>5</sub>
402	5.0	M <sub>3</sub> CHC <sub>6</sub> H <sub>5</sub>
43	7.8	CH <sub>2</sub> N(CH <sub>3</sub> ) and/or C <sub>3</sub> H <sub>7</sub>
58	13	CH <sub>2</sub> N(CH <sub>3</sub> ) <sub>2</sub>
134	2.7	CH <sub>2</sub> N(CH <sub>3</sub> )CH <sub>2</sub> C <sub>6</sub> H <sub>5</sub>

Single ion pyrograms of some characteristic products are shown in Figure 3.48. Almost all HIPS based products showed similar trends in their evolution profiles. However, in the presence of MMT10A, the formation of monomer and benzene were maximized at slightly lower temperatures, at around 444°C.

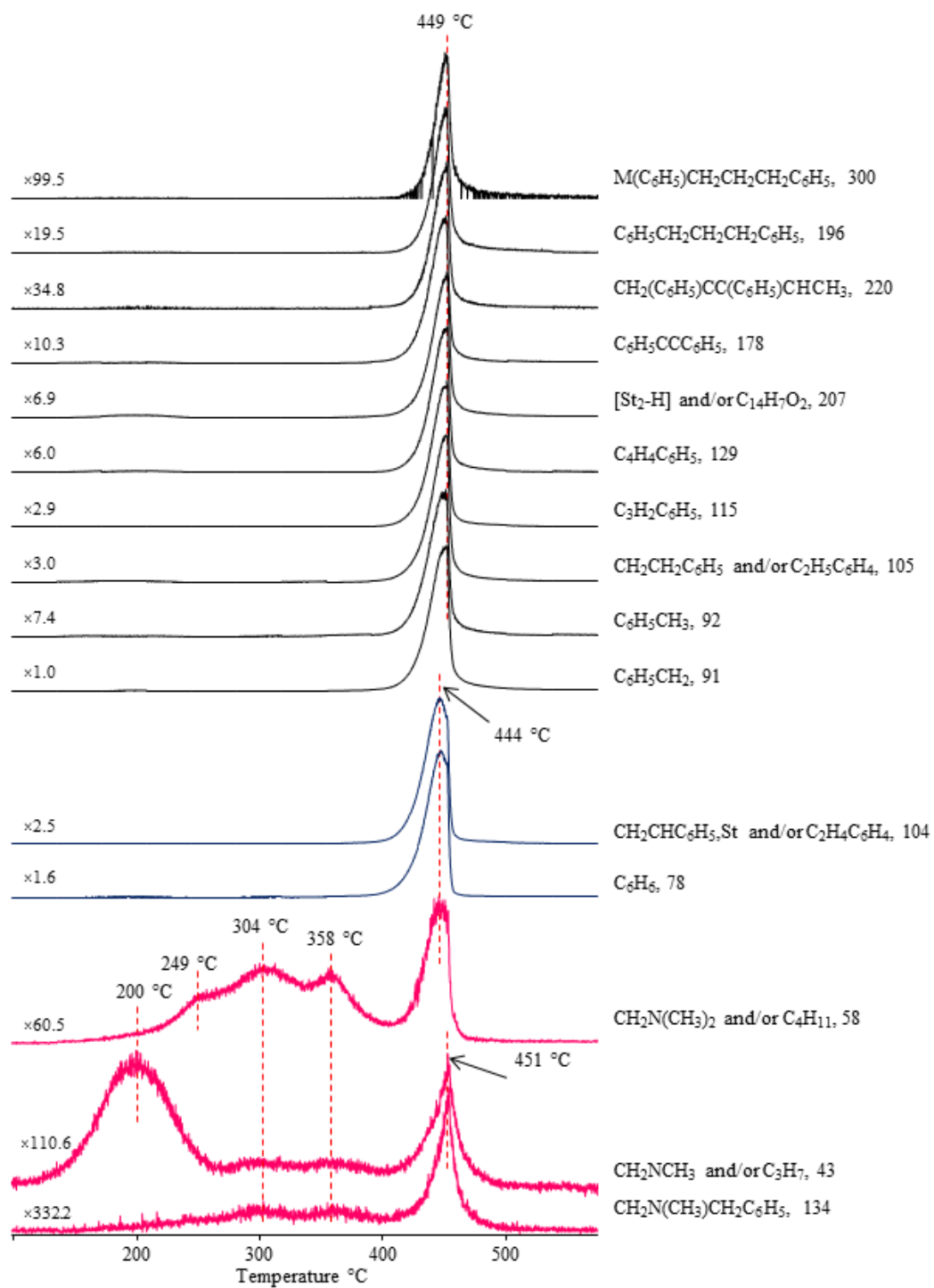
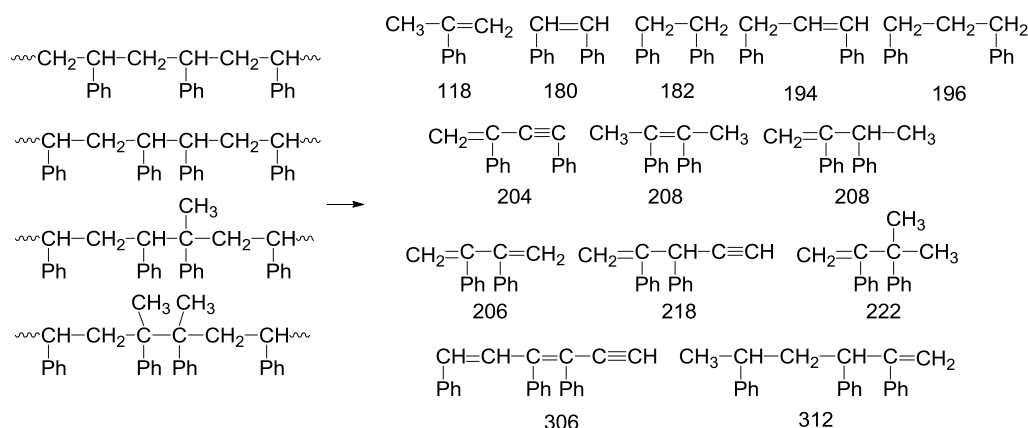


**Figure 3.48.** Single ion pyrograms of some selected fragments detected during the pyrolysis of HIPS-MMT10A.





**Scheme 3.14.** Possible unsaturated and head to head compounds.



In the case of the HIPS-MMT10A, the radicals generated by chain scission have more chance to undergo radical recombination and transfer reactions due to the barrier effect of the clay layers.

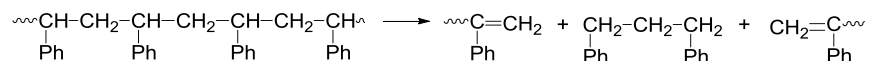
It was proposed that as molecules can undergo extensive random chain scission at any methylene linkages continued with the hydrogen abstraction, disproportionation or  $\beta$ -scission, generating different structures. If  $\beta$ -scission takes place, the generated fragments include unsaturation in every molecule. On the other hand, disproportionation generates molecules that show both saturation and unsaturation. In addition, more saturated structures were generated by hydrogen abstraction. It was suggested that in the presence of clay, all these reactions take place [79].

The products with m/z values 204, 218 and 306 Da indicated presence of H deficiency. Thus, it may be concluded that their structures may contain a carbon-carbon triple bond (Scheme 3.14).

On the other hand, it is probable that 1,3 diphenylpropane (196 Da) was mostly generated by disproportionation because of the clay layers effect (Scheme 3.15).

The increase in the yield of 1,3 diphenylpropane was in accordance with the increase in the probability of disproportionation reactions in the presence of clay.

**Scheme 3.15.** Disproportionation reaction of polystyrene.



### 3.4.1.3. HIPS-ATH-MMT10A

In a recent study [81], it has been shown that the addition of 3 wt% MMT10A and 25 wt% ATH was decreased the PHRR by ~69% compared to neat HIPS. In addition, the PMLR was decreased from ~31% to ~12% compared to neat HIPS. Furthermore, LOI was enhanced about 3.2% with respect to neat HIPS. It was determined that the char residues was increased to 18.8% for HIPS-ATH-MMT10A compared to both HIPS-MMT10A and HIPS-ATH, for which char residues were 3.1 and 15.6% respectively [81]. It was proposed that upon dehydration, a residue of about 60% of the initial amount of ATH was remained in the solid phase, independent of the presence of nanoclay [81].

In the presence of ATH and MMT10A, the TIC curve recorded during the pyrolysis of HIPS-ATH-MMT10A composite showed a sharp peak with a maximum at 441°C (Figure 3.49). The base peak is again at 91 Da, indicating that the main decomposition product was again C<sub>6</sub>H<sub>5</sub>CH<sub>2</sub>. Diagnostic peaks, recorded in the pyrolysis mass spectra of HIPS-ATH and HIPS-MMT10A, were also recorded during the pyrolysis of HIPS-ATH-MMT10A composite at 441°C. In addition the decomposition of HIPS shifted to lower temperatures about 30°C, indicating that thermal stability of HIPS chains reduced in the presence of nanoclay and ATH.

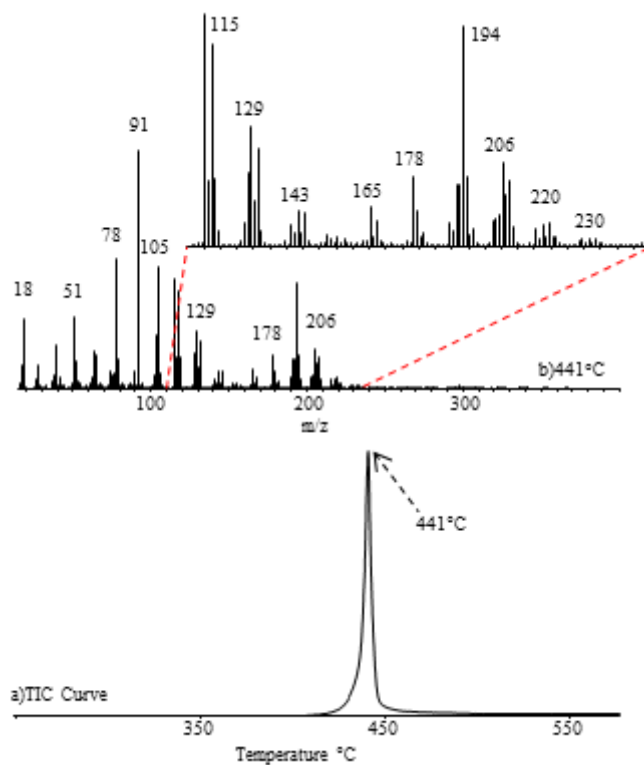


**Figure 3.49.** a) The total ion current curve and b) mass spectrum of HIPS-ATH-MMT10A at 441 °C.

In Table 3.21, the relative intensities of intense and/or characteristic peaks recorded in the spectrum and the assignments made are summarized.

**Table 3.21.** The relative intensities, RI, of some selected intense and/or characteristic peaks recorded in pyrolysis spectrum of HIPS-ATH-MMT10A at 441°C and the assignments made

m/z	RI	Assignment
78	541	C <sub>6</sub> H <sub>6</sub> ,
91	1000	C <sub>6</sub> H <sub>5</sub> CH <sub>2</sub>
92	170	C <sub>6</sub> H <sub>5</sub> CH <sub>3</sub>
104	380	CH <sub>2</sub> CHC <sub>6</sub> H <sub>5</sub> , M and/or C <sub>2</sub> H <sub>4</sub> C <sub>6</sub> H <sub>4</sub>
105	510	CH <sub>2</sub> CH <sub>2</sub> C <sub>6</sub> H <sub>5</sub> and/or C <sub>2</sub> H <sub>5</sub> C <sub>6</sub> H <sub>4</sub>
115	462	C <sub>3</sub> H <sub>2</sub> C <sub>6</sub> H <sub>5</sub>
118	134	C <sub>3</sub> H <sub>5</sub> C <sub>6</sub> H <sub>5</sub>
129	240	C <sub>4</sub> H <sub>4</sub> C <sub>6</sub> H <sub>5</sub>
178	138	C <sub>6</sub> H <sub>5</sub> CCC <sub>6</sub> H <sub>5</sub>
193	124	C <sub>6</sub> H <sub>5</sub> CHCHCHC <sub>6</sub> H <sub>5</sub>
196	24	C <sub>6</sub> H <sub>5</sub> CH <sub>2</sub> CH <sub>2</sub> CH <sub>2</sub> C <sub>6</sub> H <sub>5</sub>
207	104	M <sub>2</sub> -H and/or C <sub>14</sub> H <sub>7</sub> O <sub>2</sub>
208	132	St <sub>2</sub> , CH <sub>3</sub> C(C <sub>6</sub> H <sub>5</sub> )C(CH <sub>3</sub> )C <sub>6</sub> H <sub>5</sub> , CH <sub>2</sub> C(C <sub>6</sub> H <sub>5</sub> )CH(CH <sub>3</sub> )C <sub>6</sub> H <sub>5</sub>
218	42	(C <sub>6</sub> H <sub>5</sub> )CCC(C <sub>6</sub> H <sub>5</sub> )CHCH <sub>3</sub>
220	48	CH <sub>2</sub> (C <sub>6</sub> H <sub>5</sub> )CC(C <sub>6</sub> H <sub>5</sub> )CHCH <sub>3</sub>
222	18	CH <sub>2</sub> C(C <sub>6</sub> H <sub>5</sub> )C(C <sub>6</sub> H <sub>5</sub> )(CH <sub>3</sub> ) <sub>2</sub>
306	1.3	CH(C <sub>6</sub> H <sub>5</sub> )CHC(C <sub>6</sub> H <sub>5</sub> )C(C <sub>6</sub> H <sub>5</sub> )CCH
312	2.7	St <sub>3</sub> , CH <sub>3</sub> CH(C <sub>6</sub> H <sub>5</sub> )CH <sub>2</sub> CH(C <sub>6</sub> H <sub>5</sub> )C(C <sub>6</sub> H <sub>5</sub> )CH <sub>2</sub>
194	440	C <sub>6</sub> H <sub>5</sub> CHCH <sub>2</sub> CHC <sub>6</sub> H <sub>5</sub>
298	10	M <sub>2</sub> CHC <sub>6</sub> H <sub>5</sub>
402	0.1	M <sub>3</sub> CHC <sub>6</sub> H <sub>5</sub>
18	290	H <sub>2</sub> O
43	8.5	CH <sub>2</sub> N(CH <sub>3</sub> ) and/or C <sub>3</sub> H <sub>7</sub>
58	16	CH <sub>2</sub> N(CH <sub>3</sub> ) <sub>2</sub>
134	1.0	CH <sub>2</sub> N(CH <sub>3</sub> )CH <sub>2</sub> C <sub>6</sub> H <sub>5</sub>

Single ion pyrograms of some characteristic fragments are shown in Figure 3.50. All products showed almost the same trends in their evolution profiles. Thus, it can be concluded that they were generated energetically through the same decomposition pathways or through one step thermal degradation mechanism. Again, peaks, due to the series of fragments with formula M<sub>x</sub>CHC<sub>6</sub>H<sub>5</sub> (m/z = 194, 298, 402, 506, 610 and 714 Da for x = 1 to 6) were detected.

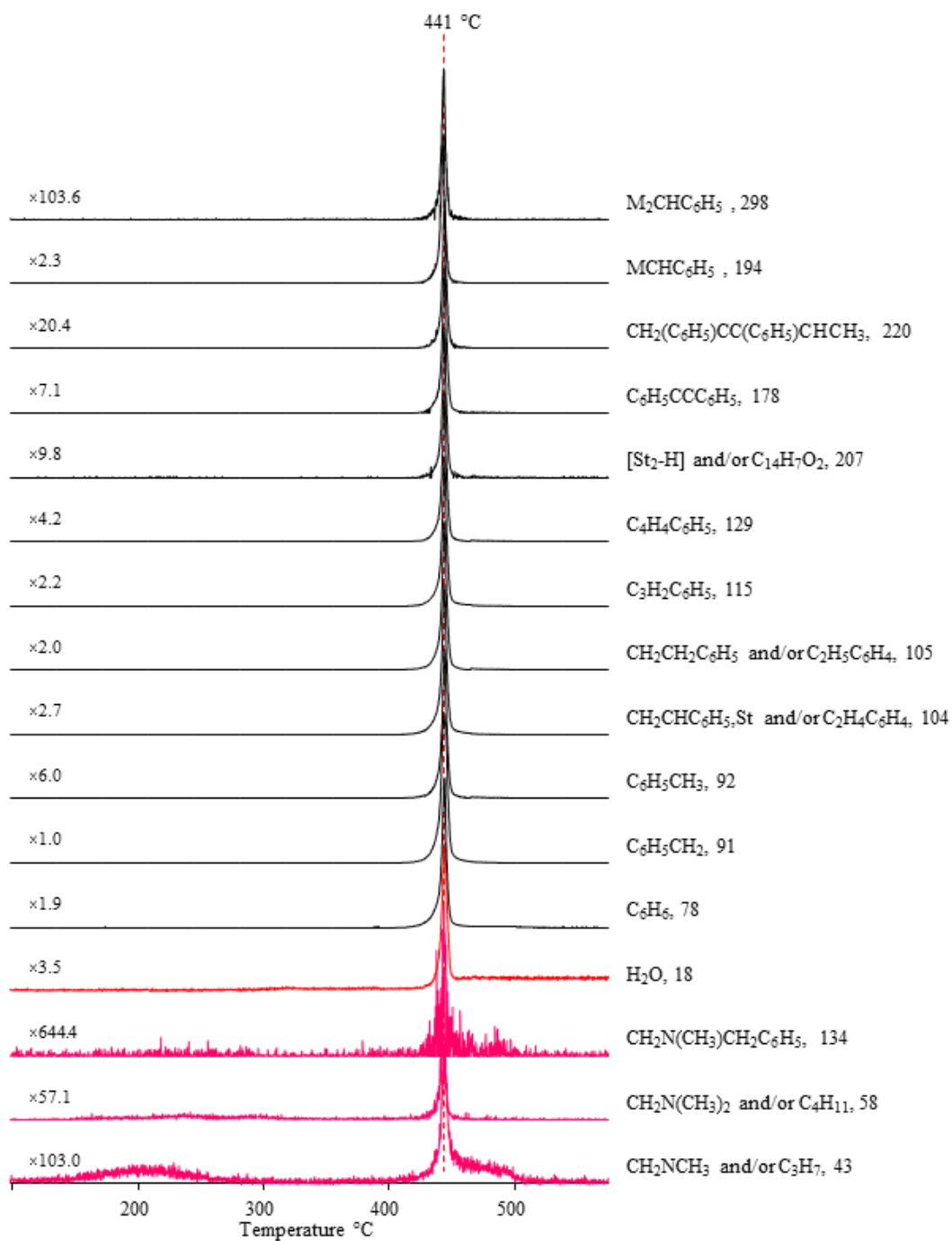


**Figure 3.50.** Single ion pyrograms of some selected fragments detected during the pyrolysis of HIPS-ATH-MMT10A.

The pyrolysis mass spectra recorded at the range of 150-250°C was dominated by typical peaks of MMT10A such as  $\text{CH}_2\text{NCH}_3$  (43 Da),  $(\text{CH}_3)_2\text{NCH}_2$  (58 Da) and  $\text{CH}_2\text{N}(\text{CH}_3)\text{CH}_2\text{C}_6\text{H}_5$  (134 Da). Again, contribution of thermal degradation products of HIPS was quite significant at the high temperature evolution of MMT10A based products (Figure 3.48).

When the composite involved both ATH and MMT10A, decomposition of HIPS was occurred over a very narrow temperature range indicating that the rate of decomposition was increased with the combination of ATH and MMT10A. In addition, the relative intensities of all products were increased even more than the case of HIPS-MMT10A. Actually, in the presence of ATH, the decomposition fragments have more possibility to undergo radical recombination reactions than in the case of HIPS-MMT10A. In Table 3.22, the relative yields of the fragments generated by radical recombination reactions are summarized in the presence of MMT10A and/or ATH.

**Table 3.22.** The comparison of relative intensities, RI, of some selected intense and/or characteristic peaks recorded in pyrolysis spectrum of HIPS, HIPS-ATH, HIPS–MMT10A and HIPS-ATH-MMT10A and the assignments made.

m/z	HIPS	HIPS-ATH	HIPS–MMT	HIPS-ATH-MMT	Assignment
	471°C	469°C	449°C	441°C	
91	947	1000	1000	1000	C <sub>7</sub> H <sub>7</sub>
92	100	113	128	170	C <sub>7</sub> H <sub>8</sub>
104	1000	740	350	380	C <sub>8</sub> H <sub>8</sub>
105	106	133	336	510	C <sub>8</sub> H <sub>9</sub>
106	6	12	63	64	C <sub>8</sub> H <sub>10</sub>
115	113	181	346	462	C <sub>9</sub> H <sub>7</sub>
118	23	24	136	134	C <sub>9</sub> H <sub>10</sub>
129	35	79	163	240	C <sub>10</sub> H <sub>9</sub>
178	15	28	96	138	C <sub>14</sub> H <sub>10</sub>
193	43	-	352	-	C <sub>15</sub> H <sub>13</sub>
194	46	37	127	440	C <sub>15</sub> H <sub>14</sub>
196	3	-	49	-	C <sub>15</sub> H <sub>16</sub>
204	4	5	62	-	C <sub>16</sub> H <sub>12</sub>
208	40	70	53	132	C <sub>16</sub> H <sub>16</sub>
218	1	1	25	42	C <sub>17</sub> H <sub>14</sub>
220	3	4	28	48	C <sub>17</sub> H <sub>16</sub>
222	1.5	4	9	18	C <sub>17</sub> H <sub>18</sub>
306	0.4	0.2	2.3	1.3	C <sub>24</sub> H <sub>18</sub>

### 3.4.2. THERMAL DEGRADATION OF POLYSTYRENE IN THE PRESENCE OF NANOPARTICLE AND FLAME RETARDANTS

For understanding the effects of nanoclays on thermal degradation characteristics of polystyrene composites, PS involving 20% BE or 5% MMT10A, PS involving 20% BE and 3% Sb<sub>2</sub>O<sub>3</sub> or 5% MMT10A and PS involving 20% BE, 3% Sb<sub>2</sub>O<sub>3</sub> and 5% MMT10A were studied by DP-MS technique separately (Table 2.4).

Polystyrene (PS) decomposes in a single step by a depolymerization reaction generating mostly styrene. The TIC curve recorded during the pyrolysis of PS showed a broad peak with a maxima at 441°C (Figure 3.51). Typical fragmentation



pattern of PS, intense peaks at  $m/z = 51, 78, 91, 104, 117, 194$  and  $207$  Da due to  $C_4H_3, C_6H_6, C_7H_7, St, C_3H_4C_6H_5, CH(C_6H_5)CH_2CHC_6H_5$  and  $St_2-H$  respectively, was noted in the pyrolysis mass spectra recorded at  $441^\circ C$  indicating that the thermal degradation of PS took via depolymerization producing mostly the monomer and low mass oligomers, 2,4-diphenylbut-1-ene (dimer) and 2,4,6-triphenylhex-1-ene (trimer). In Table 3.23, the relative intensities of intense and/or characteristic peaks recorded in the spectrum and the assignments made are summarized.

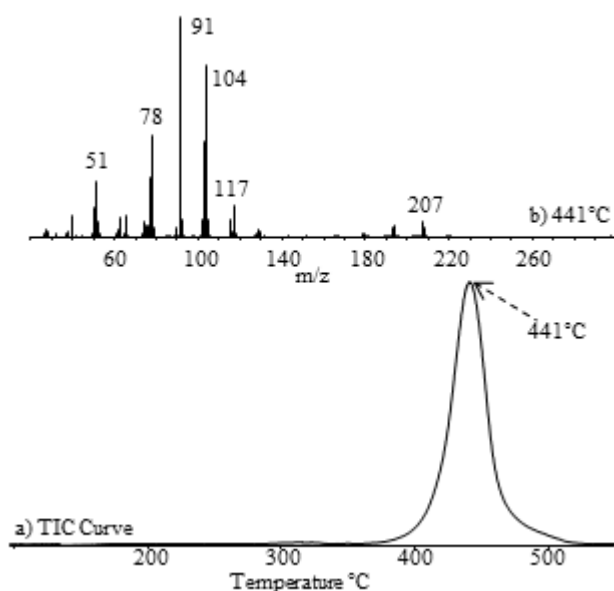


**Figure 3.51.** a) The total ion current curve and b) mass spectrum of PS at  $441^\circ C$ .

**Table 3.23.** The relative intensities, RI, of some selected intense and/or characteristic peaks recorded in pyrolysis spectrum of PS at 441°C and the assignments made.

m/z	RI	Assignment
51	254	C <sub>4</sub> H <sub>3</sub>
78	464	C <sub>6</sub> H <sub>6</sub>
91	1000	CH <sub>2</sub> C <sub>6</sub> H <sub>5</sub>
92	82	CH <sub>3</sub> C <sub>6</sub> H <sub>5</sub>
103	438	C <sub>2</sub> H <sub>2</sub> C <sub>6</sub> H <sub>5</sub>
104	783	CH <sub>2</sub> CHC <sub>6</sub> H <sub>5</sub> St
115	81	C <sub>3</sub> H <sub>2</sub> C <sub>6</sub> H <sub>5</sub>
117	143	C <sub>2</sub> H <sub>4</sub> CC <sub>6</sub> H <sub>5</sub>
129	32	C <sub>4</sub> H <sub>4</sub> C <sub>6</sub> H <sub>5</sub>
194	49	CH(C <sub>6</sub> H <sub>5</sub> )CH <sub>2</sub> CHC <sub>6</sub> H <sub>5</sub>
207	69	CH <sub>2</sub> C(C <sub>6</sub> H <sub>5</sub> )CH <sub>2</sub> CHC <sub>6</sub> H <sub>5</sub>
208	40	CH <sub>2</sub> CH(C <sub>6</sub> H <sub>5</sub> )CH <sub>2</sub> CHC <sub>6</sub> H <sub>5</sub> , St <sub>2</sub>
312	3.4	CH <sub>2</sub> CH(C <sub>6</sub> H <sub>5</sub> )CH <sub>2</sub> CH(C <sub>6</sub> H <sub>5</sub> )CH <sub>2</sub> CHC <sub>6</sub> H <sub>5</sub> , St <sub>3</sub>

In Figure 3.52, single ion pyrograms of C<sub>4</sub>H<sub>3</sub> (51 Da), C<sub>6</sub>H<sub>6</sub> (78 Da), C<sub>7</sub>H<sub>7</sub> (91 Da), [St] (104 Da), C<sub>3</sub>H<sub>4</sub>C<sub>6</sub>H<sub>5</sub> (117 Da), CH(C<sub>6</sub>H<sub>5</sub>)CH<sub>2</sub>CHC<sub>6</sub>H<sub>5</sub> (194 Da), [St<sub>2</sub>-H] (207 Da) and [St<sub>3</sub>] (312 Da) are presented. All products showed almost the same trends in their evolution profiles. Thus, it can be concluded that they were generated energetically almost through the same decomposition pathway or through one step thermal degradation mechanism.

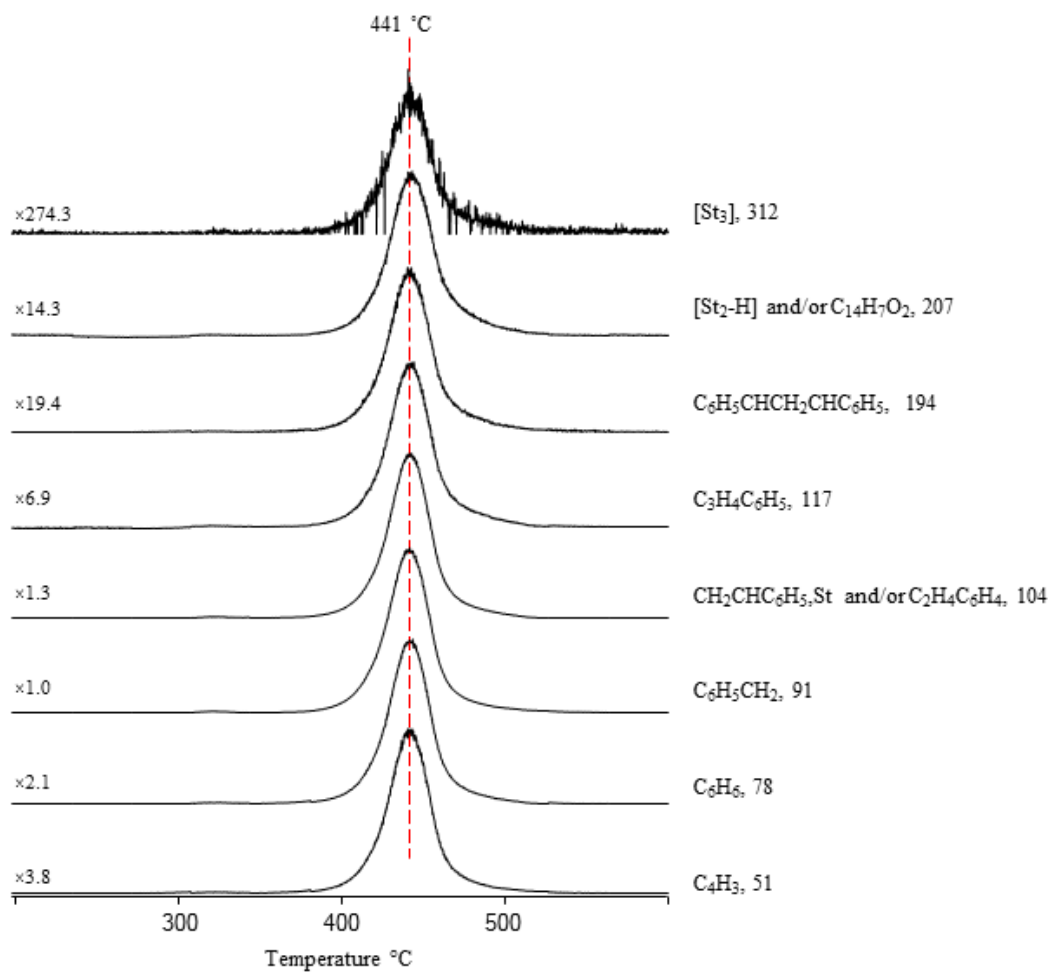


**Figure 3.52.** Single ion pyrograms of some selected fragments detected during the pyrolysis of PS.

### 3.4.2.1. PS-BE

In a recent study, it has been found that with the addition of 20 wt% BE as the dispersed phase in PS-BE blends the peak heat release rate, PHRR, was decreased about ~35% and the peak mass loss rate, PMLR, was enhanced about ~31% compare with neat PS. The ratio of total heat evolved to total mass loss, effective heat of combustion of volatiles and the product of combustion efficiency, was reduced from  $3.0 \text{ MJm}^{-2}\text{g}^{-1}$  to  $1.6 \text{ MJm}^{-2}\text{g}^{-1}$  with the corporation of BE into PS. In UL-94 test V-2 rating was obtained. Also, the limiting oxygen index, LOI, improved from 18% to 21%. It has been found that BE changes the degradation and combustion behavior of PS by accelerating dripping and following self-extinguishment [82].

In the presence of brominated epoxy, pyrolysis of PS yielded a TIC curve with a maximum at around  $448^\circ\text{C}$  (Figure 3.53). The spectra recorded at around these temperatures were dominated with characteristic peaks of PS. Those of BE can also be detected upon expansion of the spectra recorded (Figure 3.53).

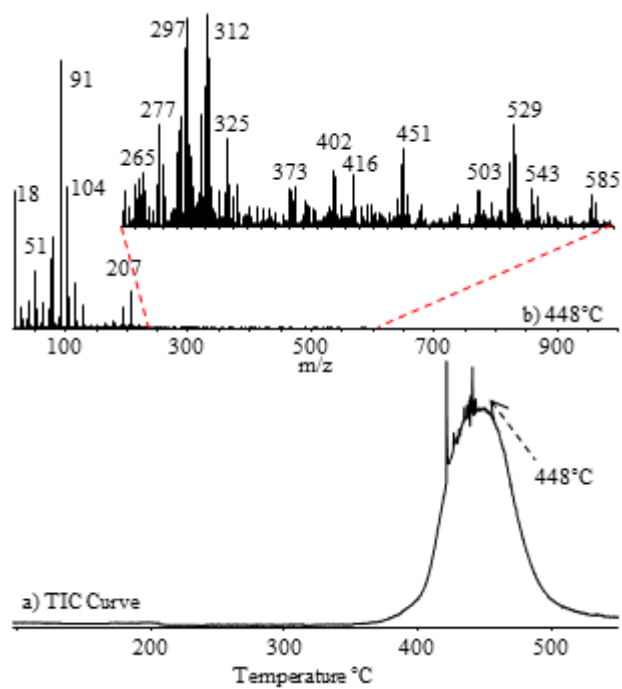


**Figure 3.53.** a) The total ion current curve and b) mass spectrum of PS-BE at 448°C.

In Table 3.24, the relative intensities of intense and/or characteristic peaks recorded in the spectrum and the assignments made are summarized.

**Table 3.24.** The relative intensities, RI, of some selected intense and/or characteristic peaks recorded in pyrolysis spectrum of PS-BE at 448°C and the assignments made.

m/z	RI	Assignment
78	351	C <sub>6</sub> H <sub>6</sub>
91	1000	CH <sub>2</sub> C <sub>6</sub> H <sub>5</sub>
92	121	CH <sub>3</sub> C <sub>6</sub> H <sub>5</sub>
103	301	C <sub>2</sub> H <sub>2</sub> C <sub>6</sub> H <sub>5</sub> [St]-H
104	541	C <sub>2</sub> H <sub>3</sub> C <sub>6</sub> H <sub>5</sub> [St]
105	123	C <sub>2</sub> H <sub>4</sub> C <sub>6</sub> H <sub>5</sub>
115	128	C <sub>3</sub> H <sub>2</sub> C <sub>6</sub> H <sub>5</sub>
129	89	C <sub>4</sub> H <sub>4</sub> C <sub>6</sub> H <sub>5</sub>
193	70	CH(C <sub>6</sub> H <sub>5</sub> )CHCHC <sub>6</sub> H <sub>5</sub>
207	131	[St <sub>2</sub> -H]
18	531	H <sub>2</sub> O
43	15	CH <sub>3</sub> CO, CH <sub>2</sub> COH
80, 82	16, 16	HBr
94, 96	3.5, 1.8	CH <sub>3</sub> Br
136, 138	0.6, 0.6	CH <sub>3</sub> COCH <sub>2</sub> Br
182, 184	2.6, 0.3	C <sub>2</sub> H <sub>2</sub> C <sub>6</sub> H <sub>4</sub> Br
286, 288	0.2, 0.3	C <sub>2</sub> H <sub>3</sub> (C <sub>6</sub> H <sub>5</sub> )C <sub>2</sub> H <sub>2</sub> C <sub>6</sub> H <sub>4</sub> Br
291,293,295	2.0, 1.6, 2.8	C <sub>6</sub> H <sub>2</sub> Br <sub>2</sub> C <sub>2</sub> H <sub>3</sub> O <sub>2</sub>
330	0.4	Br <sub>3</sub> C <sub>6</sub> H <sub>2</sub> OH
529	1.5	HO(Br <sub>2</sub> )C <sub>6</sub> H <sub>2</sub> CCH <sub>3</sub> C <sub>6</sub> H <sub>2</sub> (Br <sub>2</sub> )OH

Single ion evolution profiles of characteristic degradation products of PS followed identical trends. However, the relative yields of high mass thermal degradation fragments were increased noticeably. Furthermore, though thermal degradation of PS chains was started almost at around the same temperature ranges, evolution profiles were broadened indicating that thermal degradation was continued at higher temperatures compared to neat PS.

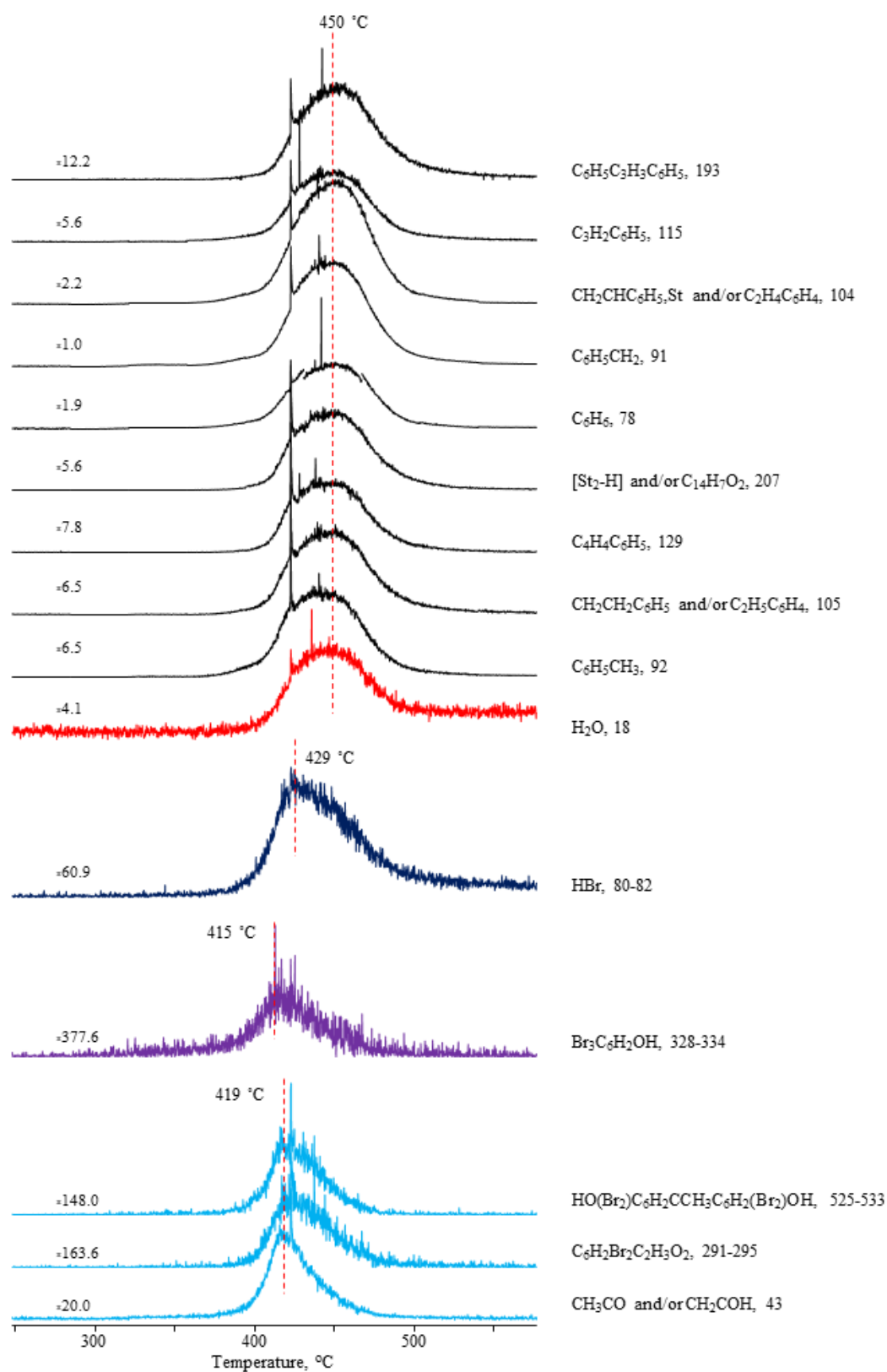


**Figure 3.54.** Single ion pyrograms of some selected fragments detected during the pyrolysis of PS-BE.

It can be concluded that thermal stability of BE chains were enhanced in the presence of PS (Section 3.1.3). As in the case of pure BE, slight differentiations were present in the evolution profiles of BE based thermal decomposition fragments. Tribromophenol (328-334 Da) produced by loss of end groups maximized at around 415°C. However, the products due to the decomposition of epoxy linkages, such as CH<sub>3</sub>CO or CH<sub>2</sub>COH (43 Da), and tetrabromo bisphenol A (525-533 Da) and all the fragments involving bisphenol A units, reached maximum yield at around 419°C. Again the generation of HBr (80-82 Da), CH<sub>3</sub>Br (94-96 Da) and CH<sub>3</sub>COCH<sub>2</sub>Br (136-138 Da) were reached maximum yield at slightly elevated temperatures, at around 429°C.

Furthermore, the relative yields of the thermal decomposition products of BE was changed in the presence of PS. Among the thermal decomposition products of BE, the relative yield of brominated fragments were reduced significantly compared to the major fragment with m/z 43 Da. The reduction was more than 2-folds for HBr, 1.7 folds for tetrabromobisphenol A and other fragments formed by decomposition of the main chain. On the other hand, the reduction was about 1.2 folds for tribromophenol generated by elimination of the end-groups. Hydrogen bromide is the major decomposition product from brominated flame retardants [89, 100]. It acts in a way to facilitate hot radical entrapment in the vapor phase, which reduces flaming ignition and heat evolution. Therefore, the reduction in the yield of HBr may be related with the reactions between brominated flame retardants and PS. Weak peaks, due to brominated monomer (182-184 Da) and dimer (286-288 Da), were noted. Moreover, noticeable enhancement in the relative intensities of H-deficient monomer peak (103 Da) may be related with loss of Br during the ionization of brominated styrene units. Furthermore, the slight increase in the char yield for PS-BE composite (~ 3.3%) may be thought to be as a result of the enhancement in the thermal stability of BE chains. Most probably crosslinked structures involving both PS and BE units were increased [82].



Evolution of H<sub>2</sub>O was observed in the temperature region where PS degradation took place, at around 450°C. The high temperature evolution of H<sub>2</sub>O was agreed with the proposed mechanism (Scheme 3.2c).

#### **3.4.2.2. PS-BE-Sb<sub>2</sub>O<sub>3</sub>**

It has been determined that the combination of BE(20 wt%) and Sb<sub>2</sub>O<sub>3</sub>(3 wt%) yielded further decrease in the PHRR about %64 with respect to neat PS and 44% with respect to PS-BE blend [82]. The BE-Sb<sub>2</sub>O<sub>3</sub> combination acts as a good flame retardant by generating SbBr<sub>3</sub>, a more powerful radical scavenger than HBr, generated by the reaction between Sb<sub>2</sub>O<sub>3</sub> and HBr. On the other hand, flaming drips could not be prevented, causing a retained UL-94 V-2 rating for PS-BE-Sb<sub>2</sub>O<sub>3</sub> as in the case of PS-BE [82].

The TIC curve of the PS-BE-Sb<sub>2</sub>O<sub>3</sub> showed two overlapping peaks with maxima at 393 and 446°C (Figure 3.55). Decomposition in two distinct regions in the presence of Sb<sub>2</sub>O<sub>3</sub> was also observed by Jakab and coworkers but due to the experimental technique used it was not possible to identify all the degradation products produced at the lower temperature region [78]. But they were able to identify the evolution of styrene and H<sub>2</sub>O. In an earlier study, it was proposed that brominated additives and SbBr<sub>3</sub> are generated during this stage of degradation [88]. In this study, both of peaks were noticed in the evolution profiles of all fragments (Figure 3.56). However, the relative intensity of the low temperature peak was higher in the evolution profiles of the degradation products of flame retardants whereas it was lower in those of PS. In Table 3.25, the relative intensities of intense and/or characteristic peaks recorded in the spectrum and the assignments made are summarized.

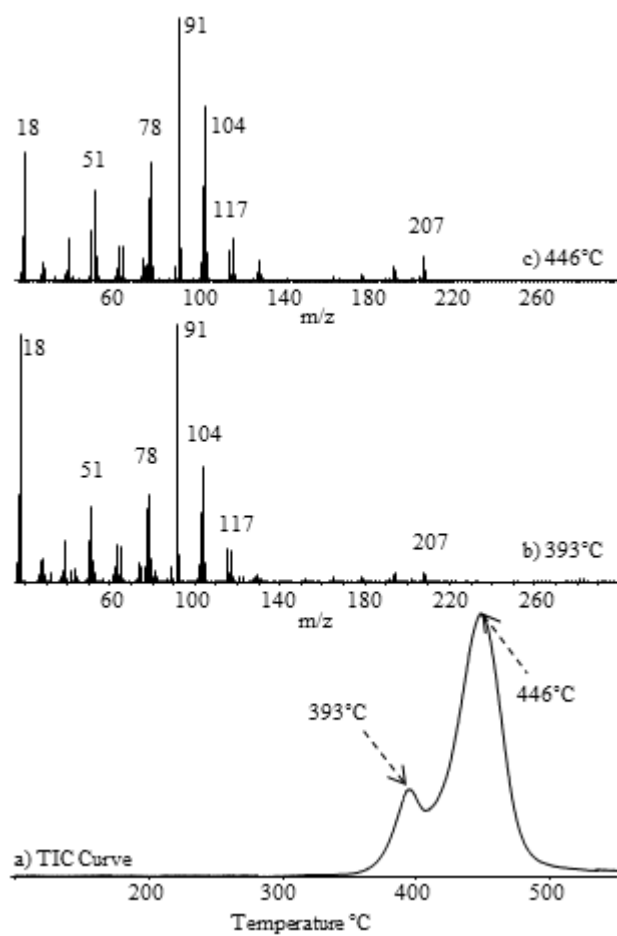


**Figure 3.55.** a) The total ion current curve and the mass spectra at **b) 393** **c) 446** °C recorded during the pyrolysis of PS-BE-Sb<sub>2</sub>O<sub>3</sub>.

**Table 3.25.** The relative intensities, RI, of some selected intense and/or characteristic peaks recorded in pyrolysis spectrum of PS-BE-Sb<sub>2</sub>O<sub>3</sub> at 393 and 446°C and the assignments made.

m/z	RI		Assignment
	393°C	446°C	
18	1000	513	H <sub>2</sub> O
78	334	483	C <sub>6</sub> H <sub>6</sub>
91	950	1000	CH <sub>2</sub> C <sub>6</sub> H <sub>5</sub>
92	96	117	CH <sub>3</sub> C <sub>6</sub> H <sub>5</sub>
104	456	686	C <sub>2</sub> H <sub>3</sub> C <sub>6</sub> H <sub>5</sub> [St]
105	76	110	C <sub>2</sub> H <sub>4</sub> C <sub>6</sub> H <sub>5</sub>
115	125	121	C <sub>3</sub> H <sub>2</sub> C <sub>6</sub> H <sub>5</sub>
129	30	79	C <sub>4</sub> H <sub>4</sub> C <sub>6</sub> H <sub>5</sub>
193	28	52	CH(C <sub>6</sub> H <sub>5</sub> )CHCHC <sub>6</sub> H <sub>5</sub>
207	32	92	[St <sub>2</sub> -H]
43	58	3.4	CH <sub>3</sub> CO, CH <sub>2</sub> COH
80	19	7.8	HBr
293	5.7	0.4	C <sub>6</sub> H <sub>2</sub> Br <sub>2</sub> C <sub>2</sub> H <sub>3</sub> O <sub>2</sub>
330	1.2		Br <sub>3</sub> C <sub>6</sub> H <sub>2</sub> OH
529	6.0	0.1	HO(Br <sub>2</sub> )C <sub>6</sub> H <sub>2</sub> CCH <sub>3</sub> C <sub>6</sub> H <sub>2</sub> (Br <sub>2</sub> )OH
137	1.3	0.3	SbO
281	14	1.2	SbBr <sub>2</sub>
362	5.8	0.6	SbBr <sub>3</sub>
276	0.5	0.1	Sb <sub>2</sub> O <sub>2</sub>
292	0.8	0.2	Sb <sub>2</sub> O <sub>3</sub>
203	6.7	9.2	SbBr,
219	4.2	6.8	SbOBr,
235	0.5	1.3	SbO <sub>2</sub> Br,
360	4.7	0.3	Sb <sub>2</sub> O <sub>2</sub> Br

PS based thermal decomposition products showed two maxima at 393 and 446°C, the second one being more intense. Again an enhancement in the relative yield of high mass fragments was observed. However, enhancement was not as noticeable as in case of PS-BE. The low temperature peaks may be related with evolution of products generated by the interactions with products generated by the reactions of brominated epoxy and Sb<sub>2</sub>O<sub>3</sub>. Single ion pyrograms of some characteristic products are shown in Figure 3.56.

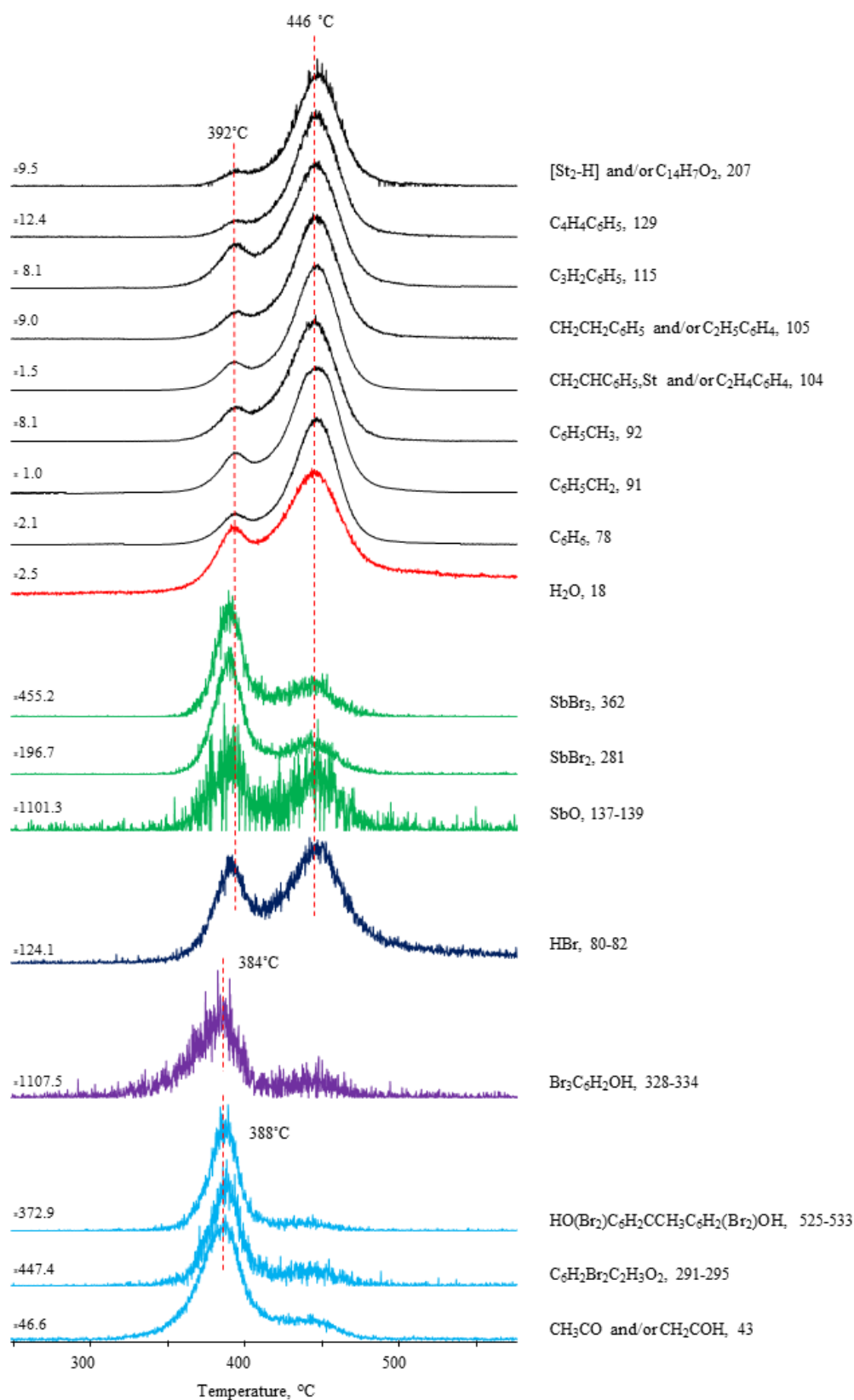


**Figure 3.56.** Single ion pyrograms of some selected fragments detected during the pyrolysis of PS-BE-Sb<sub>2</sub>O<sub>3</sub>.

Thermal decomposition products of BE showed maxima at 384 and 446°C, the first one was more intense. In the presence of Sb<sub>2</sub>O<sub>3</sub>, degradation of BE chains shifted to lower temperatures with respect to neat BE. The single evolution profiles of thermal decomposition fragments of BE showed similar trend unlike what was observed for pure BE and PS-BE composite. All products reached maximum yield at the same temperature. The characteristic peaks present in the pyrolysis mass spectra of Sb<sub>2</sub>O<sub>3</sub> were either absent or significantly weak. Only, very weak peaks due to SbO, Sb<sub>2</sub>O<sub>2</sub>, Sb<sub>3</sub>O<sub>4</sub> and Sb<sub>4</sub>O<sub>6</sub> were determined. In spite, peaks due to oxybromides and bromides of antimony such as SbBr, SbBr<sub>2</sub>, SbBr<sub>3</sub>, Sb<sub>2</sub>Br<sub>2</sub>, SbOBr, SbOBr<sub>2</sub>, SbO<sub>2</sub>Br, Sb<sub>2</sub>O<sub>2</sub>Br and Sb<sub>2</sub>OBr<sub>2</sub> were identified. In addition, their evolutions were detected at around 392°C. In the presence of brominated epoxy, the evolution of antimony compounds generated at noticeably lower temperatures than the temperature region where the pyrolysis products of pure Sb<sub>2</sub>O<sub>3</sub> were observed (Section 3.1.4). Therefore, it can be proposed that the reactions of antimony oxides with bromines of BE initiated the thermal degradation of BE, causing a reduction in the thermal stability of both BE and antimony oxides. As a result, these interactions generated the oxybromides and bromides of antimony.

Pyrolysis products of both BE and antimony compounds showed a weaker high temperature peak in their evolution profiles with a maximum at 446 °C, at which decomposition products of PS reached maximum yield. HBr evolution was more significant at around 446°C as thermal decomposition fragments of PS, unlike the general trends noticed in the evolutions of neat antimony compounds and the thermal degradation products of neat brominated epoxy polymer. In a recent study, it has been suggested that some of the flame retardant radicals reacted with the polymer matrix by radical recombination and transfer reactions, were released at the final stages of degradation [100]. Therefore, it may be proposed that the fragments decomposed at early stages of pyrolysis interacted with the host polymer, causing the degradation of the polymer to a certain extent yielded fragments with higher thermal stability. Furthermore, the higher yield of HBr in the temperature region where PS degradation took place obviously agrees the bromination of polystyrene during the degradation of brominated polyepoxy.

However, it was not possible to differentiate brominated styrene oligomers even if they were produced because of the presence of similar units in brominated poly epoxy and styrene.

Evolution of water was also observed in two temperature regions. Again, contrary to diagnostic thermal degradation products of flame retardants, the high temperature peak was more intense as in case of HBr. Therefore, it can be concluded that bromination and oxidation of polystyrene chains took place due to the reactions with decomposition products of flame retardants. These reactions seemed to be more efficient in the presence of  $\text{Sb}_2\text{O}_3$ .

### **3.4.2.3. PS-MMT10A**

Isitman et al. determined that the incorporation of 5 wt% organoclay into PS significantly caused charring about 7.9 wt% [82]. Also, the flame spread rate was reduced from 6.9 to 4.2  $\text{kWm}^{-2}\text{s}^{-1}$ . In the presence of organoclay, LOI value slightly increased by ~1%, and dripping was hindered in UL-94 vertical tests, while no enhancement was obtained in the UL-94 rating with respect to neat PS [82].

In the presence of MMT10A, pyrolysis of PS yielded a sharp peak with maximum at around 457°C in the TIC curve (Figure 3.57). The abundance of high mass products was increased and extensive fragmentation was detected. As a result of increase in the probability of radical recombination reactions, many additional structures may be generated. The TIC curve PS-MMT10A also shows two weak peaks at around 202 and 322°C in accordance to the thermal degradation of MMT10A based products.

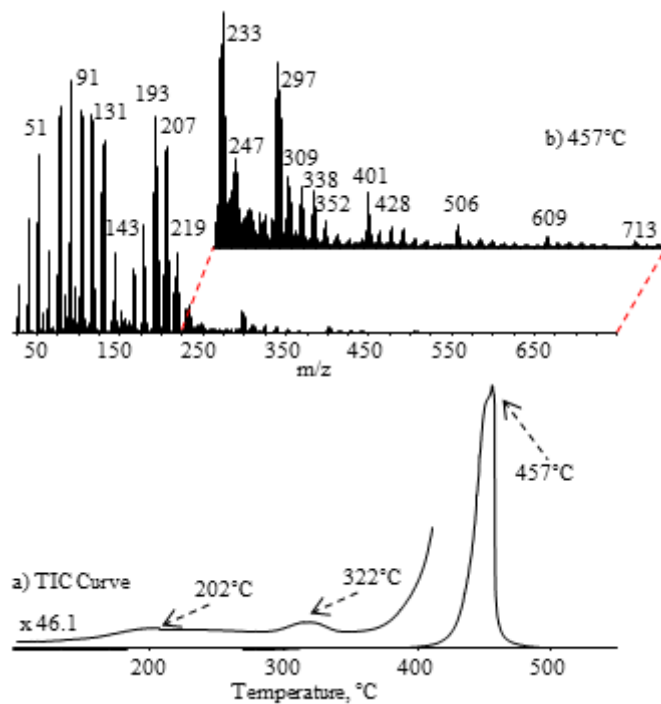


**Figure 3.57.** a) The total ion current curve and b) mass spectrum of PS-MMT10A at 457°C.

In Table 3.26, the relative intensities of intense and/or characteristic peaks recorded in the spectrum and the assignments made are summarized.

**Table 3.26.** The relative intensities, RI, of some selected intense and/or characteristic peaks recorded in pyrolysis spectrum of PS- MMT10A at 457°C and the assignments made.

m/z	RI	Assignment
78	894	C <sub>6</sub> H <sub>6</sub>
91	1000	CH <sub>2</sub> C <sub>6</sub> H <sub>5</sub>
92	634	CH <sub>3</sub> C <sub>6</sub> H <sub>5</sub>
104	848	CH <sub>2</sub> CHC <sub>6</sub> H <sub>5</sub> , St
105	855	C <sub>2</sub> H <sub>4</sub> C <sub>6</sub> H <sub>5</sub>
115	865	C <sub>9</sub> H <sub>7</sub>
129	748	C <sub>4</sub> H <sub>4</sub> C <sub>6</sub> H <sub>5</sub>
131	763	StC <sub>2</sub> H <sub>3</sub>
178	431	C <sub>6</sub> H <sub>5</sub> C≡CC <sub>6</sub> H <sub>5</sub>
206	580	CH <sub>2</sub> C(C <sub>6</sub> H <sub>5</sub> )C(C <sub>6</sub> H <sub>5</sub> )CH <sub>2</sub>
207	742	CH <sub>2</sub> C(C <sub>6</sub> H <sub>5</sub> )CH <sub>2</sub> CHC <sub>6</sub> H <sub>5</sub>
208	284	St <sub>2</sub> , CH <sub>3</sub> C(C <sub>6</sub> H <sub>5</sub> )C(CH <sub>3</sub> )C <sub>6</sub> H <sub>5</sub> , CH <sub>2</sub> C(C <sub>6</sub> H <sub>5</sub> )CH(CH <sub>3</sub> )C <sub>6</sub> H <sub>5</sub>
220	157	CH <sub>2</sub> (C <sub>6</sub> H <sub>5</sub> )CC(C <sub>6</sub> H <sub>5</sub> )CHCH <sub>3</sub>
193	854	CH <sub>2</sub> C(C <sub>6</sub> H <sub>5</sub> )CHC <sub>6</sub> H <sub>5</sub>
297	90	CH <sub>2</sub> C(C <sub>6</sub> H <sub>5</sub> )CH(C <sub>6</sub> H <sub>5</sub> )St
401	26	CH <sub>2</sub> C(C <sub>6</sub> H <sub>5</sub> )CH(C <sub>6</sub> H <sub>5</sub> )St <sub>2</sub>
505	8.5	CH <sub>2</sub> C(C <sub>6</sub> H <sub>5</sub> )CH(C <sub>6</sub> H <sub>5</sub> )St <sub>3</sub>
609	4.9	CH <sub>2</sub> C(C <sub>6</sub> H <sub>5</sub> )CH(C <sub>6</sub> H <sub>5</sub> )St <sub>4</sub>
194	657	MCHC <sub>6</sub> H <sub>5</sub>
298	77	M <sub>2</sub> CHC <sub>6</sub> H <sub>5</sub>
402	26	M <sub>3</sub> CHC <sub>6</sub> H <sub>5</sub>
506	11	M <sub>4</sub> CHC <sub>6</sub> H <sub>5</sub>
610	3.3	M <sub>5</sub> CHC <sub>6</sub> H <sub>5</sub>
714	2.0	M <sub>6</sub> CHC <sub>6</sub> H <sub>5</sub>
196	291	HMCH <sub>2</sub> C <sub>6</sub> H <sub>5</sub>
300	63	HM <sub>2</sub> CH <sub>2</sub> C <sub>6</sub> H <sub>5</sub>
404	16	HM <sub>3</sub> CH <sub>2</sub> C <sub>6</sub> H <sub>5</sub>
508	5.3	HM <sub>4</sub> CH <sub>2</sub> C <sub>6</sub> H <sub>5</sub>
612	1.7	HM <sub>5</sub> CH <sub>2</sub> C <sub>6</sub> H <sub>5</sub>
716	1.3	HM <sub>6</sub> CH <sub>2</sub> C <sub>6</sub> H <sub>5</sub>
43	11	CH <sub>2</sub> NCH <sub>3</sub> and/or C <sub>3</sub> H <sub>7</sub>
58	82	CH <sub>2</sub> N(CH <sub>3</sub> ) <sub>2</sub> and/or C <sub>4</sub> H <sub>11</sub>
134	6.4	CH <sub>2</sub> N(CH <sub>3</sub> )CH <sub>2</sub> C <sub>6</sub> H <sub>5</sub>



Single ion pyrograms of some characteristic products are shown in Figure 3.58. Thermal degradation products of PS followed identical trends in their evolution profiles. Nevertheless, the relative yields of high mass thermal degradation fragments of PS were increased significantly in the presence of MMT10A. Furthermore, degradation of PS based products was maximized at around 458°C, indicating a shift of 17°C. This shows that in the presence of MMT10A, the thermal stability of PS chains was enhanced.

The overlapping peaks, recorded at around 150-350°C in pyrolysis mass spectra, at 43, (CH<sub>2</sub>NCH<sub>3</sub>), 58, ((CH<sub>3</sub>)<sub>2</sub>NCH<sub>2</sub>) and 134 Da, (CH<sub>2</sub>N(CH<sub>3</sub>)CH<sub>2</sub>C<sub>6</sub>H<sub>5</sub>) was related to MMT10A. These fragments also evolved in the temperature region where PS degradation took place. However, due to the same m/z values, contribution of thermal degradation products of PS has to be considered.

As discussed earlier by Jang and Wilkie [79], the accommodation of decomposed polymers within the clay layers, simplifies the entrapment of decomposition products for a long time before they are released into the vapor phase. In addition, the tortuous pathway generated by clay layers may prevent the diffusion of volatiles and the generation of a clay-catalyzed carbonaceous char can also restrict heat and mass transfer across itself. These two effects, that are hindered diffusion and carbonaceous char generation, are termed as the “barrier effects.” [82] MMT retards the degradation of PS chains by barrier effect. In addition, the TIC curve shows a sharp peak at higher temperatures compared to neat PS. Thus, it can be concluded that the evolution of fragments produced by depolymerization was completed in a narrow temperature region indicating an increase in the rate of depolymerization.

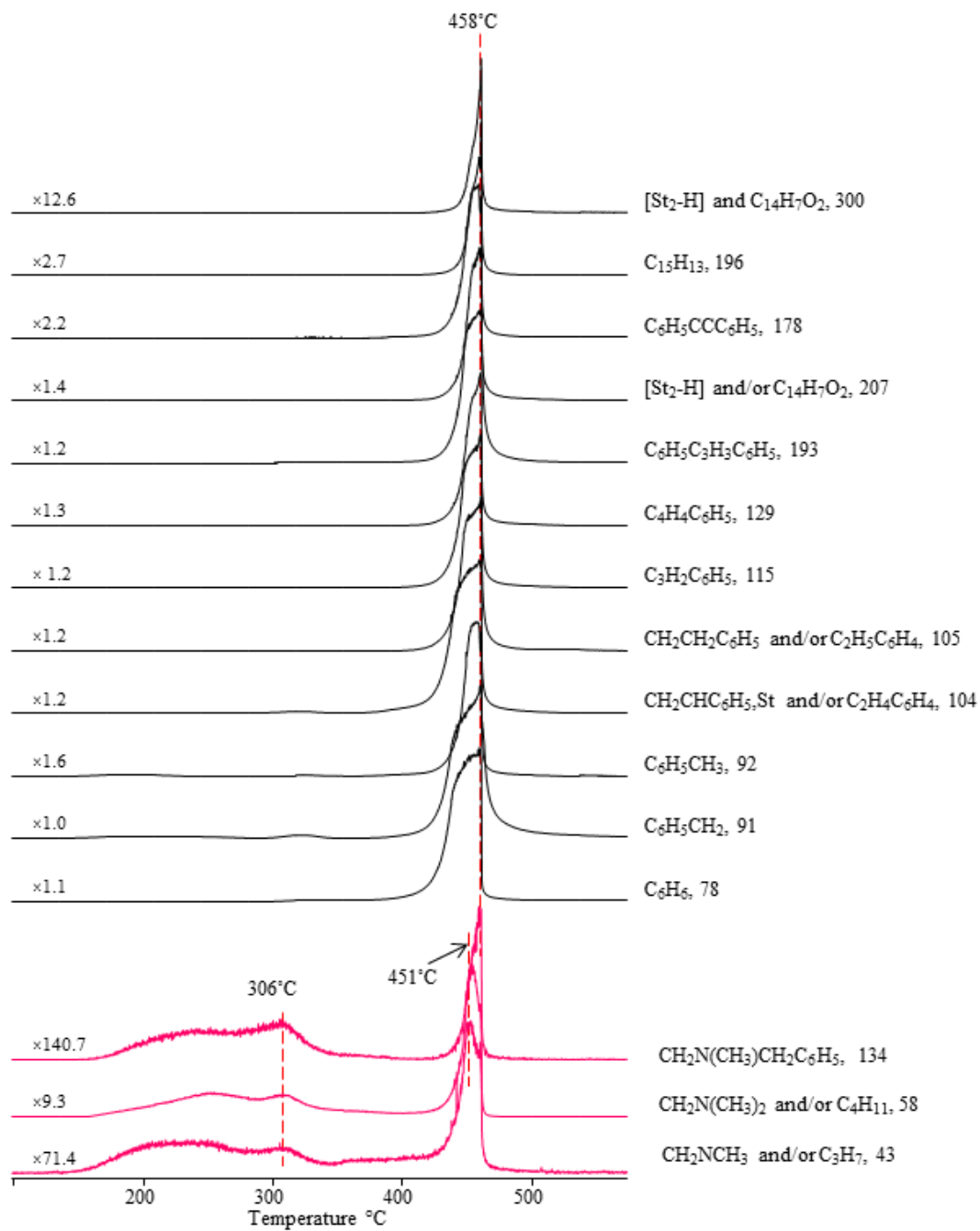


**Figure 3.58.** Single ion pyrograms of some selected fragments detected during the pyrolysis of PS-MMT10A.

In the presence of clay, extensive fragmentation was detected. Generation of additional fragments, most probably involving head-to-head compounds, can be proposed. These head-to-head compounds were thought to be generated by radical recombination reactions. In neat polystyrene,  $\text{CH}_2\text{C}(\text{C}_6\text{H}_5)\text{CH}(\text{C}_6\text{H}_5)\text{M}$  (297 Da) was formed by dissociation of the trimer, but in the presence of nanoclay, despite the absence of trimer,  $\text{CH}_2\text{C}(\text{C}_6\text{H}_5)\text{CH}(\text{C}_6\text{H}_5)\text{M}$  was produced again. Presence of peaks due to products such as  $(\text{C}_6\text{H}_5)\text{CC}(\text{C}_6\text{H}_5)$  (178 Da),  $(\text{C}_6\text{H}_5)(\text{CH}_2)\text{CCH}(\text{C}_6\text{H}_5)$  (193 Da),  $(\text{C}_6\text{H}_5)\text{CH}_2\text{CH}(\text{CH}_3)(\text{C}_6\text{H}_5)$  (196 Da),  $(\text{C}_6\text{H}_5)(\text{CH}_2)\text{CC}(\text{CH}_2)(\text{C}_6\text{H}_5)$  (206 Da),  $(\text{C}_6\text{H}_5)(\text{CH}_3)\text{CHC}(\text{CH}_2)(\text{C}_6\text{H}_5)$  (208 Da),  $(\text{C}_6\text{H}_5)(\text{CH}_2)\text{CC}(\text{CHCH}_3)(\text{C}_6\text{H}_5)$  (220 Da) and  $(\text{CH}_3)(\text{C}_6\text{H}_5)\text{CHCH}_2\text{CH}(\text{C}_6\text{H}_5)\text{CH}_2(\text{C}_6\text{H}_5)$  (300 Da) also supported the proposed mechanism (Figure 3.59). Furthermore, these findings suggested that there were some differences in decomposition pathway in the presence of clay. Because of the effects of the clay layers, the radicals which were generated through chain scission have more possibility to undergo radical transfer and recombination reactions. In addition, for the PS-MMT10A composite, the trace of  $\alpha$ -methylstyrene in neat PS increased its abundance more than 36 folds.

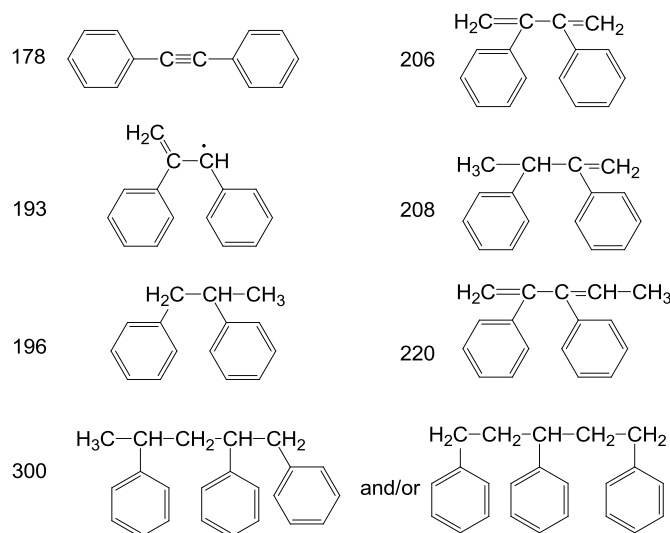


**Figure 3.59.** Possible head-to-head compounds.

Peaks, due to the series of fragments with formula  $\text{HMxCH}_2\text{C}_6\text{H}_5$  ( $m/z = 196, 300, 404, 508, 612$  and  $716$  Da for  $x = 1$  to  $6$ ) were detected. It was likely that 1,3-diphenylpropane (196 Da) was mostly generated by disproportionation because of the effects of the clay (Scheme 3.15). The enhancement in the yield of 1,3-diphenylpropane suggested that disproportionation reactions was increased in the presence of clay. Moreover, peaks, due to the series of fragments with formula  $\text{MxCHC}_6\text{H}_5$  ( $m/z = 194, 298, 402, 506, 610$  and  $714$  Da for  $x = 1$  to  $6$ ) were detected.

#### 3.4.2.4. PS-BE-MMT10A

In a recent study [82], it has been detected that organoclay incorporation into PS-BE blend (20 wt% brominated epoxy and 5 wt% MMT10A) was decreased the flame spread rate from  $4.5$  to  $2.1 \text{ kW m}^{-2} \text{ s}^{-1}$  which corresponds to the same performance showed by PS-BE- $\text{Sb}_2\text{O}_3$  ( $2.1 \text{ kW m}^{-2} \text{ s}^{-1}$ ). The addition of organoclay in PS-BE increased LOI by 6% compared to neat PS. It is noteworthy that LOI of PS-BE-MMT10A was the same as PS-BE- $\text{Sb}_2\text{O}_3$ , which indicated that organoclays acted as efficiently as  $\text{Sb}_2\text{O}_3$ . However, in UL-94 test V-2 rating was changed to nonclassified because self-extinguishment by dripping was prevented by organoclay. This may be related to enhancement of the melt viscosity of nanocomposites. The decomposition characteristic of PS was changed in the presence of brominated additive [82].

PS-BE-MMT10A composite degraded in a single step by depolymerization reaction. The TIC curve recorded during the pyrolysis of PS-BE-MMT10A composite showed a sharp peak with a maximum at  $442^\circ\text{C}$  and a shoulder at  $372^\circ\text{C}$  (Figure 3.60). Typical fragmentation pattern of PS, intense peaks at  $m/z = 78, 91, 92, 104, 105, 115, 129, 193$  and  $207$  Da due to  $\text{C}_6\text{H}_6, \text{C}_6\text{H}_5\text{CH}_2, \text{C}_6\text{H}_5\text{CH}_3, \text{C}_2\text{H}_3\text{C}_6\text{H}_5(\text{St}), \text{C}_2\text{H}_4\text{C}_6\text{H}_5, \text{C}_3\text{H}_2\text{C}_6\text{H}_5, \text{C}_4\text{H}_4\text{C}_6\text{H}_5, \text{C}_6\text{H}_5\text{C}_3\text{H}_3\text{C}_6\text{H}_5,$  and  $\text{St}_2\text{-H}$  respectively, was noted in the pyrolysis mass spectrum recorded at  $442^\circ\text{C}$ . In addition, characteristic fragmentation pattern of BE and MMT10A, intense peaks at  $m/z = 43, 80, 293, 330, 529, 585, 58$  and  $134$  Da due to  $\text{CH}_3\text{CO}, \text{HBr},$

$C_6H_2Br_2C_2H_3O_2$ ,  $Br_3C_6H_2OH$ ,  $HO(Br_2)C_6H_2CCH_3C_6H_2(Br_2)OH$ ,  
 $C_3H_5O_2(Br_2)C_6H_2CCH_3C_6H_2(Br_2)OH$ ,  $NC_3H_8$  and  $N(CH_3)_2CH_2C_6H_5$  respectively,  
were observed in the pyrolysis mass spectra recorded at around 372 and 442°C.  
Peaks, due to the series of products with formula  $MxCHC_6H_5$  ( $m/z = 194, 298,$   
 $402, 506, 610$  and  $714$  Da for  $x = 1$  to  $6$ ) were detected as in the case of PS-  
MMT10A composite. In Table 3.27, the relative intensities of intense and/or  
characteristic peaks recorded in the spectrum and the assignments made are  
summarized.

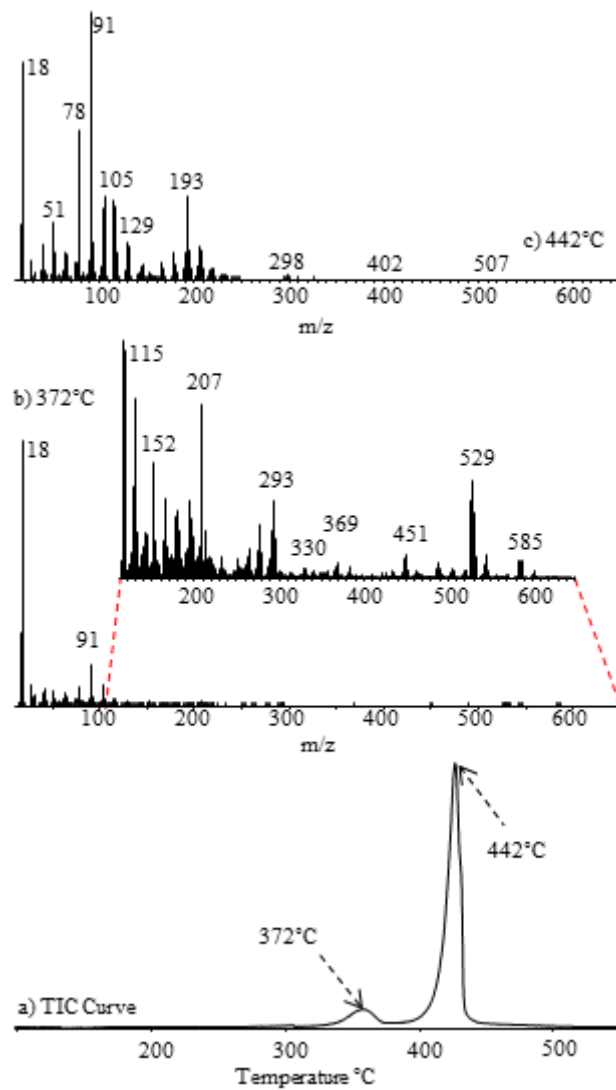


**Figure 3.60.** a) The total ion current curve and the mass spectra at b) 372 c) 442°C recorded during the pyrolysis of PS-BE-MMT10A.

**Table 3.27.** The relative intensities, RI, of some selected intense and/or characteristic peaks recorded in pyrolysis spectrum of PS-BE-MMT10A at 372 and 442 °C and the assignments made.

m/z	RI		Assignment
	372 °C	442 °C	
18	1000	809	H <sub>2</sub> O
28	78	69	CO
43	62	6.3	CH <sub>3</sub> CO, CH <sub>2</sub> COH
51	56	208	C <sub>4</sub> H <sub>3</sub>
78	65	553	C <sub>6</sub> H <sub>6</sub>
91	151	1000	CH <sub>2</sub> C <sub>6</sub> H <sub>5</sub>
92	28	133	CH <sub>3</sub> C <sub>6</sub> H <sub>5</sub>
104	72	265	C <sub>2</sub> H <sub>3</sub> C <sub>6</sub> H <sub>5</sub> [St]
105	23	306	C <sub>2</sub> H <sub>4</sub> C <sub>6</sub> H <sub>5</sub>
115	22	293	C <sub>3</sub> H <sub>2</sub> C <sub>6</sub> H <sub>5</sub>
129	16	140	C <sub>4</sub> H <sub>4</sub> C <sub>6</sub> H <sub>5</sub>
131	7.7	122	CH <sub>2</sub> C(C <sub>6</sub> H <sub>5</sub> )CH <sub>2</sub> CH <sub>2</sub>
178	5.6	100	C(C <sub>6</sub> H <sub>5</sub> )CC <sub>6</sub> H <sub>5</sub>
191	2.6	99	C(C <sub>6</sub> H <sub>5</sub> )CCHC <sub>6</sub> H <sub>5</sub>
193	6.7	308	CH(C <sub>6</sub> H <sub>5</sub> )CHCHC <sub>6</sub> H <sub>5</sub>
207	16	104	[St <sub>2</sub> -H]
208	5.6	40	St <sub>2</sub> , CH <sub>3</sub> C(C <sub>6</sub> H <sub>5</sub> )C(CH <sub>3</sub> )C <sub>6</sub> H <sub>5</sub>
194	7.1	105	MCHC <sub>6</sub> H <sub>5</sub>
298	0.5	10	M <sub>2</sub> CHC <sub>6</sub> H <sub>5</sub>
402	0.1	2.6	M <sub>3</sub> CHC <sub>6</sub> H <sub>5</sub>
506	0.9	0.4	M <sub>4</sub> CHC <sub>6</sub> H <sub>5</sub>
610		0.3	M <sub>5</sub> CHC <sub>6</sub> H <sub>5</sub>
714		0.1	M <sub>6</sub> CHC <sub>6</sub> H <sub>5</sub>
58	6.8	7.1	NC <sub>3</sub> H <sub>8</sub>
134	0.8	1.4	N(CH <sub>3</sub> ) <sub>2</sub> CH <sub>2</sub> C <sub>6</sub> H <sub>5</sub>
79	21	91	Br
80	17	8.1	H <sup>79</sup> Br
212	4.4	0.6	C <sub>6</sub> H <sub>3</sub> BrOHC <sub>3</sub> H <sub>5</sub>
252	0.6	3.2	C <sub>6</sub> H <sub>3</sub> Br <sub>2</sub> OH
265	2.6	0.8	C <sub>6</sub> H <sub>2</sub> Br <sub>2</sub> OCH <sub>3</sub>
277	4.8	1.3	C <sub>6</sub> H <sub>2</sub> Br <sub>2</sub> OC <sub>2</sub> H <sub>3</sub>
293	7.0	1.2	C <sub>6</sub> H <sub>2</sub> Br <sub>2</sub> C <sub>2</sub> H <sub>3</sub> O <sub>2</sub>
332	0.9	0.6	Br <sub>3</sub> C <sub>6</sub> H <sub>2</sub> OH
369	1.4	0.4	Br <sub>3</sub> C <sub>6</sub> H <sub>2</sub> OC <sub>3</sub> H <sub>4</sub>
451	2.1	0.1	HO(Br)C <sub>6</sub> H <sub>3</sub> CCH <sub>3</sub> C <sub>6</sub> H <sub>2</sub> (Br <sub>2</sub> )OH
529	9.0		HO(Br <sub>2</sub> )C <sub>6</sub> H <sub>2</sub> CCH <sub>3</sub> C <sub>6</sub> H <sub>2</sub> (Br <sub>2</sub> )OH
544	2.1		HO(Br <sub>2</sub> )C <sub>6</sub> H <sub>2</sub> C(CH <sub>3</sub> ) <sub>2</sub> C <sub>6</sub> H <sub>2</sub> (Br <sub>2</sub> )OH
585	1.6		C <sub>3</sub> H <sub>5</sub> O <sub>2</sub> (Br <sub>2</sub> )C <sub>6</sub> H <sub>2</sub> CCH <sub>3</sub> C <sub>6</sub> H <sub>2</sub> (Br <sub>2</sub> )OH

Single ion evolution profiles of characteristic decomposition fragments of PS followed identical trends (Figure 3.61). The relative yields of high mass thermal degradation fragments increased compared to what was noted for neat PS and PS-BE. On the other hand, relative yields of monomer (104 Da), protonated monomer (105 Da), dimer (208 Da) and dehydrated dimer (207 Da) were decreased compared to PS-MMT10A and PS-BE-Sb<sub>2</sub>O<sub>3</sub>-MMT10A while those of all other fragments were increased. All these findings indicate that upon combination of BE and MMT10A, depolymerization reactions were suppressed.

Single ion evolution profiles of characteristic decomposition fragments of BE followed identical trends as in the case of PS-BE-Sb<sub>2</sub>O<sub>3</sub>. Thermal stability of BE chains was decreased in the presence of MMT10A. All BE based products reached maximum yield at around 371°C. These fragments were also detected in the temperature region where PS degradation took place, at around 442°C. The evolution of HBr (80-82) and tribromophenol (328-334) in this region was more pronounced. In addition the relative yields of the thermal degradation products of BE were changed in the presence of nanoclay. Among the thermal decomposition fragments of BE, the relative yields of brominated fragments were decreased noticeably compared to PS-BE. The decrease was 2.5 folds for tribromophenol, 2 folds for HBr, tetrabromobisphenol A and other fragments generated by decomposition of the main chain of BE oligomer.



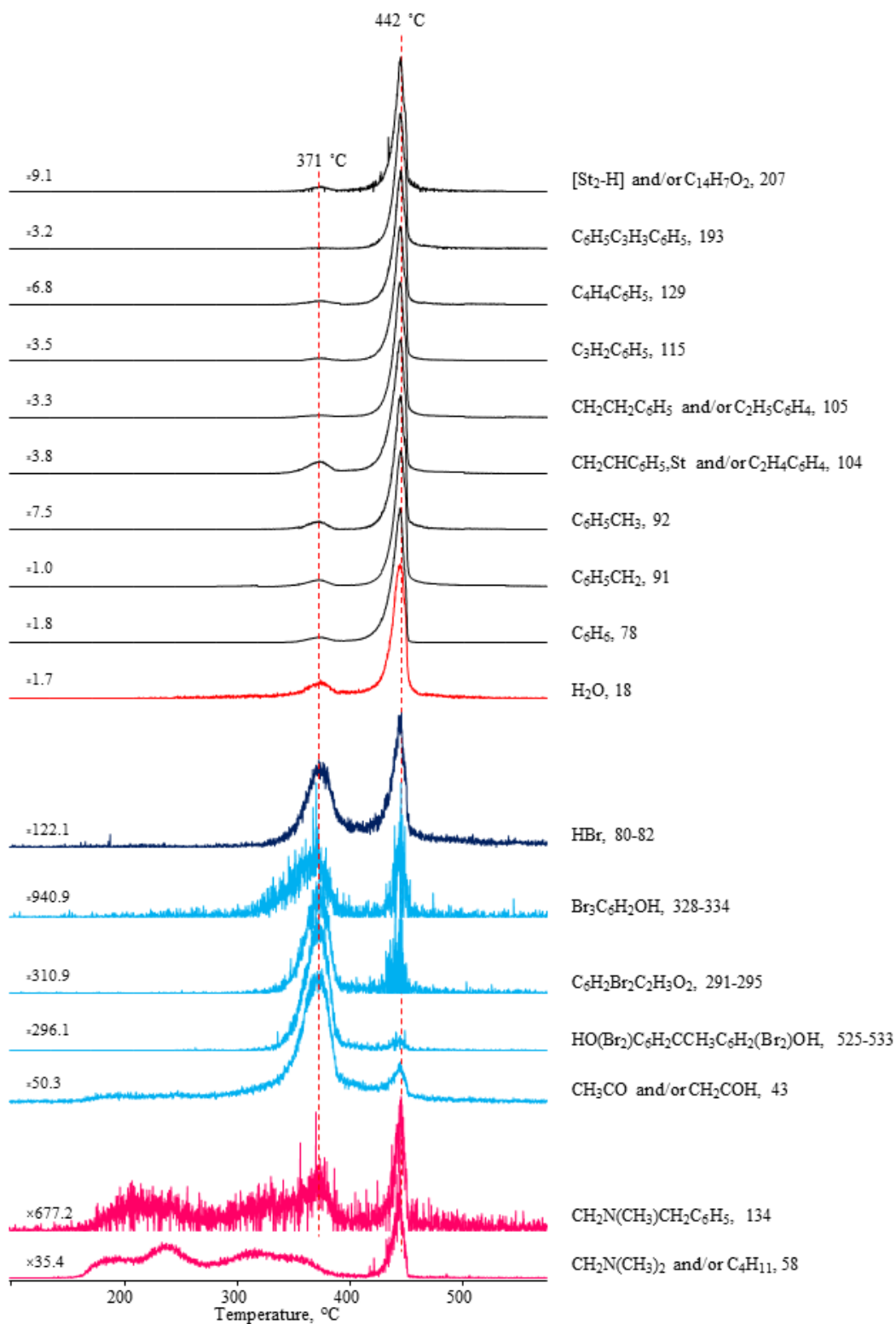


**Figure 3.61.** Single ion pyrograms of some selected fragments detected during the pyrolysis of PS-BE-MMT10A.

Though the thermal decomposition of PS chains was started at almost the same temperature region, the evolution profiles were sharpened indicating that release of thermal degradation products was completed in a narrow temperature interval. Although the rate of depolymerization was increased, the thermal stability of PS chains was not changed. The evolution of BE products had shown similar trends with those of PS products during the pyrolysis of PS-BE composite. However, in the presence of MMT10A, the generation of BE based fragments were decreased in the temperature region where PS degradation took place. As a conclusion, it can be thought that the interactions between BE and PS were hindered by the effect of clay layers.

The overlapping peaks, recorded at around 150-400°C in pyrolysis mass spectra, at 43, (CH<sub>2</sub>NCH<sub>3</sub>), 58, ((CH<sub>3</sub>)<sub>2</sub>NCH<sub>2</sub>) and 134 Da, (CH<sub>2</sub>N(CH<sub>3</sub>)CH<sub>2</sub>C<sub>6</sub>H<sub>5</sub>) was related to decomposition of organic part of MMT10A. These fragments evolved in the temperature region where PS degradation took place. Again, the high temperature evolution of MMT25A based products may be expressed by the contribution of thermal degradation fragments of PS.

Furthermore, as in the case of PS-BE-Sb<sub>2</sub>O<sub>3</sub> composite, the higher yields of HBr and water, in the temperature region where PS degradation took place, supported bromination and oxidation of polystyrene due to the reactions with decomposition products of flame retardants.

#### **3.4.2.5. PS-BE-Sb<sub>2</sub>O<sub>3</sub>-MMT10A**

In a recent study [82], it has been shown that the fire growth rate was further lowered from 4.2 to 1.4 kWm<sup>-2</sup>s<sup>-1</sup> for PS-BE-Sb<sub>2</sub>O<sub>3</sub>-MMT10A by the act of halogenated flame retardant, Sb<sub>2</sub>O<sub>3</sub> and nanoclay additives. The addition of organoclay in PS-BE-Sb<sub>2</sub>O<sub>3</sub> increased LOI by 1.5% [82].

PS-BE-Sb<sub>2</sub>O<sub>3</sub>-MMT10A composite (20 wt% brominated epoxy, 5 wt% MMT10A and 3 wt% antimony oxide) degraded in two-steps at around 384 and 453°C. The

TIC curve recorded during the pyrolysis of PS-BE-Sb<sub>2</sub>O<sub>3</sub>-MMT10A composite is given in Figure 3.62. Typical fragmentation pattern of PS, intense peaks at  $m/z = 78, 91, 92, 104, 105, 115, 129$  and  $207$  Da due to C<sub>6</sub>H<sub>6</sub>, C<sub>6</sub>H<sub>5</sub>CH<sub>2</sub>, C<sub>6</sub>H<sub>5</sub>CH<sub>3</sub>, C<sub>2</sub>H<sub>3</sub>C<sub>6</sub>H<sub>5</sub>(St), C<sub>2</sub>H<sub>4</sub>C<sub>6</sub>H<sub>5</sub>, C<sub>3</sub>H<sub>2</sub>C<sub>6</sub>H<sub>5</sub>, C<sub>4</sub>H<sub>4</sub>C<sub>6</sub>H<sub>5</sub> and St<sub>2</sub>-H respectively, was observed in the pyrolysis mass spectrum recorded at 453 °C. In addition diagnostic peaks of BE, Sb<sub>2</sub>O<sub>3</sub> and MMT10A, intense peaks at  $m/z = 43, 80, 293, 330, 529, 137, 281, 362, 58$  and  $134$  Da due to CH<sub>3</sub>CO, HBr, C<sub>6</sub>H<sub>2</sub>Br<sub>2</sub>C<sub>2</sub>H<sub>3</sub>O<sub>2</sub>, Br<sub>3</sub>C<sub>6</sub>H<sub>2</sub>OH, HO(Br<sub>2</sub>)C<sub>6</sub>H<sub>2</sub>CCH<sub>3</sub>C<sub>6</sub>H<sub>2</sub>(Br<sub>2</sub>)OH, SbO, SbBr<sub>2</sub>, SbBr<sub>3</sub>, CH<sub>2</sub>N(CH<sub>3</sub>)<sub>2</sub> and N(CH<sub>3</sub>)<sub>2</sub>CH<sub>2</sub>C<sub>6</sub>H<sub>5</sub> respectively, were observed in the pyrolysis mass spectra recorded at 384 and 453 °C. As in the case of PS-MMT10A and PS-BE-MMT10A, peaks, due to the series of fragments with formula M<sub>x</sub>CHC<sub>6</sub>H<sub>5</sub> ( $m/z = 194, 298, 402, 506, 610$  and  $714$  Da for  $x = 1$  to  $6$ ) were detected.

Thermal decomposition products of BE showed maxima at 378 and 451 °C, indicating that degradation of BE chains shifted to lower temperatures compared to neat BE, in the presence of Sb<sub>2</sub>O<sub>3</sub> and MMT10A. The relative yields of the thermal degradation products of BE were changed in the presence of MMT10A and Sb<sub>2</sub>O<sub>3</sub>. In Table 3.28, the relative intensities of intense and/or characteristic peaks recorded in the spectrum and the assignments made are summarized.

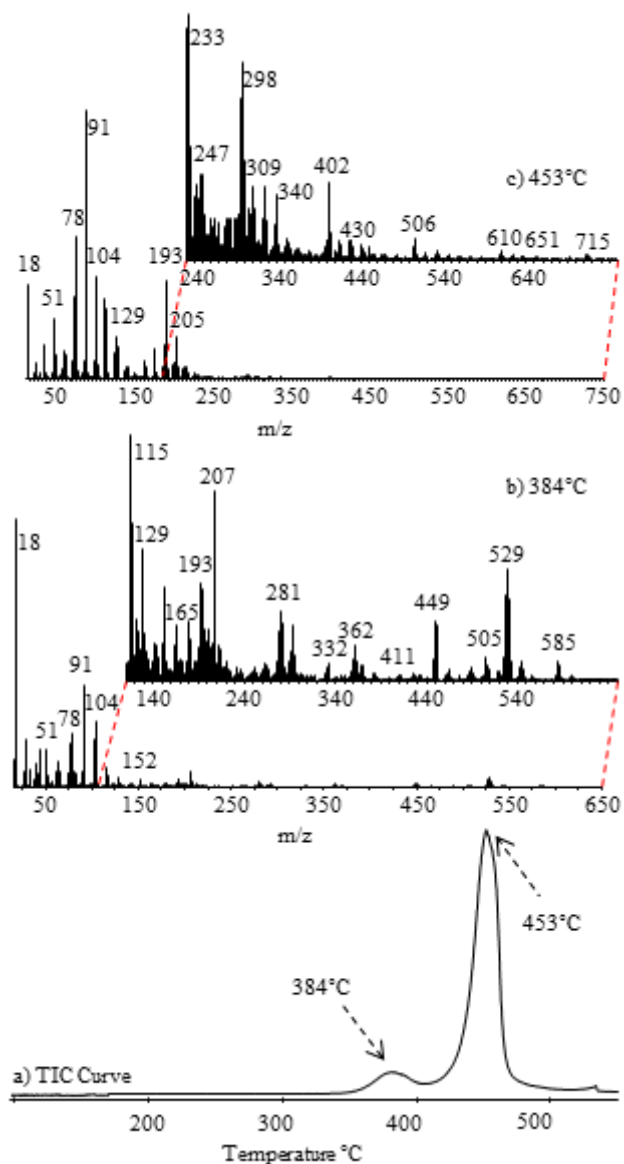


**Figure 3.62.** a) The total ion current curve and the mass spectra at **b)** 384, **c)** 453 °C recorded during the pyrolysis of PS-BE-Sb<sub>2</sub>O<sub>3</sub>-MMT10A.

**Table 3.28.** The relative intensities, RI, of some selected intense and/or characteristic peaks recorded in pyrolysis spectrum of PS-BE-Sb<sub>2</sub>O<sub>3</sub>-MMT10A at 384 and 453 °C and the assignments made.

m/z	RI		Assignment
	384 °C	453 °C	
18	1000	351	H <sub>2</sub> O
28	178	60	CO
43	139	4.0	CH <sub>3</sub> CO, CH <sub>2</sub> COH
51	139	224	C <sub>4</sub> H <sub>3</sub>
78	199	530	C <sub>6</sub> H <sub>6</sub>
91	380	1000	CH <sub>2</sub> C <sub>6</sub> H <sub>5</sub>
92	43	125	CH <sub>3</sub> C <sub>6</sub> H <sub>5</sub>
104	245	381	C <sub>2</sub> H <sub>3</sub> C <sub>6</sub> H <sub>5</sub> [St]
105	61	332	C <sub>2</sub> H <sub>4</sub> C <sub>6</sub> H <sub>5</sub>
115	73	301	C <sub>3</sub> H <sub>2</sub> C <sub>6</sub> H <sub>5</sub>
129	39	155	C <sub>4</sub> H <sub>4</sub> C <sub>6</sub> H <sub>5</sub>
131	14	119	CH <sub>2</sub> C(C <sub>6</sub> H <sub>5</sub> )CH <sub>2</sub> CH <sub>2</sub>
178	18	113	C(C <sub>6</sub> H <sub>5</sub> )CC <sub>6</sub> H <sub>5</sub>
191	14	122	C(C <sub>6</sub> H <sub>5</sub> )CCHC <sub>6</sub> H <sub>5</sub>
193	29	362	CH(C <sub>6</sub> H <sub>5</sub> )CHCHC <sub>6</sub> H <sub>5</sub>
207	56	138	[St <sub>2</sub> -H]
194	27	130	MCHC <sub>6</sub> H <sub>5</sub>
298	1.6	7.8	M <sub>2</sub> CHC <sub>6</sub> H <sub>5</sub>
402	0.3	4.7	M <sub>3</sub> CHC <sub>6</sub> H <sub>5</sub>
506	1.5	1.3	M <sub>4</sub> CHC <sub>6</sub> H <sub>5</sub>
58	7.6	12	NC <sub>3</sub> H <sub>8</sub>
134	6.1	1.4	N(CH <sub>3</sub> ) <sub>2</sub> CH <sub>2</sub> C <sub>6</sub> H <sub>5</sub>
79	86	92	Br
80	51	9.7	H <sup>79</sup> Br
212	11	0.6	C <sub>6</sub> H <sub>3</sub> BrOHC <sub>3</sub> H <sub>5</sub>
252	3.8	1.1	C <sub>6</sub> H <sub>3</sub> Br <sub>2</sub> OH
265	4.6	2.5	C <sub>6</sub> H <sub>2</sub> Br <sub>2</sub> OCH <sub>3</sub>
277	9.8	1.7	C <sub>6</sub> H <sub>2</sub> Br <sub>2</sub> OC <sub>2</sub> H <sub>3</sub>
293	16	2.8	C <sub>6</sub> H <sub>2</sub> Br <sub>2</sub> C <sub>2</sub> H <sub>3</sub> O <sub>2</sub>
332	4.9	0.6	Br <sub>3</sub> C <sub>6</sub> H <sub>2</sub> OH
369	4.4	0.4	Br <sub>3</sub> C <sub>6</sub> H <sub>2</sub> OC <sub>3</sub> H <sub>4</sub>
451	16	0.8	HO(Br)C <sub>6</sub> H <sub>3</sub> CCH <sub>3</sub> C <sub>6</sub> H <sub>2</sub> (Br <sub>2</sub> )OH
529	33	0.2	HO(Br <sub>2</sub> )C <sub>6</sub> H <sub>2</sub> CCH <sub>3</sub> C <sub>6</sub> H <sub>2</sub> (Br <sub>2</sub> )OH
544	5.8	0.2	HO(Br <sub>2</sub> )C <sub>6</sub> H <sub>2</sub> C(CH <sub>3</sub> ) <sub>2</sub> C <sub>6</sub> H <sub>2</sub> (Br <sub>2</sub> )OH
585	6.0	0.2	C <sub>3</sub> H <sub>5</sub> O <sub>2</sub> (Br <sub>2</sub> )C <sub>6</sub> H <sub>2</sub> CCH <sub>3</sub> C <sub>6</sub> H <sub>2</sub> (Br <sub>2</sub> )OH
137	2.0	1.2	SbO
281	21	2.5	SbBr <sub>2</sub>
362	11	0.6	SbBr <sub>3</sub>
203	6.5	58	SbBr,
219	4.2	45	SbOBr,
235	1.8	6.7	SbO <sub>2</sub> Br,
360	6.6		Sb <sub>2</sub> O <sub>2</sub> Br

Single ion profiles of characteristic products are given in Figure 3.63. The relative yields of the thermal decomposition fragments of BE were increased noticeably in the presence of both  $\text{Sb}_2\text{O}_3$  and MMT10A compared to what was observed during the pyrolysis of PS-BE- $\text{Sb}_2\text{O}_3$  composite. The increase was 2.8-folds for tetrabromobisphenol A, 1.7 folds for tribromophenol and more than 1.2-folds for other fragments generated by decomposition of BE.

The characteristic peaks present in the pyrolysis mass spectra of  $\text{Sb}_2\text{O}_3$  were weak. However, peaks due to oxybromides and bromides of antimony such as  $\text{SbBr}$ ,  $\text{SbBr}_2$ ,  $\text{SbBr}_3$ ,  $\text{Sb}_2\text{Br}_2$ ,  $\text{SbOBr}$ ,  $\text{SbOBr}_2$ ,  $\text{SbO}_2\text{Br}$ ,  $\text{Sb}_2\text{O}_2\text{Br}$  and  $\text{Sb}_2\text{OBr}_2$  were noticed as in the spectrum of PS-BE- $\text{Sb}_2\text{O}_3$  composite. In addition in the presence of MMT10A, relative yields of oxybromides and bromides of antimony were increased significantly. For instance, the increase was 4-folds for  $\text{SbOBr}_2$ , 2.5-folds for  $\text{SbBr}$ . However, because of the effects of clay layers, the release of gaseous decomposition products such as  $\text{HBr}$  was decreased. In this respect, enhancement in the time period for the reaction of  $\text{HBr}$  with  $\text{Sb}_2\text{O}_3$  caused an increase in the yield of  $\text{SbBr}_3$ . Thus, it can be concluded that the reactions of antimony oxides with bromines were increased in the presence of MMT10A.

The overlapping peaks, recorded at around 150-400°C in pyrolysis mass spectra, at 58,  $((\text{CH}_3)_2\text{NCH}_2)$  and 134 Da,  $(\text{CH}_2\text{N}(\text{CH}_3)\text{CH}_2\text{C}_6\text{H}_5)$  was due to the degradation of organic part of MMT10A. Again, these fragments evolved in the temperature region where PS degradation took place, because of the contributions of thermal degradation products of PS.

The yields of thermal decomposition fragments of PS chains were maximized at higher temperature regions than PS-BE- $\text{Sb}_2\text{O}_3$  and PS-BE-MMT10A indicating improvement in the thermal stability of PS chains in the presence of mixture of BE,  $\text{Sb}_2\text{O}_3$  and MMT10A. Evolution of water,  $\text{HBr}$  was also mainly noted in the temperature region where of PS degradation took place. Furthermore, unlike what was observed during the pyrolysis of PS-BE- $\text{Sb}_2\text{O}_3$  composite,  $\text{Sb}_2\text{O}_3$  based products showed higher yield in this temperature region.

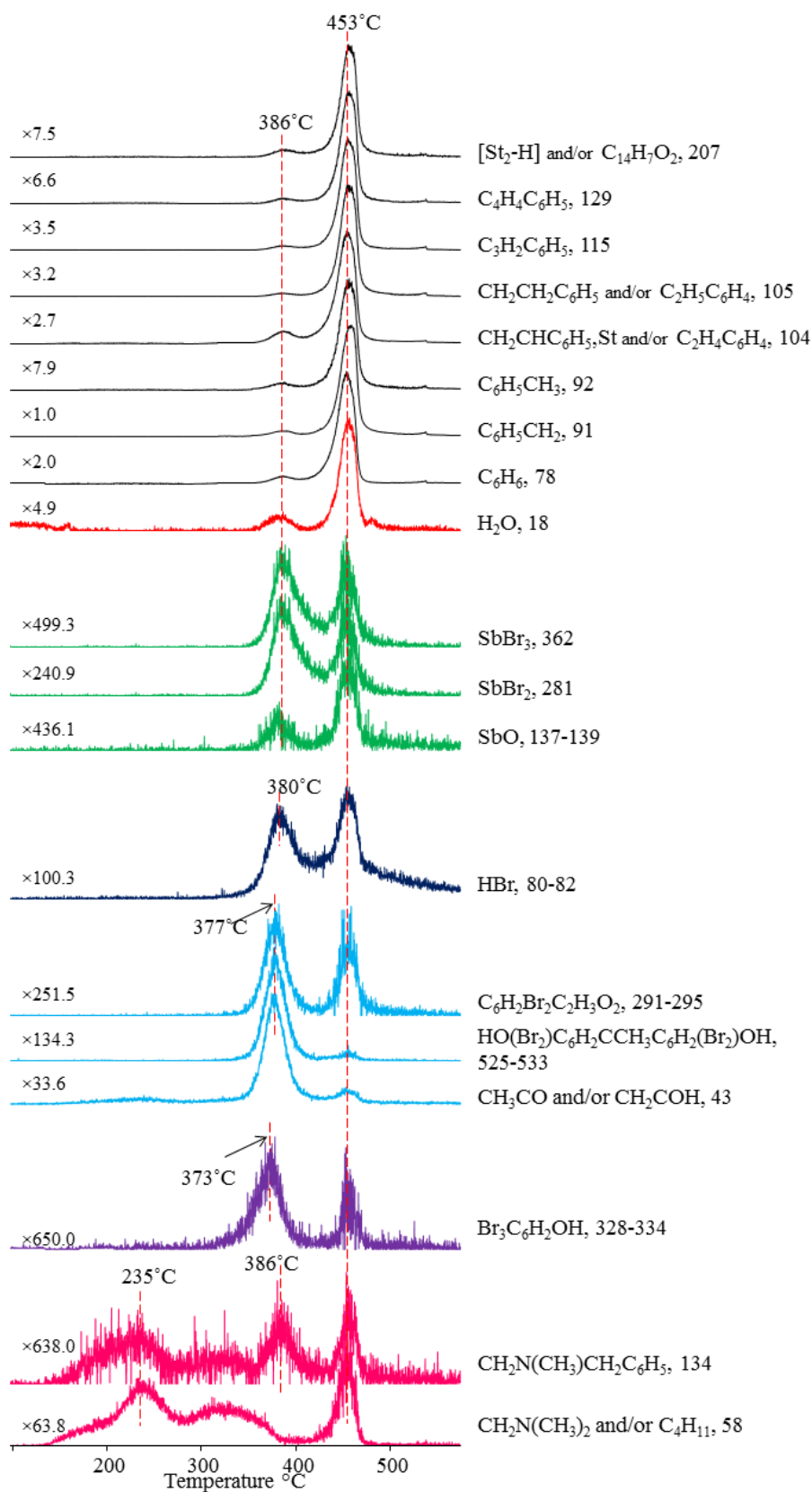


**Figure 3.63.** Single ion pyrograms of some selected fragments detected during the pyrolysis of PS-BE-Sb<sub>2</sub>O<sub>3</sub>-MMT10A.





## CHAPTER 4

### CONCLUSION

In this work, the effects of addition of nanoparticles on thermal decomposition characteristics of composites of polyamide 6 (PA6) and polylactide, (PLA) and polystyrenes, (HIPS and PS) involving flame retardants were analyzed via direct pyrolysis mass spectrometry (DP-MS) technique.

- The effects of halloysite (HNT) or organically modified montmorillonites (MMT25A or MMT30B) on thermal decomposition characteristics of PA6 with or without aluminium diethylphosphinate, AlPi, were investigated.
  - By the addition of HNT, the thermal stability of PA6 chains was decreased. The yields of fragments generated by hydrolysis and aminolysis were enhanced indicating the increase in the possibility of the reactions between carbonyl groups and ammonia.
  - MMT25A had no influence on the thermal stability of PA6. Yet, a reduction in the yields of fragments produced by aminolysis reactions was observed.
  - For the composites involving MMT30B, thermal stability of PA6 was increased, as a consequence of the reactions between PA6 and MMT30B. As the amount of MMT30B added was increased, the intermolecular interactions between the PA6 chains were increased.
  - In the presence of AlPi, thermal stability of PA6 chains was decreased and the rate of depolymerization increased.

- Upon addition of HNT, thermal degradation of PA6-AIPi composite was shifted slightly to higher temperature regions. On the other hand, the relative yields of almost all fragments were decreased indicating the decrease in the interactions between PA6 and AIPi.
  - Incorporation of MMT25A increased the thermal stability of PA6-AIPi composite.
  - Thermal stability has enhanced again by addition of MMT30B to PA6-AIPi composite. Overlapping peaks at the evolution profiles of MMT30B based products were indicating that the reactions among amine and carbonyl groups and phosphinates may take place.
- DP-MS analyses of PLA-AIPi composites involving nanoparticles, halloysite (HNT) or organically modified montmorillonite (MMT30B) or SiO<sub>2</sub> were performed to investigate the effects of additives.
- Thermal stability of poly(lactide) in the presence of AIPi was decreased due to the attack of phosphinate groups to carbonyl groups of PLA. As a consequence, extensive fragmentation of PLA took place.
  - With the addition of MMT30B, thermal stability of PLA was slightly increased. Trans-esterification reactions between the PLA and hydroxy ethylene groups of ammonium salt generated units involving CO-OC<sub>2</sub>H<sub>4</sub>N.
  - SiO<sub>2</sub> had no effect on the thermal stability of PA6. Yet, generation of dimeric four coordinate compounds involving Al-O-P linkages was reduced, but monomeric aluminium phosphinate compounds were promoted.
  - In the presence of HNT, thermal stability of PLA was reduced. The interactions between PLA and AIPi based products were hindered, thus, degradation of components of PLA-AIPi resembled to the corresponding pure forms.

- The effects of organically modified montmorillonite (MMT10A) on thermal degradation characteristics of HIPS with or without aluminium hydroxide, ATH, were also studied.
  - Upon addition of MMT10A, thermal stability of PA6 was decreased. The possibility of radical recombination reactions was enhanced, thus, products involving head-to-head linkages, double and triple bonds were generated.
  - Presence of ATH did not influence the thermal stability of HIPS, yet, it improved the effects of clay.
  
- The effects of organically modified montmorillonite (MMT10A) on thermal degradation characteristics of PS with or without bromophenol end-capped brominated epoxy, (BE) or antimony trioxide, ( $\text{Sb}_2\text{O}_3$ ) were investigated.
  - Thermal stability of PS was improved noticeably in the presence of BE. In addition, oxidation/hydrolysis and bromination of PS were detected.
  - Thermal stability of PS was decreased due to the interactions of  $\text{Sb}_2\text{O}_3$  with BE. Generations of oxybromides and bromides of antimony were noted. It has been determined that bromination and oxidation/hydrolysis of PS were more efficient in the presence of  $\text{Sb}_2\text{O}_3$ .
  - In the presence of MMT10A thermal stability of PS chains was enhanced. Products involving head-to-head linkages as a result of radical recombination reactions were identified.
  - Upon addition of BE and MMT10A, thermal stability of PS chains was not affected. However, the interactions between BE and PS were hindered.
  - Thermal stability of PS chains was enhanced for composite involving a mixture of BE,  $\text{Sb}_2\text{O}_3$  and MMT10A. The relative yields of brominated fragments, oxybromides and bromides of antimony were increased. Thus, it can be concluded that the reactions of antimony oxides with bromines were increased in the presence of MMT10A.



## REFERENCES

- 1 Allen, N.S., Edge, M., *Fundamentals of Polymer Degradation and Stabilization*, Elsevier Applied Science, London, 1992, 1.
- 2 Schnabel, W., *Polymer Degradation - Principles and Practical Applications*, Akademie-Verlag, Berlin, 1981, 13.
- 3 Andersson, T., Wesslen, B., Sandstrom, J., *Journal of Applied Polymer Science*, 2002, 86, 7, 1580.
- 4 Pospisil, J., Horak, Z., Krulis, Z., Nespurek, S., Kuroda, S., *Polymer Degradation and Stability*, 1999, 65, 3, 405.
- 5 Price, D.M., Reading, M., Hammiche, A., Pollock, H.M., *International Journal of Pharmaceutics*, 1999, 192, 1, 85.
- 6 Gouin, F., *Plastiques & Elastomeres Magazine*, 2000, 52, 7, 33.
- 7 Hutchinson, J.M., *Journal of Thermal Analysis and Calorimetry*, 2003, 72, 2, 619.
- 8 Kruse, Y.M., Wong H.W., Broadbelt, L.J., *Industrial and Engineering Chemistry Research*, 2003, 42, 12, 2722.
- 9 Chamot, E., *Polymer Preprints*, 2001, 42, 1, 396.
- 10 Zuev, V.V., Bertini F., Audisio, G., *Polymer Degradation and Stability*, 2001 71, 2, 213.
- 11 Carroccio, S., Puglisi, C., Montaudo, G., *Macromolecular Chemistry and Physics*, 1999, 200, 10, 2345.

- 12 Kopinke, F.D., Remmler M., Mackenzie, K., *Polymer Degradation and Stability*, 1996, 52, 1, 25-38.
- 13 Innes, J.D., *Flame retardants and their market applications*, *Flame retardants 101: basic dynamics, past efforts create future opportunities*, Baltimore: Fire Retardant Chemicals Association, 1996, 61–9.
- 14 Price, D., Anthony, G., Carty, P., *Introduction: polymer combustion, condensed phase pyrolysis and smoke formation*, In: Horrocks, A.R., Price, D., editors, *Fire retardant materials*, Cambridge, UK: Woodhead Publishing Ltd, 2001, 1–30.
- 15 Hirschler, M.M., *Chemical aspects of thermal decomposition of polymeric materials*, In: Grand, A.F., Wilkie, C.A., editors, *Fire retardancy of polymeric materials*, New York, NY: Marcel Dekker Inc, 2000, 28–79.
- 16 Sutker, B.J., *Flame retardants*, In: Gerhartz, W., editor, *Ullman's encyclopedia of industrial chemistry*, vol. 14, Weinheim, Germany: Wiley–VCH Verlag, 2002, 1–19.
- 17 Irvine, D.J., McCluskey, J.A., Robinson, I.M., *Fire hazards and some common polymers*, *Polymer Degradation and Stability*, 2000, 67, 383–96.
- 18 Pal, G., Macskasy, H., *Plastics: Their behavior in fires*, Elsevier, New York, 1991.
- 19 Laoutid, F., Bonnaud, L., Alexandre, M., Lopez-Cuesta, J.M., Dubois, Ph., *Materials Science and Engineering R*, 2009, 63, 100-125.
- 20 Horrocks, A.R., Price, D., *Fire Retardant Materials*, CRC Press, Boston, 2001.
- 21 Wilkie, C.A., *An introduction to the use of fillers and nanocomposites in fire retardancy*, In: Le Bras, M., Wilkie, C.A., Bourbigot, S., editors, *Fire retardancy of polymers: new applications of mineral fillers*, Cambridge, UK: Royal Society of Chemistry, 2005, 1–15.

- 22 Camino, G., Costa, L., Luda, D., Cortemiglia, M.P., Overview of fire retardant mechanisms, *Polymer Degradation and Stability*, 1991, 33, 131–54.
- 23 Skinner, G.A., Flame retardancy, the approaches available, In: Pritchard, G., editor, *Plastics additives, an A-Z reference*, London, UK: Chapman and Hall, 1998, 260–7.
- 24 Kiliaris, P., Papaspyrides, C.D., Polymer/layered silicate (clay) nanocomposites: An overview of flame retardancy *Progress in Polymer Science*, 2010, 35, 902–58.
- 25 Woycheshin, E.A., I., Sobolev, J., *Fire Retardant Chem.*, 1975, 2, 224.
- 26 Levchik, S., in: Morgan, A.B., Wilkie, C.A., Editors, *Flame Retardant Polymer Nanocomposites*, Vol.1, Wiley, Hoboken, 2007.
- 27 Babushok, V., Tsang, W., *Combust Flame*, 2000, 124, 488.
- 28 Camino, G., *Polymer Degradation and Stability*, 1984, 12, 213.
- 29 Hastie, J.W., Res, J., *Nat. Bur. Stand. Sect., A Phys. Chem.*, 1973, 77, 733.
- 30 Lewin, M., Weil, E.D., Mechanism and Modes of Action in Flame Retardancy of, in: *Fire Retardant Materials*, Horrocks, A.R. Price, D., Editors, Woodhead Publishing Limited, Cambridge 2001, 31.
- 31 Pearce, E.A., Weil, E.D., Barinov, V.Y., Fire Smart, in: *Fire and Polymers*, Nelson, G.L., Wilkie, C.A., Editors, American Chemical Society, Washington 2001, 37.
- 32 Braun, U., Balabanovich, A.I., Schartel, B., Knoll, U., Artner, J., Ciesielski, M., Doring, M., Perez, R., Sandler, J.K., Altstadt, W., Hoffmann, V., Pospiech, T.D., *Polymer*, 2006, 47, 8495.
- 33 Troitzsch, J., *Plastics Flammability Handbook*, Hanser, Munchen, 2004.

- 34 Costa, L., Camino, G., Luda, D., Cortemiglia, P., *Fire and Polymers*, 425, ACS Symposium, Washington DC, 1990.
- 35 Gilman, J.W., Kashiwagi, T., Harris J., Lomakin, R.H.S., Lichtenhan, J.D., Jones, P., Bolf, A., in: Al-Malaika, S., Wilkie, C., Golovoy C.A., Editors, *Chemistry and Technology of Polymer Additives*, Blackwell Science, London, 1999.
- 36 Zanetti, M., Kashiwagi, T., Falqui, L., Camino, G., *Chem. Mater.* 2002, 14, 881.
- 37 Lewin, M., *Polym. Adv. Technol.*, 2006, 17, 758.
- 38 Song, R., Wang, Z., Meng, X., Zhang, B., Tang, T., *J. Appl. Polym. Sci.*, 2007, 106, 3488.
- 39 Jang, B.N., Costache, M., Wilkie, C.A., *Polymer*, 2005, 46, 10678-10687.
- 40 Peeterbroeck, S., Laoutid, F., Taulemesse, J.M., Monteverde, F., Lopez-Cuesta, J.M., Nagy, J.B., Alexandre, M., Dubois, P., *Funct., Adv., Mater.*, 2007, 17, 2787.
- 41 Jin, Z., Pramoda, K.P., Xu, G., Goh, S.H., *Chem. Phys. Lett.*, 2001, 337, 43.
- 42 Cooper, C.A., Ravich, D., Lips, D., Mayer, J., Wagner, H.D., *Compos. Sci. Technol.*, 2002, 62, 1105.
- 43 Cipiriano, B.H., Kashiwagi, T., Raghavan, S.R., Yang, Y., Grulke, E.A., Yamamoto, K., Shields, J.R., Douglas, J.F., *Polym.*, 2007, 48, 6086.
- 44 Kashiwagi, T., Du, F., Winey, K.I., Groth, K.M., Shields, J.R., Bellayer, S.P., Kim, H., Douglas, J.F., *Polym.*, 2005, 46, 471.
- 45 Schartel, B., Potschke, P., Knoll, U., Abdel-Goad, M., *Eur. Polym. J.*, 2005, 41, 1061.



- 46 Bocchini, S., Frache, A., Camino, G., Claes, M., Eur., Polym., J., 2007, 43, 3222.
- 47 Kashiwagi, T., Grulke, E., Hilding, J., Groth, K., Harris, R.H., Butler, K., Shields, J., Kharchenko, S., Douglas, J., Polym., 2004, 39, 4227.
- 48 Ravindra, K., Manasi, G., Sheetal, G., Bijoy, K.P., Ravindra, K., J Adv Scient Res, 2012, 3, 2, 25-29.
- 49 Souza, A.C., Pires, A.T.N., Soldi, V., Journal of Thermal Analysis and Calorimetry, 2002, 70, 2, 405.
- 50 Broadbelt, L.J., Klein, M.T., Dean, B.D., Andrews, S.M., Journal of Polymer Science: Polymer Chemistry Edition, 1997, 35, 15, 3305.
- 51 Bahr, U., Luderwald, I., Muller, R., Schulten, H.R., Pyrolysis field desorption mass spectrometry of polymers, III., Aliphatic polyamides, Angewandte Makromolekulare Chemie 1984, 120, 163–175.
- 52 Ballistreri, A., Garozzo, D., Giufrida, M., Impallomeni, G., Montaudo, G., Primary thermal decomposition processes in aliphatic polyamides, Polymer Degradation and Stability, 1988, 23, 25.
- 53 Montaudo, G., Mass spectrometrical determination of cyclic oligomer distributions in polymerization and degradation reactions, Macromolecules, 1991, 24, 5829–5833.
- 54 Levchik, S.V., Weil, E.D., Lewin, M., Thermal Decomposition of Aliphatic Nylons, Polymer International, 1999, 48, 532-557.
- 55 Herrera, M., Wilhelm, M., Matuschek, G., Kettrup, A., Thermoanalytical and pyrolysis studies of nitrogen containing polymers, Journal of Analytical and Applied Pyrolysis 2001, 58, 173–188.
- 56 Herrera, M., Matuscheki, G., Kettrup, A., Main products and kinetics of the thermal degradation of polyamides, Chemosphere, 2001, 42, 601–607.

- 57 Dussel, H.J., Rosen, H., Hummel, D.O., *Makromol Chem.*, 1976, 177, 2343.
- 58 Hornsby, P.R., Wang, J., Rother, R., Jackson, G., Wilkinson, G., and Cossick, K., *Polymer Degradation and Stability*, 1996, 51, 235.
- 59 Song, L., Hu, Y., Lin, Z., Xuan, S., Wang, S., Chen, Z., Preparation and properties of halogen-free flame-retarded polyamide 6/organoclay nanocomposite, *Polymer Degradation and Stability*, 2004, 86, 3, 535–40.
- 60 Bok, N.J., Wilkie C.A., The effect of clay on the thermal degradation of polyamide 6 in polyamide 6/clay nanocomposites, *Polymer*, 2005, 46, 3264–3274.
- 61 Braun, U., Schartel, B., Fichera, M.A., Jager, C., Flame Retardancy Mechanisms of Aluminium Phosphinate in Combination with Melamine Polyphosphate and Zinc Borate in Glass-Fibre Reinforced Polyamide 6,6. *Polymer Degradation and Stability*, 2007, 92, 1528-1545.
- 62 Isitman, N.A., Gunduz, H.O., Kaynak, C., Nanoclay synergy in flame retarded/glass fibre reinforced polyamide 6, *Polymer Degradation and Stability* 2009, 24, 2241–2250.
- 63 Isbasar, C., Bayramlı, E., Hacıoğlu, J., Direct Pyrolysis Mass Spectrometry Analysis of PA-6 Containing Melamine and Boron Compounds, *Polymer Composites*, 2013, 34, 1389-1395.
- 64 Gupta, AP., Kumar, V., New emerging trends in synthetic biodegradable polymers - polylactide: a critique, *Eur Polym J*, 2007, 43, 10, 4053-4074.
- 65 Kopinke, F.D., Remmler, M., Mackenzie, K., Mörder, M., Wachen. O., Thermal decomposition of biodegradable polyester-II., Poly(lactic acid), *Polymer Degradation and Stability*, 1996, 3, 329-342.
- 66 Pluta, M., Gałęski, A., Alexandre, M., Paul, M.A., Dubois, P., *J. Appl. Polym. Sci.*, 2002, 86, 1497.

- 67 Paul, M.A., Alexandre, M., Degee, P., Henrist, C., Rulmont, A., Dubois, P., *Polymer* 2003, 44, 443.
- 68 Isitman, N.A., Dogan, M., Bayramli, E., Kaynak, C., The role of nanoparticle geometry in flame retardancy of polylactide nanocomposites containing aluminium phosphinate, *Polymer Degradation and Stability*, 2012, 97, 1285-1296.
- 69 Peterson, J.D., Vyazovkin, S., Wight, C.A., *Macromolecular Chemistry and Physics*, 2001, 202, 6, 775.
- 70 Saido, K., Kodera, Y., Taguchi, H., Tomono, K., Ishihara, Y., Kuroki, T., *Polymer Preprints*, 2002, 43, 2, 1162.
- 71 Nagasaki, Y., Yamazaki, N., Kato, M., *Macromolecular Rapid Communications*, 1996, 17, 2, 123.
- 72 Howell, B.A., Cui, Y., Priddy, D.B., *Polymer Preprints*, 2002, 43, 1, 360.
- 73 Demirelli, K., Coskun, M., *Polymer Plastics Technology and Engineering*, 1999, 38, 1, 167.
- 74 Lehrle, R.S., Atkinson, D.J., Bate, D.M., Gardner, P.A., Grimbley, M.R., Groves, S.A., Place, S.A., and Williams, R.J., *Polymer Degradation and Stability*, 1996, 52, 2, 183.
- 75 Pielichowski, K., Stoch, L., *Journal of Thermal Analysis*, 1994, 45, 5, 1239.
- 76 Faravelli, T., Pinciroli, M., Pisano, F., Bozzano, G., Dente M., Ranzi, E., *Journal of Analytical and Applied Pyrolysis*, 2001, 60, 103–121.

- 77 Luijk, R., Govers, H.A.J., Eijkel, G.B., Boon, J.J., Thermal degradation characteristics of high impact polystyrene/decabromodiphenylether/antimony oxide studied by derivative thermogravimetry and temperature resolved pyrolysis-mass spectrometry: formation of polybrominated dibenzofurans, antimony (oxy) bromides and brominated styrene oligomers, *Journal of Analytical and Applied Pyrolysis*, 1991, 20, 303-319.
- 78 Jakab, E., Uddin, M.A., Bhaskar, T., Sakata, Y., *Journal of Analytical and Applied Pyrolysis*, 2000, 68-69, 83-99.
- 79 Jang, B.N., Wilkie, C.A., The thermal degradation of polystyrene nanocomposite, *Polymer*, 2005, 46, 2933-42.
- 80 Grause, G., Ishibashi, J., Kameda, T., Bhaskar, T., Yoshioka, T., Kinetic studies of the decomposition of flame retardant containing high-impact polystyrene, *Polymer Degradation and Stability*, 2010, 95, 1129-1137.
- 81 Isitman, N.A., Kaynak, C., Tailored flame retardancy via nanofiller dispersion state: synergistic action between a conventional flame-retardant and nanoclay in high-impact polystyrene, *Polymer Degradation and Stability*, 2010, 95, 9, 1759-68.
- 82 Isitman, N.A., Sipahioglu, B.M., Kaynak, C., Nanomorphology and fire behavior of polystyrene/organoclay nanocomposites containing brominated epoxy and antimony oxide, *Polym., Adv., Technol.*, 2012, 23, 984-991.
- 83 Hacaloğlu, J., *Pyrolysis Mass Spectrometry for Molecular Ionization Methods. The Encyclopedia of Mass Spectrometry: Ionization Methods*, Volume 6, Edited by Michael L. Gross & Richard M. Caprioli. Elsevier Science Ltd, 2007, 925-938.
- 84 Uyar, T., Nur, Y., Hacaloglu, J., Besenbacher, F., Electrospinning of functional poly(methyl methacrylate) nanofibers containing cyclodextrin-menthol inclusion complexes, *Nanotechnology*, 2009, 20, 12.

- 85 Orhan, T., Isitman, N.A., Hacıoğlu, J., Kaynak, C., Thermal Degradation Mechanisms of Aluminium Phosphinate, Melamine Polyphosphate and Zinc Borate in Poly(Methyl Methacrylate), *Polymer Degradation and Stability*, 2011, 96, 1780-1787.
- 86 Wang, Y., Parkin, S., Atwood, D., Ligand-Tetrahydrofuran Coupling in Chelated Aluminum Phosphinates, *Inorganic Chemistry*, 2002, 41, 558-565.
- 87 Mitra, A., Parkin, S., Atwood, D.A., Aluminum Phosphinate and Phosphates of Salen Ligands, *Inorganic Chemistry*, 2006, 45, 3970-3975.
- 88 Blazso, M., Czegeny, Z., Csoma, C., Pyrolysis and debromination of flame retarded polymers of electronic scrap studied by analytical pyrolysis, *Journal of Analytical and Applied Pyrolysis*, 2002, 64, 249-261.
- 89 Ballistreri, A., Foti, S., Montaudo, G., Pappalardo, S., Scamporrino, E., Thermal decomposition of flame retardants-mixtures of chlorinated polymers with  $Sb_2O_3$  and  $(Bio)_2CO_3$ , *J Appl. Polym. Sci. Polym. Chem.*, 1979, 17, 2469-2475.
- 90 Isbasar, C., Hacıoğlu, J., Investigation of Thermal Degradation Characteristics of Polyamide-6 Containing Melamine or Melamine Cyanurate via Direct Pyrolysis Mass Spectrometry, *Journal of Analytical and Applied Pyrolysis*, 2012, 98, 221-230.
- 91 Kopinke, F.D., Remmler, M., Mackenzie, K., Milder, M., Wachsen, O., Thermal decomposition of biodegradable polyesters-11. Poly(lactic acid) *Polymer Degradation and Stability*, 1996, 43, 329-342.
- 92 Kuroki, T., Honda, T., Sekiguchi, Y., Ogawa, T., Sawaguchi, T., Ikemura, T., Thermal Degradation of Polystyrene, *Nippon Kagaku Kaishi*, 1977, 6, 894-901.

- 93 Sousa, P.A., Bouster, C., Vermande, P., Veron, J., Study of the pyrolysis of polystyrenes: II. Study of transfer reactions by identification of the most important by-products, *Journal of Analytical and Applied Pyrolysis*, 1981, 3, 19–34.
- 94 Krauze, M., Trzeszczynski, J., Dzieciol, M., *Polimery*, (Warsaw, Poland) 2003, 48, 701–8.
- 95 Schroeder, U., Ebert, K.H., Hamielec, A.W., On the Kinetics and Mechanism of Thermal Degradation of Polystyrene, *Makromol. Chem.*, 1984, 185, 991–1001.
- 96 McNeill, I.C., Zulfiqar, M., Kousar, T., A detailed investigation of the products of the thermal degradation of polystyrene, *Polymer Degradation and Stability*, 1990, 28, 131–51.
- 97 Guyot, A., Recent developments in the thermal degradation of polystyrene, *Polymer Degradation and Stability*, 1986, 15, 219–35.
- 98 McNeill, I.C., Stevenson, W.T.K., Thermal degradation of styrene-butadiene diblock copolymer: Part 1 Characteristics of polystyrene and polybutadiene degradation, *Polymer Degradation and Stability*, 1985, 10, 247-265.
- 99 Guaita, M., Chiantore, O., Costa, L., Changes in degree of polymerization in the thermal degradation of polystyrene, *Polymer Degradation and Stability*, 1985, 12, 315-332.
- 100 Grause, G., Karakita, D., Ishibashi, J., Kameda, T., Bhaskar, T., Yoshioka, T., TG-MS investigation of brominated products from the degradation of brominated flame retardants in high-impact polystyrene, *Chemosphere*, 2011, 85, 368-373.

## CURRICULUM VITAE

### Personal Details:

Name and Surname: Hatice KAYA  
Address: Çankaya / ANKARA  
E-mail: haticey8@yahoo.com  
Place/Date of Birth: Ankara / 1984

### Education:

Fatih Sultan Mehmet High School **High School** (1998-2001)  
Ankara, Turkey

Middle East Technical University **B.Sc. in Chemistry** (2002-2006)  
Ankara, Turkey Department of Chemistry

Middle East Technical University **M.Sc. in Organic Chemistry** (2006-2009)  
Ankara, Turkey Department of Chemistry  
“Studies on The Reactions of Acyl Phosphonates with Aldehydes in The Presence of Proline” under the supervision of Prof. Dr. Ayhan Sıtkı Demir

Middle East Technical University **Ph.D. in Department of PST**(2009-2013)  
Ankara, Turkey  
“Effects of Nanoparticles on Thermal Characteristics of Polyamide-6, Polylactide and Polystyrene Involving Various Flame Retardants” under the supervision of Prof. Dr. Jale Hacaloğlu

## Professional Experience:

General Directorate of Mineral Research and Exploration Ankara, Turkey	<b>Chemist, M.Sc.</b> (2010-present) Department of Mineral Analysis, Water Analysis Laboratory
Middle East Technical University Ankara, Turkey	<b>Research Assistant</b> (2007-2010) Department of Chemistry
Turkish Petroleum Corporation (TPAO) Ankara, Turkey	<b>Intern</b> (Summer 2005) Department of Research Center General Directorate of Technology

## Special Skills:

<b>Instrumental skills:</b>	Analytical Methods: HPLC, ICP-OES, ICP-MS, Py-MS, IC.
<b>Language skills:</b>	Turkish (native language) English (proficient in writing & speaking) Spanish (beginner)
<b>Computer skills:</b>	Documentation: MS Office Scientific Tools: ChemOffice, MassLynx, IgorPro MSD ChemStation, Scifinder

## Honors & Awards:

Middle East Technical University Ankara, Turkey	Chemistry Department Honor Student
TÜBİTAK	Merit Scholarship (2006-2008)



## **Publications:**

### **Articles in Press**

1. Kaya, H. and Hacaloglu, J. Thermal degradation of polystyrene composites. Part I. The effect of brominated polyepoxy and antimony oxide. *J. Anal. Appl. Pyrol.* 2014, 105, 301-308.
2. Kaya H, and Hacaloglu J. Thermal Degradation of Poly(lactide)/Aluminium Diethylphosphinate Composites. Submitted to *Polymer Degradation and Stability* 2013.
3. Kaya, H, Kaynak, C and Hacaloglu, J. Effects of Nanoparticles on Thermal Degradation of Poly(lactide) containing aluminium diethylphosphinate composites. *Polymer Composites* 2013.

### **Articles in Preparation**

1. Kaya, H. Isitman, N.A., Kaynak, C and Hacaloglu, J. Thermal degradation of polystyrene composites. Part II. In the presence of organoclay nanocomposites.
2. Kaya H, Hacaloglu J. Direct Pyrolysis mass spectrometry analyses of Polyamides 6 composites.
3. Kaya H, Isitman N.A., Kaynak C, Hacaloglu J. The role of organo-montmorillonite on Thermal Degradation of Polyamide 6 composites.
4. Kaya H, Kaynak C, Hacaloglu J. The effect of presence of nanoparticles on thermal degradation characteristics of Polyamide 6 composites.
5. Kaya H, Kaynak C, Hacaloglu J. Effects of nanoclays on thermal degradation of high impact polystyrene in the presence of aluminium hydroxide